

**THEORETICAL MODELING TO ACCESS THE
SURFACE PHENOMENON OF LIQUID
TERNARY ALLOYS**



**A THESIS SUBMITTED TO THE
CENTRAL DEPARTMENT OF PHYSICS
INSTITUTE OF SCIENCE AND TECHNOLOGY
TRIBHUVAN UNIVERSITY
NEPAL**

**FOR THE AWARD OF
DOCTOR OF PHILOSOPHY
IN PHYSICS**

**BY
UPENDRA MEHTA
FEBRUARY 2023**

**THEORETICAL MODELING TO ACCESS THE
SURFACE PHENOMENON OF LIQUID
TERNARY ALLOYS**



**A THESIS SUBMITTED TO THE
CENTRAL DEPARTMENT OF PHYSICS
INSTITUTE OF SCIENCE AND TECHNOLOGY
TRIBHUVAN UNIVERSITY
NEPAL**

**FOR THE AWARD OF
DOCTOR OF PHILOSOPHY
IN PHYSICS**

**BY
UPENDRA MEHTA
FEBRUARY 2023**

DECLARATION

This thesis entitled “**Theoretical Modeling to Access the Surface Phenomenon of Liquid Ternary Alloys**” which is being submitted to the Central Department of Physics, Institute of Science and Technology (IOST), Tribhuvan University, Nepal for the award of the degree of Doctor of Philosophy (Ph.D.), is a research work carried out by me under the supervision of Prof. Dr. Devendra Adhikari of Department of Physics, Mahendra M.A.M. Campus, Tribhuvan University, Biratnagar, Nepal and co-supervised by Prof. Dr. Ishwar Koirala of Central Department of Physics, Tribhuvan University, Kirtipur, Kathmandu, Nepal.

This research is original and has not been submitted earlier in part or full in this or any other form to any university or institute, here or elsewhere, for the award of any degree.

.....
Upendra Mehta

RECOMMENDATION

This is to recommend that **Upendra Mehta** has carried out research entitled “**Theoretical Modeling to Access the Surface Phenomenon of Liquid Ternary Alloys**” for the award of Doctor of Philosophy (Ph.D.) in **Physics** under our supervision. To our knowledge, this work has not been submitted for any other degree.

He has fulfilled all the requirements laid down by the Institute of Science and Technology (IOST), Tribhuvan University, Kirtipur for the submission of the thesis for the award of Ph.D. degree.

.....
Prof. Dr. Devendra Adhikari

Supervisor

(Professor)

Mahendra Morang Adarsha Multiple Campus
Tribhuvan University
Biratnagar, Nepal

.....
Prof. Dr. Ishwar Koirala

Co-supervisor

(Professor)

Central Department of Physics
Tribhuvan University
Kirtipur, Kathmandu, Nepal

FEBRUARY 2023

LETTER OF APPROVAL

[Date: 21-05-2023]-

On the recommendation of Prof. Dr. **Devendra Adhikari**, Department of Physics, M.M.A.M. Campus, Tribhuvan University, Biratnagar, Nepal and Prof. Dr. **Ishwar Koirala**, Central Department of Physics, Tribhuvan University, Kathmandu, Nepal, this Ph.D. thesis submitted by **Upendra Mehta**, Central Department of Physics, Tribhuvan University, Kathmandu, Nepal entitled “**THEORETICAL MODELING TO ACCESS THE SURFACE PHENOMENON OF LIQUID TERNARY ALLOYS**” is forwarded by Central Department Research Committee (CDRC) to the Dean, IOST, T.U..

.....

Dr. Om Prakash Niraula

Professor

Head

Central Department of Physics,

Tribhuvan University

Kirtipur, Kathmandu

Nepal

ACKNOWLEDGMENTS

Firstly, I would like to express my immense gratitude to my research supervisor Prof. Dr. Devendra Adhikari, Mahendra Morang Adarsh Multiple Campus, Tribhuvan University, Biratnagar, Nepal and co-supervisor Prof. Dr. Ishwar Koirala, Central Department of Physics, Tribhuvan University, Kirtipur, Nepal for their support, scientific as well as motivational inspirations, guidance and mentorship to carry this research work.

I would like to extend my special appreciation to Dr. Ram Prasad Koirala and Dr. Shashit Kumar Yadav, Department of Physics, Mahendra Morang Adarsha Multiple Campus, Tribhuvan University, Biratnagar, Nepal for their unwavering support and insightful suggestions which played a crucial role in each step of my research work.

I am thankful to Prof. Dr. Om Prakash Niraula (HoD), Prof. Dr. Narayan Prasad Adhikari, Prof. Dr. Raju Khanal, and Prof. Dr. Hari Prasad Lamichhane, Central Department of Physics, Tribhuvan University, Kirtipur, Nepal for their support, encouragement, and inspiration to handle this work. I am also appreciative to all the faculty members and non-teaching staff of the department for their motivational support.

I would like to acknowledge Prof. Dr. Ashok Kumar (HoD), Dr. Indu Shekhar Jha, Mr. Jamil Akhtar and all the faculty members of Department of Physics, Mahendra Morang Adarsha Multiple Campus, Tribhuvan University, Biratnagar, for their valuable suggestions and encouragement. I am also grateful to all the non-teaching staff of the department for their good wishes.

I would also like to acknowledge the cooperation and assistance of my research colleagues, Ramesh Kumar Gohivar and Arjun Dhungana, whose collaboration has been invaluable to the success of this undertaking.

I am thankful to Mr. Rajesh Kumar Bachchan, Mr. Janardan Mehta and younger brother Abhilekh Pratik Mehta for assisting me with the computational work during my research.

My sincere thanks go to Mrs. Sarita Adhikari for her continuous support, encouragement, and inspiration during this work.

For the love, understanding and support, I would like to thank my beloved wife Mrs. Shakuntala Mehta and daughters Sejal and Bhabya. I would also like to thank my brother Rajendra Mehta, his wife Mrs. Meera Singh and daughters Shritika and Deepali for support and good wishes during my ups and downs.

Moreover, I would like to show my gratitude to my father-in-law, Bhajan Lal Mehta, mother-in-law Kunti Devi, and brothers-in-law Sanjay and Dhananjay for their continuous support during the period of research work.

Last but not the least, I would like to show my immense gratitude to my father Mr. Kadam Lal Mehta for the encouragement and inspiration and my mother, Uma Devi for nurturing and standing by me in all up and down situations of my life.

Upendra Mehta
February, 2023

ABSTRACT

The Redlich-Kister (R-K) polynomial was used to optimise the linear temperature dependent interaction energy parameters for excess Gibbs free energy of mixing of binary subsystems of Fe–Si–Ti, Al–Sn–Zn and Al–Cu–Fe ternary liquid alloys using experimental data for excess entropy of mixing and enthalpy of mixing. The optimised parameters of binary subsystems were then used in the Chou equation (General Solution Model) for the excess Gibbs free energy of mixing of ternary liquid alloys to evaluate the partial excess free energy of mixing of components. These partial excess free energies of components of ternary liquid alloys were then used in the Butler equation to compute the surface concentrations of components and surface tensions of these ternary systems from the corner of each element at cross-sections of 3 : 1, 1 : 1 and 1 : 3. In addition, the excess surface tension of the binary subsystems at four different temperatures was used to compute the temperature dependent coefficients of the R-K polynomial for the binary subsystems of the previously mentioned ternary alloy. These coefficients were then used in the Kohler, Toop, and Chou equation to obtain the surface tension of the ternary alloys at different temperatures and concentrations. The obtained values of surface tension using these geometrical models were then compared with those obtained using the Butler equation.

It was found that the component with the lowest surface tension leads to the highest surface concentration and the surface concentration of components increases as their bulk concentration increases and vice versa. Furthermore, it was observed that the interaction between the binary pairings affected the surface concentration of a component in these ternary alloys. All three binary subsystems of Fe–Si–Ti ternary system were found to be ordering in nature and the surface concentration of the components was also affected by the interaction between these binary pairs. The surface concentration of Ti was found to increase with the decrease of its bulk concentration at the low content of Ti in the alloys. This unusual behaviour was observed due to the higher interaction energy between Fe and Si than between Fe and Ti in Fe–Si–Ti ternary liquid alloys.

It was observed that the surface concentration of each component in Al–Sn–Zn ternary liquid alloy increased with increasing the respective bulk concentration at all cross-sections. In this case, surface concentration was determined by the surface tension of the individual components, as all the binary sub-systems of this ternary alloys were of segregating nature.

In case of Al–Cu–Fe liquid ternary alloys, binary sub-systems Al–Cu and Al–Fe are of ordering in nature while Cu–Fe is strongly segregating. When observed from the Fe corner, the surface concentration of Cu increased from 0.060 to 0.081 while the bulk

concentration decreased from 0.225 to 0.088 at the cross-section $x_{\text{Al}} : x_{\text{Cu}} = 3 : 1$. This unusual trend of increasing surface concentration of Cu with the decrease of its bulk concentration may be due to the ordering tendency of Fe with Al and the segregating nature of Fe with Cu.

The surface concentration of components changes towards the ideal value (bulk concentration) at elevated temperatures. The surface concentration of Fe and Ti was found to increase while that of Si was found to decrease when the temperature of the alloy was increased from 1873 K to 2173 K. The surface concentration of Fe and Ti were found less than their respective bulk concentration and mole fraction concentration of Si in the surface was found to be much higher than the bulk phase. Similar results were noticed for the variation of surface concentration with temperature in the case of Al–Sn–Zn and Al–Cu–Fe ternary liquid alloys.

The surface tension of liquid ternary alloys was found to decrease rapidly with the rise in bulk concentration of the component having the least surface tension in pure state. The value of temperature coefficient of surface tension was found to vary with composition of the alloys. The surface tension of all ternary liquid alloys studied in this work decreased linearly with increase in temperature, regardless of composition.

LIST OF SYMBOLS

a_x	: Activity of a component at its bulk concentration x
G	: Absolute Gibbs free energy of mixing
G_i	: Absolute partial Gibbs free energy of i th component
G_i^0	: Absolute Gibbs free energy of i th component of alloy in pure state
G_{ij}^{XS}	: Excess Gibbs free energy of mixing of ij binary system
G_M^{XS}	: Excess Gibbs free energy of mixing
$G_{i,b}^{XS}$: Partial excess free energy of i^{th} component in bulk phase of alloy
$G_{i,s}^{XS}$: Partial excess free energy of i^{th} component in surface phase of alloy
A_{ij}^k	: Coefficients of k^{th} term of of R-K polynomial for ij binary system
β	: Ratio of partial excess free energy of surface phase to bulk phase
A_i	: Partial monolayer surface area of i^{th} component of one mole of substance in solution phase
A_i^0	: Monolayer surface area of i^{th} component of one mole of substance in its pure state
A	: Weighted mean of surface area of component of one mole of alloy
R	: Universal gas constant
k_B	: Boltzmann constant
σ	: Surface tension of alloy
σ_i	: Partial surface tension of i^{th} component in alloy
σ_i^0	: Surface tension of i^{th} component of alloy in its pure state
$S_{cc}(0)$: Concentration fluctuation in long wavelength limit
$S_{cc}^{id}(0)$: Ideal value of Concentration fluctuation in long wavelength limit
H_M	: Heat of mixing
S_M	: Entropy of mixing
S_M^{XS}	: Excess entropy of mixing
x_i	: Bulk concentration of i^{th} components in ternary alloy
x_i^s	: Surface concentration of i^{th} component in alloy
X_{ij}	: Sub-binary concentration in ternary alloy
ρ_i	: Density of i^{th} component of alloy
ρ_i^0	: Density of i^{th} component of alloy near their melting temperatures
z^s	: Coordination number of an atom in surface phase
z^b	: Coordination number of an atom in bulk phase
N_A	: Avagadro's number
M_i	: Molar mass of i^{th} component in alloy
$\eta_{i(jk)}$: Deviation sum of square for ij and ik binary subsystems
ξ_{ij}	: Similarity coefficients for ij binary system

- Ω : Total no. of ways of arrangement of atoms
 w : Interchange energy
 ϵ_{AB} : Bond energy between A–B
 ϵ_{AA} : Bond energy between A–A
 ϵ_{BB} : Bond energy between B–B
 ω_R : Rayleigh surface oscillation frequency

LIST OF TABLES

	Page No.
Table 1: Optimised coefficients of R-K polynomial for G_M^{xs} of binary subsystems of Fe–Si–Ti liquid ternary alloys	46
Table 2: G_M^{xs} (kJ/mol) of binary subsystems of Fe–Si–Ti liquid ternary alloys	46
Table 3: Values of density (ρ_0) and surface tension (σ_0) of elements near their melting temperature (T_0) and variation of density and surface tension with temperature	48
Table 4: Surface tension of binary sub-systems of Fe–Si–Ti liquid alloys at 1873 K	48
Table 5: Surface concentration of Fe, Si and Ti in Fe–Si–Ti liquid ternary alloys from Fe corner at 1873 K	52
Table 6: Surface concentration of Fe, Si and Ti in Fe–Si–Ti liquid ternary alloys from Si corner at 1873 K	52
Table 7: Surface concentration of Fe, Si and Ti in Fe–Si–Ti liquid ternary alloys from Ti corner at 1873 K	55
Table 8: Surface concentration of components in Fe–Si–Ti liquid alloys at different temperatures for a fixed bulk composition $x_{Fe} : x_{Si} : x_{Ti} = 0.4 : 0.15 : 0.45$	55
Table 9: Optimised coefficients of R-K polynomial for excess surface tension of binary subsystems of Fe–Si–Ti liquid ternary alloys .	57
Table 10: Surface tension of Fe–Si–Ti ternary alloys from Fe corner at 1873 K	58
Table 11: Surface tension of Fe–Si–Ti ternary alloys from Si corner at 1873 K	58
Table 12: Surface tension of Fe–Si–Ti ternary alloys from Ti corner at 1873 K	59
Table 13: Variation of surface tension of Fe–Si–Ti liquid alloys with temperature	61
Table 14: Optimised coefficients of R-K polynomial for G_M^{xs} of binary subsystems of Al–Sn–Zn liquid ternary alloys	63
Table 15: G_M^{xs} (kJ/mol) of binary subsystems of Al–Sn–Zn liquid ternary alloys.	64
Table 16: Surface tension ($N\ m^{-1}$) of binary subsystems of Al–Sn–Zn liquid alloys at 973 K	65

Table 17: Surface concentration of Al, Sn and Zn in Al–Sn–Zn liquid ternary alloys from Al corner at 973 K	67
Table 18: Surface concentration of Al, Sn and Zn in Al–Sn–Zn liquid ternary alloys from Sn corner at 973 K	67
Table 19: Surface concentration of Al, Sn and Zn in Al–Sn–Zn liquid ternary alloys from Zn corner at 973 K	69
Table 20: Surface concentration of components in Al–Sn–Zn liquid alloys at different temperature for a fixed bulk composition $x_{Al} : x_{Sn} : x_{Zn} = 0.333 : 0.333 : 0.334$	72
Table 21: Optimised coefficients of R-K polynomial for excess surface tension of binary subsystems of Al–Sn–Zn liquid ternary alloys	73
Table 22: Surface tension of Al–Sn–Zn ternary alloys from Al corner at 973 K	73
Table 23: Surface tension of Al–Sn–Zn ternary alloys from Sn corner at 973 K	74
Table 24: Surface tension of Al–Sn–Zn ternary alloys from Zn corner at 973 K	74
Table 25: Surface Tension of Al–Sn–Zn liquid ternary alloys at different temperatures	78
Table 26: Optimised coefficients of R-K polynomial for G_M^{xs} of binary subsystems of Al–Cu–Fe liquid ternary alloys	80
Table 27: G_M^{xs} (kJ/mol) of binary subsystems of Al–Cu–Fe liquid ternary alloys.	81
Table 28: Surface tension ($N m^{-1}$) of binary subsystems of Al–Cu–Fe liquid alloys at 1823 K	82
Table 29: Surface concentration of components in Al–Cu–Fe liquid ternary alloys from Al corner at 1823 K	84
Table 30: Surface concentration of components in Al–Cu–Fe liquid ternary alloys from Cu corner at 1823 K	87
Table 31: Surface concentration of components in Al–Cu–Fe liquid ternary alloys from Fe corner at 1823 K	87
Table 32: Surface concentration of components in Al–Cu–Fe liquid alloys at different temperature for a fixed bulk composition $x_{Al} : x_{Cu} : x_{Fe} = 0.1 : 0.45 : 0.45$	90
Table 33: Optimised coefficients of R-K polynomial for excess surface tension of binary subsystems of Al–Cu–Fe liquid ternary alloys	91
Table 34: Surface tension of Al–Cu–Fe ternary alloys from Al corner at 1823 K	91

Table 35: Surface tension of Al–Cu–Fe ternary alloys from Cu corner at 1823 K	92
Table 36: Surface tension of Al–Cu–Fe ternary alloys from Fe corner at 1823 K	92
Table 37: Surface Tension of Al–Cu–Fe liquid ternary alloys at different temperatures.	96
Table 38: Partial excess free energy of components in Fe–Si–Ti ternary liquid alloy at 1873 K from Fe corner at three cross-section . .	119
Table 39: Partial excess free energy of components in Fe–Si–Ti ternary liquid alloy at 1873 K from Si corner at at three cross-section .	120
Table 40: Partial excess free energy of components in Fe–Si–Ti ternary liquid alloy at 1873 K from Ti corner at three cross-sections . .	121
Table 41: Partial excess free energy of components in Al–Sn–Zn ternary liquid alloy at 973 K from Al corner at three cross-sections . .	122
Table 42: Partial excess free energy of components in Al–Sn–Zn ternary liquid alloy at 973 K from Sn corner at three cross-sections . .	123
Table 43: Partial excess free energy of components in Al–Sn–Zn ternary liquid alloy at 973 K from Zn corner at three cross-section . . .	124
Table 44: Partial excess free energy of components in Al–Cu–Fe ternary liquid alloy at 1823 K from Al corner at three cross-sections . .	125
Table 45: Partial excess free energy of components in Al–Cu–Fe ternary liquid alloy at 1823 K from Cu corner at three cross-sections .	126
Table 46: Partial excess free energy of components in Al–Cu–Fe ternary liquid alloy at 1823 K from Fe corner at three cross-sections . .	127
Table 47: Ternary concentrations of Fe–Si–Ti liquid alloy for iso-surface tension lines at 1873 K	128
Table 48: Ternary concentrations of Al–Sn–Zn liquid alloy for iso-surface tension lines at 973 K	129
Table 49: Ternary concentrations of Al–Cu–Fe liquid alloy for iso-surface tension lines at 1823 K	130

LIST OF FIGURES

	Page No.
Figure 1: Selections of binary concentration points using ternary plots in different geometrical models.	6
Figure 2: Variation of excess surface tensions of binary subsystems of Al–Sn–Zn ternary liquid alloys with bulk concentration.	7
Figure 3: Representation of concentrations of binary subsystems in liquid ternary alloys.	27
Figure 4: Representation of binary concentrations corresponds to a ternary point in Mugginau model.	27
Figure 5: Representation of binary concentrations corresponds to a ternary point in Kohler model.	29
Figure 6: Representation of binary concentrations corresponds to a ternary point in Toop model.	31
Figure 7: Representation of binary concentrations corresponds to a ternary point in Chou model.	32
Figure 8: Variation of G_M^{xs}/RT of Fe–Si binary alloys with the order of interaction energy parameters.	42
Figure 9: Variation of G_M^{xs}/RT of different binary liquid alloys with bulk concentration (x_1).	43
Figure 10: Variation of G_M^{xs} of binary subsystems of Fe–Si–Ti liquid alloys with concentration.	47
Figure 11: Variation of surface tension of sub-binary system of Fe–Si–Ti ternary alloy at 1873 K.	49
Figure 12: Variation of surface concentration of components in Fe–Si–Ti ternary alloys with bulk concentration from Fe corner at three cross-sections.	51
Figure 13: Variation of surface concentration of components in Fe–Si–Ti ternary alloys with bulk concentration from Si corner at three cross-sections.	53
Figure 14: Variation of surface concentration of components in Fe–Si–Ti ternary alloys with bulk concentration from Ti corner at three cross-sections.	54
Figure 15: Variation of surface concentration of components in the Fe–Si–Ti ternary alloys with temperature at a fixed bulk concentration.	56

Figure 16: Iso surface tension (mN m^{-1}) lines of Fe–Si–Ti liquid ternary alloys at 1873 K.	57
Figure 17: Variation of surface tension of Fe–Si–Ti liquid ternary alloys with bulk concentration from Fe corner.	59
Figure 18: Variation of surface tension of Fe–Si–Ti liquid ternary alloys with bulk concentration from Si corner.	60
Figure 19: Variation of surface tension of Fe–Si–Ti liquid ternary alloys with bulk concentration from Ti corner at three different cross-sections.	60
Figure 20: Variation of surface tension of Fe–Si–Ti liquid ternary alloys with temperature at five different bulk concentrations.	61
Figure 21: Variation of G_M^{XS} of binary subsystems of Al–Sn–Zn liquid alloys with concentration.	64
Figure 22: Variation of surface tension of binary subsystems of Al–Sn–Zn liquid alloys with bulk concentration at 973 K.	65
Figure 23: Variation of surface concentration of components in Al–Sn–Zn ternary alloys with bulk concentration from Al corner at three cross-sections.	68
Figure 24: Variation of surface concentration of components in Al–Sn–Zn ternary alloys with bulk concentration from Sn corner at three cross-sections.	70
Figure 25: Variation of surface concentration of components in Al–Sn–Zn ternary alloys with bulk concentration from Zn corner at three cross-sections.	71
Figure 26: Variation of surface concentration of components in Al–Sn–Zn liquid ternary alloys with temperature at a fixed bulk concentration.	72
Figure 27: Iso-surface tension (mN m^{-1}) lines of Al–Sn–Zn liquid alloys at 973 K. Triangles on Sn–Zn line (Pstrus et al., 2006) and square on Al–Sn line (Goumiri et al., 1979) represent experimental data.	75
Figure 28: Variation of surface tension of Al–Sn–Zn liquid alloys at 973 K from Al corner at three different cross-sections.	76
Figure 29: Variation of surface tension of Al–Sn–Zn liquid alloys at 973 K from Sn corner at three different cross-sections.	77
Figure 30: Variation of surface tension of Al–Sn–Zn liquid alloys at 973 K from Zn corner at three different cross-sections.	77

Figure 31: Variation of surface tension (N m^{-1}) of Al–Sn–Zn liquid ternary alloys with temperature (K) at five different bulk compositions.	78
Figure 32: Variation of G_M^{XS} of binary subsystems of Al–Cu–Fe liquid alloys with concentration.	81
Figure 33: Variation of surface tension of binary subsystems of Al–Cu–Fe liquid ternary alloys with concentration at 1823 K.	83
Figure 34: Variation of surface concentration of components in Al–Cu–Fe ternary alloys with bulk concentration from Al corner at three bulk concentrations.	85
Figure 35: Variation of surface concentration of components in Al–Cu–Fe ternary alloys with bulk concentration from Cu corner at three bulk concentrations.	86
Figure 36: Variation of surface concentration of components in Al–Cu–Fe ternary alloys with bulk concentration from Fe corner at three cross-sections.	89
Figure 37: Variation of surface concentration of components in the Al–Cu–Fe ternary alloys with temperature at a fixed bulk concentration.	90
Figure 38: Iso-surface tension lines (mN m^{-1}) of Al–Cu–Fe liquid alloys at 1823 K.	93
Figure 39: Variation of surface tension of Al–Cu–Fe liquid alloys at 1823 K from Al corner at three different cross-sections.	94
Figure 40: Variation of surface tension of Al–Cu–Fe liquid alloys at 1823 K from Cu corner at three different cross-sections.	95
Figure 41: Variation of surface tension of Al–Cu–Fe liquid alloys at 1823 K from Fe corner at three different cross-sections.	95
Figure 42: Variation of surface tension (N m^{-1}) of Al–Cu–Fe liquid ternary alloys with temperature at five different compositions.	96

TABLE OF CONTENTS

	Page No.
Declaration	ii
Recommendation	iii
Letter of Approval	iv
Acknowledgements	v
Abstract	vii
List of Symbols	ix
List of Tables	xi
List of Figures	xiv
CHAPTER 1	1
1. INTRODUCTION	1
1.1 General background	1
1.2 System selection	3
1.3 Geometrical models	5
1.4 Problem statement	8
1.5 Objectives of the Work	9
1.6 Organization of the work	9
CHAPTER 2	10
2. LITERATURE REVIEW	10
2.1 General background	10
2.2 A brief review of thermodynamic properties of liquid alloys	10
2.3 Surface properties	14
CHAPTER 3	22
3. MATERIALS AND METHODS	22
3.1 Thermodynamic properties	22
3.1.1 Gibbs free energy of mixing	23
3.1.2 Gibbs free energy of mixing for ideal solution	23
3.1.3 Excess Gibbs free energy of mixing of alloys	25
3.2 General discription of different ternary models	25
3.3 Mugginau Model	27

3.4	Kohler Model	29
3.5	Toop model	30
3.6	Chou or General Solution Model (GSM)	31
3.7	Surface properties	35
CHAPTER 4		41
4.	RESULTS AND DISCUSSION	41
4.1	Effect of interaction energy parameters on mixing properties of liquid alloys	41
4.2	Fe–Si–Ti ternary system	44
4.2.1	Excess Gibbs free energy of mixing of Fe–Si, Si–Ti and Fe–Ti binary systems	45
4.2.2	Surface tensions of binary subsystems of Fe–Si–Ti alloy	48
4.2.3	Surface properties of Fe–Si–Ti liquid ternary alloy	50
4.2.3.1	Surface concentration of components in Fe–Si–Ti liquid ternary alloy	50
4.2.3.2	Surface tension of Fe–Si–Ti liquid ternary alloys	56
4.3	Al–Sn–Zn ternary system	62
4.3.1	Excess Gibbs free energy of mixing of Al–Sn, Al–Zn and Sn–Zn binary systems	63
4.3.2	Surface tensions of binary subsystems of Al–Sn–Zn alloys	65
4.3.3	Surface properties of Al–Sn–Zn liquid ternary alloys	66
4.3.3.1	Surface concentrations of components in Al–Sn–Zn liquid ternary alloys	66
4.3.3.2	Surface tension of Al–Sn–Zn liquid ternary alloys	73
4.4	Al–Cu–Fe ternary system	79
4.4.1	Excess Gibbs free energy of mixing of Al–Cu, Al–Fe and Cu–Fe binary systems	80
4.4.2	Surface tensions of binary subsystems of Al–Cu–Fe alloys	82
4.4.3	Surface properties of Al–Cu–Fe liquid ternary alloys	84
4.4.3.1	Surface concentrations of components in Al–Cu–Fe liquid ternary alloys	84
4.4.3.2	Surface tension of Al–Cu–Fe liquid ternary alloys	91
CHAPTER 5		98
5.	CONCLUSIONS AND RECOMMENDATIONS	98
5.1	Conclusions	98
5.2	Recommendations of the work	100

CHAPTER 6	101
6. SUMMARY	101
7. REFERENCE	104
APPENDIX	119
A: Data for Partial excess free energy of mixing of components in ternary liquid alloys.	119
B: Data for iso-surface tension lines of ternary liquid alloys.	128
C: Paper published in international journals	131
D: Paper published in national journals	131
E: Participation in Conferences and Workshops	132

CHAPTER 1

1. INTRODUCTION

1.1 General background

Alloys are uniform blends of two or more elements, at least one of which must be a metal. In order to develop new materials with required properties, alloying phenomenon is followed. New materials with improved properties are necessary to satisfy the global demand for the newest technological advancements. With this regard, alloying is carried out and has established itself as a successful technique for developing new materials. For this, a desired metal is considered as substrate and additional microgranules (metals or non-metals) are added using various processing techniques. Even though, alloys are used for a variety of purposes in solid state, such as in the military, domestic, industrial, etc., they are grown from their liquid states (Adhikari, 2013). Therefore, the energetic of initial melt determines the mixing behaviours of solid alloys.

Experimental methods to determine mixing properties of materials at each temperature are tedious for several reasons. The metals or microgranules become reactive with the walls of the container as well as with the atmospheric conditions at high temperatures (Duan et al., 2018; Fima & Novakovic, 2018; Yadav, 2018). This contamination significantly changes the surface properties of the liquid alloys. A few parts per million of oxygen can significantly change the surface tension of the melts (Egry, Ricci, et al., 2010). Surface tension of Fe and Ni was found to decrease exponentially with time when exposed to oxygen/helium gas flow at constant composition (Seyhan & Egry, 1999). Furthermore, it is difficult to change the composition of alloys continuously throughout the entire range and testing their properties experimentally at all the composition to retrieve quality product. This also increases the laboratory costs, making the alloys industry's product very expensive for consumers. As a result, the use of theoretical modeling to explain and understand the various mixing properties of liquid alloys has become mandatory in metallurgical science.

Several theoreticians working in this field have spent a considerable amount of time over the period of many years developing various theoretical models. In this limelight, different theoretical models (Hoar & Melford, 1957; Zhang et al., 1997; Kaptay, 2004; Picha et al., 2004; Brillo & Egry, 2005; Mekler & Kaptay, 2008; Fima & Kucharski, 2008; Schmitz et al., 2009; Zhou et al., 2011; Sklyarchuk et al., 2012; Yadav et al., 2016) and computational techniques (Chushak & Baumketner, 1999; Han et al., 2013;

M. I. Jordan & Mitchell, 2015; Allen & Tildesley, 1987; Trybula et al., 2018; Belova et al., 2019; W. Wang et al., 2019; Zou et al., 2021; Yi et al., 2021) have been developed to assess and explain the alloying properties of binary and multi-component systems. In this work, the surface properties of many ternary liquid alloys, such as Fe–Si–Ti, Al–Sn–Zn and Al–Cu–Fe have been studied at different temperature using various theoretical models. The surface properties of the above mentioned liquid alloys have been computed using the thermodynamic database of constituent binary subsystems.

The surface properties and stability phase are greatly affected by the thermodynamic functions. The strength of bonding between the constituent atoms in a complex is determined by the minimum or maximum value of excess free energy of mixing (G_M^{xs}) of the system called extremum value. The system is said to be weakly interacting when the extremum value of G_M^{xs}/RT lies in between 0 and -1 (Costa et al., 2014). For moderately interacting systems, this value lies in between -1 and -2 and less than -2 for strongly interacting systems. The positive values of G_M^{xs}/RT of liquid mixture signifies the segregating nature of liquid mixture. Another thermodynamic function that influence the nature of complex and stability of phase is enthalpy of mixing (H_M) and it can be directly measured from experiments using calorimetric method. Short range ordered liquid alloys have large negative value of H_M and segregating liquid alloys are characterised by a low negative or positive value of H_M . The concentration fluctuation in the long wavelength limit ($S_{cc}(0)$) has been developed as a unique tool for investigating the configuration of the local arrangement of atoms in a liquid mixture. First of all, Bhatia & Thornton (1970) presented the quantitative statistical idea of $S_{cc}(0)$ and then used by several researchers (Bhatia & Hargrove, 1974; R. N. Singh, 1987; R. N. Singh & Sommer, 1997; Novakovic, 2010; Adhikari, 2011; Yadav et al., 2016) to comprehend the hetero-coordinating or homo-coordinating nature of binary liquid alloys.

An understanding of the surface properties of liquid systems holds crucial importance due to various reasons. By studying surface properties, valuable insights can be obtained regarding phase transitions, kinetics of equilibrium phases, wettability and catalytic activities. Such knowledge allows researchers to delve deeper into the behavior and characteristics of liquid systems, enabling advancements in fields ranging from materials science to chemical engineering. As a result, several theoreticians and experimentalists have long been working in this field to better understand the surface properties of various liquid alloys.

As stated previously, researchers have developed many theoretical modeling equations to assess the mixing behaviours of binary liquid alloys. To investigate the thermodynamic properties of ternary liquid alloys, however, limited models, known as geometrical models have been purposed. These models include Kohler model, Toop model, Mugginau model, Hillert model, General Solution Model or Chou model etc. The applicability of

these models is based on the thermodynamic database of constituent binary subsystems. Later, these models were employed to study and explain the surface properties (Yan et al., 2007; Plevachuk et al., 2011; Fima & Novakovic, 2018; Mehta et al., 2022) and transport properties (Dogan & Arslan, 2016, 2018) of ternary liquid alloys. The geometrical models were employed to compute the thermo-physical properties of several ternary liquid alloys. However, the complete thermodynamic database for most of the ternary and higher order alloys are not available to date.

Therefore, we intend to investigate the surface properties of Fe–Si–Ti, Al–Sn–Zn, and Al–Cu–Fe ternary liquid alloys at different temperatures and compositions using theoretical models like Toop model (Toop, 1965), Kohler model (Kohler, 1960) and Chou or General Solution Model (GSM) (Chou & Chang, 1989; Chou, 1995; Chou et al., 1996). The thermodynamic data of G_M^{xs} is used for the computation of surface properties. Initially, the temperature-dependent self-consistent parameters of binary subsystems of ternary liquid alloys were optimised for G_M^{xs} using data of H_M and excess entropy of mixing (S_M^{xs}) in the framework of Redlich-Kister (R-K) polynomials (Redlich & Kister, 1948). Secondly, these temperature dependent parameters were then used to compute the surface tensions of the binary subsystems using Bulter equation (Butler, 1932) at various temperatures and concentrations. The excess surface tensions of the binary systems were then computed at various compositions as the deviation of the surface tension values from that obtained using the weighted mean. These data of excess surface tensions were used to optimise the coefficients of R-K polynomial for excess surface tension. Different geometrical models were employed to study the surface tension of the ternary alloys in terms of the optimised coefficients of the sub-binaries.

1.2 System selection

In this work, the thermodynamic and surface properties of ternary systems have been described using the interaction between the molecules of the sub-binary pairs. The G_M^{xs} and partial excess Gibbs free energy (G_i^{xs}) of ternary liquid alloys have been computed using different geometrical modeling equations with the aid of interaction energy parameters of binary systems. The ternary systems considered for the study in this work have been chosen based on whether the binary pairing exhibit ordering or segregating nature. Studies reveal that the mixing properties of ternary and multi-component systems are significantly influenced by the degree of interaction between the atoms in the binary subsystems of the ternary alloys. So, it has been investigated how interaction between such binary pairings affect the surface properties of ternary systems.

These effects can be more conveniently interpreted in terms of the structural function, called concentration fluctuation in long wavelength limit ($S_{cc}(0)$) of the sub-binary pairs.

It gives information regarding the local pairing of atoms in the immediate vicinity of the liquid mixtures. At a concentration and temperature, when the value of $S_{cc}(0)$ of a binary system is less than its ideal value ($S_{cc}^{id}(0)$), the system shows ordering tendency. If $S_{cc}(0) > S_{cc}^{id}(0)$, then the system shows segregating nature and in case of $S_{cc}(0) = S_{cc}^{id}(0)$, then it shows ideal mixing tendency (R. N. Singh, 1987; Prasad et al., 1995; Adhikari, Singh, & Jha, 2010; Novakovic et al., 2012; R. P. Koirala et al., 2013; Adhikari, 2013; Yadav et al., 2015). Herein, $S_{cc}^{id}(0)$ at bulk concentrations x_1 and x_2 of binary liquid alloys can be expressed using the relation

$$S_{cc}^{id}(0) = x_1 x_2 \quad (1.1)$$

The experimental values of $S_{cc}(0)$ for the binary subsystems can be obtained using the experimental data of activity (a) of components in the alloys with the help of relation (Bhatia & Hargrove, 1974; R. N. Singh, 1987; Adhikari, 2013; Costa et al., 2014; Yadav, 2018)

$$S_{cc}(0) = x_2 a_1 \left(\frac{\partial a_1}{\partial x_1} \right)_{T,P}^{-1} = x_1 a_2 \left(\frac{\partial a_2}{\partial x_2} \right)_{T,P}^{-1} \quad (1.2)$$

where a_1 and a_2 are the activities of components in binary liquid alloys at bulk concentrations x_1 and x_2 respectively. The values of $\partial a / \partial x$ can be computed using the equation

$$\frac{\partial a}{\partial x} = \frac{1}{12h} [a_{x+3} - 6a_{x+2} + 18a_{x+1} - 10a_x - 3a_{x-1}] \quad (1.3a)$$

for the concentration ranging from $x=0.1$ to 0.7 and herein, $h = 0.1$ is the interval between the two consecutive bulk concentrations. The values of $\partial a / \partial x$ for the bulk concentration $x = 0.8$ and 0.9 can be expressed as

$$\frac{\partial a}{\partial x} = \frac{1}{12h} [3a_{x+1} + 10a_x - 18a_{x-1} + 6a_{x-2} - a_{x-3}] \quad (1.3b)$$

The extent of deviation between $S_{cc}(0)$ and $S_{cc}^{id}(0)$ also represents the nature of bonding between the atoms. The stable complexes are formed at those stoichiometric compositions where there are greater negative deviations of $S_{cc}(0)$ from its respective ideal value. At this condition, G_M^{xs} and H_M have high negative values and the activity of liquid alloys show greater negative deviation from Raoult's law (ideal value).

In this work, the surface properties of three ternary liquid alloys namely Fe–Si–Ti, Al–Sn–Zn, and Al–Cu–Fe have been investigated. The computed values of $S_{cc}(0)$ of the binary subsystems Fe–Si (Adhikari et al., 2011; Novakovic et al., 2022) and Si–Ti (Yadav et al., 2020) binary liquid alloys were found to be much less than their respective

ideal values at all concentrations showing the ordering tendency of these alloys. The G_M^{xs} of these binary systems were found to be negative and there was negative deviation of activity of components from Raoult's law. The value of $S_{cc}(0)$ of Fe–Ti liquid alloys were found to be lower than its ideal value showing the compound forming tendency of these alloys (Akinlade & Boyo, 2022). Furthermore, activity of components in Fe–Ti binary liquid alloys were found to be less than their ideal values and G_M^{xs} was found to be negative at all compositions showing the ordering nature of this binary alloy (Mehta, Koirala, et al., 2020). Hence, all the binary subsystems of Fe–Si–Ti ternary alloys are of ordering nature.

The values of $S_{cc}(0)$ of binary subsystems Al–Sn (Prasad & Mikula, 2006b; Odusote et al., 2016), Sn–Zn and Zn–Al (Prasad & Mikula, 2006b) of Al–Sn–Zn ternary system show positive deviation from the ideal values. The G_M^{xs} of all the binary subsystems of Al–Sn–Zn ternary liquid alloys were found to be positive in liquid phase at all the compositions (Prasad & Mikula, 2006b). These studies show that the binary subsystems of Al–Sn–Zn ternary liquid alloys are of segregating nature. In case of Al–Cu–Fe ternary system, $S_{cc}(0)$ of Al–Cu (Trybula et al., 2018) and Fe–Al (Yadav et al., 2018) show negative deviation from their respective ideal values. These binary subsystems are characterised by negative values of G_M^{xs} and negative deviation of activity of components from their ideal values in liquid state. These properties show that Al–Fe and Al–Cu binary systems are of ordering nature (Mehta, Yadav, Koirala, & Adhikari, 2020). Cu–Fe system is characterised by positive deviation of activity from Raoult's law and have positive value of G_M^{xs} at all compositions in liquid state which explain the segregating nature of this alloy.

In these selected ternary liquid alloys, the effect of a broad spectrum of interactions between the components were imposed to study the surface properties of the alloys.

1.3 Geometrical models

Based on the features of its binary constituents, a number of methods can be employed to study the thermo-physical properties of a ternary solution phase. Fundamentally, there are two different ways to assess the mixing behaviour of liquid alloys called theoretical approaches and empirical solution models. A theoretical approach is a basic analysis of current conceptions that serves as a foundation for reasoning. Although theoretical models give clear physical meaning, they are fruitful only in certain constrained conditions (Chou & Chang, 1989). An empirical model is a useful and more flexible technique to describe thermodynamic behaviour to study and explain the properties of ternary alloys, even though it may not give a clear physical picture. As a result, this kind of paradigm

has been used to address a wide range of practical problems. Geometrical models used to study the properties of alloys in this work belongs to the empirical methods.

Geometrical models are frequently used for studying the thermodynamic properties of ternary alloys in terms of energetic interactions between their binary subsystems. Hillert (1980) classified the geometrical models into two classes called symmetrical and asym-

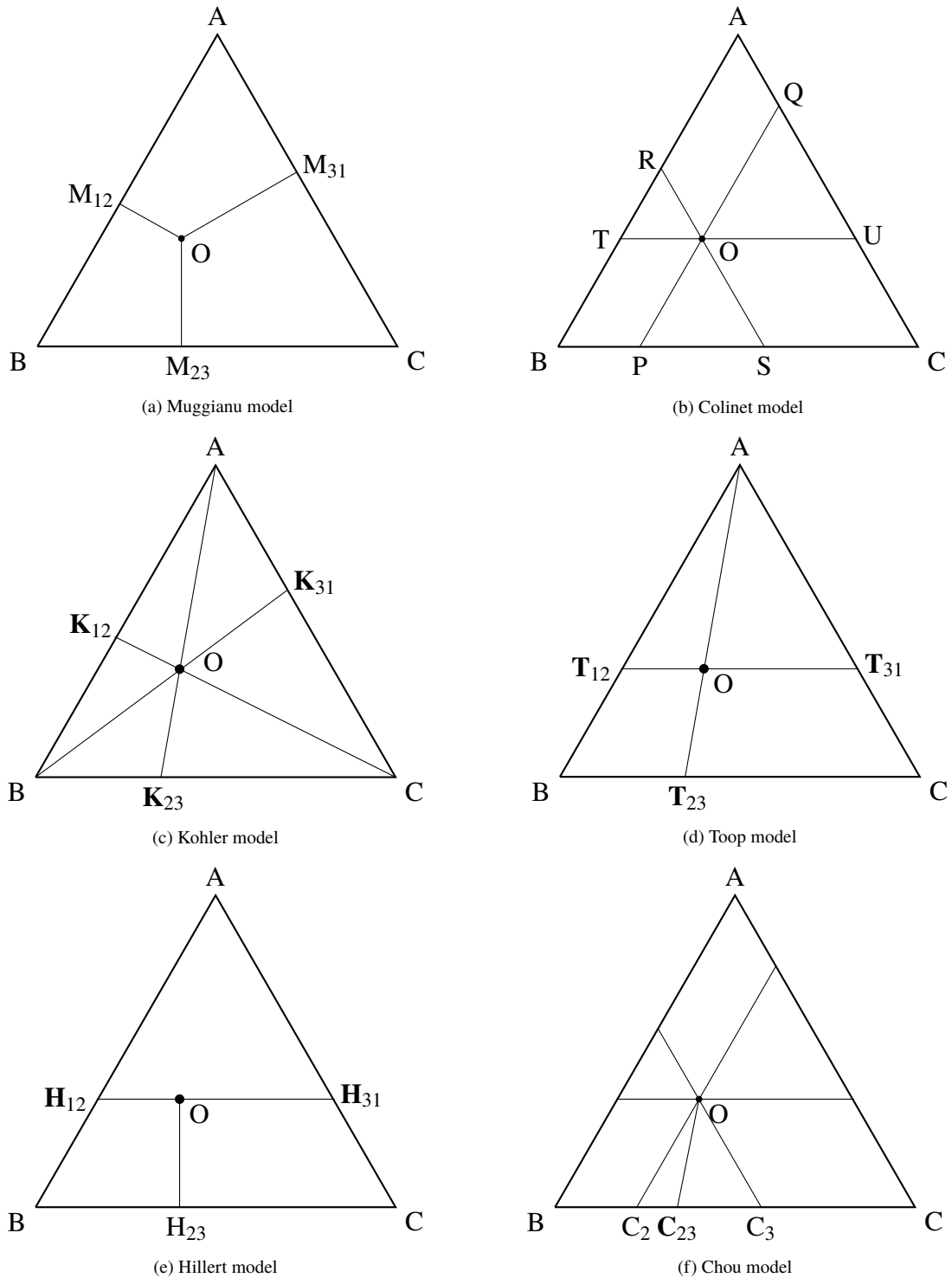


Figure 1: Selections of binary concentration points using ternary plots in different geometrical models.

metrical. A model is recognised as symmetrical if the expression of the corresponding geometrical model preserves its own form on interchanging the concentrations of constituent components x_1 , x_2 and x_3 in the cyclic order. The Muggianu, Colinet, and Kohler models are the symmetrical models. In asymmetrical models, the interchange of concentrations x_1 , x_2 and x_3 in cyclic order does not preserve the identity of the equation obtained for the given model. The Toop and Hillert models are grouped as asymmetric models. The basic difference between these geometrical models is the way of defining the three sub-binary concentrations corresponding to a given ternary concentration. The specified points on the sides of triangle ABC represent the binary concentrations for the respective model as shown in Figure 1 (a-e). Among the three components, if two are substituted the same, these geometrical models are not reducible to corresponding binary subsystems and hence these models are assumed to be inadequate. Additionally, in the case of asymmetrical models, it necessitates human intervention in order to find the symmetrical element and rearrange three components to the three apexes of a triangle for their applicability.

Chou & Chang (1989) summarised the five different geometrical models used for the evaluation of G_M^{xs} of ternary liquid alloys. To overcome the constraints related to the symmetric and asymmetric model, Chou & Chang (1989); Chou (1995); Chou et al. (1996) proposed another model, the general solution model (GSM) also called the Chou model. In this model, any of the three components can be placed at any apex of the triangle. Furthermore, the binary concentrations corresponding to a ternary

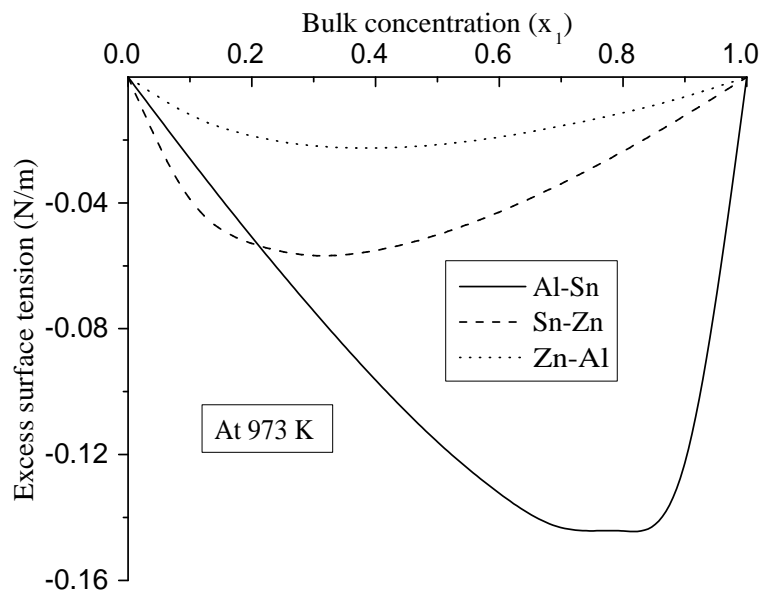


Figure 2: Variation of excess surface tensions of binary subsystems of Al–Sn–Zn ternary liquid alloys with bulk concentration.

concentration depend on interaction among the binary pairs. In the case of the above mentioned geometrical models, whatever the strength of interaction between the binary pairs, the ternary concentration is fixed to a single point (K_{23} or T_{23} or H_{23} , Figure 1(c-e)). But in the case of GSM, for a given ternary concentration, the binary concentrations C_{23} may vary in between points C_2 to C_3 depending on strength of interactions between A–B and A–C binary systems (Figure 1(f)).

To apply asymmetric geometrical models, a symmetrical element has to be chosen among the three components of the ternary alloys. The variation of excess surface tensions of Sn–Zn and Zn–Al binary subsystems are found to be similar to each other, whereas that of Al–Sn is found to be different, as shown in Figure 2. As Zn is the common element in Sn–Zn and Zn–Al binary alloys, it is considered as symmetrical element in Al–Sn–Zn ternary alloys to apply the Toop model for study of thermodynamic and surface properties of ternary alloys.

1.4 Problem statement

The knowledge of the mixing behaviours of initial melts is necessary for the characterization, fabrication, and design of new materials with improved properties. There is a great deal of interest in creating new alloys due to their desirable properties like light weight, high strength, corrosion and oxidation resistance, less toxic, high conductivity or resistivity and so on. Alloying as a processing route has evolved as an important machinery act to obtain desired materials with anticipated properties. These data cannot be obtained completely from the experimental measurements because they are difficult to handle at high temperatures and are also tedious, time-consuming, and costly. Furthermore, statistical approaches are used to obtain preliminary knowledge about the parameters governing the micro-structures of materials in order to perform and design new experimental procedures. These demonstrate the importance of developing theoretical modeling for assessing the alloying behaviours of binary and multi-component systems.

Therefore, we have employed different theoretical models to study and predict the surface properties of a few ternary liquid alloys at different temperatures in this work. The thermodynamic database of sub-binary pairs has been used for the purpose.

1.5 Objectives of the Work

General Objective

To assess the surface properties of ternary Fe–Si–Ti, Al–Sn–Zn and Al–Cu–Fe liquid alloys using the Butler equation and different geometrical models.

Specific Objectives

- i. To optimise the interaction energy parameters for excess free energy of mixing of binary liquid alloys using the data of excess free energy of mixing, Enthalpy of mixing and excess entropy of mixing.
- ii. To use the optimised parameters to study surface tension and surface concentration of Al–Cu–Fe, Al–Sn–Zn and Fe–Si–Ti liquid ternary alloys using the Butler equation and to compare the computed surface tension of aforementioned alloys with the values computed by using the Chou, Kohler and Toop models.

1.6 Organization of the work

The current work is divided into the following chapters:

CHAPTER 2: This chapter contains a brief explanation of the literature reviewed in order to undertake this research work on the thermodynamic and surface properties of various binary, ternary and multi-component alloys.

CHAPTER 3: This chapter includes the formulations of different geometrical models like Mugginau, Kohler, Toop, and General solution model (chou model) associated with thermodynamic functions like G_M^{xs} , H_M , and S_M^{xs} , and surface properties like surface tension and surface concentrations of the ternary liquid alloys. Furthermore, it includes the Bulter equation for calculation of the surface properties of liquid mixtures.

CHAPTER 4: This chapter includes the results and discussion associated with the thermodynamic and surface properties of the constituent binary subsystems and Fe–si–Ti, Al–Sn–Zn and Al–Cu–Fe ternary liquid alloys. The variations of surface concentrations of components with concentration and temperature are also briefly explained and discussed in the same chapter.

CHAPTER 5: This chapter includes the conclusions seeked from this work and recommendations for the relevant work.

CHAPTER 6: The brief summary of this work is presented in this chapter.

CHAPTER 2

2. LITERATURE REVIEW

2.1 General background

Alloying phenomena are commonly used to develop new materials with desired properties. The physical and chemical properties of alloys are entirely different from those of individual components. Pure elements, which make up the alloy, are typically very soft and have lower tensile strength than the alloys. The chemical reactivity of atoms in alloys has been found to be much less than their reactivity in pure states. Thus, the atoms during the alloying processes acquire a more stable state and have high oxidation and corrosion resistance. Moreover, the alloying process improves the casting properties of the metals; for example, soft gold can be converted into hard gold by alloying with copper. The breaking stress of iron can be improved from 300 MPa upto 2000 MPa by on alloying it to make steel (H. D. Young et al., 2013). The melting temperature of an alloy can be less than that of its individual components when mixed in a certain proportion. The melting temperature of lead is 327 °C and that of tin is 232 °C. However, melting temperature of Pb–Sn alloys were found to be 183 °C when blended uniformly at composition of 63 wt% of Sn and 37 wt% of Pb and is thus used for the soldering purpose in electronic devices. Due to the advancement in thermo-physical properties, both theoreticians and experimentalists have been working in this field for decades to assess the mixing properties of binary and multi-component systems.

The following subsections provide a brief overview of the literature on the thermodynamic and surface characteristics of binary and ternary alloy systems.

2.2 A brief review of thermodynamic properties of liquid alloys

Since decades, different kinds of theoretical models were developed in order to assess the mixing behaviours of binary liquid mixtures (Guggenheim, 1945; Prigogine & Defay, 1954; A. S. Jordan, 1970; Bhatia & Hargrove, 1974; Lele & Ramachandrarao, 1981; Srikanth & Jacob, 1988; W. H. Young, 1992; R. N. Singh & Sommer, 1997; Srikanth et al., 1999; Adhikari, Singh, & Jha, 2010; Jha et al., 2012; I. Koirala et al., 2013; R. P. Koirala et al., 2013; Yadav et al., 2015). Likewise, several attempts were made by researchers working in the field of material science to study and explain the mixing behaviours of ternary liquid alloys using different experimental techniques (Nogi et al.,

1991; Knott & Mikula, 2002; Egry et al., 2005; Knott et al., 2005; L. Wang et al., 2007; Chen et al., 2009; Moser et al., 2009; Plevachuk et al., 2011; J. Wang et al., 2011; Zhou et al., 2011; Fima, 2012; Sklyarchuk et al., 2012; Pstrus, 2013; Dreval et al., 2018). The Butler model was most preferentially used as theoretical modeling equation linking the thermodynamic properties with the surface phenomenon for comparative study in due course. Later, the theoreticians of this field attempted to explain the thermodynamic and surface properties of ternary liquid alloys by developing different geometrical models.

In due course, a number of geometrical models have been proposed by different theoreticians (Kohler, 1960; Toop, 1965; Colinet, 1967; Muggianu et al., 1975; Hillert, 1980, 1983; Chou, 1987; Chou & Wei, 1997) to evaluate G_M^{xs} of ternary liquid alloys in terms of the interaction energy parameters of its binary subsystems. Kohler (1960) proposed a geometrical model to express the G_M^{xs} of ternary liquid alloys in terms of the interaction energy parameters of the binary subsystems. Similarly, Toop (1965) and Muggianu et al. (1975) proposed two more geometrical models to explain the G_M^{xs} of ternary liquid alloys in terms of mole fraction concentration of components of the alloy and interaction energy parameters of binary subsystems. Hillert (1980) summarised the geometrical models and classified them as symmetric and asymmetric models. The Kohler, Colinet and Muggianu models were termed as symmetrical models because interchange of mole fraction concentration of components in cyclic order preserve the form of the equation for G_M^{xs} of the ternary alloys. Similarly, Toop model and Hillert model (Hillert, 1980, 1983) were termed as asymmetrical because changing the positions of mole fraction concentration of components in cyclic order does not preserve the form of the expression of G_M^{xs} .

Later, Chou (1987) summarised the above mentioned geometrical models and showed that the Muggianu and Colinet models do not contain the ternary interaction term in their expression for G_M^{xs} of ternary liquid alloys. The ternary interaction terms were not taken into account in the Hillert model and Toop model. Though, these terms were considered in the Kohler model but their contributions were negligible. Therefore, Chou (Chou, 1987; Chou & Chang, 1989) proposed a new model to study the thermodynamic properties of ternary liquid alloys. This model is more applicable for the ternary alloy systems as the ternary interaction terms appreciably contribute to the thermodynamic properties. This model is also called general solution model (GSM) and the details regarding the consideration of number of interaction terms is described in the works of Chou & Chang (1989), Chou (1995) and Chou et al. (1996).

The basic difference between these geometrical models is the way of selection of sub-binary concentrations for a given bulk concentration of ternary alloys. The sub-binary concentration depends on the interaction energy parameters of the binary subsystems in case of GSM. But this dependency does not prevail in other geometrical models. The

details of these geometrical models have been described in the Section (3.1).

Several researchers (Manasijević et al., 2003; Arroyave et al., 2003; Turchanin et al., 2008; Chen et al., 2009; Egry, Holland-Moritz, et al., 2010; Dogan & Arslan, 2018) have used the above mentioned geometrical models to estimate the thermodynamic properties of the ternary liquid alloys. Manasijević et al. (2003) carried out a comparative study of H_M and G_M^{xs} of Ga–Sb–Pb liquid alloys at 973 K and 1073 K using the GSM, Kohler and Toop modeling equations. The computed results were in good agreement with each other. However, computed results were not compared with any experimental data in order to prove the superiority among the different models.

Prasad & Mikula (2006b) studied G_M^{xs} of Al–Sn–Zn liquid alloys at 973 K using Chou and Kohler model from Al corner at cross-section $x_{Sn} : x_{Zn} = 2 : 1$ and compared the computed values with the experimental data (Knott & Mikula, 2002). It had been found that the computed results using the modeling equations were in good agreement with each other but had slightly positive deviation from the experimental data in the range $0.2 < x_{Al} < 0.8$.

Knott et al. (2005) measured H_M of Al–Sn–Zn and Ag–Sn–Zn ternary liquid alloys at 973 K using the calorimetric method and compared the obtained experimental data with the computed values using the Mugginau, Kohler and Toop models. The values of H_M for Al–Sn–Zn ternary alloy system were found to be positive when computed from Al corner at three different cross-sections $x_{Sn} : x_{Zn} = 2 : 1, 1 : 1$ and $1 : 2$. Similarly, H_M for Ag–Sn–Zn liquid alloys were computed from Zn corner at cross-sections $x_{Sn} : x_{Zn} = 3 : 1, 1 : 1$ and $1 : 3$. These were found to be negative at cross-section $x_{Ag} : x_{Sn} = 3 : 1$ and positive at cross-section $x_{Ag} : x_{Sn} = 1 : 3$.

Kostov et al. (2008) studied the activity, integral Gibbs free energy of mixing and G_M^{xs} of sub-binary and ternary alloy system of Ti–Al–Fe alloys at 1873, 2000 and 2073 K using the software FactSage. It was observed that there was negative deviation of activity of components from the Raoult's law and negative values of integral Gibbs free energy of mixing and G_M^{xs} at all concentrations of the sub-binary and ternary alloy systems.

Živković et al. (2014) studied the variation of activity of Cu with its bulk concentrations in Cu–Al–Ag and Cu–Al–Au alloys at 1100 K from three cross-sections using the GSM and found that there was negative deviation of activity from the Raoult's law. They also computed the G_M^{xs} the ternary alloys from Cu corner at the three cross-sections and found negative values of G_M^{xs} at the compositions. The G_M^{xs} of Cu–Al–Ag ternary alloy system were compared with the experimental data and found good agreement between them. The phase equilibria of the Al–Fe–Me were studied by Balanetsky et al. (2015) in its Al rich region and phase relationship were studied by Zheng et al. (2018) in the Al rich region as well as in Fe–Mn rich region using CALPHAD over wide composition

range from room temperature to well above the melting point of the alloys to establish the phase transformation for Al-based alloys as well as for steel.

Costa et al. (2014) studied the thermodynamic and surface properties of sub-binaries and Co–Cr–Ni liquid ternary alloys at different concentrations at 1873 K. They used quasi-chemical approximation to evaluate G_M^{xs} and activity of components in the binary subsystems. The activity of components in Cr–Co and Cr–Ni were slightly less than the values given by Raoult’s law (ideal value). These data show that the alloys have compound forming tendency and is weakly interacting in nature. The activities of the components in the Co–Ni liquid alloys were extremely close to the ideal value, with slightly positive deviation, indicating a weakly segregating tendency. The thermodynamic properties of these binary subsystems were used to study the thermodynamic properties of this ternary alloys in the frame of GSM and surface properties using the Butler equation. They found that the surface tension of the ternary alloys increased with the increase in bulk concentration of Co at a fixed bulk concentration of Cr. Similarly, at constant bulk concentration of Cr, the surface tension of the alloys seems to be increased with the increase in bulk concentration of Ni.

Dreval et al. (2018) measured the H_M of Co–Cu–Ti liquid alloys at 1873 K using isoperibolic calorimeter. The measured values of H_M changes from lower positive value at very low bulk concentration of Ti to higher negative value at very low bulk concentration of Cu near equiatomic bulk concentration of Co and Ti in this alloy.

Mehta et al. (2021) studied the thermodynamic and surface properties of Ti–Al–Fe liquid alloys using the interaction energy parameters for G_M^{xs} from COST 507 (Ansara et al., 1998) by applying Kohler, Toop and Chou model at different temperatures. The computed values of G_M^{xs} and activity of components (a_i) of the ternary alloy system were found to be in excellent agreement with the available literature data (Kostov et al., 2008) obtained using the software FactSage. Thermodynamic properties of Ti–Si–Fe liquid alloys have been studied by Mehta, Koirala, et al. (2020) at different temperatures and concentration using Kohler, Toop and Chou models from Fe corner at five different cross-sections ($x_{Si} : x_{Ti} = 9 : 1, 7 : 3, 5 : 5, 3 : 7$ and $1 : 9$). The computed values of G_M^{xs} and surface tension (σ_{123}) of the ternary alloy system were found to decrease with the increase in temperatures.

Yadav et al. (2021) studied the thermodynamic and surface properties of Ti–Al–Si liquid alloys at different temperatures using Kohler, Toop and Chou models from Ti corners at five different cross-sections $x_{Al} : x_{Si} = 9 : 1, 7 : 3, 5 : 5, 3 : 7$ and $1 : 9$. The variation of G_M^{xs} of this ternary alloy system was symmetrical about $x_{Ti} = 0.5$ at all the above mentioned cross-sections. The negative value of G_M^{xs} of this ternary alloy system was found to increase with the increase in bulk concentration of Si and decrease with

the increase in bulk concentration of Al.

2.3 Surface properties

Surface tension is a property of a liquid surface and defined as the variation of surface energy of liquid due to change in the surface area of the liquid solution. It arises due to interaction between atoms or molecules at the surface phase and the interaction of atoms or molecules of surface phase with the bulk phase. Like thermodynamic properties, several researches have been working since decades to assess the surface properties of liquid alloys. The experimental techniques, such as levitating droplet oscillating method (Nogi et al., 1991; Egry et al., 2005; H. P. Wang et al., 2008; Zhou et al., 2011), sessile drop method (Fima, 2012; Sklyarchuk et al., 2012), large drop method (Plevachuk et al., 2011) and maximum bubble pressure method (Moser et al., 2009; Pstrus, 2013) were used to measure the surface tension of liquid alloys.

The first and foremost concept of surface tension of liquid had been described by Gibbs (1879) as the variation of Gibbs free energy of the liquid with its surface area at constant pressure, absolute temperature, and amount of matter. The Gibbs free energy of liquid may change with the variation of pressure, temperature and the amount of matter. When these factors are kept constant and variation of Gibbs free energy is observed with the variation in the surface area of the components of liquid.

Butler (1932) used the concept of monolayer surface area of liquid as a separate phase being in thermodynamic equilibrium with another separate bulk phase of the liquid. Under this assumption, he derived the relation for surface tension of multi-component liquid alloys as

$$\sigma = \sigma_i^0 + \frac{RT}{A_i} \ln \left(\frac{x_i^s \gamma_i^s}{a_i} \right) \quad (i = 1, 2, 3..) \quad (2.1)$$

where σ_i is the surface tension of i^{th} component in the pure state, A_i is the surface area of one mole of the component, x_i^s is surface concentration of the component in the liquid mixture, γ_i^s is the activity coefficient of i^{th} component in the surface phase of the solution and a_i is the activity of the respective component in the bulk phase.

Skapski (1948), for the first time expressed the monolayer surface area of an individual component of a liquid mixture as

$$A_i = f N_A^{1/3} V_i^{2/3} = f N_A^{1/3} \left(\frac{M_i}{\rho_i} \right)^{2/3} \quad (2.2)$$

where, M_i is the mass of one mole of the pure element, ρ_i is the density of the element

in the liquid state at the concerned temperature and V_i is the volume of one mole of the pure component in the liquid state. The term f is the geometrical structure factor and its value depends on the packing fraction. The value of f was estimated to be 1.09 for hexagonal close-packed structure, 1.12 for the body-centered cubic structure, and 1.04 for liquid mercury.

Guggenheim (1952) proposed a statistical approach based on the assumption of the existence of double layers of atoms on the surface phase of a binary solution, similar to a particular plane of a crystal lattice such that the composition of only the outer layer differs from that of the bulk. He designated the surface coordination numbers as p and q for the respective layers and assumed similar arrangements of atoms on the surface as well as in the bulk. He also assigned the interchange energy $w = z(2\varepsilon_{AB} - \varepsilon_{AA} - \varepsilon_{BB})$, where ε_{AB} , ε_{AA} , and ε_{BB} are the bond energies of binary alloy systems A–B, A–A, and B–B respectively, and z is the coordination number. He derived the expression for the surface tension in terms of w and surface composition x_i^s by constructing grand partition function in the quasi-crystalline model as (Guggenheim, 1952)

$$\begin{aligned}\sigma &= \sigma_1 + \frac{k_B T}{A} \ln \left(\frac{x_1^s}{\gamma_1 x_1} \right) + [p(x_2^s)^2 + q(x_2)^2] \frac{w}{A} \\ &= \sigma_2 + \frac{k_B T}{A} \ln \left(\frac{x_2^s}{\gamma_2 x_2} \right) + [p(x_1^s)^2 + q(x_1)^2] \frac{w}{A}\end{aligned}\quad (2.3)$$

where γ_i ($i = 1, 2$) are the activity coefficients of the monomers and $A = x_1 A_1 + x_2 A_2$ is the weighted mean atomic surface area of the components in the alloys. The values of p and q are chosen depending upon the types of crystal structures of the components of the alloy such that $p + 2q = 1$. Additionally, for close-packed crystal structures, such as fcc and hcp lattices $z = 12$, $p = 0.5$, and $q = 0.25$ whereas for simple cubic lattice $z = 6$, $p = 2/3$ and $q = 1/6$ and for bcc lattice $z = 8$, $p = 3/5$, and $q = 1/5$. On the basis of this model, researchers (Novakovic, 2010; R. P. Koirala et al., 2014; Yadav, 2018) have explained the surface properties of different binary liquid alloys. Nogi et al. (1991) measured the surface tension of the Cu-Ni binary liquid alloys using the levitated droplet method and the sessile drop method at 1773 K at different compositions. The surface tension of the alloys were found to be greater when measured using the levitated droplet method than that of the sessile drop method at all the compositions of the alloys for which the experiment was carried out. The surface tension of the pure Cu and Ni liquid elements measured using the sessile drop method were in agreement with the data available in Gale & Totemeier (2004). The G_i^{xs} in the surface and the bulk phases depends on the coordination number of the atoms in the respective phases. The atoms in the surface phase have a reduced coordination number with respect to that of the bulk, and the partial excess free energy of the surface phase is found to be less than that of the

bulk phase and proportional to the coordination numbers.

A term β is defined as the ratio of coordination number of atoms in the surface (Z_s) to that in the bulk (Z_b) relation $\beta = Z_s/Z_b = G_{i,s}^{xs}/G_{i,b}^{xs}$. Tanaka & Iida (1994) studied the surface tension of some binary alloys using the Bulter equation for $\beta = 1/2, 2/3, 3/4$ and 1 and compared the results with each other as well as with the experimental data. The deviation between the computed results of the surface tension of segregating binary alloys Cu–Fe and Cu–Pb for $\beta = 0.5$ and $\beta = 1$ lies within 30 mN m^{-1} . The maximum deviation of surface tension of these alloys for this range of β with experimental results was found to be 40 mN m^{-1} . But the results were found to differ for Al–Cu and Ni–Si ordering alloys in which there was significant deviation between the computed values using this range of β . The experimental data were found to be scattered around the curves of surface tension verses concentration computed using β equal to $2/3$ and $3/4$. Therefore, it was difficult to select the appropriate values of β for the further calculations. From these results, it was concluded that the G_M^{xs} of the ordering alloys were affected due to the interaction of atoms with the first as well as second nearest neighbouring atoms.

Tanaka et al. (1996) estimated the value of β equal to 0.83 for the mixing of liquid metals and 0.94 for the mixing of ionic compounds in a liquid state. Later, Novakovic et al. (2006) computed the surface properties of Cu–Sn, Cu–Ti, and Sn–Ti binary liquid alloys using a quasi-chemical approximation of those of Cu–Sn and Cu–Ti liquid alloys on the basis of a compound formation model.

Kaptay (2005b) established the equation for the geometrical structure factor (f) in terms of surface packing fraction (f_s) and volume packing fraction (f_b) given as

$$f = \left(\frac{3f_b}{4} \right)^{2/3} \frac{\pi^{1/3}}{f_s} \quad (2.4)$$

For simple liquid metal, the average value of f_b has been estimated to be 0.65 ± 0.02 and that of f_s has been estimated to be 0.906 ± 0.02 . Using these data, the value of f is estimated to be 1.00 ± 0.02 (Mekler & Kaptay, 2008).

Egry et al. (2005) measured the density and surface tension of the Cu–Fe–Ni ternary liquid alloys over a wide temperature range using the electromagnetic levitation method. It was found that the concentration dependence of the surface tension of the ternary liquid alloys was highly non-linear and could be predicted precisely using the Bulter Equation. Brillo et al. (2006) measured the surface tension of the Ni–Cu–Fe liquid alloys at 1800 K using a non-contact technique and found that the computed values of the surface tension of this ternary alloys using the Butler equation were in good agreement with the experimental result. They used the value of β equal to 0.75 and f equal to 1.091.

Yan et al. (2007) studied the surface tension of Sn–Ga–In ternary liquid alloys at 773 K using Kohler, Toop, GSM, and the Butler models in regular solution approximation and compared the result with the experimental data. The deviation between the computed and observed values was the least for the Toop model. However, the results computed using the Chou and the Butler models were also in good agreement with the experiment results. But the values obtained using the Kohler model showed a relatively large deviation from experimental values. The superiority of the general solution model over other models is that it is free from the concept of symmetric or asymmetric distribution of the components in the ternary alloys and the concentration of binary subsystems for a particular ternary composition depends on the interaction energy between the binary pairs. In contrast, the symmetric element has to be chosen by comparing the plots of excess surface tensions of sub-binary pairs in order to the Toop model.

The surface tension and density of Fe–Cu–Mo liquid ternary alloys were measured by H. P. Wang et al. (2008) using a levitating droplet oscillating method from undercooled to superheated liquid stages at three different compositions in the absence of oxygen gas. The surface tension of a liquid drop of mass m was calculated from the measurement of surface oscillation frequencies (ω_R) using the Rayleigh equation of the form

$$\sigma = \frac{3}{8}\pi m\omega_R^2 \quad (2.5)$$

The surface tension was observed to vary linearly with the temperature at all the three compositions with negative temperature coefficient. Egry et al. (2008) assessed the surface tension of Fe–Al and Fe–Ni liquid alloys across a large concentration and temperature range using the oscillating drop method in electromagnetic levitating state of the sample. Furthermore, they studied the surface tension of these alloys using theoretical approach like extended form of ideal solution model and the Butler equation. They noticed that surface tension varied linearly with temperature.

The density and surface tension of the Ag–Bi–Sn alloy were measured experimentally using the sessile drop method at different temperatures and concentrations by Fima & Kucharski (2008). It was found that the density of these alloys decrease linearly with the increase in temperature at all concentrations, while the surface tension of the alloys decrease non-linearly with the increase in temperature except at very low bulk concentrations of Ag. However, the surface tension was found to decrease linearly with the increase in temperature at a higher bulk concentration of Ag. These measured values of surface tension were found to be in good agreement with the values obtained using the Butler model.

Plevachuk et al. (2011) measured the surface tension of the Bi–Pb–Sn ternary liquid alloys over the temperature ranging from 380 K to 750 K at a concentration $\text{Bi}_{46}\text{Pb}_{29}\text{Sn}_{25}$

using the large drop method. The surface tension of this alloy was found to be 403.5 mN m^{-1} at 550 K. They computed the surface tension of the system at this temperature using the Butler equation and geometrical models (Kohler, Toop, Chou). The experimental result was found to be in good agreement with the value (413.8 mN m^{-1}) computed using the Butler equation. Among the geometrical models, the Chou model was found to be more appropriate with respect to other models.

Sklyarchuk et al. (2012) used the sessile drop method to measure the surface tension of Ag–Sb–Sn liquid ternary alloys at four different concentrations over a wide temperature range, from melting temperature to 1100 K. They found that the surface tension of the liquid alloys decrease linearly with the increase in temperature at all concentrations. They computed the surface tension of this ternary alloy system using the Butler model. The computed values of the surface tension of the alloys were found in good agreement with the experimental results.

The surface tension of In–Sn–Zn ternary liquid was measured by Pstrus (2013) using the maximum gas bubble pressure at different concentrations in the temperature range of 550 to 1150 K. Furthermore, he computed the surface tension of the liquid alloys using the Butler equation at 673 K and 1073 K and compared the result with the experimental data. He found that the surface tension of the liquid alloys change linearly with temperature and observed the negative value of temperature coefficient of surface tension. There was good agreement between the computed values with the experimental data at higher temperature and lower contents of zinc (upto 35 at.%). He also concluded that the surface concentrations of the components were largely deviated from the bulk composition.

Novakovic et al. (2014) studied the surface tension and surface segregation of Cr–Nb–Re ternary liquid alloys using the thermodynamic database of the binary subsystems in conjunction with the Butler equation at 2473 K. They used $\beta = 0.75$ and $f = 1.091$. The surface tension of these alloys were found to increase with the increase in bulk concentration of Nb at a fixed bulk concentration of Re. At constant bulk concentration of Nb, the surface tension was found to increase gradually with the increase of bulk concentration of Re.

The surface tension of the Ti–Al liquid alloys was studied by Xuyang et al. (2017) experimentally by the sessile drop method and compared with the values computed using Butler equation and seven other modified ideal solution models at 1758 K. Their research revealed that the experimental results agreed well with the values calculated using the Butler equation.

Due to the availability of the experimental results for the majority of ternary liquid alloys, several researchers have used various geometrical models (GSM, Toop, Kohler, Mugginau, Hillert, etc.) in conjunction with the Butler model to compare the surface

properties of ternary and multi-component liquid alloys. Though these geometrical models were originally developed to explore thermodynamic properties, they were later applied to the research of surface and transport properties of ternary and multi-component liquid alloys.

Fima & Novakovic (2018) studied the surface tension of the Cd–Sn–Zn ternary liquid alloys at 773 K at different concentrations using the Butler model and three geometrical model (GSM, Toop, Kohler). They used $\beta = 0.83$ and $f = 1.091$ in the Butler Equation and compared the results with the available experimental data. It was found that the experimental data agreed well with the values obtained using the Butler equation and then followed by the Chou model. The deviations were relatively greater for the values computed using the Kohler and Toop models.

Arslan & Dogan (2019a) studied the surface tension and surface concentrations of Ni–Cu–Fe liquid alloys at 1800 K using GSM, Mugginau, Kohler, Toop, Hillert, Guggenheim, Butler, Egry, and ideal solution models and compared the results with the experimental data. The mean square deviation of the computed values was the least for the values obtained using the Butler model. The surface tension of Ag–Au–Cu liquid alloys were measured by Arslan & Dogan (2019b) using the sessile drop method, and they also theoretically computed the values using the Butler model and some geometrical models at 1381 K. The values computed using the Toop model were found to be in good agreement with the experimental data. In this ternary alloy system, the excess surface tension of the sub-binary Au–Cu system was found to be positive while that of the Ag–Au and Ag–Cu systems was found to be negative. This shows that the Ag element should be selected as an asymmetrical element for the calculation of surface tension using an asymmetric (Toop) model. The theoretical values obtained using this model were found to be closer to the experimental data at some cross-sections. Meanwhile, at some cross-sections, the results predicted by the Butler equation was found to be closer to the experimental data than those from the Toop model.

The thermodynamic and surface properties of sub-binaries and Al–Cu–Fe ternary alloy system in the liquid state at different temperatures have been studied by Mehta, Yadav, Koirala, & Adhikari (2020) using the Butler Equation in the regular solution approximation. These values were also calculated using the Kohler, Toop, and Chou models. The G_M^{xs} for Al–Cu and Al–Fe systems was found to be negative and that of the Cu–Fe liquid alloys were found to be positive. Therefore, Al was selected as an asymmetrical element in the calculations of the G_M^{xs} and surface tension of a ternary alloy system using the Toop model. They found that the Al atoms segregated onto the surface phase while Fe and Cu remained in the bulk phase of the ternary solution at 1773 K. Likewise, the thermodynamic and surface properties of Cu–Fe–Si, Ti–Al–Fe and Ti–Si–Fe ternary liquid alloys were studied at different temperatures using the abovementioned theoretical

models by Mehta et al. (2021); Mehta, Koirala, et al. (2020). Later, Yadav et al. (2021) studied the thermodynamic properties of Ti–Al–Si liquid ternary alloys using Kohler, Toop, and Chou models using the thermodynamic data of the binary subsystems. The surface properties of this ternary alloy system at different temperatures were studied using the Butler equation along with the above mentioned geometrical models. All the sub-binary pairs of the ternary alloy system were found to be ordering in nature. Among them, Al–Si binary alloys were found to be very weakly interacting, Al–Ti were found to be moderately interacting and Si–Ti were found to be strongly interacting. In general, the activity of a component increases with the increase of its bulk concentration and vice versa. But some peculiar effects were depicted in the activity of ternary alloy system when computed from the Ti corner at lower bulk concentrations of Al. In this range of concentration, the activity of Al was found to increase in the beginning, although the bulk concentration of Al was lowered gradually in that range.

Recently, Gohivar et al. (2021) studied the thermodynamic and surface properties of Al–Sn–Zn ternary liquid alloys using different theoretical models. The surface tension was computed using the Butler equation, Chou, Toop, and Kohler models at different temperatures. For this purpose, they optimised the exponential-temperature dependent interaction energy parameters for G_M^{xs} of the binary subsystems using the experimental data of H_M and S_M^{xs} . These parameters were then used to compute the G_i^{xs} of individual components of the system. The surface concentrations of the components of alloys were calculated with the help of which the surface properties of the ternary alloy system were computed at different temperatures using the Butler equation in regular solution approximation. The surface concentration of Al was found to be increasing and that of Sn was found to be decreasing with the increase in temperature. Further, they found that the surface concentration of Zn did not change significantly with an increase in temperature. The surface tension of the system was found to decrease with increase in temperature as expected.

From the literature survey, it can be stated that the study of surface tension of binary and multi-component liquid alloys is very important to understand their physical properties. Further, there are very limited available experimental as well as literature databases for surface properties of ternary liquid alloys to date. Therefore, several researchers working in this field are putting their optimal efforts into devising new and effective experimental techniques or in developing new or renovated modeling equations to assess the surface properties of ternary liquid alloys at different temperatures.

With this regard, an effort has been made in this work to assess the surface properties of Fe–Si–Ti, Al–Sn–Zn, and Al–Cu–Fe liquid ternary alloys at different temperatures. We used the Butler equations to study the surface concentration of components and surface tension of the liquid alloys at different compositions. Furthermore, Kohler,

Toop and Chou geometrical models were employed to compute the surface tension of these ternary alloy systems on the basis of the thermodynamic data of the constituent binary subsystems. For this purpose, the linear temperature-dependent (T-dependent) interaction energy parameters for G_M^{xs} for the binary subsystems have been optimised in the framework of Redlich-Kister polynomials. The least square fitting method has been employed for the optimisation process using available experimental or literature data on H_M and S_M^{xs} of the respective binary subsystems. The validity of the optimised parameters can also be obtained by comparing the theoretical results with the reference base data. Then, afterward, they have been used to compute the G_i^{xs} and finally the excess surface tension of ternary alloy systems.

CHAPTER 3

3. MATERIALS AND METHODS

The surface properties (surface tension and surface concentration) of the ternary liquid alloys have been studied in this work. These properties have been computed using the thermodynamic database of the constituent binary subsystems of the ternary liquid alloys. The Butler equation along with different geometrical models have been used as modeling equations for this purpose.

The expressions related to the different models considered in the work are presented in the following sections of this chapter.

3.1 Thermodynamic properties

The surface properties of alloys are correlated with G_M^{xs} of these alloys through the partial excess free energy of each component of the system. The concept of Gibbs free energy of mixing of a thermodynamic system have been introduced in terms of a state function, which provides the information about the spontaneity of physical or chemical changes of the system. For spontaneous physical or chemical change, the entropy of the universe should always increase i.e.

$$\Delta S_{\text{universe}} = \Delta S_{\text{system}} + \Delta S_{\text{surrounding}} \geq 0 \quad (3.1)$$

$$\Delta S_{\text{surrounding}} = \frac{Q_{\text{surrounding}}}{T} \quad (3.2)$$

and

$$Q_{\text{surrounding}} = -Q_{\text{system}} \quad (3.3)$$

Using Equations (3.2) & (3.3) in Equation (3.1), we obtain

$$\Delta S_{\text{system}} - \frac{Q_{\text{system}}}{T} \geq 0 \quad (3.4)$$

The enthalpy of a system is defined as the heat transformed to the system at constant pressure.

$$\Delta H_{\text{system}} = Q_{P, \text{system}} \quad (3.5)$$

The Equation (3.4) takes the form for spontaneous change of state of a system and can be arranged in the form

$$\Delta H_{\text{system}} - T\Delta S_{\text{system}} \leq 0 \quad (3.6)$$

The term on left hand side of the equation is a state function called change in Gibbs free energy (ΔG) of the system. Thus, for a spontaneous reaction, we must have

$$\Delta G = \Delta H_{\text{system}} - T\Delta S_{\text{system}} \leq 0 \quad (3.7)$$

The absolute Gibbs free energy (G) is defined using the relation

$$G = H - TS \quad (3.8)$$

3.1.1 Gibbs free energy of mixing

Let us suppose one mole of a liquid mixture consists of X_A and X_B mole fraction of components A and B respectively. If G_A and G_B are the molar Gibbs free energy of the respective components, then the total Gibbs free energy of the system before mixing is given by

$$G_{\text{initial}} = G_A X_A + G_B X_B \quad (3.9)$$

When the components are mixed, the final Gibbs free energy of the system (G_{final}) can be given as

$$G_{\text{final}} = G_{\text{initial}} + \Delta G_M \quad (3.10)$$

where ΔG_M is called the Gibbs free energy of mixing of the solution. Using the relations $G_{\text{initial}} = H_{\text{initial}} - TS_{\text{initial}}$ and $G_{\text{final}} = H_{\text{final}} - TS_{\text{final}}$ and putting $\Delta H_M = H_{\text{final}} - H_{\text{initial}}$ and $\Delta S_M = S_{\text{final}} - S_{\text{initial}}$, we obtain

$$\Delta G_M = G_{\text{final}} - G_{\text{initial}} = \Delta H_M - T\Delta S_M \quad (3.11)$$

where ΔH_M is the enthalpy of mixing.

3.1.2 Gibbs free energy of mixing for ideal solution

A solution is said to be ideal if there is no interaction between its constituent molecules. For such solution, $\Delta H_M = 0$ and Gibbs free energy of mixing is due to the entropy of

mixing of the solution. i.e.

$$\Delta G_M = -T\Delta S_M \quad (3.12)$$

Statistically, entropy is the measurement of randomness of a system and it is described quantitatively by the Boltzmann Equation

$$S = k_B \ln \Omega \quad (3.13)$$

where k_B is the Boltzmann constant. The entropy of a system may be due to the distinguished number of vibrations of atoms or molecules that set up in a solid solution, which is known as thermal contribution to entropy. When entropy changes due to the distinguished ways of arrangements of atoms or molecules in a solution, then it is called a configurational contribution to entropy. In the case of an ideal solution, the change in volume of the system or heat change during mixing is zero. In this case, the change in entropy is only due to the configurational contribution. The configurational entropy of the system is zero before mixing because there is only one kind of atom in the lattice and hence only one distinguished arrangement of atoms is possible and hence $S_1 = k_B \ln 1 = 0$. The change in entropy of mixing then becomes

$$\Delta S_M^{\text{id}} = S_2 = k_B \ln \Omega \quad (3.14)$$

Let, N_1 and N_2 are the number of molecules of the components A and B respectively in one mole solutions. Then, the number of distinguished ways of arrangements of the molecules in the solution is given by

$$\Omega = \frac{(N_1 + N_2)!}{N_1!N_2!} \quad (3.15)$$

When Equation (3.15) is used in the Equation (3.14), we get

$$\Delta S_M^{\text{id}} = k_B [\ln(N_1 + N_2)! - \ln N_1! - \ln N_2!] \quad (3.16)$$

Using the Stirling approximation, $\ln N! = N \ln N - N$, for large value of N in the above relation, one can obtain

$$\Delta S_M^{\text{id}} = k_B [\ln(N_1 + N_2)! - N_1 \ln N_1 + N_1 - N_2 \ln N_2 + N_2] \quad (3.17)$$

Since, the prepared solution is one mole, the total number of atoms must be equal to the Avogadro's number (N_A). Therefore, $N_1 = X_A N_A$ and $N_2 = X_B N_A$. Putting these values

in Equation (3.17) and applying the condition $X_A + X_B = 1$, we obtain

$$\begin{aligned}\Delta S_M^{\text{id}} &= k_B[N_A \ln N_A - N_A - X_A N_A \ln(X_A N_A) + X_A N_A - X_B N_A \ln(X_B N_A) + X_B N_A \\ &= -R(X_A \ln X_A + X_B \ln X_B)\end{aligned}\quad (3.18)$$

where $R (= k_B N_A)$ is the universal gas constant. The Gibbs free energy of mixing of the ideal solution is given by the relation,

$$\Delta G_M^{\text{id}} = RT(X_A \ln X_A + X_B \ln X_B) \quad (3.19)$$

This equation shows that G_M^{xs} of an ideal solution does not depend on the interaction energy between the molecules of the components of the solution and depends solely on the mole fraction of the components in the solution. Furthermore, when the temperature of the system increases, so does its entropy, whereas the Gibbs free energy of mixing of the ideal solution decreases.

3.1.3 Excess Gibbs free energy of mixing of alloys

The self-consistent thermodynamic database for binary and multi-component liquid alloys is generated by taking references to excess Gibbs free energy of mixing (ΔG_M^{xs}). The G_M^{xs} is the deviation of ΔG_M^{id} from the integral Gibbs free energy of mixing (ΔG_M) and can be expressed as

$$G_M^{\text{xs}} = \Delta G_M - \Delta G_M^{\text{id}} \quad (3.20)$$

3.2 General discription of different ternary models

Hillert (1980) and Chou & Chang (1989) summarised the ternary models for the study of thermodynamic properties of liquid ternary alloys in terms of interaction energy parameters of sub-binary pairs. On the basis of geometrical models, the general expression for the G_M^{xs} for ternary alloys can be expressed as

$$G_M^{\text{xs}} = \sum_{ij} W_{ij} G_{ij}^{\text{xs}} \quad (ij = 12, 23, 31) \quad (3.21)$$

where G_{ij}^{xs} is the excess free energy of mixing for the binary subsystems of the ternary alloys. Redlich & Kister (1948) expressed the G_M^{xs} of binary alloys using a polynomial

equation of order n in terms of concentration of components as

$$G_{ij}^{xs} = x_i x_j \sum_{k=0}^n A_{ij}^k (x_i - x_j)^k \quad (3.22)$$

where A_{ij}^k are termed as the coefficients of R-K polynomial for G_{ij}^{xs} . These coefficients are concentration independent and temperature-dependent parameters. Equation (3.22) has been used by many researchers (Manasijević et al., 2003; Egry, Holland-Moritz, et al., 2010; Fima, 2012; Fima & Novakovic, 2018) to compute other thermo-physical quantities such as enthalpy, excess surface tension, excess viscosity of the binary liquid alloys.

The probability weighted factor (W_{ij}) can be expressed as (Chou et al., 1996)

$$W_{ij} = \frac{x_i x_j}{X_i X_j} \quad (3.23)$$

In this equation, x_i and x_j are mole fractions of components in a ternary alloys and X_i and X_j are the mole fractions of the binary pairs present in the ternary alloys. The fundamental difference between the geometrical models is how the binary concentration coordinates (X_i, X_j) corresponding to the ternary compositions are chosen.

The points A, B and C at the vertices of the ternary diagram in Figure 3 represent pure components, i.e. ($x_1 = 1, x_2 = 0, x_3 = 0$) at point A, ($x_1 = 0, x_2 = 1, x_3 = 0$) at point B and ($x_1 = 0, x_2 = 0, x_3 = 1$) at point C. The points on the sides AB, BC and CA represent the binary compositions of sub-binary pairs A–B, B–C and C–A respectively. Each point inside the region bounded by three sides of the ternary diagram represents a unique ternary concentration.

Let, O is an arbitrary point representing the mole fraction concentration (x_1, x_2, x_3) of components A, B and C respectively, inside the ternary diagram ABC which satisfy the condition

$$x_1 + x_2 + x_3 = 1 \quad (3.24)$$

The lines PQ, TU and RS are drawn parallel to the sides AB, BC and CA respectively so that the concentrations of components A, B, and C on the lines TU, RS and PQ are x_1, x_2 and x_3 respectively. The lengths BT (=OP=OS=CU) is equal to x_1 , CS (=OU=OQ=AR) is equal to x_2 and AQ (=OR=OT=BP) is equal to x_3 .

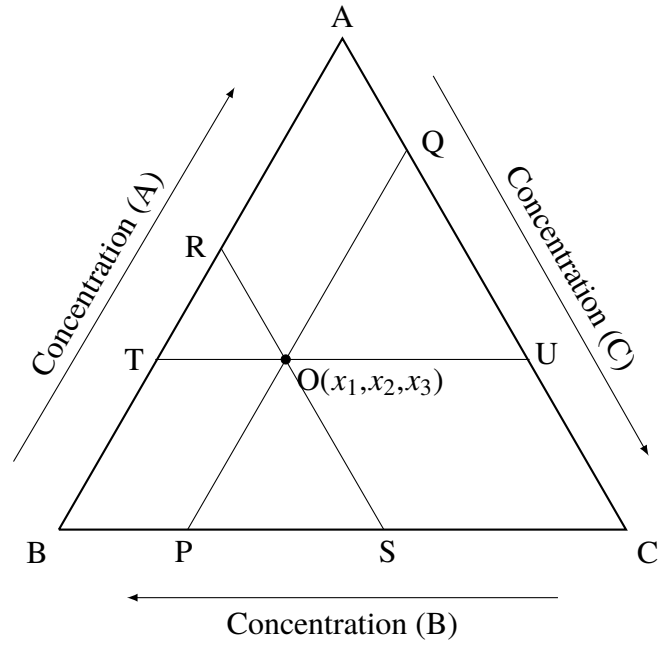


Figure 3: Representation of concentrations of binary subsystems in liquid ternary alloys.

3.3 Mugginau Model

Let, OM_{12} , OM_{23} and OM_{31} are the perpendiculars drawn from the point O on the sides AB , BC and CA respectively (Figure 4). Then, coordinates of the points M_{12} , M_{23} and M_{31} in the ternary diagram represents the sub-binary concentrations in the Mugginau model. If (X_2, X_3) be the binary concentration of the components B and C corresponds

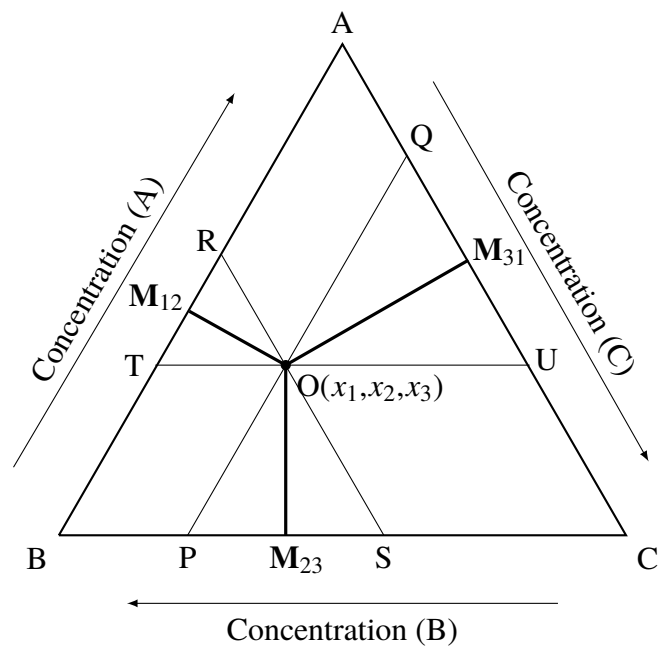


Figure 4: Representation of binary concentrations corresponds to a ternary point in Mugginau model.

to the point M_{23} so that $CM_{23}=X_2$ and $BM_{23}=X_3$ which are related by the equation

$$X_2 + X_3 = 1 \quad (3.25)$$

The total length of any one side of the triangle in ternary diagram is unity or 100%. Therefore, we can write

$$\begin{aligned} BP + PS + SC &= 1 \\ \text{OR, } x_3 + PS + x_2 &= 1 \end{aligned} \quad (3.26)$$

From Equations (3.24) and (3.26), one can obtain $PS = x_1$. Since the triangle OPS is equilateral, $M_{23}S=PS/2=x_1/2$. Hence,

$$X_2 = CM_{23} = M_{23}S + CS = \frac{x_1}{2} + x_2 = \frac{1 - x_2 - x_3}{2} + x_2 = \frac{1 + x_2 - x_3}{2} \quad (3.27)$$

Similarly, one can obtain

$$X_3 = BM_{23} = 1 - CM_{23} = \frac{1 - x_2 + x_3}{2} \quad (3.28)$$

In the same way, the binary concentrations at the points M_{12} and M_{31} can be expressed as

$$\begin{aligned} (X_1, X_2) &= \left(\frac{1 + x_1 - x_2}{2}, \frac{1 - x_1 + x_2}{2} \right) \quad \text{and} \\ (X_3, X_1) &= \left(\frac{1 + x_3 - x_1}{2}, \frac{1 - x_3 + x_1}{2} \right) \end{aligned}$$

In general, the binary concentration (X_i, X_j) of binary subsystems "ij" corresponds to the ternary concentration point (x_1, x_2, x_3) in the Muggianu model is $((1 + x_i - x_j)/2, (1 - x_i + x_j)/2)$, where 'ij' = (12, 23, 31). Now, using Equation(3.23) into Equation (3.21) and putting the values of sub-binary concentrations, we obtain the expression for excess free energy of mixing of ternary alloys for Muggianu model as (Muggianu et al., 1975)

$$\begin{aligned} G_M^{xs} &= \frac{4x_1x_2}{(1 + x_1 - x_2)(1 - x_1 + x_2)} G_{12}^{xs}(1 + x_1 - x_2, 1 - x_1 + x_2) \\ &+ \frac{4x_2x_3}{(1 + x_2 - x_3)(1 - x_2 + x_3)} G_{23}^{xs}(1 + x_2 - x_3, 1 - x_2 + x_3) \\ &+ \frac{4x_3x_1}{(1 + x_3 - x_1)(1 - x_3 + x_1)} G_{31}^{xs}(1 + x_3 - x_1, 1 - x_3 + x_1) \end{aligned} \quad (3.29)$$

3.4 Kohler Model

The lines drawn from the vertices A, B, and C through the point $O(x_1, x_2, x_3)$ intersect the opposite sides at points K_{23} , K_{31} and K_{12} shown in Figure 5. The coordinates of the points K_{23} , K_{31} and K_{12} represents the binary concentrations in Kohler model.

Let, (X_2, X_3) be the coordinates of the point K_{23} so that the length BK_{23} becomes equal to X_3 and the length CK_{23} becomes equal to X_2 satisfying the Equation 3.25. Since the line TU is parallel to the side BC. Using geometry, it can be written as

$$\frac{OT}{OU} = \frac{BK_{23}}{CK_{23}}$$

or, $\frac{x_3}{x_2} = \frac{X_3}{X_2}$ (3.30)

Now, putting $X_3 = 1 - X_2$ in Equation (3.30) and solving for X_2 , we obtain

$$X_2 = \frac{x_2}{x_2 + x_3}$$
 (3.31)

Similarly, solving for X_3 , we get

$$X_3 = \frac{x_3}{x_2 + x_3}$$
 (3.32)

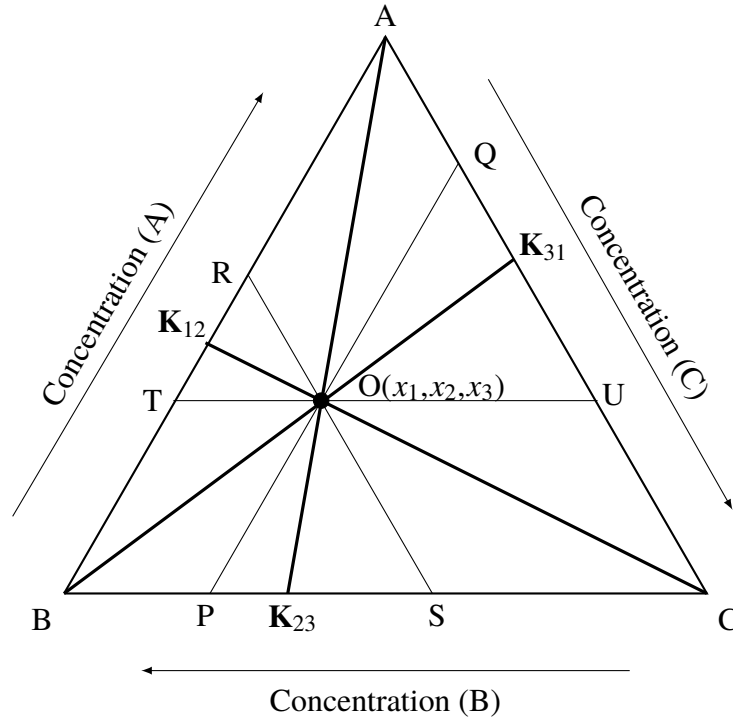


Figure 5: Representation of binary concentrations corresponds to a ternary point in Kohler model.

In the same manner, binary concentrations corresponds to the points K_{12} and K_{31} are

$$(X_1, X_2) = \left(\frac{x_1}{x_1 + x_2}, \frac{x_2}{x_1 + x_2} \right) \quad \text{and} \quad (X_3, X_1) = \left(\frac{x_3}{x_3 + x_1}, \frac{x_1}{x_3 + x_1} \right)$$

In general, the binary concentrations (X_i, X_j) of the binary subsystems 'ij' corresponding to a ternary concentration point (x_1, x_2, x_3) in Kohler model can be expressed as

$$(X_i, X_j) = \left(\frac{x_i}{x_i + x_j}, \frac{x_j}{x_i + x_j} \right)$$

where 'ij' = (12, 23, 31). Now, using Equation(3.23) into Equation (3.21) and putting the values of sub-binary concentrations, we obtain the expression for excess free energy of mixing for ternary alloys in Kohler model (Kohler, 1960; Manasijević et al., 2003; Yan et al., 2007; Egry, Holland-Moritz, et al., 2010)

$$\begin{aligned} G_M^{xs} = & (x_1 + x_2)^2 G_{12}^{xs} \left(\frac{x_1}{x_1 + x_2}, \frac{x_2}{x_1 + x_2} \right) + (x_2 + x_3)^2 G_{23}^{xs} \left(\frac{x_2}{x_2 + x_3}, \frac{x_3}{x_2 + x_3} \right) \\ & + (x_3 + x_1)^2 G_{31}^{xs} \left(\frac{x_3}{x_3 + x_1}, \frac{x_1}{x_3 + x_1} \right) \end{aligned} \quad (3.33)$$

3.5 Toop model

A line is drawn from the vertex A through the point O which intersect the side BC at point T_{23} shown in Figure 6. The line parallel to the side BC, passing through the point O, intersects the side AB and AC at points T_{12} and T_{31} . The coordinates of the points T_{12} , T_{23} and T_{31} are binary concentrations for binary subsystems A–B, B–C and C–A respectively. The point T_{23} in the Toop model is at identical position to that of K_{23} in the Kohler model and have the same concentration for B–C binary subsystem. The value of ternary concentration is x_1 at every point on the line joining the points T_{12} and T_{31} . Hence, binary concentration of the binary subsystem A–B becomes $(x_1, 1 - x_1)$ and that for the binary subsystem C–A becomes $(1 - x_1, x_1)$ in the Toop model. Now, using Equation(3.23) into Equation (3.21) and putting the values of sub-binary concentrations, we obtain the expression for excess free energy of mixing of ternary alloys for the Toop model as

$$\begin{aligned} G_M^{xs} = & \left(\frac{x_2}{x_2 + x_3} \right) G_{12}^{xs}(x_1, 1 - x_1) + (x_2 + x_3)^2 G_{23}^{xs} \left(\frac{x_2}{x_2 + x_3}, \frac{x_3}{x_2 + x_3} \right) \\ & + \left(\frac{x_3}{x_2 + x_3} \right) G_{13}^{xs}(x_1, 1 - x_1) \end{aligned} \quad (3.34)$$

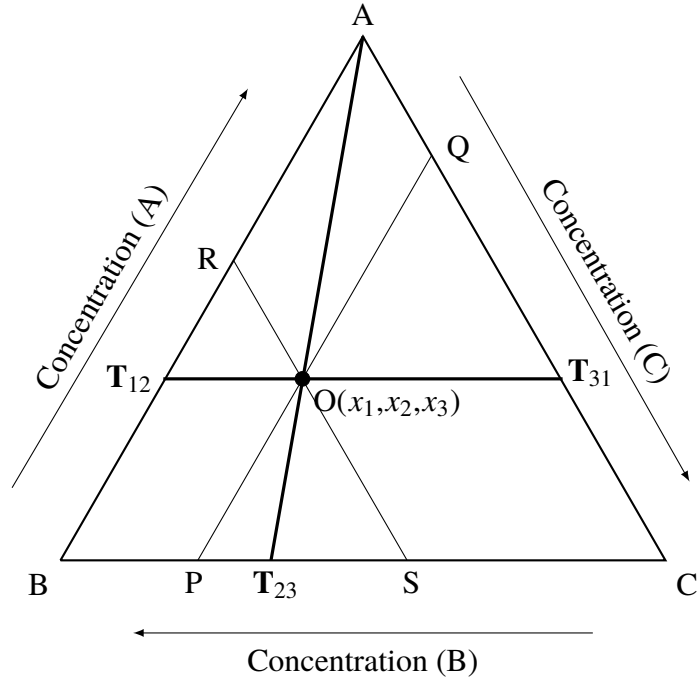


Figure 6: Representation of binary concentrations corresponds to a ternary point in Toop model.

3.6 Chou or General Solution Model (GSM)

Hillert (1980) classified geometrical models into the symmetric and asymmetric groups. A model is called symmetric if the thermo-physical properties of the ternary alloys do not change when any element is substituted for x_1 or x_2 or x_3 . The Mugginau model and the Kohler model are symmetric models. The Toop model is an asymmetrical model in which all the elements cannot be placed on an equal footing unlike symmetrical model. Therefore, symmetric element has to be chosen to apply this model.

There are some inherent problems with the symmetric and asymmetric models. The symmetrical models for the computation of the properties of ternary alloys do not reduce to binary when any two components are made identical. The problem with the asymmetric model is how to distribute the three components at the three vertices of the triangle. To get rid of these problems, Chou & Chang (1989) proposed a new model for the prediction of the mixing properties of ternary alloys called the General Solution Model (GSM).

Consider an arbitrary point C_{23} having the binary concentrations $(X_{2(23)}, X_{3(23)})$ in the Chou model (Figure 7) for the binary system B–C with the help of a parameter ξ_{23} ($0 < \xi_{23} < 1$) using the relations $X_{2(23)} = x_2 + \xi_{23}x_1$ and $X_{3(23)} = 1 - X_{2(23)}$. When ξ_{23} approaches zero then $(X_{2(23)}, X_{3(23)})$ approaches $(x_2, x_1 + x_3)$ which is the binary concentration corresponding to the point S in Figure 7. Similarly, when ξ_{23} approaches 1 then $(X_{2(23)}, X_{3(23)})$ approaches $(x_2 + x_1, x_3)$ which is the binary concentration corresponding

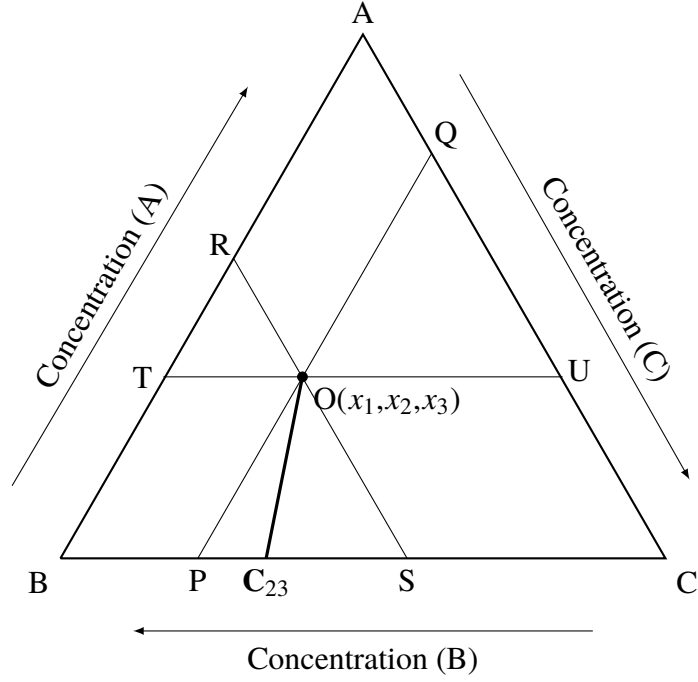


Figure 7: Representation of binary concentrations corresponds to a ternary point in Chou model.

to the point P in Figure 7. As the value of ξ_{23} changes from 0 to 1, then the point C_{23} moves from the point S to P. This term ξ_{23} is called similarity coefficients and is related with G_M^{xs} of the binary subsystems of the ternary alloys. The choice of the sub-binary concentrations in the ternary alloys depends on the relative magnitude of G_M^{xs} of the binary subsystems related through the terms ξ and expressed as

$$(X_1, X_2) = (X_{1(12)}, X_{2(12)}) = (x_1 + \xi_{12}x_3, 1 - X_{1(12)}) \quad (3.35a)$$

$$(X_2, X_3) = (X_{2(23)}, X_{3(23)}) = (x_2 + \xi_{23}x_1, 1 - X_{2(23)}) \quad (3.35b)$$

$$(X_3, X_1) = (X_{3(31)}, X_{1(31)}) = (x_3 + \xi_{31}x_2, 1 - X_{3(31)}) \quad (3.35c)$$

The similarity coefficients ξ_{12} , ξ_{23} and ξ_{31} for the sub-binaries A–B, B–C and C–A respectively are defined in terms of deviation sum of squares (η) by the relations,

$$\xi_{12} = \frac{\eta_{1(23)}}{\eta_{1(23)} + \eta_{2(13)}}, \quad \xi_{23} = \frac{\eta_{2(13)}}{\eta_{2(13)} + \eta_{3(12)}}, \quad \xi_{31} = \frac{\eta_{3(12)}}{\eta_{3(12)} + \eta_{1(23)}} \quad (3.36)$$

The deviation sum of squares (η) are defined in terms of G_M^{xs} of the binary subsystems

using the relations

$$\begin{aligned} \eta_{1(23)} &= \int_0^1 (G_{12}^{xs} - G_{13}^{xs})^2 dx_1, & \eta_{2(13)} &= \int_0^1 (G_{21}^{xs} - G_{23}^{xs})^2 dx_2, \\ \eta_{3(12)} &= \int_0^1 (G_{31}^{xs} - G_{32}^{xs})^2 dx_3 \end{aligned} \quad (3.37)$$

Now, expanding Equation (3.22) for G_{12}^{xs} , G_{23}^{xs} and G_{31}^{xs} of the respective binary systems A–B, B–C and C–A and terminating the terms after $n=3$, we obtain

$$G_{12}^{xs} = X_1 X_2 [A_{12}^0 + A_{12}^1 (X_1 - X_2) + A_{12}^2 (X_1 - X_2)^2 + A_{12}^3 (X_1 - X_2)^3] \quad (3.38a)$$

$$G_{23}^{xs} = X_2 X_3 [A_{23}^0 + A_{23}^1 (X_2 - X_3) + A_{23}^2 (X_2 - X_3)^2 + A_{23}^3 (X_2 - X_3)^3] \quad (3.38b)$$

$$G_{31}^{xs} = X_3 X_1 [A_{31}^0 + A_{31}^1 (X_3 - X_1) + A_{31}^2 (X_3 - X_1)^2 + A_{31}^3 (X_3 - X_1)^3] \quad (3.38c)$$

Now, using Equations (3.38a) and (3.38c) into Equation (3.37) to evaluate the value of $\eta_{1(23)}$ under the condition $A_{ij}^k = (-1)^k A_{ji}^k$ and eliminating X_2 and X_3 with the help of relations $X_1 + X_2 = 1$ and $X_1 + X_3 = 1$, we get

$$\begin{aligned} \eta_{1(23)} &= \int_0^1 X_1^2 (1 - X_1)^2 [(A_{12}^0 - A_{13}^0) + (A_{12}^1 - A_{13}^1)(2X_1 - 1) \\ &\quad + (A_{12}^2 - A_{13}^2)(2X_1 - 1)^2 + (A_{12}^3 - A_{13}^3)(2X_1 - 1)^3]^2 dX_1 \end{aligned} \quad (3.39)$$

Expanding and integrating this equation, one can obtain

$$\begin{aligned} \eta_{1(23)} &= \frac{1}{30}(A_{12}^0 - A_{13}^0)^2 + \frac{1}{210}(A_{12}^1 - A_{13}^1)^2 + \frac{1}{630}(A_{12}^2 - A_{13}^2)^2 \\ &\quad + \frac{1}{1386}(A_{12}^3 - A_{13}^3)^2 + \frac{1}{105}(A_{12}^0 - A_{13}^0)(A_{12}^2 - A_{13}^2) \\ &\quad + \frac{1}{315}(A_{12}^1 - A_{13}^1)(A_{12}^3 - A_{13}^3) \end{aligned} \quad (3.40)$$

Similarly, we can obtain the relations,

$$\begin{aligned} \eta_{2(13)} &= \frac{1}{30}(A_{23}^0 - A_{21}^0)^2 + \frac{1}{210}(A_{23}^1 - A_{21}^1)^2 + \frac{1}{630}(A_{23}^2 - A_{21}^2)^2 \\ &\quad + \frac{1}{1386}(A_{23}^3 - A_{21}^3)^2 + \frac{1}{105}(A_{23}^0 - A_{21}^0)(A_{23}^2 - A_{21}^2) \\ &\quad + \frac{1}{315}(A_{23}^1 - A_{21}^1)(A_{23}^3 - A_{21}^3) \end{aligned} \quad (3.41)$$

$$\begin{aligned}
\eta_{3(12)} = & \frac{1}{30}(A_{31}^0 - A_{32}^0)^2 + \frac{1}{210}(A_{31}^1 - A_{32}^1)^2 + \frac{1}{630}(A_{31}^2 - A_{32}^2)^2 \\
& + \frac{1}{1386}(A_{31}^3 - A_{32}^3)^2 + \frac{1}{105}(A_{31}^0 - A_{32}^0)(A_{31}^2 - A_{32}^2) \\
& + \frac{1}{315}(A_{31}^1 - A_{32}^1)(A_{31}^3 - A_{32}^3)
\end{aligned} \tag{3.42}$$

The weight probability of the three binary subsystems can be expressed as

$$W_{12} = \frac{x_1 x_2}{X_{1(12)} X_{2(12)}}, \quad W_{23} = \frac{x_2 x_3}{X_{2(23)} X_{3(23)}}, \quad W_{31} = \frac{x_3 x_1}{X_{3(31)} X_{1(31)}} \tag{3.43}$$

Using Equations (3.35), (3.38) and (3.43) into Equation (3.21) for G_M^{xs} of the ternary alloys for the GSM can be expressed as

$$\begin{aligned}
G_M^{xs} = & x_1 x_2 [A_{12}^0 + A_{12}^1(x_1 - x_2) + A_{12}^2(x_1 - x_2)^2 + A_{12}^3(x_1 - x_2)^3] \\
& + x_2 x_3 [A_{23}^0 + A_{23}^1(x_2 - x_3) + A_{23}^2(x_2 - x_3)^2 + A_{23}^3(x_2 - x_3)^3] \\
& + x_3 x_1 [A_{31}^0 + A_{31}^1(x_3 - x_1) + A_{31}^2(x_3 - x_1)^2 + A_{31}^3(x_3 - x_1)^3] \\
& + F x_1 x_2 x_3
\end{aligned} \tag{3.44}$$

where F is the ternary interaction term and is expressed as (Chou et al., 1996)

$$\begin{aligned}
F = & (2\xi_{12} - 1)[A_{12}^3(3(x_1 - x_2)^2 x_3 + 3(x_1 - x_2)x_3^2(2\xi_{12} - 1) + x_3^3(2\xi_{12} - 1)^2) \\
& + A_{12}^2((2\xi_{12} - 1)x_3 + 2(x_1 - x_2)) + A_{12}^1] \\
& + (2\xi_{23} - 1)[A_{23}^3(3(x_2 - x_3)^2 x_1 + 3(x_2 - x_3)x_1^2(2\xi_{23} - 1) + x_1^3(2\xi_{23} - 1)^2) \\
& + A_{23}^2((2\xi_{23} - 1)x_1 + 2(x_2 - x_3)) + A_{23}^1] \\
& + (2\xi_{31} - 1)[A_{31}^3(3(x_3 - x_1)^2 x_2 + 3(x_3 - x_1)x_2^2(2\xi_{31} - 1) + x_2^3(2\xi_{31} - 1)^2) \\
& + A_{31}^2((2\xi_{31} - 1)x_2 + 2(x_3 - x_1)) + A_{31}^1]
\end{aligned} \tag{3.45}$$

The partial excess free energy of mixing of the components (G_i^{xs}) in the binary and ternary liquid alloys are frequently expressed using the relation (Yan et al., 2007; Egry, Holland-Moritz, et al., 2010)

$$G_i^{xs} = G_M^{xs} + \sum_{j=1}^m (\delta_{ij} - x_j) \frac{\partial G_M^{xs}}{\partial x_j} \tag{3.46}$$

The summation is taken upto $m = 2$ for binary alloys and $m = 3$ for ternary alloys.

Equation (3.46) can be expanded to obtain G_i^{xs} in the ternary alloys as

$$G_1^{xs} = G_M^{xs} + \frac{\partial G_M^{xs}}{\partial x_1} - \left(x_1 \frac{\partial G^{xs}}{\partial x_1} + x_2 \frac{\partial G_M^{xs}}{\partial x_2} + x_3 \frac{\partial G_M^{xs}}{\partial x_3} \right) \quad (3.47a)$$

$$G_2^{xs} = G_M^{xs} + \frac{\partial G_M^{xs}}{\partial x_2} - \left(x_1 \frac{\partial G^{xs}}{\partial x_1} + x_2 \frac{\partial G_M^{xs}}{\partial x_2} + x_3 \frac{\partial G_M^{xs}}{\partial x_3} \right) \quad (3.47b)$$

$$G_3^{xs} = G_M^{xs} + \frac{\partial G_M^{xs}}{\partial x_3} - \left(x_1 \frac{\partial G^{xs}}{\partial x_1} + x_2 \frac{\partial G_M^{xs}}{\partial x_2} + x_3 \frac{\partial G_M^{xs}}{\partial x_3} \right) \quad (3.47c)$$

These values of G_i^{xs} of the components are used to calculate the surface tensions and surface concentrations of the components of the ternary alloys using the Butler equation.

3.7 Surface properties

Gibbs (1879) expressed the surface tension of a liquid mixture in terms of variation of absolute Gibbs free energy of mixing due to change in surface area of the liquid at constant pressure, temperature and number of moles of the components in the liquid solution and given by the relation

$$\sigma = \left(\frac{dG}{dA} \right)_{P,T,n} \quad (3.48)$$

The total Gibbs free energy of the solution is considered as the sum of Gibbs free energy of the bulk phase (G_b) and that of the surface phase (G_s). When the surface area of the liquid tends to zero, the total Gibbs free energy of the solution becomes G_b . Therefore, integrating Equation (3.48) under the boundary conditions $G = G_b$ when $A = 0$ and $G = G$ when $A = A$ gives the relation

$$G = G_b + \sigma A \quad (3.49)$$

Similarly, the surface tension (σ_i^0) of the pure component i can be expressed in terms of absolute Gibbs free energy (G_i^0) of that component in pure state as

$$\sigma_i^0 = \left(\frac{dG_i^0}{dA_i^0} \right)_{P,T,n_i} \quad (3.50)$$

where A_i^0 are the surface area of the pure component. The integration of Equation (3.50) under the identical boundary condition used for the liquid mixture yields

$$G_i^0 = G_{b,i}^0 + \sigma_i^0 A_i^0 \quad (3.51)$$

The absolute partial Gibbs free energy of mixing of a component in a solution can be expressed as

$$G_i = G_i^0 + \Delta G_i \quad (3.52)$$

where ΔG_i is the change in Gibbs free energy on transforming n_i mole of pure liquid into the solution phase. The absolute Gibbs free energy of mixing of the solution is equal to the sum of absolute partial Gibbs free energy of the components in the solution i.e.

$$G = \sum_i G_i \quad (3.53)$$

The similar equation is there for the Gibbs free energy of mixing of the components in the solution and expressed as

$$\Delta G = \sum_i \Delta G_i \quad (3.54)$$

where ΔG is the absolute Gibbs free energy of mixing defined using the relation

$$G = G^0 + \Delta G \quad (3.55)$$

The partial surface area occupied by the atoms or molecules of the components along the surface is related with the total surface area by the equation

$$A = \sum_i A_i \quad (3.56)$$

The equation for the partial surface tension of the components in the solution, identical to Equation (3.48) can be expressed as

$$\sigma_i = \left(\frac{dG_i}{dA_i} \right)_{P,T,n_i} \quad (3.57)$$

Integration of Equation (3.57) under the boundary condition $G_i = G_{b,i}$ when $A_i = 0$ and $G_i = G_i$ when $A_i = A_i$ yields

$$G_i = G_{b,i} + \sigma_i A_i \quad (3.58)$$

Now, using Equation (3.58) into Equation (3.53), we obtain

$$G = \sum_i G_i = \sum_i G_{b,i} + \sum_i \sigma_i A_i = G_b + \sum_i \sigma_i A_i \quad (3.59)$$

On comparing Equations (3.49) and (3.59), one can obtain

$$\sigma A = \sum_i \sigma_i A_i \quad (3.60)$$

Now, combining Equations (3.60) and (3.56), we obtain

$$\sum_i A_i (\sigma - \sigma_i) = 0 \quad (3.61)$$

This equation has infinite number of solutions and the simplest one is

$$\sigma = \sigma_i \quad (i = 1, 2, 3 \dots) \quad (3.62)$$

When two or more pure liquids are mixed to make a solution, the components spread on the surface of the solution such that the partial surface tension of each component becomes equal. The components have unequal partial surface tension in the nonequilibrium condition and Marangoni flow occurs in the solution in which the component having lower surface tension flows towards the surface of the solution to replace the component having higher surface tension. Thus, Marangoni flow takes place till the partial surface tension of each of the components becomes equal and the Gibbs free energy of mixing becomes minimal.

Now, using Equation (3.52) into Equation (3.57), we obtain

$$\sigma_i = \left[\frac{d(G_i^0 + \Delta G_i)}{dA_i} \right]_{P,T,n_i} \quad (3.63)$$

The first term on right hand side of Equation (3.63) can expressed as

$$\frac{dG_i^0}{dA_i} = \left[\frac{dG_i^0}{dA_i} \frac{dA_i^0}{dA_i^0} \frac{dn_{s,i}}{dn_{s,i}} \right] = \left[\frac{dG_i^0}{dA_i^0} \frac{dA_i^0}{dn_{s,i}} \frac{dn_{s,i}}{dA_i} \right] = \sigma_i^0 \frac{A_i^0}{A_i} \quad (3.64)$$

where $n_{s,i}$ is the number of moles of component i in the surface, A_i is the partial surface area of one mole of component i in the solution phase and A_i^0 is the surface area of one mole of component i in the pure state. When a solution is prepared by mixing the components in the liquid state, then the system tends to shift from a nonequilibrium condition to an equilibrium condition in which the surface area of a component may increase or decrease due to Marangoni flow, so that the Gibbs free energy of the bulk phase and the liquid phase may change. If the surface area of a component i increases due to the flow of component i from the bulk to the surface, then the second term on the

right hand side of Equation (3.63) can be expressed as

$$\left[\frac{d(\Delta G_i)}{dA_i} \right]_{P,T,n_i} = \frac{\Delta G_{s,i} - \Delta G_{b,i}}{A_i} \quad (3.65)$$

where ΔG_i^s is the partial molar Gibbs free energy of mixing, which corresponds to the transformation of one mole of component i from the surface of the pure state to the solution phase, and ΔG_i^b is the corresponding quantity for the bulk phase. The standard thermodynamic relation for the partial Gibbs free energy of mixing of component i having mole fraction concentration x_i at temperature T is defined by the relation

$$\Delta G_{b,i} = RT \ln x_i + \Delta G_{b,i}^{xs} \quad (3.66)$$

where $\Delta G_{b,i}^{xs}$ is the partial excess molar Gibbs free energy of component i in the solution. There is similar equation for the partial Gibbs free energy of mixing of the surface phase

$$\Delta G_{s,i} = RT \ln x_i^s + \Delta G_{s,i}^{xs} \quad (3.67)$$

Using Equations (3.66) and (3.67) into Equation (3.65), we obtain

$$\left[\frac{d(\Delta G_i)}{dA_i} \right]_{P,T,n_i} = \frac{RT}{A_i} \ln \left(\frac{x_i^s}{x_i} \right) + \frac{\Delta G_{s,i}^{xs} - \Delta G_{b,i}^{xs}}{A_i} \quad (3.68)$$

When Equations (3.64) and (3.68) are used in Equation (3.63), the expression for partial surface tension of the components in the solution takes the form

$$\sigma = \sigma_i^0 \frac{A_i^0}{A_i} + \frac{RT}{A_i} \ln \left(\frac{x_i^s}{x_i} \right) + \frac{\Delta G_{s,i}^{xs} - \Delta G_{b,i}^{xs}}{A_i} \quad (3.69)$$

Assuming that the molar surface area of a component in its pure state is the same as its partial surface area in the solution phase i.e. $A_i = A_i^0$ (Kaptay, 2016), the expression for the surface tension of a ternary liquid solution can be obtained using Equation (3.62) as (Costa et al., 2014; Kaptay, 2015; Fima & Novakovic, 2018; Yadav et al., 2016; Tanaka et al., 1998; Egry, Holland-Moritz, et al., 2010; B. P. Singh et al., 2014; Mekler & Kaptay, 2008)

$$\begin{aligned} \sigma &= \sigma_1^0 + \frac{RT}{A_1} \ln \left(\frac{x_1^s}{x_1} \right) + \frac{G_{s,1}^{xs} - G_{b,1}^{xs}}{A_1} \\ &= \sigma_2^0 + \frac{RT}{A_2} \ln \left(\frac{x_2^s}{x_2} \right) + \frac{G_{s,2}^{xs} - G_{b,2}^{xs}}{A_2} \\ &= \sigma_3^0 + \frac{RT}{A_3} \ln \left(\frac{x_3^s}{x_3} \right) + \frac{G_{s,3}^{xs} - G_{b,3}^{xs}}{A_3} \end{aligned} \quad (3.70)$$

The sum of mole fraction concentration of components in the solution for the surface phase x_i^s and that for the bulk phase x_i must be unity separately i.e. $x_1^s + x_2^s + x_3^s = 1$ and $x_1 + x_2 + x_3 = 1$. The partial molar excess free energy for surface phase and bulk phase of an individual component are proportional to the coordination number of that component in the surface phase (Z^s) and bulk phase (Z^b) of the solution and is related by the equation

$$G_{s,i}^{xs} = \beta G_{b,i}^{xs} \quad (3.71)$$

where $\beta = Z^s/Z^b$ represents the ratio of the coordination number of each atoms in the surface phase to that of the bulk phase. Kaptay (2005a) determined that the acceptable value for the simple liquid element is 0.818. A_i^0 are the monolayer surface area of one mole of pure element i and its value is computed using Equation (2.2).

The surface tension of the liquid ternary alloys have been computed using the Chou, Toop and Kohler model using the optimised parameters for excess surface tension of the binary subsystems. For this purpose, the same sets of equations were used which were employed for calculation of G_M^{xs} . However, parameters A_{ij}^K used for G_M^{xs} were replaced by corresponding coefficients L_{ij}^K for excess surface tension of the alloys. The ideal value of surface tension is the weighted mean of the surface tension of the components involved in the alloys and defined by the equation

$$\sigma^{\text{ideal}} = \sum_i (x_i \sigma_i^0) \quad (3.72)$$

The excess surface tension (σ^{xs}) of the binary and multi-component alloys is defined as the deviation of surface tension of the alloys from its ideal value and expressed as

$$\sigma^{xs} = \sigma - \sigma^{\text{ideal}} = \sigma - \sum_i (x_i \sigma_i^0) \quad (3.73)$$

where σ_i^0 are the surface tensions of the pure constituents of the alloys at the working temperature. The surface of liquid metals undergoes oxidation or combines with the other components of the alloys, which deviate the experimental result from reality, and non-linear variation of the experimental data of surface tension with the temperature can be observed. For most of the liquid elements, surface tension decreases linearly with the increase in temperature when measured in the condition in which partial pressure of oxygen is maintained below 10^{-10} Nm^{-2} (Mills & Su, 2006; Fima & Novakovic, 2018). Therefore, researchers used the linear variation of the surface tension of pure liquid elements with temperatures. The surface tension ($\sigma_i^0(T)$) and density ($\rho_i(T)$) of pure elements at temperature T are obtained in terms of surface tension ($\sigma_i^0(T_0)$) and density

$(\rho_i(T_0))$ near their melting temperature T_0 are expressed using the linear equations

$$\sigma_i^0(T) = \sigma_i^0(T_0) + \frac{\partial \sigma_i^0}{\partial T}(T - T_0), \quad \text{and} \quad \rho_i(T) = \rho_i(T_0) + \frac{\partial \rho_i}{\partial T}(T - T_0) \quad (3.74)$$

where $\partial \sigma_i^0 / \partial T$ and $\partial \rho_i / \partial T$ are the temperature derivative of surface tension and density of the individual components in their pure state respectively.

CHAPTER 4

4. RESULTS AND DISCUSSION

The importance of knowledge regarding the surface properties of liquid alloys has already been highlighted in the previous chapters. The surface properties of three liquid ternary alloys, such as Fe–Si–Ti, Al–Sn–Zn and Al–Cu–Fe at different temperatures were investigated at different temperatures in this work. For this purpose, the self-consistent set of T-dependent interaction parameters for G_M^{xs} were first optimised using the available experimental or literature data of H_M and S_M^{xs} . These parameters were optimised in the framework of the Redlich-Kister (R-K) polynomials. The surface properties of the preferred systems were then computed at different temperatures using the thermodynamic data of the constituent sub-binary alloys. The Butler equation and geometrical models like Chou or GSM, Toop and Kohler models were used for the computation processes.

The alloys studied in this work were chosen based on the degree of interaction between their constituent sub-binary pairs. In the following sub-sections, the results and discussion of the theoretical investigations are presented.

4.1 Effect of interaction energy parameters on mixing properties of liquid alloys

The value of G_M^{xs} in liquid alloys indicate the bonding strength between the atoms in the complex and G_M^{xs} depends on the concentrations as well as temperature of the liquid mixture. The weak interaction in a binary system is characterised by the significantly smaller negative or positive extremum value of H_M . However, the strongly interacting binary system has a substantially greater negative extremum value of H_M . It is important to note that the ordering systems have the negative G_M^{xs} value while segregating systems have positive G_M^{xs} values.

Equation (3.22) is the R-K polynomial of order n and is used to compute the G_M^{xs} of a binary system at different bulk concentrations in terms of interaction energy parameters (A_{ij}^k) ($k=0, 1, 2, \dots$). These parameters are concentration-independent and T-dependent quantities. The G_M^{xs} depends on H_M and S_M^{xs} of a binary system and hence A_{ij}^k also depends on these two quantities.

Therefore, A_{ij}^k can be expressed as (Kaptay, 2017)

$$A_{ij}^k = a_{ij}^k + b_{ij}^k T \quad (k = 0, 1, 2, 3 \dots) \quad (4.1)$$

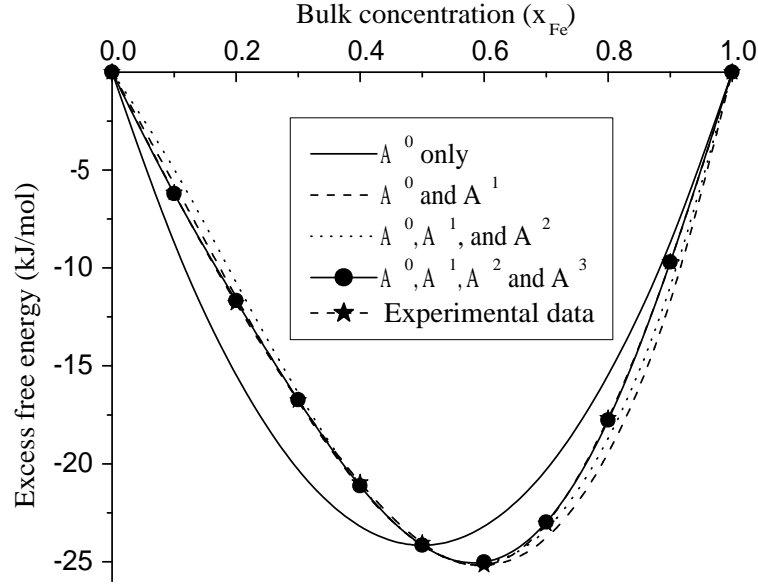


Figure 8: Variation of G_M^{xs}/RT of Fe–Si binary alloys with the order of interaction energy parameters.

where a_{ij}^k represents the H_M contribution and b_{ij}^k represents the S_M^{xs} contribution on A_{ij}^k . The value of A_{ij}^0 has significant effect on G_M^{xs} and provides information regarding the strength and nature of interaction between the atoms constituting the system. The other terms A_{ij}^k with $k > 0$ are the coefficient of $x_i x_j (x_i - x_j)^k$ in the R-K polynomial and have a minor effect on the G_M^{xs} , as seen in Figure 8. When the G_M^{xs} of Fe–Si binary alloys were computed using only A_{ij}^0 , then there was a maximum deviation of 29% and minimum deviation of 0.4% between the computed value and the experimental data. When A_{ij}^0 and A_{ij}^1 were used to compute G_M^{xs} of this system, the results were very close to the experimental data. Similarly, when four interaction energy parameters were employed to compute G_M^{xs} , the values obtained tends to agree well with the reference experimental data. These findings revealed that, despite the significant contribution of A_{ij}^0 to the computed values of G_M^{xs} , its higher order terms are used as the correction factors (Figure 8).

The contributions of A_{ij}^k terms to G_M^{xs} decrease as k increases and hence, terms with larger value of k were neglected. Furthermore, for the even value of k , A_{ij}^k has the same value and sign for ‘ij’ and ‘ji’ system and opposite sign for odd values of k i.e. $A_{ij}^k = (-1)^k A_{ji}^k$. When the concentrations of both components in an alloy are equal, there is contribution of only A_{ij}^0 to G_M^{xs} of the alloy.

Figure 9 depicts the variation of G_M^{xs}/RT of a few binary liquid alloys with different bulk concentration in order to investigate the effect of interaction energy parameters on G_M^{xs} . A strongly interacting binary system is characterised by relatively greater negative value

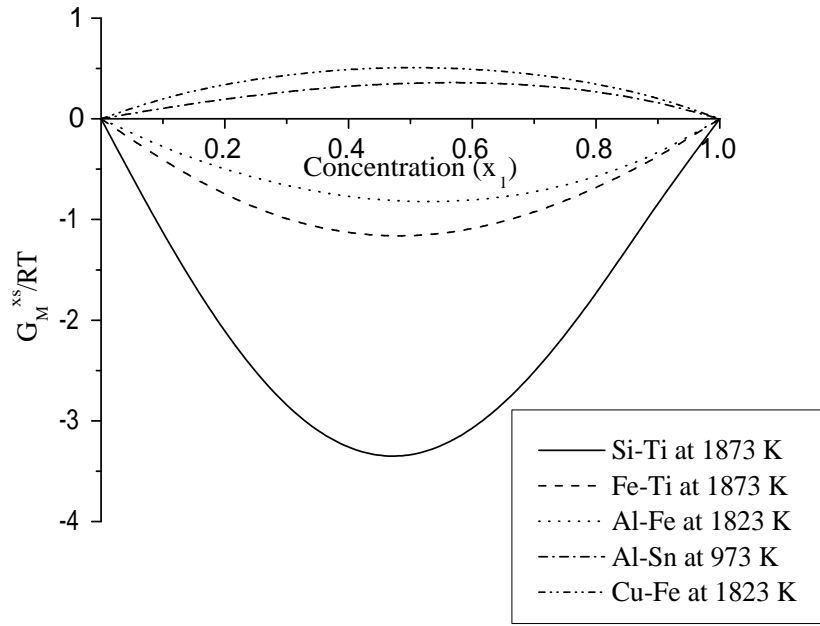


Figure 9: Variation of G_M^{xs}/RT of different binary liquid alloys with bulk concentration (x_1).

of A_{ij}^0 and a_{ij}^0 . For example, Si–Ti binary liquid alloys are strongly interacting binary system at 1873 K as the extremum value of G_M^{xs}/RT at this temperature was found to be -3.30 which is much less than -2 . The value of a_{ij}^0 and A_{ij}^0 for Si–Ti binary system at 1873 K was found to be -231000 J/mol and -208000 J/mol respectively which can be observed from Table 1.

Similarly, the extremum value of G_M^{xs}/RT of Fe–Ti binary liquid alloys were found to be -1.16 which indicate that this binary system is moderately interacting and ordering in nature ($-2 < G_M^{xs}/RT < -1$). The values of a_{ij}^0 and A_{ij}^0 of Fe–Ti liquid alloys at 1873 K was found to be -86900 J/mol and -72200 J/mol respectively. The negative values of these parameters for Fe–Ti system was less than that for Si–Ti system. Furthermore, the values of a_{ij}^0 and A_{ij}^0 of Al–Fe binary liquid mixture at 1823 K were found to be -78900 J/mol and -49600 J/mol. The extremum value of G_M^{xs}/RT of Al–Fe liquid mixture was found to be -0.880 which suggest that Al–Fe binary system is a weakly interacting and ordering in nature. The Al–Fe system has lower value of A_{ij}^0 and a_{ij}^0 than the moderately interacting Fe–Si system and much lower value than the strongly interacting Si–Ti system. These findings indicate that the relatively higher negative values of a_{ij}^0 and A_{ij}^0 characterise greater bonding strength in an ordering binary liquid alloys.

Positive values of G_M^{xs} indicate the segregating binary alloys. The extremum values of G_M^{xs}/RT of Al–Sn alloys were found to be 0.360 at 973 K and 0.508 at 1823 K for Cu–Fe alloys. These results show that segregating tendency of Cu–Fe system has a higher

segregating tendency than the Al–Sn system.

The values of A_{ij}^0 and a_{ij}^0 are both positive for these two binary systems. The values of a_{ij}^0 and A_{ij}^0 of Al–Sn binary system were found to be 16130 J/mol and 11456 J/mol at 973 K respectively. Similarly, values of a_{ij}^0 and A_{ij}^0 of Cu–Fe system were found to be 35620 J/mol and 30780 J/mol at 1823 K respectively. These observations suggest that the system is more segregating if the positive values of the parameters a_{ij}^0 and A_{ij}^0 increase.

The negative value of enthalpy contributing term a_{ij}^0 was found to be significantly greater than that of the entropy contributing term $b_{ij}^0.T$ for strongly ordering binary systems, resulting in higher negative values for G_M^{xs} . The positive values of $b_{ij}^0.T$ increase linearly as the temperature of the system increases, leading the negative values of A_{ij}^0 and G_M^{xs} to decrease and the system to shift its ideal state. Above a certain temperature, the value of $b_{ij}^0.T$ exceeds the negative values of a_{ij}^0 , leading the G_M^{xs} of the system to become positive, indicating a transition from ordering to segregating behaviour. This shift at higher temperature is unexplained due to the evaporation of liquid alloys, which yields the alloying process impossible.

To overcome this problem, Kaptay (2017) suggested the exponential temperature dependent interaction energy parameters expressed as

$$A_{ij}^k = h_{ij}^k \exp\left(-\frac{T}{\tau_{ij}^k}\right) \quad (k = 0, 1, 2, \dots) \quad (4.2)$$

where h_{ij}^k represents the contribution of H_M on A_{ij}^k . $\tau_{ij}^k > 0$ is the measure of a temperature at which A_{ij}^k changes sign from negative to positive values if the linear model is used to determine it. Consequently, the exponential model can be used at temperatures ranging from the melting point to considerably above it. Many researchers, however, accept the linear model for computing thermodynamic properties of liquid alloys closer to melting temperature.

4.2 Fe–Si–Ti ternary system

There is extensive use of iron alloys for various applications, including building, vehicles and bridges. Due to their excellent mechanical strength-to-weight ratio, corrosion resistance and high melting point, Titanium-based alloys are utilized for engineering in the automobile and aerospace industries (Kostov et al., 2007, 2008). The addition of titanium to steel improves the toughness of heat-affected area of thick steel sheets (J. Lee et al., 2006) and yield strength by 188 MPa (Bo et al., 2013). The alloying of iron and titanium with silicon enhances the reactivity of filler metals, thereby reducing their

melting temperature, and they are commonly used as joining agents in ceramics (Weitzer et al., 2008). Due to the multipurpose uses, many researchers (Watson & Brown, 1974; Bouchard & Bale, 1995; J. Lee et al., 2006; Weitzer et al., 2008; Raghavan, 2009; Park et al., 2010; Mehta, Koirala, et al., 2020; Ushioda et al., 2011) studied Fe–Si–Ti sub-binary and ternary alloys. The concentration-dependent surface tension of Fe–Ti liquid alloys at 1873 K has been studied by J. Lee et al. (2006) using the constrained drop method and found that the surface tension of the alloy decreases with the increase in the bulk concentration of Ti. Watson and Brown (Watson & Brown, 1974) studied the ductility and strength of Fe-2.5% Si-1.4%Ti alloy and estimated the high strength (1100-1200 MPa) and poor ductility of the specimen when aged to peak hardness. Aging of the specimen improves the ductility at the expense of its strength. Ushioda et al. (2011) studied the mechanical properties of Fe–Si solid alloys in the Fe-rich region and found that the yield strength of iron can be increased by 40% with the addition of 1.9 at.% of silicon. Thermodynamic studies of the Fe–Si, Fe–Ti, and Si–Ti systems in liquid state reveal a strong interaction between the components of these binary subsystems (Bouchard & Bale, 1995).

According to literature (Ansara et al., 1998; Zhu et al., 2001), the compounds Fe_2Si and Fe_5Si_3 , FeSi , FeSi_2 , and Fe_2Si_5 are formed in Fe–Si system in solid solution. There are two intermetallic phases Fe_2Ti and FeTi in Fe–Ti binary solid-phase (Hong et al., 2012). Similarly, Ti_5Si_4 , Ti_5Si_3 , and Ti_3Si intermediate phases exist in Ti–Si binary solid solution (Sabooni et al., 2012). The intermediate metallic phases detected in the ternary solid alloys are FeSi_2Ti , FeSiTi , $\text{Fe}_4\text{Si}_3\text{Ti}$, Fe_2SiTi , and $\text{Fe}_7\text{Si}_2\text{Ti}$ over the entire range of concentration (Raghavan, 2009). The sizeable negative deviation of activity of components from the ideal value in these binary subsystems at 1873 K (Mehta, Koirala, et al., 2020) suggests a substantial interaction between the components in the binary pairs. In the present work, we studied the surface properties of Fe–Si–Ti liquid ternary alloys. The thermodynamic databases of the binary Fe–Si, Si–Ti, and Fe–Ti sub-systems are required to compute the surface properties of sub-binary and ternary alloy system. So, first, we obtained the required thermodynamic parameters in the following section.

4.2.1 Excess Gibbs free energy of mixing of Fe–Si, Si–Ti and Fe–Ti binary systems

Using experimental data (Hultgren et al., 1973) of H_M and S_M^{xs} , We optimised the T-dependent interaction energy parameters for G_M^{xs} of Fe–Si binary liquid alloys. To optimise the interaction energy parameters, we used the data of G_M^{xs} of Si–Ti binary liquid alloys at 2000 K, 2400 K, and 2473 K from the work of Kostov et al. (2007). Similarly, we obtained the T-dependent interaction energy parameters for G_M^{xs} of Fe–Ti liquid binary alloys with the help of H_M and G_M^{xs} of Fe–Ti binary liquid system from the

Table 1: Optimised coefficients of R-K polynomial for G_M^{xs} of binary subsystems of Fe–Si–Ti liquid ternary alloys

Systems	Optimised parameters (A^K) (J/mol)	
Fe–Si	A^0	$-151700 + 29.40T$
	A^1	$-37230 - 2.29T$
	A^2	$36620 - 12.62T$
	A^3	$29600 - 1.38T$
Fe–Ti	A^0	$-86950 + 7.87T$
	A^1	$17990 - 6.05T$
	A^2	$19930 - 6.53T$
	A^3	$-13180 + 4.82T$
Si–Ti	A^0	$-231200 + 12.50T$
	A^1	30540
	A^2	58460

Table 2: G_M^{xs} (kJ/mol) of binary subsystems of Fe–Si–Ti liquid ternary alloys

x_1	Fe–Si at 1873 K		Si–Ti at 2000K		Fe–Ti at 1873 K	
	Calculated	Expt.*	Calculated	Ref**	Calculated	Expt.***
0.1	-6.22	-6.17	-17.39	-17.08	-6.34	-6.36
0.2	-11.66	-11.79	-32.56	-32.83	-11.61	-11.57
0.3	-16.74	-16.76	-43.90	-44.57	-15.41	-15.39
0.4	-21.13	-20.96	-50.39	-50.92	-17.57	-17.61
0.5	-24.16	-24.05	-51.55	-51.55	-18.05	-18.10
0.6	-25.01	-25.17	-47.46	-46.94	-16.95	-16.95
0.7	-22.98	-23.07	-38.77	-38.11	-14.40	-14.38
0.8	-17.77	-17.68	-26.69	-26.42	-10.62	-10.60
0.9	-9.70	-9.71	-12.99	-13.30	-5.77	-5.78

*Hultgren et al. (1973), **Kostov et al. (2007), ***Thiedemann et al. (1995)

work of Thiedemann et al. (1995). The optimised parameters for G_M^{xs} of the sub-binary alloys of the Fe–Si–Ti ternary alloy system are presented in Table 1.

Using the optimised parameters in Equation (3.22), we computed the values of G_M^{xs} of Fe–Si, Si–Ti, and Fe–Ti binary liquid alloys at different concentrations. Table 2 depicts the computed values of G_M^{xs} of these binary systems as well as data from the literature. The variation of G_M^{xs} of the binary subsystems of the Fe–Si–Ti ternary alloy with the bulk concentrations is displayed in Figure 10. The computed values of G_M^{xs} of the Fe–Si and Fe–Ti binary systems agreed well with the experimental data (Hultgren et al., 1973). At $x_{Fe} = 0.5$, the experimental and computed values of G_M^{xs} were (-24.05 ± 6.279) kJ/mol and -24.16 kJ/mol respectively at 1873 K. These results show that the theoretical and experimental data are in consistent with each other (Figure 10). The extremum value of G_M^{xs} of the Fe–Si binary system was found to be -25.05 kJ/mol at 1873 K at the bulk concentration of $x_{Fe} = 0.58$ which indicated that the system to be asymmetric

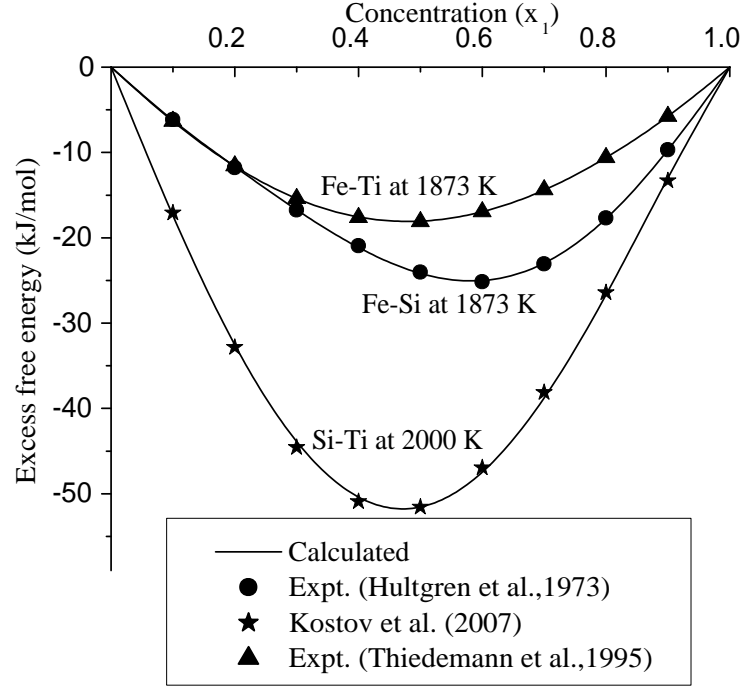


Figure 10: Variation of G_M^{xs} of binary subsystems of Fe–Si–Ti liquid alloys with concentration.

and ordering in nature. The maximum deviation of the computed values from the experimental data of Hultgren et al. (1973) was found to be about 1.0% at the bulk concentration of $x_{Fe} = 0.2$. The extremum value of G_M^{xs}/RT in this work was found to be -1.61 . The graphical study of variation of G_M^{xs}/RT with bulk concentration at 1873 K in the literature (Adhikari, Jha, & Singh, 2010) was found to be -1.63 at bulk composition of $x_{Fe} = 0.6$.

For Si–Ti binary system, both the literature (Kostov et al., 2007) and computed values of G_M^{xs} were found to be equal -51.55 kJ/mol at 2000 K and $x_{Si} = 0.5$ (Figure 10). This high negative value of G_M^{xs} revealed the system to be a strongly interacting and ordering in nature. The highest variation in the value of G_M^{xs} between the computed values in this work using the optimised parameters and the data obtained using the software FactSage by Kostov et al. (2007) was about 2.3% at bulk concentration of $x_{Si} = 0.9$. The estimated extremum value of G_M^{xs}/RT of Si–Ti binary liquid alloy at 2000 K were found to be -3.15 in the work of Yadav et al. (2020) using the quasi-lattice model. This data is equivalent to the value of G_M^{xs} equal to -52.38 kJ/mol which is quite close (deviation of about 1.6%) to the data presented in Table 34. The extremum value of G_M^{xs} of Si–Ti binary liquid alloys computed using the interaction energy parameter given in Ansara et al. (1998) was found to be -53.72 kJ/mol at equiatomic bulk composition which is 4% below the value obtained in this work.

The experimental and computed extremum values of G_M^{xs} of the Fe–Ti binary system were found to be -18.05 kJ/mol and -18.10 kJ/mol respectively at equiatomic bulk

concentration. Both of these values were found to be in consistent with each other (Figure 10). This binary system was found to be moderately interacting as the value G_M^{xs}/RT at 1873 K was found to be -1.16 . The maximum deviation of the computed values using the optimised parameters in this work with the experimental data (Thiedemann et al., 1995) was found to be 0.3% at bulk composition of $x_{Fe} = 0.2$ at 1873 K.

These investigations yielded the validity of the optimised parameters for G_M^{xs} of the binary subsystems, which were hence used to compute the surface concentration and surface tension of sub-binary and liquid ternary alloys of the Fe–Si–Ti ternary alloy system.

4.2.2 Surface tensions of binary subsystems of Fe–Si–Ti alloy

Using the Butler equation, we computed the surface tensions of sub-binary liquid alloys of the Fe–Si–Ti ternary alloy system. The surface tension and density of individual components of the alloy near their melting temperature T_0 as well as their temperature derivative terms were taken from Smithell’s Metal Reference Book (Gale & Totemeier, 2004) and are presented in Table 3. Equation (3.74) was used to compute the surface

Table 3: Values of density (ρ_0) and surface tension (σ_0) of elements near their melting temperature (T_0) and variation of density and surface tension with temperature

Elements	T_0 (K)	ρ_0 (kg m ⁻³)	$\partial\rho/\partial T$ (kg m ⁻³ K ⁻¹)	σ_0 (N m ⁻¹)	$\partial\sigma/\partial T$ (N m ⁻¹ K ⁻¹)
Al	933	2385	-0.35	0.914	-0.00035
Cu	1356	8000	-0.80	1.303	-0.00023
Fe	1809	7015	-0.883	1.872	-0.00049
Si	1683	2530	-0.35	0.865	-0.00013
Sn	505	6980	-0.61	0.560	-0.00009
Ti	1958	4110	-0.702	1.650	-0.00026
Zn	692	6575	-0.98	0.782	-0.00017

Source- (Gale & Totemeier, 2004)

Table 4: Surface tension of binary sub-systems of Fe–Si–Ti liquid alloys at 1873 K

Bulk concentration (x_1)	Surface tension (N m ⁻¹) at 1873 K		
	Fe–Si	Si–Ti	Ti–Fe
0.1	0.879	1.661	1.849
0.2	0.916	1.627	1.853
0.3	0.965	1.544	1.851
0.4	1.033	1.408	1.841
0.5	1.124	1.250	1.822
0.6	1.240	1.106	1.795
0.7	1.378	0.995	1.763
0.8	1.532	0.921	1.729
0.9	1.692	0.875	1.698

tensions and densities of the pure components of the alloy at working temperature T . The G_i^{xs} of the components in the binary alloys was computed using Equations (3.22) and (3.46). These parameters were used in Equation (3.70) to compute the surface tensions of the above mentioned binary subsystems.

The computed values of the surface tensions of the Fe–Si, Si–Ti, and Ti–Fe binary liquid alloys at 1873 K are presented in Table 4. Figure 11 shows the variation of surface tensions of these binary systems as the function of concentration. In the Fe–Si binary system, the surface tension of pure Si (8.40 N m^{-1}) was found to be significantly lower than that of Fe (1.841 N m^{-1}). The estimated value of surface tension of Fe was found to be 1.837 N m^{-1} by J. Lee et al. (2004) at 1873 K. This value of surface tension of pure Fe is in excellent agreement with the data (Gale & Totemeier, 2004) used in this work. Surface tension of the Fe–Si system decreased with the increase in the bulk concentration of Si and range of variation of surface tension was found to be more with respect to other binary subsystems of the Fe–Si–Ti ternary alloy system (Figure 11). The results of this work are consistent with the work of Tanaka & Iida (1994). The surface tension of Si–Ti liquid alloys were found to decrease as the bulk concentration of Si increased (Figure 11). The gradual increase in the bulk concentration of Fe at 1873 K was observed to cause the surface tensions of the Fe–Ti binary liquid alloys to vary from 1.672 N m^{-1} to 1.841 N m^{-1} . J. Lee et al. (2006) observed the similar trend of variation of surface tension of this alloy at 1823 K. The surface tension of Fe and Ti were comparable and the range of variation of the surface tension of the Fe–Ti

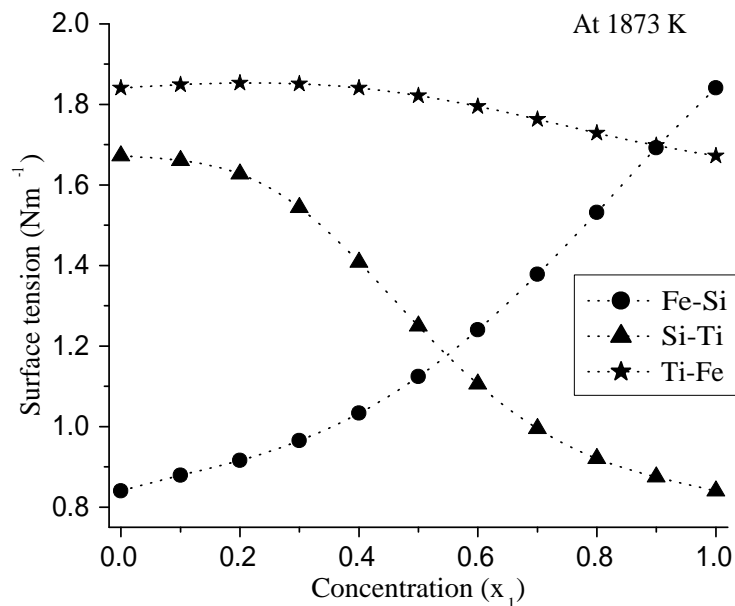


Figure 11: Variation of surface tension of sub-binary system of Fe–Si–Ti ternary alloy at 1873 K.

binary liquid alloys were found to be the least over the entire range of concentration in comparison with the other two binary subsystems.

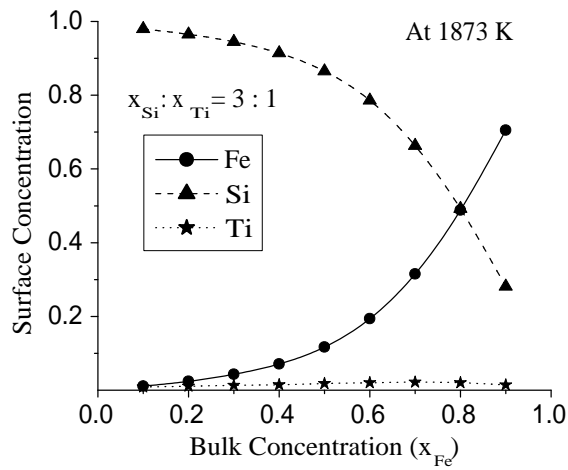
4.2.3 Surface properties of Fe–Si–Ti liquid ternary alloy

4.2.3.1 Surface concentration of components in Fe–Si–Ti liquid ternary alloy

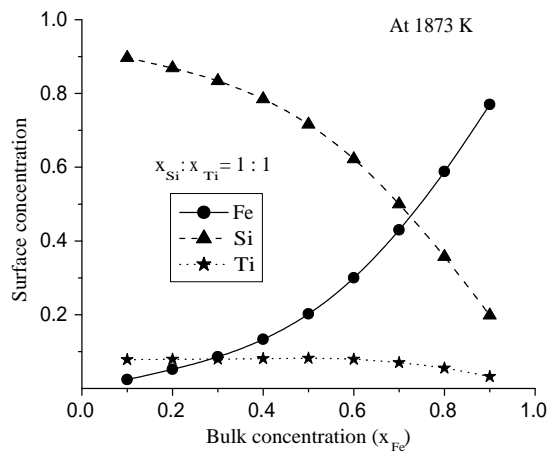
Using the Butler equation (Equation (3.70)), We computed the surface concentration of components present in a liquid ternary alloy. We used the data of surface tension and density of the pure components near their melting temperature from Table 3 and used in Equation (3.74) to compute the surface tension of the pure components at working temperatures. The value of monolayer surface area of one mole of pure component is obtained using Equation (2.2). Equations (3.22) and (3.46) were used for the calculation of the G_i^{xs} of the components in the ternary alloys. The computed values of G_i^{xs} of components in the liquid alloys at three different cross-sections ($x_{Si} : x_{Ti} = 3 : 1$, $1 : 1$ and $1 : 3$) are presented in Appendix A (Tables 38-40).

The surface concentration of components from Fe corner at the above mentioned cross-sections are presented in Table 5. The variation of surface concentration of components in Fe–Si–Ti ternary alloys with the bulk concentration from Fe corner at 1873 K are shown in Figures 12 (a-c). When observed from Fe corner at cross-sections $x_{Si} : x_{Ti} = 3 : 1$, the surface concentration of Fe increased with rising bulk concentration and that of Si decreased with decreasing bulk concentration. However, the surface concentration of Ti was found to increase from 0.009 to 0.022 even though its bulk concentration decreased in the region of 0.225 to 0.075.

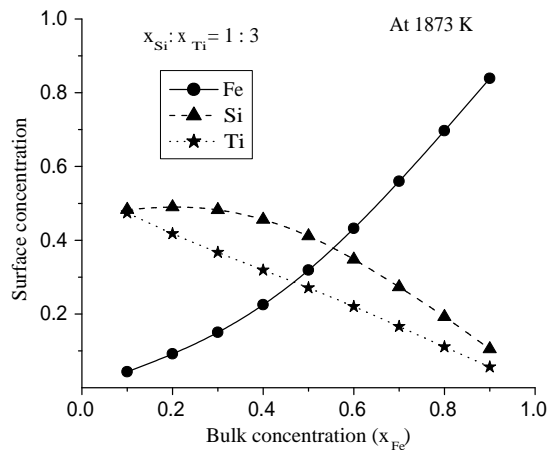
This unusual trend of variation of the surface concentration of Ti can be explained in terms of interaction energy between binary pairs and the surface tension of the individual components of this alloy in a liquid state. The surface tensions of Fe, Si and Ti are found to be 1.841, 0.840 and 1.672 N m⁻¹ in their pure state at 1873 K. As a result, surface concentration of Fe was found to be much less than its bulk concentration while that of Si was found to be much higher than its bulk concentration. Therefore, Fe atoms prefer to form complexes with Si atoms rather than with Ti atoms as the interaction between Fe and Si was found to be more energetically favourable than that between Fe and Ti (Figure 10). Similar effect can also be observed at cross-sections $x_{Si} : x_{Ti} = 1 : 1$ (Figure 12(b)). However, the surface concentration of Ti was relatively higher at cross-section $x_{Si} : x_{Ti} = 1 : 1$ than at cross-section $x_{Si} : x_{Ti} = 3 : 1$ due to the higher bulk concentration of Ti in the former case. The surface concentration of Ti was found to decrease constantly when the bulk concentration of Ti decreased from the Fe corner at cross-section $x_{Si} : x_{Ti} = 1 : 3$ (Figure 12(c)). In this case, surface concentration of



(a)



(b)



(c)

Figure 12: Variation of surface concentration of components in Fe–Si–Ti ternary alloys with bulk concentration from Fe corner at three cross-sections.

Table 5: Surface concentration of Fe, Si and Ti in Fe–Si–Ti liquid ternary alloys from Fe corner at 1873 K

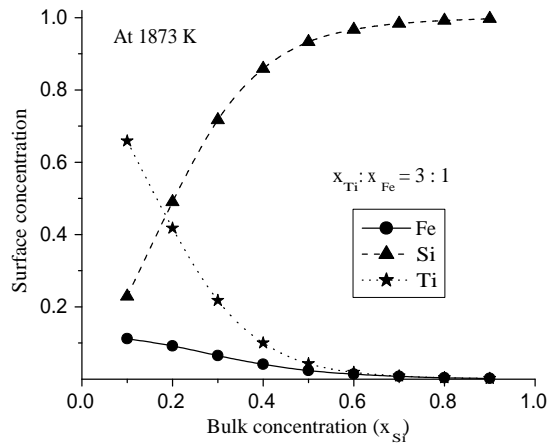
x_{Fe}	Surface concentration								
	$x_{Si} : x_{Ti} = 3 : 1$			$x_{Si} : x_{Ti} = 1 : 1$			$x_{Si} : x_{Ti} = 1 : 3$		
	Fe	Si	Ti	Fe	Si	Ti	Fe	Si	Ti
0.1	0.011	0.980	0.009	0.024	0.897	0.078	0.043	0.483	0.474
0.2	0.024	0.965	0.011	0.052	0.869	0.079	0.092	0.490	0.418
0.3	0.043	0.945	0.013	0.086	0.834	0.080	0.150	0.482	0.367
0.4	0.071	0.914	0.015	0.133	0.785	0.081	0.225	0.456	0.319
0.5	0.117	0.865	0.018	0.202	0.716	0.082	0.319	0.411	0.271
0.6	0.194	0.786	0.020	0.300	0.622	0.079	0.432	0.348	0.220
0.7	0.315	0.663	0.022	0.430	0.500	0.070	0.560	0.273	0.166
0.8	0.488	0.492	0.020	0.588	0.357	0.055	0.697	0.192	0.111
0.9	0.705	0.281	0.014	0.770	0.198	0.032	0.839	0.105	0.056

Table 6: Surface concentration of Fe, Si and Ti in Fe–Si–Ti liquid ternary alloys from Si corner at 1873 K

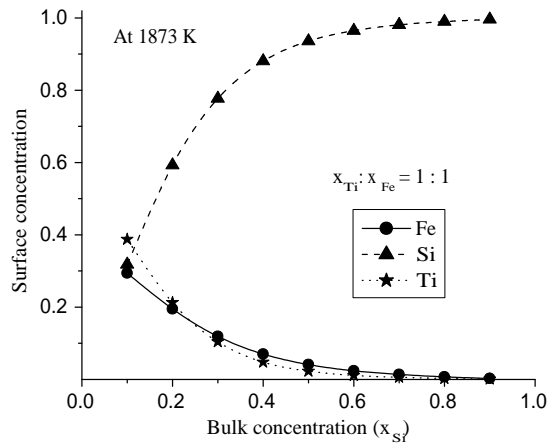
x_{Si}	Surface concentration								
	$x_{Ti} : x_{Fe} = 3 : 1$			$x_{Ti} : x_{Fe} = 1 : 1$			$x_{Ti} : x_{Fe} = 1 : 3$		
	Fe	Si	Ti	Fe	Si	Ti	Fe	Si	Ti
0.1	0.112	0.229	0.659	0.294	0.318	0.388	0.496	0.354	0.149
0.2	0.092	0.490	0.418	0.195	0.593	0.213	0.300	0.622	0.079
0.3	0.065	0.717	0.218	0.119	0.777	0.104	0.170	0.791	0.039
0.4	0.041	0.859	0.100	0.070	0.881	0.048	0.096	0.885	0.019
0.5	0.024	0.933	0.043	0.041	0.936	0.023	0.055	0.935	0.010
0.6	0.014	0.967	0.019	0.024	0.965	0.011	0.033	0.962	0.005
0.7	0.008	0.984	0.009	0.014	0.981	0.006	0.020	0.978	0.003
0.8	0.004	0.992	0.004	0.007	0.990	0.003	0.011	0.988	0.001
0.9	0.002	0.997	0.002	0.003	0.996	0.001	0.005	0.995	0.001

Ti was found to be less than that of Si, irrespective of its higher bulk concentration. Furthermore, the surface concentration of Si was found to increase from 0.483 to 0.490 in the beginning (Table 5) and then start decreasing continuously, even though its bulk concentration decreased continuously over the entire range of concentrations (Figure 12 (c)).

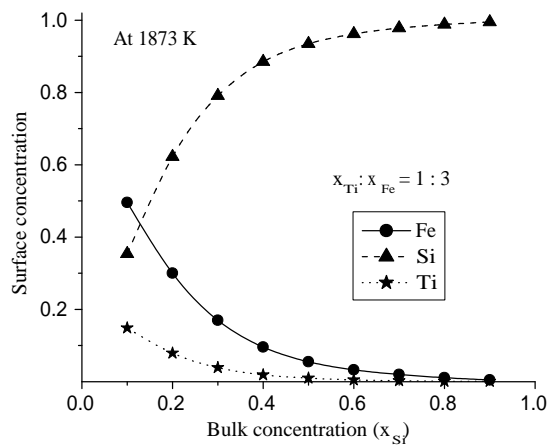
The computed values of surface concentration of components from Si corner at 1873 K at the above mentioned cross-sections are presented in Table 6 and plotted as a function of composition in Figures 13 (a-c). The surface concentrations of Fe and Ti were found to be less than their respective bulk concentrations while that of Si was found to be significantly higher than its bulk concentration. Furthermore, the usual trend of variations in the surface concentration of the components was depicted when viewed from Si corner, in which the surface concentrations of components were found to increase or decrease with the increase or decrease of their respective bulk concentrations.



(a)

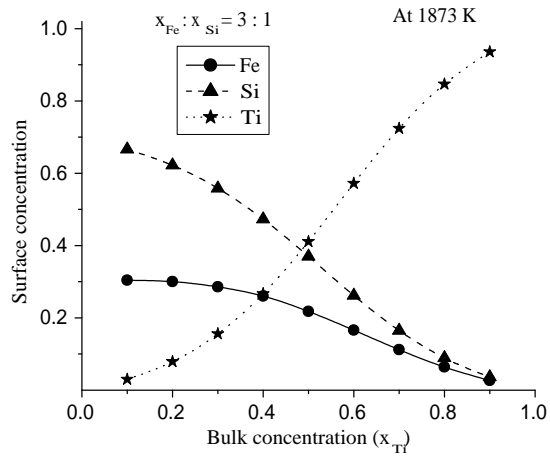


(b)

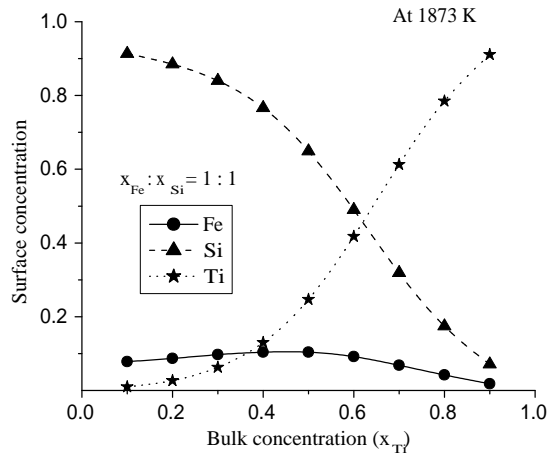


(c)

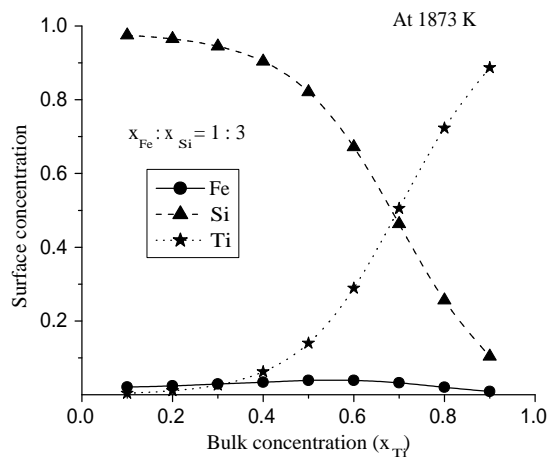
Figure 13: Variation of surface concentration of components in Fe–Si–Ti ternary alloys with bulk concentration from Si corner at three cross-sections.



(a)



(b)



(c)

Figure 14: Variation of surface concentration of components in Fe–Si–Ti ternary alloys with bulk concentration from Ti corner at three cross-sections.

Table 7: Surface concentration of Fe, Si and Ti in Fe–Si–Ti liquid ternary alloys from Ti corner at 1873 K

x_{Ti}	Surface Concentration								
	$x_{Fe} : x_{Si} = 3 : 1$			$x_{Fe} : x_{Si} = 1 : 1$			$x_{Fe} : x_{Si} = 1 : 3$		
	Fe	Si	Ti	Fe	Si	Ti	Fe	Si	Ti
0.1	0.304	0.666	0.030	0.078	0.913	0.010	0.021	0.975	0.004
0.2	0.300	0.622	0.079	0.087	0.885	0.027	0.024	0.965	0.011
0.3	0.286	0.558	0.156	0.097	0.840	0.063	0.029	0.945	0.026
0.4	0.260	0.473	0.267	0.104	0.766	0.130	0.034	0.904	0.062
0.5	0.218	0.370	0.411	0.104	0.649	0.247	0.039	0.821	0.140
0.6	0.166	0.262	0.572	0.092	0.490	0.418	0.039	0.672	0.289
0.7	0.112	0.165	0.724	0.068	0.319	0.613	0.032	0.463	0.505
0.8	0.064	0.089	0.847	0.042	0.174	0.785	0.020	0.256	0.723
0.9	0.027	0.036	0.936	0.018	0.071	0.911	0.009	0.104	0.887

The calculated values of surface concentrations of components of the ternary alloy system from Ti corners at three cross-sections are presented in Table 7 and plotted in Figures 14 (a-c). When viewed from Ti corner, the usual trends of variation in surface concentrations of components were observed at relatively higher bulk concentrations of Fe than Si (Figure 14(a)). Herein, the surface concentration of a component was found to increase with the increase in its respective bulk concentration and vice versa. When the bulk concentration of Fe was maintained at approximately equal to or less than that of Si, the surface concentration of Fe was found to increase at first and then decrease, although there was a continuous decrease in its bulk concentration over the entire range (Figures 14 (b,c)). When the bulk concentration of Ti was increased, excess Si atoms moved from the surface region to the bulk region due to the very strong energetic interaction between Si and Ti with respect to the interaction between other binary pairs. This leads to a slight increase in the surface concentration of Fe in spite of the decrease in its bulk concentration.

Surface concentrations of components for a fixed bulk concentration $x_{Fe} : x_{Si} : x_{Ti} = 40 : 15 : 45$ at 1873, 1973, 2073 and 2173 K are depicted in Table 8. These computed values of surface concentration are presented in Figure 15 as the function of temperature. The surface concentrations of Fe and Ti were found to be much less than their respective

Table 8: Surface concentration of components in Fe–Si–Ti liquid alloys at different temperatures for a fixed bulk composition $x_{Fe} : x_{Si} : x_{Ti} = 0.4 : 0.15 : 0.45$

Temperature (K)	Surface Concentration		
	Fe	Si	Ti
1873	0.225	0.456	0.319
1973	0.243	0.432	0.325
2073	0.260	0.410	0.330
2173	0.277	0.388	0.335

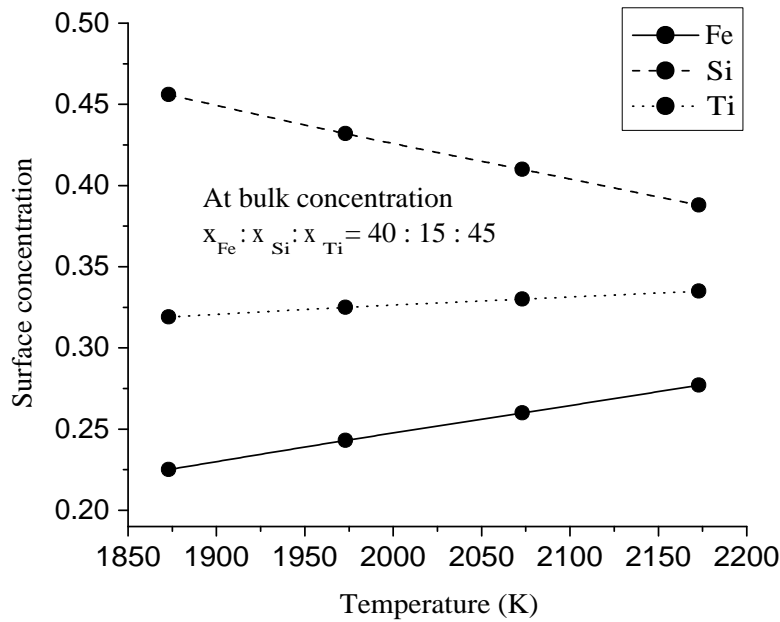


Figure 15: Variation of surface concentration of components in the Fe–Si–Ti ternary alloys with temperature at a fixed bulk concentration.

bulk concentrations and the surface concentration of Si was found to be much higher than its bulk concentration at 1873 K. It can be seen from Table 8 and Figure 15 that the surface concentration of Si decreased while that of Fe and Ti increased with the increase in temperature. From this observation, it can be concluded that the surface concentrations of the components shifted towards their respective ideal values with increase in the temperature of the alloys. This is due to a decrease in the level of interaction between the components of mixture at elevated temperatures.

4.2.3.2 Surface tension of Fe–Si–Ti liquid ternary alloys

The surface tensions of Fe–Si, Si–Ti, and Fe–Ti binary liquid alloys were computed using the Butler equation at four different temperatures. The ideal values of surface tension of the binary liquid alloys were computed using weighted values of the surface tension of individual components. The excess surface tension of the binary liquid alloys at these temperatures was computed as the deviation of the weighted values of surface tension from the values obtained using the Butler equation. These excess surface tensions of the binary systems at four different temperatures were then used to optimise the T-dependent coefficients of R-K polynomials for the surface tension, which are presented in Table 9. The Chou, Kohler and Toop models were used to compute the surface tension of Fe–Si–Ti liquid ternary alloys using these optimised parameters. Furthermore, the equation is also used to compute the surface tension of ternary alloys at the mentioned corners. The

obtained data are presented in Tables 10, 11 and 12.

The iso-surface tension lines of the Fe–Si–Ti liquid ternary alloys at 1873 K are shown in Figure 16. The data used for plotting the iso-surface tension lines of this ternary alloys are presented in Table 47 of Appendix A. Surface tension ranges between 0.840 N m^{-1} (for pure silicon) to 1.841 N m^{-1} (for pure iron) at 1873 K. The surface tension

Table 9: Optimised coefficients of R-K polynomial for excess surface tension of binary subsystems of Fe–Si–Ti liquid ternary alloys

Systems	Optimised parameters (L^k) (N m^{-1})	
Fe–Si	L^0	$-2.264 + 7.45110^{-4}T$
	L^1	$-0.582 + 3.477 \times 10^{-4}T$
	L^2	0.406
Fe–Ti	L^0	$0.105 + 8.295 \times 10^{-4}T$
	L^1	$-0.454 - 1.713 \times 10^{-4}T$
	L^2	$-0.151 + 2.396 \times 10^{-4}T$
	L^3	$-0.144 + 5.847 \times 10^{-4}T$
Si–Ti	L^0	$-0.555 + 2.984 \times 10^{-4}T$
	L^1	$-2.078 + 3.361 \times 10^{-4}T$
	L^2	$0.914 - 3.643 \times 10^{-4}T$
	L^3	$1.198 - 1.133 \times 10^{-4}T$

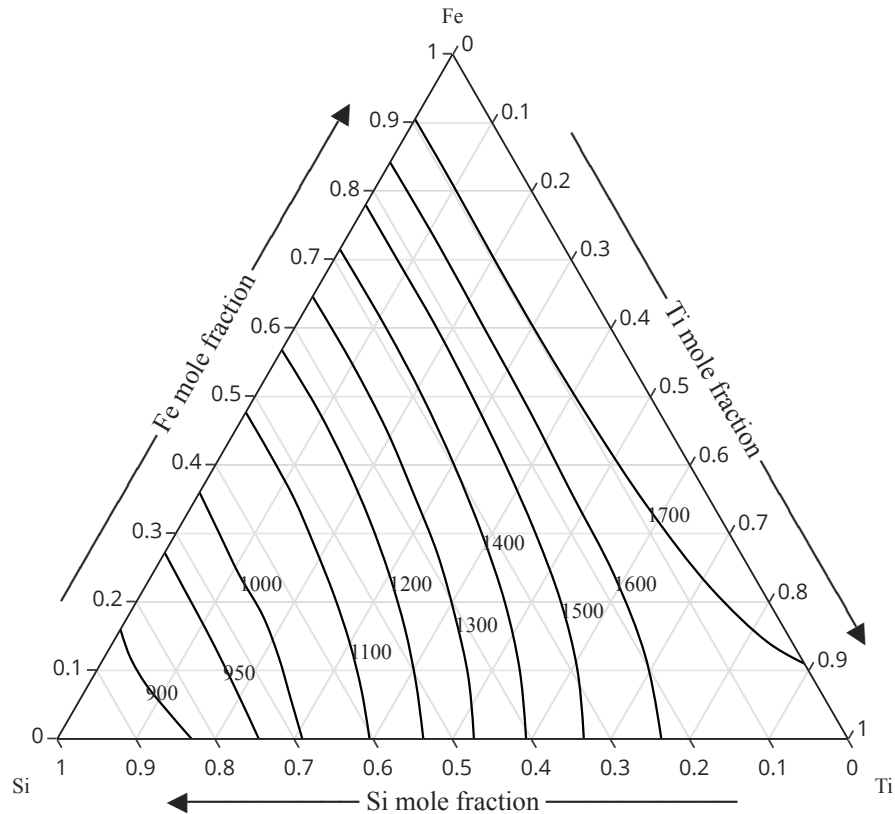


Figure 16: Iso surface tension (mN m^{-1}) lines of Fe–Si–Ti liquid ternary alloys at 1873 K.

Table 10: Surface tension of Fe–Si–Ti ternary alloys from Fe corner at 1873 K

x_{Fe}	Surface Tension (N m^{-1}) of Fe–Si–Ti liquid alloys											
	$x_{\text{Si}} : x_{\text{Ti}} = 3 : 1$				$x_{\text{Si}} : x_{\text{Ti}} = 1 : 1$				$x_{\text{Si}} : x_{\text{Ti}} = 1 : 3$			
	Chou	Toop	Kohler	Butler	Chou	Toop	Kohler	Butler	Chou	Toop	Kohler	Butler
0.1	0.995	1.002	1.002	1.004	1.277	1.289	1.288	1.283	1.578	1.594	1.592	1.602
0.2	1.046	1.055	1.055	1.057	1.304	1.324	1.322	1.320	1.580	1.606	1.605	1.615
0.3	1.107	1.115	1.116	1.118	1.343	1.364	1.367	1.365	1.595	1.624	1.629	1.633
0.4	1.182	1.186	1.190	1.192	1.396	1.414	1.422	1.420	1.622	1.649	1.660	1.658
0.5	1.272	1.273	1.278	1.283	1.460	1.473	1.485	1.485	1.657	1.678	1.693	1.688
0.6	1.375	1.374	1.381	1.390	1.533	1.540	1.555	1.558	1.696	1.711	1.726	1.721
0.7	1.490	1.487	1.495	1.507	1.612	1.615	1.628	1.633	1.736	1.745	1.757	1.753
0.8	1.611	1.609	1.614	1.623	1.692	1.693	1.702	1.703	1.775	1.779	1.786	1.781
0.9	1.731	1.730	1.732	1.729	1.770	1.770	1.773	1.769	1.810	1.811	1.813	1.809

Table 11: Surface tension of Fe–Si–Ti ternary alloys from Si corner at 1873 K

x_{Si}	Surface Tension (N m^{-1}) of Fe–Si–Ti liquid alloys.											
	$x_{\text{Ti}} : x_{\text{Fe}} = 3:1$				$x_{\text{Ti}} : x_{\text{Fe}} = 1 : 1$				$x_{\text{Ti}} : x_{\text{Fe}} = 1 : 3$			
	Chou	Toop	Kohler	Butler	Chou	Toop	Kohler	Butler	Chou	Toop	Kohler	Butler
0.1	1.675	1.688	1.689	1.699	1.691	1.710	1.723	1.721	1.695	1.706	1.720	1.716
0.2	1.580	1.606	1.605	1.615	1.551	1.579	1.589	1.585	1.534	1.540	1.555	1.558
0.3	1.459	1.488	1.485	1.488	1.407	1.430	1.435	1.433	1.380	1.381	1.391	1.397
0.4	1.324	1.345	1.343	1.341	1.269	1.284	1.285	1.286	1.242	1.244	1.249	1.252
0.5	1.188	1.202	1.200	1.198	1.145	1.156	1.156	1.159	1.125	1.133	1.134	1.134
0.6	1.067	1.077	1.076	1.078	1.044	1.055	1.055	1.057	1.034	1.046	1.046	1.043
0.7	0.976	0.984	0.984	0.986	0.969	0.981	0.982	0.979	0.966	0.980	0.980	0.974
0.8	0.916	0.923	0.923	0.921	0.917	0.928	0.929	0.921	0.918	0.928	0.929	0.921
0.9	0.880	0.883	0.884	0.876	0.881	0.886	0.886	0.877	0.881	0.885	0.885	0.878

of the ternary alloys were found to decrease as the bulk concentration of Si increased, while the surface tension of the ternary alloys increased as the bulk concentrations of Fe and Ti increased. The bulk concentration of Si is almost constant along a particular iso-surface tension line, but the bulk concentration of Fe and Ti vary significantly. This observation indicated that the surface tension of this ternary alloy system is unaffected by changing the bulk concentration of Fe and Ti for a given bulk concentration of Si. This effect appears due to the comparable values of surface tension of Fe and Ti in their pure liquid states. When the variation of surface concentration of components were studied from the Si corner, it was observed that the rate of increase of surface concentration of Si was greater than the rate of increase of bulk concentration in the range $x_{\text{Si}} < 0.4$. However, in the range $x_{\text{Si}} > 0.4$, the surface concentration increased at a slower rate than the bulk concentration (Table 6). Due to this effect, rate of increase of surface tension of the ternary alloy system was found to decrease gradually with the increase in bulk concentration of Si at all cross-sections.

The variation of surface tension of the Fe–Si–Ti liquid alloys with concentration at 1873 K from the Fe corner at three different cross-sections $x_{\text{Si}} : x_{\text{Ti}} = 3 : 1$, $1 : 1$ and $1 : 3$ are shown in Figure 17. It can be observed that the values of surface tension computed using the geometrical models are in good agreement with the values obtained using the Bulter equation at all concentrations. At the lower bulk concentration of Fe, the

Table 12: Surface tension of Fe–Si–Ti ternary alloys from Ti corner at 1873 K

x_{Ti}	Surface Tension ($N\ m^{-1}$) of Fe–Si–Ti liquid alloys											
	$x_{Fe} : x_{Si} = 3:1$				$x_{Fe} : x_{Si} = 1 : 1$				$x_{Fe} : x_{Ti} = 1 : 3$			
	Chou	Toop	Kohler	Butler	Chou	Toop	Kohler	Butler	Chou	Toop	Kohler	Butler
0.1	1.490	1.488	1.497	1.509	1.178	1.183	1.185	1.185	0.983	0.995	0.996	0.991
0.2	1.533	1.540	1.555	1.558	1.248	1.253	1.258	1.261	1.046	1.055	1.055	1.057
0.3	1.578	1.598	1.614	1.609	1.330	1.346	1.351	1.350	1.138	1.147	1.146	1.148
0.4	1.620	1.646	1.659	1.655	1.419	1.446	1.449	1.447	1.252	1.267	1.265	1.262
0.5	1.655	1.679	1.688	1.690	1.505	1.537	1.537	1.540	1.376	1.395	1.393	1.391
0.6	1.680	1.697	1.702	1.709	1.580	1.606	1.605	1.615	1.492	1.511	1.508	1.514
0.7	1.693	1.702	1.704	1.712	1.635	1.650	1.649	1.661	1.585	1.598	1.596	1.606
0.8	1.694	1.697	1.697	1.704	1.666	1.672	1.670	1.679	1.644	1.649	1.648	1.654
0.9	1.686	1.686	1.686	1.689	1.676	1.676	1.676	1.679	1.668	1.668	1.668	1.670

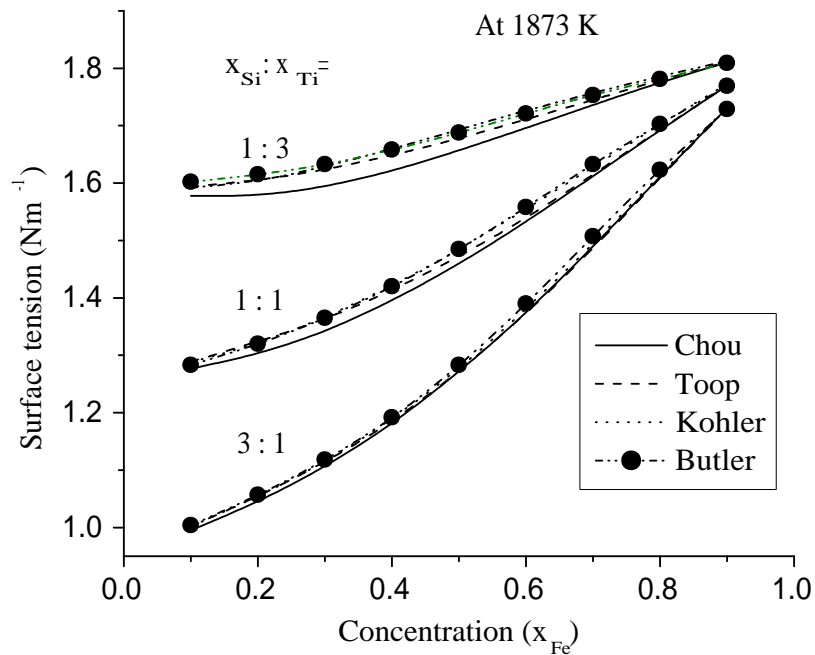


Figure 17: Variation of surface tension of Fe–Si–Ti liquid ternary alloys with bulk concentration from Fe corner.

values of surface tension of these alloys at the above mentioned cross-sections were found to be distinctly separated from each other. These graphs drawn from the Fe corner at the three cross-sections tend to intersect at a point as the bulk concentration of Fe becomes very high. The large variations in the surface tensions among the three cross-sections at lower bulk concentrations of Fe may be due to the presence of high bulk concentrations of Si and Ti having distinctly different values of surface tension. At higher bulk concentrations of Fe, the bulk concentrations of Si and Ti are negligible and hence there is a major contribution of Fe to the surface tension of this liquid ternary alloys. This is why, at very high bulk concentration of Fe, the graphs at the three cross-sections tend to coincide (Figure 17).

The variation of surface tension of the ternary alloys from the Si corner at three cross-sections is displayed in Figure 18. As the surface tension of Si is the lowest among the constituents present in this alloy, the surface tension of the alloy was found to decrease non-linearly with the increase in bulk concentration of Si. Due to the comparable values

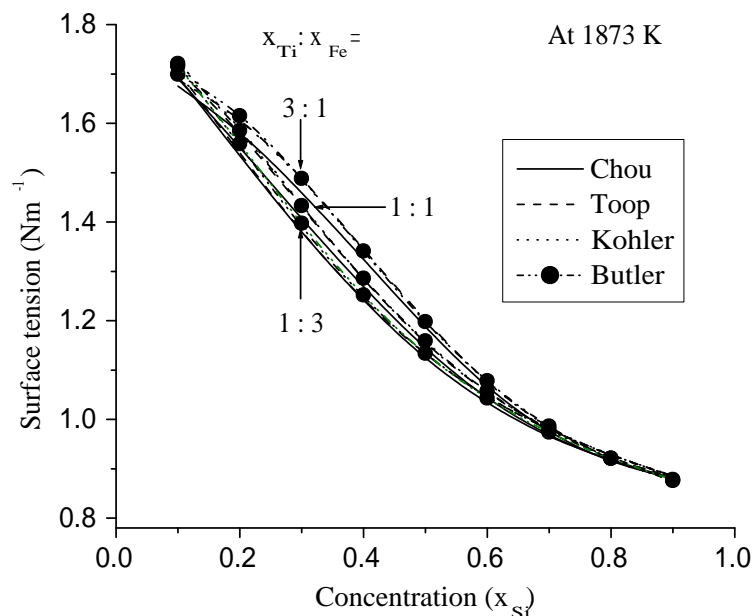


Figure 18: Variation of surface tension of Fe–Si–Ti liquid ternary alloys with bulk concentration from Si corner.

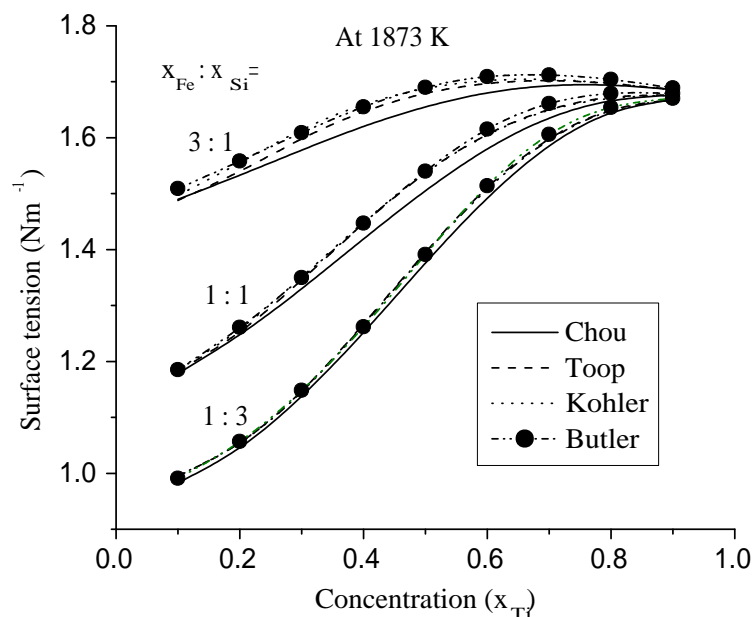


Figure 19: Variation of surface tension of Fe–Si–Ti liquid ternary alloys with bulk concentration from Ti corner at three different cross-sections.

of the surface tensions of Fe and Ti in their pure liquid states, the surface tension of the Fe–Si–Ti liquid alloys do not change significantly on shifting from one cross-section to another for a fixed bulk concentration of Si. This may be the reason why these plots tends to coincide each other (Figure 18). The variations of the surface tension of this ternary alloys from the Ti corner at all three cross-sections (Figure 19) were found to be similar to those observed from the Fe corner (Figure 17).

Table 13 shows the surface tensions of the Fe–Si–Ti liquid ternary alloys at temperatures 1873, 1973, 2073 and 2173 K for five fixed bulk concentrations and are depicted graphically in Figure 20. It can be observed that the surface tension of the liquid ternary alloys were decreased linearly with the increase in temperature at all the compositions. The temperature coefficient of surface tension ($\partial\sigma/\partial T$) was found to change from $-0.000386 \text{ N m}^{-1}\text{K}^{-1}$ (less that that of Fe) to $-0.00026 \text{ N m}^{-1}\text{K}^{-1}$ (more than that of Ti) at the two bulk compositions $x_{\text{Fe}} : x_{\text{Si}} : x_{\text{Ti}} = 90 : 8 : 2$ and $x_{\text{Fe}} : x_{\text{Si}} : x_{\text{Ti}} = 2 : 8 : 90$. The value of $\partial\sigma/\partial T$ was found to be the same ($-0.00013 \text{ N m}^{-1}\text{K}^{-1}$

Table 13: Variation of surface tension of Fe–Si–Ti liquid alloys with temperature

Temperature (K)	Surface Tension (N m^{-1}) at Bulk concentrations $x_{\text{Fe}} : x_{\text{Si}} : x_{\text{Ti}} =$				
	10 : 80 : 10	15 : 45 : 40	40 : 45 : 15	2 : 8 : 90	90 : 8 : 2
1873	0.919	1.182	1.252	1.666	1.723
1973	0.914	1.176	1.237	1.641	1.686
2073	0.902	1.162	1.224	1.615	1.647
2173	0.891	1.150	1.213	1.589	1.609

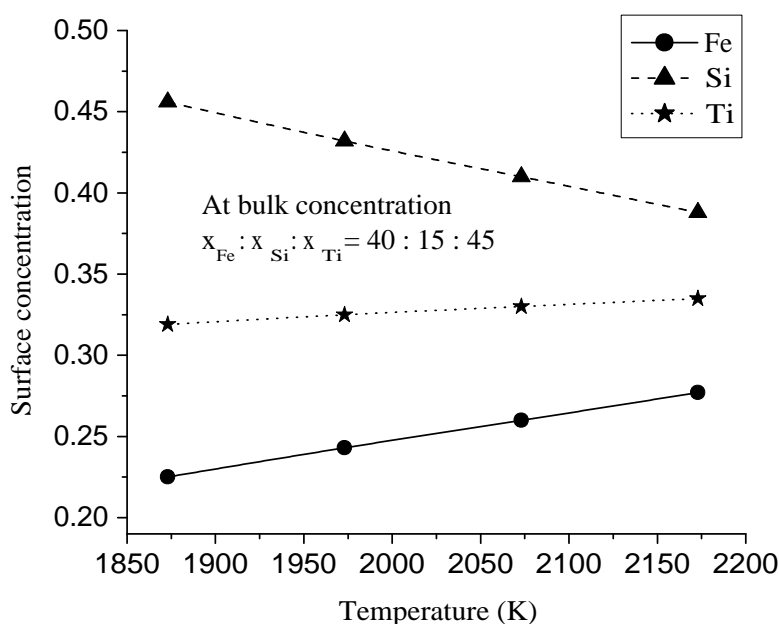


Figure 20: Variation of surface tension of Fe–Si–Ti liquid ternary alloys with temperature at five different bulk concentrations.

equal to that of pure Si) at the bulk compositions $x_{\text{Fe}} : x_{\text{Si}} : x_{\text{Ti}} = 40 : 45 : 15$ and $x_{\text{Fe}} : x_{\text{Si}} : x_{\text{Ti}} = 15 : 45 : 40$. These observations show that the value of $\partial\sigma/\partial T$ shift towards the value of Fe at its very high bulk concentration. Similarly, the value of $\partial\sigma/\partial T$ tends to shift towards the value of Ti at its very high bulk concentration provided that the maintained bulk concentration of Si was low. When the bulk concentration of Si was increased, the value of $\partial\sigma/\partial T$ tends to shift to the value of pure Si ($-0.00013 \text{ N m}^{-1}\text{K}^{-1}$). The value of $\partial\sigma/\partial T$ was found to be $-0.00012 \text{ N m}^{-1}\text{K}^{-1}$ at the bulk composition $x_{\text{Fe}} : x_{\text{Si}} : x_{\text{Ti}} = 10 : 80 : 10$. The constant value of $\partial\sigma/\partial T$ of the liquid alloys at higher bulk concentration of Si may be due to the occupation of major surface area of the liquid alloys by Si atoms. Table 6 shows that When the bulk concentration of Si was increased above 0.4, the surface concentration exceeded 0.85.

4.3 Al–Sn–Zn ternary system

Many researchers are interested in developing lead-free materials with desirable qualities due to the negative impact of lead-containing materials on human health. Sn-based binary and multi-component alloys are used to make lead-free solders (Knott et al., 2005; Prasad & Mikula, 2006b; Odusote et al., 2017). Among the various Sn-based alloys under consideration, $\text{Sn}_{91}\text{Zn}_9$ is a suitable kind of alloys for soldering purpose having a eutectic temperature of $198 \text{ }^\circ\text{C}$ (Moser et al., 1985; Ansara et al., 1998; Kamal et al., 2005; Yu et al., 2001), which is only $15 \text{ }^\circ\text{C}$ higher the traditional Sn–Pb soldering alloys. Due to the poor wettability and corrosion resistance of Sn–Zn alloys, aluminium is a suitable third element for this binary system to increase the wettability and corrosion resistance as well as to increase the oxidation resistance (Prasad & Mikula, 2006b). Steel sheets are galvanized with the Al–Zn alloys to enhance their corrosion resistance (Giorgi et al., 2018). Therefore, the Al–Sn–Zn alloys is one of the most promising substitutes for lead-free material to be used for soldering purposes.

Odusote et al. (2017) studied the activities of components in the binary subsystems of Al–Sn–Zn ternary alloys as well as the activity of Al in the ternary alloys at three cross-sections $x_{\text{Sn}} : x_{\text{Zn}} = 2 : 1, 1 : 1$ and $1 : 2$ in the temperature range of 1073 K to 1373 K . They observed that the activity of Al does not change considerably across the different molar cross-sections. Prasad & Mikula (2006a,b) investigated the G_{M}^{xs} of the ternary alloy system using GSM and Kohler model and the surface properties at three different cross-sections $x_{\text{Sn}} : x_{\text{Zn}} = 2 : 1, 1 : 1$ and $1 : 2$ using the Butler equation. They found the theoretical results to be in good agreement with the experimental data at the cross-section $x_{\text{Sn}} : x_{\text{Zn}} = 1 : 1$. Meanwhile, their theoretical results deviated somewhat positively with respect to the experimental data at the cross-sections $x_{\text{Sn}} : x_{\text{Zn}} = 2 : 1$ and $1 : 2$ but the nature of compositional variations of both the data were found similar.

They observed that the energetics of Sn–Zn is not significantly affected by the addition of Al. The surface segregation of Sn was found to be much higher than that of Al and Zn at all the above mentioned cross-sections (Prasad & Mikula, 2006b).

Gohivar et al. (2021) studied the thermodynamic, surface, and transport properties of ternary alloy system at different concentrations in the temperature range of 973 K to 1273 K. The surface properties of the ternary alloy system were computed using the Butler equation, GSM, Toop, and Kohler models. For the comparative study, the results of geometrical models have been compared with those of the Butler equation. They found that the surface tension of the alloys computed using these models was in excellent agreement when viewed from the Al corner at a very high bulk concentration of Sn. Meanwhile, some deviations were depicted among them at moderate and lower bulk concentrations of Sn.

4.3.1 Excess Gibbs free energy of mixing of Al–Sn, Al–Zn and Sn–Zn binary systems

The interaction energy parameters for G_M^{xs} of the binary subsystems Al–Sn, Sn–Zn and Al–Zn of Al–Sn–Zn liquid ternary alloys were optimised using the experimental data (Hultgren et al., 1973) of H_M and S_M^{xs} of the respective binary systems in the frame of the R-K polynomial. The temperature dependent optimised parameters of these binary systems are presented in Table 14. The theoretical values of G_M^{xs} of these binary systems were computed using Equation (3.22) with the aid of the above determined parameters and are presented in Table 15.

Table 14: Optimised coefficients of R-K polynomial for G_M^{xs} of binary subsystems of Al–Sn–Zn liquid ternary alloys

Systems	Optimised parameters (A^K) (J/mol)	
Al–Sn	A^0	16132 $-4.806T$
	A^1	3977 $-0.941T$
	A^2	2990 $-2.546T$
Al–Zn	A^0	10273 $-3.811T$
	A^1	$-204 + 1.355T$
	A^2	619 $+ 0.070T$
	A^3	$-95 - 2.166T$
Sn–Zn	A^0	12311 $-8.425T$
	A^1	$-5505 + 3.920T$
	A^2	2870 $-2.696T$

Table 15: G_M^{xs} (kJ/mol) of binary subsystems of Al–Sn–Zn liquid ternary alloys.

x_1	Al–Sn at 973 K		Sn–Zn at 750K		Al–Zn at 1000 K	
	Calculated	Expt.*	Calculated	Expt.*	Calculated	Expt.*
0.1	0.840	0.833	0.773	0.774	0.643	0.645
0.2	1.569	1.578	1.254	1.252	1.041	1.038
0.3	2.166	2.177	1.502	1.494	1.314	1.310
0.4	2.607	2.608	1.569	1.566	1.507	1.511
0.5	2.864	2.859	1.498	1.499	1.616	1.624
0.6	2.901	2.888	1.323	1.331	1.608	1.612
0.7	2.680	2.671	1.071	1.080	1.446	1.440
0.8	2.156	2.160	0.761	0.766	1.106	1.101
0.9	1.281	1.293	0.403	0.402	0.600	0.603

*Hultgren et al. (1973)

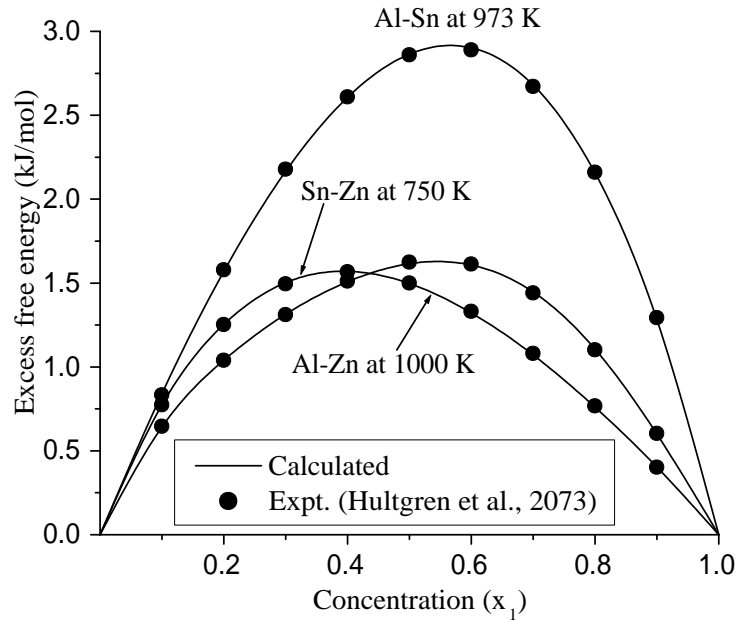


Figure 21: Variation of G_M^{xs} of binary subsystems of Al–Sn–Zn liquid alloys with concentration.

To validate the current optimisation approach, the G_M^{xs} values of binary systems were computed at temperatures for which experimental data was available. The compositional dependence of these values is displayed in Figure 21. The experimental and computed values of G_M^{xs} of Al–Sn sub-binary alloys at 973 K were found to be (2.859 ± 0.419) kJ/mol and 2.864 kJ/mol at equi-atomic composition. Likewise, the experimental and computed values of G_M^{xs} were respectively found to be (1.499 ± 0.146) kJ/mol and 1.498 kJ/mol for Sn–Zn system at 750 K and (1.624 ± 0.419) kJ/mol and 1.616 kJ/mol for Al–Zn system at 1000 K. The experimental data for all the binary systems were taken from (Hultgren et al., 1973). The values of G_M^{xs} of all the sub-binary alloys were found

positive at all the bulk concentrations, indicating they are segregating in nature (Figure 21). Moreover, the experimental and theoretical data of G_M^{xs} of these binary subsystems were found to be in well agreement at all concentrations which validate the present optimisation procedure.

4.3.2 Surface tensions of binary subsystems of Al–Sn–Zn alloys

The surface tensions of the Al–Sn, Sn–Zn and Zn–Al systems were computed using the Butler equation (Equation (3.50)). Herein, the required parameters for the process were

Table 16: Surface tension ($N\ m^{-1}$) of binary subsystems of Al–Sn–Zn liquid alloys at 973 K

Bulk concentration (x_1)	Surface tension ($N\ m^{-1}$)		
	Al–Sn	Sn–Zn	Zn–Al
0	0.518	0.734	0.900
0.1	0.530	0.674	0.871
0.2	0.543	0.638	0.848
0.3	0.558	0.613	0.828
0.4	0.574	0.593	0.811
0.5	0.593	0.576	0.796
0.6	0.615	0.562	0.782
0.7	0.642	0.549	0.768
0.8	0.679	0.538	0.756
0.9	0.739	0.527	0.745
1	0.900	0.518	0.734

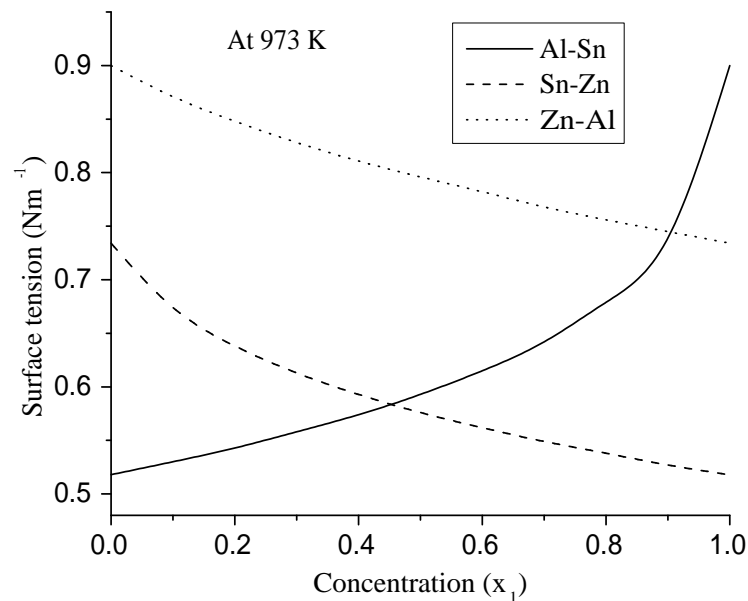


Figure 22: Variation of surface tension of binary subsystems of Al–Sn–Zn liquid alloys with bulk concentration at 973 K.

taken from Smithell Metal Reference Book (Gale & Totemeier, 2004) and are presented in the Table 3. The densities and surface tensions of the pure components of this ternary alloy system were obtained at working temperatures using Equation (3.74). The computed values of the surface tensions of these binaries at 973 K are presented in Table 16 and are plotted as a function of concentration in Figure 22. The values of surface tensions of pure Al, Sn, and Zn melts, used as the input parameters, in this work at 973 K were 0.900, 0.518, and 0.734 N m⁻¹ respectively. The surface tension value of Al, Sn and Zn employed in the work of Prasad & Mikula (2006a) were 0.89, 0.52 and 0.74 N m⁻¹ respectively. These values strongly agree with each other. As the surface tension of Al was the highest among the constituent elements, the surface tensions of Al–Sn and Zn–Al liquid alloys were found to increase with the increase in bulk concentration of Al. Experimentally measured (Goumiri et al., 1979) surface tension of the Al–Sn liquid alloys at bulk concentrations $x_{Sn} = 0.1, 0.2, 0.3$ and 0.4 were found to be 0.74, 0.69, 0.65 and 0.63 N m⁻¹ at 973 K. The maximum deviation of the experimental data with respect to the corresponding computed values presented in Table 16 is 2.4%. The graphical representation of concentration dependent of surface tension of this alloy in the work of Prasad & Mikula (2006a) was similar to the variation shown in Figure 22. The surface tension measured by Trybula et al. (2016) at bulk compositions $x_{Zn} = 0.49$ and 0.75 at 973 K was 0.80747 ± 0.00085 N m⁻¹ and 0.77675 ± 0.00175 N m⁻¹ respectively. The computed values of this alloy at same temperature and the respective compositions were found to be 0.797 and 0.762 N m⁻¹. The respective deviations of these computed values from the experimental data are 1.2 % and 1.8 %. The surface tension of the Sn–Zn liquid alloys was found to increase with the increase in bulk concentration of Zn. The surface tension of the Sn–Zn alloys estimated by Pstrus et al. (2006) at equi-atomic composition was 0.5802 ± 0.0093 N m⁻¹ at 773 K while the computed value in this work was found to be 0.590 N m⁻¹. These values agree well with each other.

4.3.3 Surface properties of Al–Sn–Zn liquid ternary alloys

4.3.3.1 Surface concentrations of components in Al–Sn–Zn liquid ternary alloys

We used GSM (Equation (3.44)) for G_M^{xs} into Equation (3.47) to calculate G_i^{xs} for the individual components of the alloys at the mentioned corners and cross-sections. The obtained data are presented in Tables 41-43 of Appendix A. These values were then used in the Butler equation (Equation (3.70)) for the calculation of the surface concentration of individual components of the system from Al, Sn, and Zn corners at three different cross-sections, 3 : 1, 1 : 1 and 1 : 3. The required parameters for the process were taken from Smithell’s Metal Reference Book (Gale & Totemeier, 2004) and presented in Table-3. Surface tension and density of individual components of these alloys at

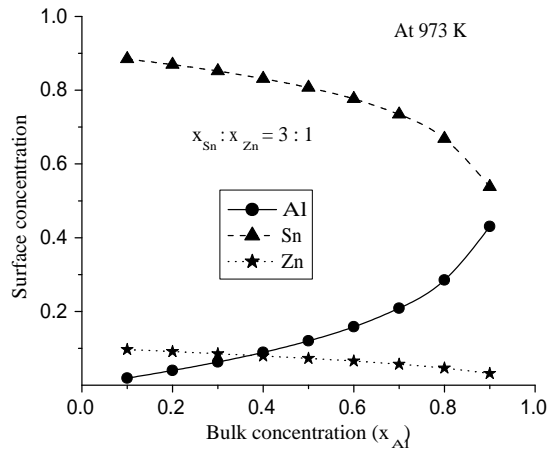
Table 17: Surface concentration of Al, Sn and Zn in Al–Sn–Zn liquid ternary alloys from Al corner at 973 K

x_{Al}	Surface Concentration								
	$x_{Sn} : x_{Zn} = 3 : 1$			$x_{Sn} : x_{Zn} = 1 : 1$			$x_{Sn} : x_{Zn} = 1 : 3$		
	Al	Sn	Zn	Al	Sn	Zn	Al	Sn	Zn
0.1	0.019	0.885	0.097	0.022	0.754	0.224	0.028	0.551	0.421
0.2	0.040	0.869	0.091	0.046	0.743	0.211	0.058	0.542	0.399
0.3	0.063	0.852	0.085	0.073	0.729	0.198	0.093	0.531	0.376
0.4	0.089	0.832	0.079	0.104	0.711	0.184	0.133	0.518	0.350
0.5	0.120	0.807	0.073	0.141	0.690	0.169	0.180	0.499	0.321
0.6	0.158	0.776	0.065	0.185	0.662	0.153	0.236	0.475	0.289
0.7	0.209	0.734	0.057	0.244	0.622	0.133	0.309	0.440	0.251
0.8	0.285	0.669	0.046	0.332	0.560	0.108	0.414	0.385	0.201
0.9	0.430	0.538	0.032	0.492	0.435	0.072	0.589	0.281	0.130

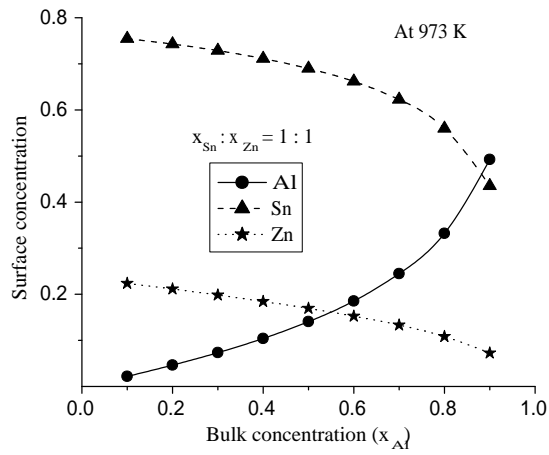
Table 18: Surface concentration of Al, Sn and Zn in Al–Sn–Zn liquid ternary alloys from Sn corner at 973 K

x_{Sn}	Surface Concentration								
	$x_{Zn} : x_{Al} = 3 : 1$			$x_{Zn} : x_{Al} = 1 : 1$			$x_{Zn} : x_{Al} = 1 : 3$		
	Al	Sn	Zn	Al	Sn	Zn	Al	Sn	Zn
0.1	0.081	0.371	0.548	0.171	0.427	0.402	0.271	0.503	0.226
0.2	0.058	0.542	0.399	0.121	0.596	0.283	0.185	0.662	0.153
0.3	0.045	0.651	0.305	0.091	0.697	0.212	0.138	0.750	0.112
0.4	0.034	0.730	0.235	0.070	0.768	0.162	0.105	0.811	0.084
0.5	0.026	0.793	0.180	0.053	0.824	0.123	0.080	0.857	0.063
0.6	0.020	0.846	0.134	0.040	0.869	0.091	0.060	0.894	0.046
0.7	0.014	0.891	0.095	0.028	0.908	0.064	0.042	0.926	0.032
0.8	0.009	0.931	0.060	0.018	0.942	0.040	0.027	0.953	0.020
0.9	0.004	0.967	0.028	0.008	0.973	0.019	0.013	0.978	0.010

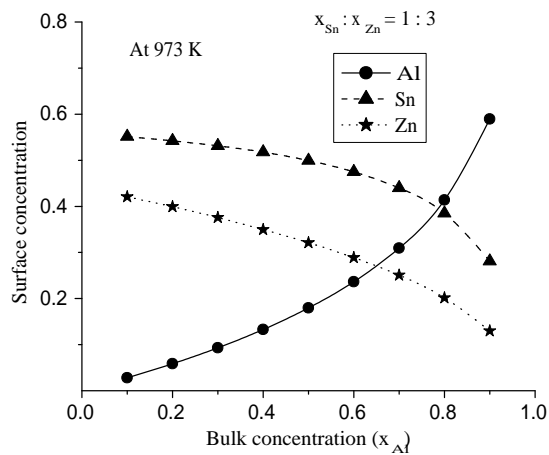
working temperature (T) were obtained using Equation (3.74) and the necessary data from Table 3. The computed surface concentrations of the components are presented in Tables 17, 18 and 19. Figure 23(a) shows the variation of surface concentrations of components with the bulk concentration from the Al corner at cross-section $x_{Sn} : x_{Zn} = 3 : 1$. It was observed that the surface concentrations of the components increased or decreased proportionally to their bulk concentrations. The surface concentration of Sn was found to be much higher than its bulk concentrations and those of Al and Zn were found to be much lower than their respective bulk concentrations at all the cross-sections (Figures 23(a-c)). Present investigations showed that the surface concentrations of Al, Sn and Zn were found to be 0.083, 0.723, and 0.194 respectively, at equi-atomic bulk concentration at 973 K. As the binary subsystems are segregating in nature, variations of surface concentrations from the Sn corner (Figures 24) or Zn corner (Figures 25) at all the cross-sections were observed to be similar to those from the Al corner. The unusual surface concentration variations observed in Fe–Si–Ti liquid ternary alloys were not



(a)



(b)



(c)

Figure 23: Variation of surface concentration of components in Al–Sn–Zn ternary alloys with bulk concentration from Al corner at three cross-sections.

Table 19: Surface concentration of Al, Sn and Zn in Al–Sn–Zn liquid ternary alloys from Zn corner at 973 K

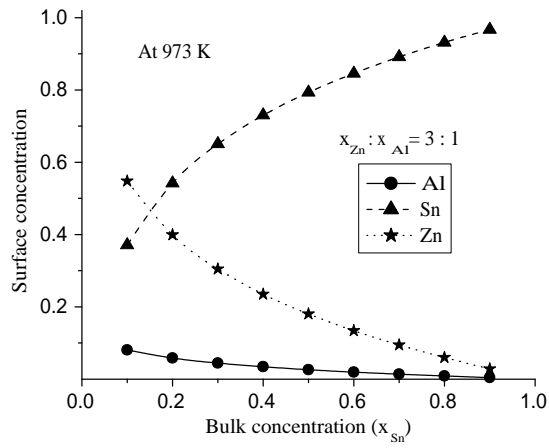
x_{Zn}	Surface Concentration								
	$x_{Al} : x_{Sn} = 3 : 1$			$x_{Al} : x_{Sn} = 1 : 1$			$x_{Al} : x_{Sn} = 1 : 3$		
	Al	Sn	Zn	Al	Sn	Zn	Al	Sn	Zn
0.1	0.201	0.724	0.075	0.100	0.846	0.053	0.043	0.914	0.044
0.2	0.185	0.662	0.153	0.093	0.796	0.111	0.040	0.869	0.091
0.3	0.169	0.598	0.233	0.086	0.742	0.172	0.036	0.821	0.143
0.4	0.151	0.532	0.317	0.077	0.683	0.239	0.033	0.766	0.201
0.5	0.131	0.463	0.406	0.068	0.617	0.314	0.029	0.705	0.266
0.6	0.110	0.388	0.502	0.058	0.542	0.399	0.025	0.633	0.342
0.7	0.086	0.307	0.606	0.047	0.454	0.499	0.021	0.546	0.433
0.8	0.061	0.218	0.720	0.035	0.346	0.618	0.016	0.434	0.550
0.9	0.033	0.119	0.848	0.020	0.207	0.773	0.009	0.276	0.715

observed in Al–Sn–Zn alloys. This may be due to the homo-coordinating nature of the individual components of the Al–Sn–Zn ternary alloy system.

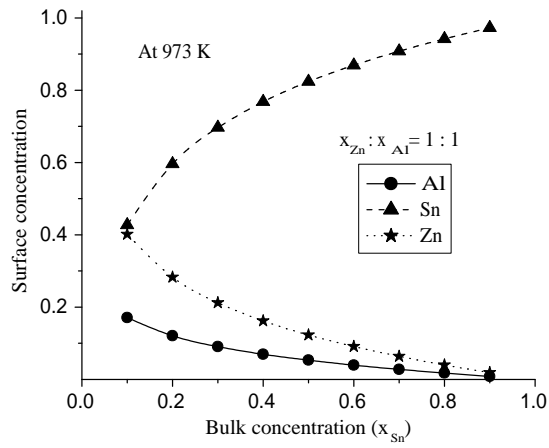
Prasad & Mikula (2006a) investigated the surface concentration of Sn in the Al–Sn–Zn liquid ternary alloys at 973 K from Al corner at cross-sections $x_{Sn} : x_{Zn} = 1 : 2$, $1 : 1$ and $2 : 1$. The graphical analysis revealed that the surface concentration of Sn decreased from 0.85 to 0.84 and increases again up to 0.85 in the range where the bulk concentration of Sn was continually decreased from 0.50 to 0.2 when viewed from the Al corner at cross-section $x_{Sn} : x_{Zn} = 1 : 1$. This down and up trend of variation of surface concentration of Sn cannot be explained on the basis of the segregating tendency of all the binary subsystems of this ternary alloys. The surface concentration of Sn was found to be decreasing continuously with the decrease in its bulk concentration when viewed from Al corner at the same cross-section (Figure 23 (b)) in this work. The rate of increase of the surface concentration of Sn was found to be much greater than the rate of increase of bulk concentration at all cross-section in the range of $x_{Sn} < 0.3$. The surface concentration of Sn increases at a slower rate than its bulk concentration when $x_{Sn} > 0.4$ which can be seen from Table 18.

The graphical study showed that the surface concentration of Sn was increased from about 0.75 to 0.92 with the change in bulk concentration of Sn from 0.33 to 0.67 in the Sn–Zn binary alloys at 973 K. Furthermore, the surface concentration of Sn was found to be about 0.85 at equi-atomic bulk concentration in the work of Prasad & Mikula (2006a) while calculated value in this work was found to be 0.723 only. The deviations between these results may be due to the input parameters used in the simplification of the Butler equation for the calculation of surface concentrations of components.

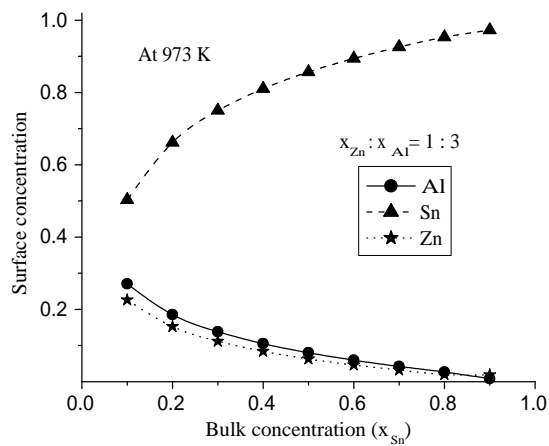
The computed values of surface concentrations at temperatures of 973, 1073, 1173, and 1273 K at equi-atomic bulk composition are presented in Table 20. The surface



(a)

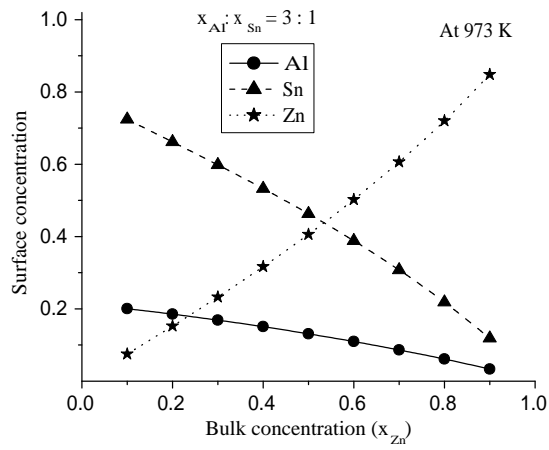


(b)

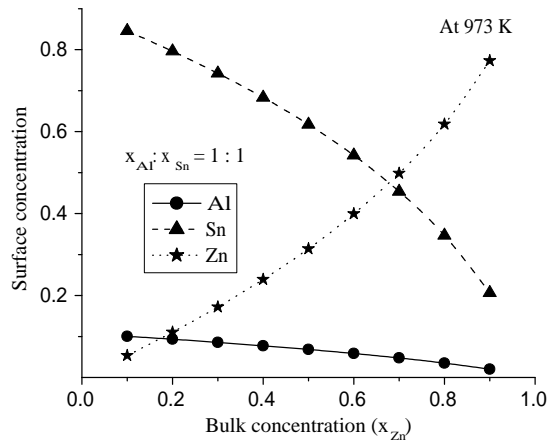


(c)

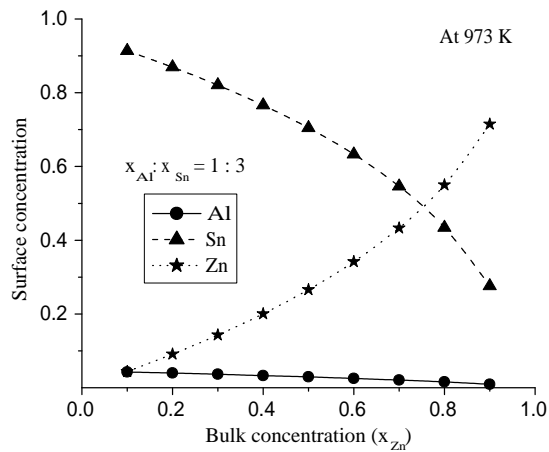
Figure 24: Variation of surface concentration of components in Al-Sn-Zn ternary alloys with bulk concentration from Sn corner at three cross-sections.



(a)



(b)



(c)

Figure 25: Variation of surface concentration of components in Al-Sn-Zn ternary alloys with bulk concentration from Zn corner at three cross-sections.

concentrations of the components Al and Zn were found to increase with increasing temperature, whereas Sn was found to decrease, as shown graphically in Figure 26. At 973 K, the surface concentrations of Al and Zn were found to be lower than their respective bulk concentrations, whereas the surface concentration of Sn was found to be much higher than its bulk concentration. It can be further observed that the surface concentrations of the components tend to approach their respective ideal values (bulk concentrations) with the increase in temperature. This may be due to the exchange of components of the liquid mixture between the surface and bulk phases to attain equilibrium, which was disturbed by the increase in temperature of the ternary alloy system, called Marangoni flow ((Tadmor, 2009; Yadav et al., 2016)). This trend of the shifting of surface concentrations towards bulk concentration at elevated temperatures reveals that liquid alloys tend to shift towards ideality.

Table 20: Surface concentration of components in Al–Sn–Zn liquid alloys at different temperature for a fixed bulk composition $x_{Al} : x_{Sn} : x_{Zn} = 0.333 : 0.333 : 0.334$.

Temperature (K)	Surface Concentration		
	Al	Sn	Zn
973	0.083	0.723	0.194
1073	0.107	0.682	0.212
1173	0.131	0.643	0.226
1273	0.154	0.608	0.238

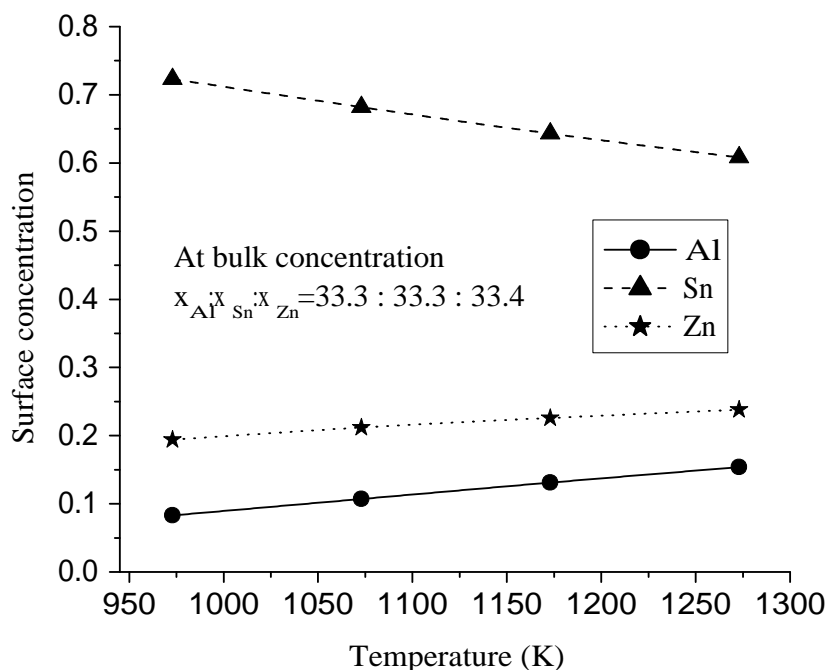


Figure 26: Variation of surface concentration of components in Al–Sn–Zn liquid ternary alloys with temperature at a fixed bulk concentration.

4.3.3.2 Surface tension of Al–Sn–Zn liquid ternary alloys

The computed values of the surface tensions of binary subsystems of Al–Sn–Zn liquid alloys using the Butler equations at temperatures of 973, 1073, 1173, and 1273 K were used to find their excess surface tensions. The excess surface tensions of the binary subsystems were used to optimise the coefficients of the R-K polynomials for excess surface tension using the least deviation method. The T-dependent optimised coefficients of R-K polynomial for excess surface tension are presented in Table 21. The surface tension of the Al–Sn–Zn liquid ternary alloys were computed at 973 K using the Chou, Toop, Kohler and the Butler equations from Al, Sn, and Zn corners at three different cross-sections 3 : 1, 1 : 1 and 1 : 3. The concentration dependent variations of excess surface tension of Sn–Zn and Zn–Al binary systems were similar to each other, while that of the Al–Sn system was found to be different. Therefore, the Zn element was selected as symmetrical element x_1 , Al was selected as x_2 and Sn as x_3 in order to apply the Toop model. The obtained data are presented in Tables (22), (23) and (24).

Table 21: Optimised coefficients of R-K polynomial for excess surface tension of binary subsystems of Al–Sn–Zn liquid ternary alloys

Systems	Optimised parameters (L^K) (N m^{-1})	
Al–Sn	L^0	$-0.949 + 5.191 \times 10^{-4}T$
	L^1	$-0.821 + 4.908 \times 10^{-4}T$
	L^2	$-1.596 + 1.102 \times 10^{-3}T$
	L^3	$-1.477 + 1.048 \times 10^{-3}T$
Al–Zn	L^0	$-0.232 + 1.524 \times 10^{-4}T$
	L^1	$-0.104 + 7.013 \times 10^{-5}T$
	L^2	$-0.066 + 4.429 \times 10^{-5}T$
	L^3	$-0.038 + 3.640 \times 10^{-5}T$
Sn–Zn	L^0	$-0.372 + 1.801 \times 10^{-4}T$
	L^1	$0.281 - 1.640 \times 10^{-4}T$
	L^2	$-0.374 + 2.578 \times 10^{-4}T$
	L^3	$0.298 - 2.147 \times 10^{-4}T$

Table 22: Surface tension of Al–Sn–Zn ternary alloys from Al corner at 973 K

x_{Al}	Surface Tension (N m^{-1}) of Al–Sn–Zn liquid alloys at 973 K											
	$x_{\text{Sn}} : x_{\text{Zn}} = 3:1$				$x_{\text{Sn}} : x_{\text{Zn}} = 1:1$				$x_{\text{Sn}} : x_{\text{Zn}} = 1:3$			
	Chou	Toop	Kohler	Butler	Chou	Toop	Kohler	Butler	Chou	Toop	Kohler	Butler
0.1	0.555	0.559	0.559	0.555	0.590	0.597	0.595	0.588	0.640	0.649	0.643	0.637
0.2	0.570	0.573	0.573	0.568	0.607	0.615	0.613	0.601	0.658	0.669	0.661	0.650
0.3	0.588	0.590	0.590	0.583	0.626	0.633	0.631	0.615	0.677	0.684	0.676	0.664
0.4	0.608	0.609	0.609	0.599	0.646	0.647	0.646	0.631	0.697	0.694	0.687	0.679
0.5	0.628	0.626	0.626	0.617	0.665	0.660	0.658	0.649	0.716	0.705	0.700	0.697
0.6	0.648	0.642	0.642	0.639	0.685	0.673	0.672	0.670	0.737	0.720	0.717	0.717
0.7	0.670	0.662	0.661	0.666	0.710	0.694	0.693	0.697	0.761	0.744	0.742	0.742
0.8	0.705	0.698	0.698	0.702	0.745	0.732	0.732	0.732	0.792	0.780	0.779	0.774
0.9	0.772	0.769	0.769	0.760	0.802	0.798	0.797	0.785	0.835	0.831	0.831	0.820

Table 23: Surface tension of Al–Sn–Zn ternary alloys from Sn corner at 973 K

x_{Sn}	Surface Tension ($N\ m^{-1}$) of Al–Sn–Zn liquid alloys at 973 K											
	$x_{Zn} : x_{Al} = 3:1$				$x_{Zn} : x_{Al} = 1 : 1$				$x_{Zn} : x_{Al} = 1 : 3$			
	Chou	Toop	Kohler	Butler	Chou	Toop	Kohler	Butler	Chou	Toop	Kohler	Butler
0.1	0.700	0.705	0.697	0.690	0.724	0.715	0.709	0.707	0.740	0.723	0.721	0.723
0.2	0.658	0.669	0.661	0.650	0.676	0.677	0.672	0.660	0.684	0.673	0.672	0.670
0.3	0.628	0.638	0.633	0.621	0.642	0.647	0.645	0.629	0.649	0.645	0.644	0.636
0.4	0.604	0.611	0.609	0.599	0.615	0.619	0.619	0.605	0.621	0.621	0.621	0.610
0.5	0.584	0.589	0.588	0.581	0.591	0.594	0.594	0.585	0.597	0.597	0.597	0.589
0.6	0.567	0.570	0.570	0.565	0.571	0.573	0.573	0.568	0.574	0.575	0.575	0.572
0.7	0.552	0.555	0.555	0.551	0.554	0.556	0.556	0.554	0.555	0.556	0.556	0.556
0.8	0.540	0.542	0.542	0.539	0.541	0.543	0.543	0.541	0.541	0.542	0.542	0.542
0.9	0.529	0.530	0.530	0.528	0.530	0.531	0.531	0.529	0.531	0.532	0.532	0.529

Table 24: Surface tension of Al–Sn–Zn ternary alloys from Zn corner at 973 K

x_{Zn}	Surface Tension ($N\ m^{-1}$) of Al–Sn–Zn liquid alloys											
	$x_{Al} : x_{Sn} = 3:1$				$x_{Al} : x_{Sn} = 1 : 1$				$x_{Al} : x_{Sn} = 1 : 3$			
	Chou	Toop	Kohler	Butler	Chou	Toop	Kohler	Butler	Chou	Toop	Kohler	Butler
0.1	0.672	0.662	0.662	0.665	0.609	0.609	0.609	0.600	0.559	0.560	0.560	0.559
0.2	0.685	0.673	0.672	0.670	0.620	0.621	0.621	0.608	0.570	0.573	0.573	0.568
0.3	0.695	0.684	0.681	0.676	0.629	0.634	0.633	0.617	0.581	0.586	0.586	0.578
0.4	0.701	0.694	0.688	0.682	0.638	0.646	0.643	0.627	0.593	0.600	0.599	0.590
0.5	0.705	0.703	0.695	0.689	0.648	0.658	0.652	0.637	0.606	0.615	0.612	0.603
0.6	0.709	0.710	0.701	0.696	0.658	0.669	0.661	0.650	0.620	0.629	0.625	0.618
0.7	0.713	0.716	0.708	0.703	0.670	0.680	0.672	0.664	0.637	0.645	0.640	0.635
0.8	0.718	0.720	0.715	0.712	0.686	0.692	0.686	0.681	0.659	0.664	0.660	0.658
0.9	0.725	0.726	0.724	0.722	0.706	0.708	0.706	0.703	0.690	0.691	0.690	0.687

The iso-surface tension lines for the Al–Sn–Zn liquid ternary alloys at 973 K is shown in Figure 27. From this figure, it can be seen that the bulk concentration of Sn was not changing significantly along a given iso-surface tension line while the bulk concentrations of Al and Zn were changing rapidly. This effect is noticed due to the fact that Sn has the lowest surface tension among the constituents of this ternary alloy system, hence the surface concentration of Sn changes considerably more rapidly than the rate at which its bulk concentration increased. The surface tension of Al and Zn were closer to each other and higher than that of Sn at 973 K. Therefore, surface tension of the ternary alloys was immune to change on changing the bulk concentration of Al and Zn at a fixed bulk concentration of Sn in the Al–Sn–Zn alloys. The surface tension variation of this ternary liquid system was shown to be more sensitive to the bulk concentration change of Sn at its lower bulk concentration. This effect is observed due to a higher rate of increase of surface concentration of Sn than the rate of increase of its bulk concentration when $x_{Sn} < 0.3$. The rate of decrease in surface tension has been observed to decrease progressively as the bulk concentration of Sn has increased.

The experimental data of surface tension of Al–Sn liquid alloys at 973 K from the work of Goumiri et al. (1979), shown using squares in the ternary plot, are in good agreement with the computed values. Similarly, the experimental data (Pstrus et al., 2006) on the

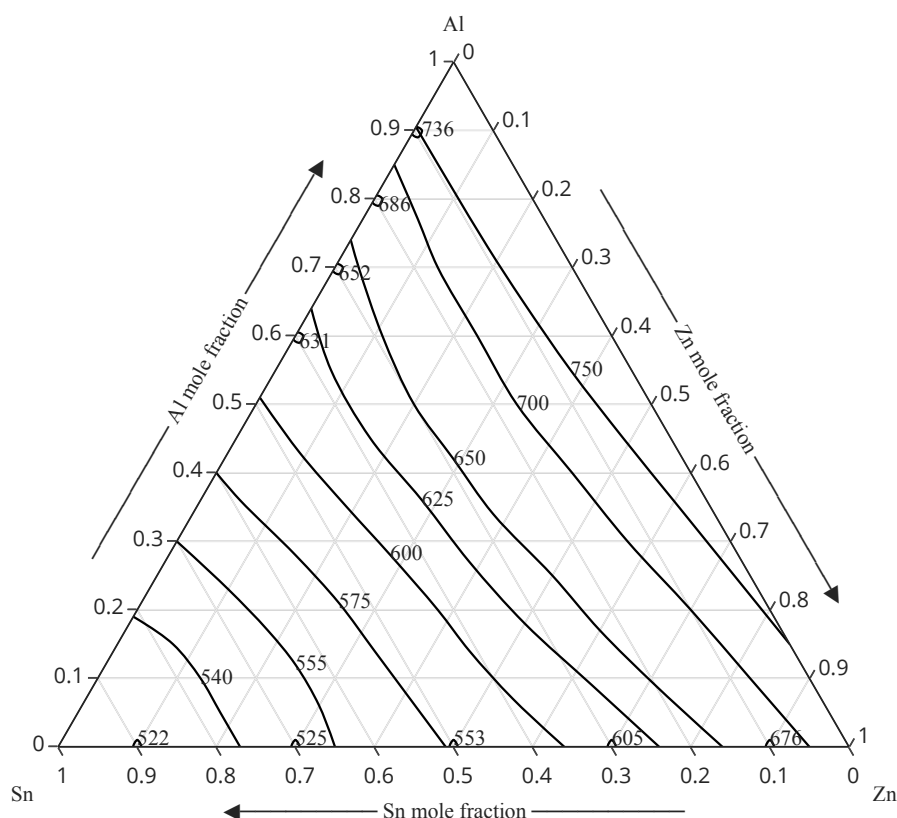


Figure 27: Iso-surface tension (mN m^{-1}) lines of Al–Sn–Zn liquid alloys at 973 K. Triangles on Sn–Zn line (Pstrus et al., 2006) and square on Al–Sn line (Goumiri et al., 1979) represent experimental data.

surface tension of the Sn–Zn liquid alloys at 973 K deviate slightly from the computed values shown in the ternary plot using triangles (Figure 27).

The variation of surface tension of the Al–Sn–Zn liquid ternary alloys at 973 K from the Al corner at three cross-sections $x_{\text{Sn}} : x_{\text{Zn}} = 3 : 1, 1 : 1$ and $1 : 3$ are shown in Figure 28. The surface tension of the liquid ternary alloys were found to increase with the increase in bulk concentrations of Al at all the three cross-sections. This effect was observed due to the highest value of surface tension of this component among the constituents of this ternary alloys at 973 K. Prasad & Mikula (2006a) studied the surface properties of these alloys and found that the surface tension of these ternary alloys were found to decrease slightly and then start to increase again at cross-section $x_{\text{Sn}} : x_{\text{Zn}} = 1 : 1$ from the Al corner. However, the surface tension was found to increase gradually and continuously in the identical condition in this work (Figure 28). When the bulk concentration of Al was increased from 0.1 to 0.9 at cross-section $x_{\text{Sn}} : x_{\text{Zn}} = 1 : 1$, the surface tension increased from 0.570 to 0.770 N m^{-1} in the work of (Prasad & Mikula, 2006a).

The value of surface tension was found to increase continuously from 0.588 to 0.785 N m^{-1} in this work. These data were found to be in appreciable agreement with each

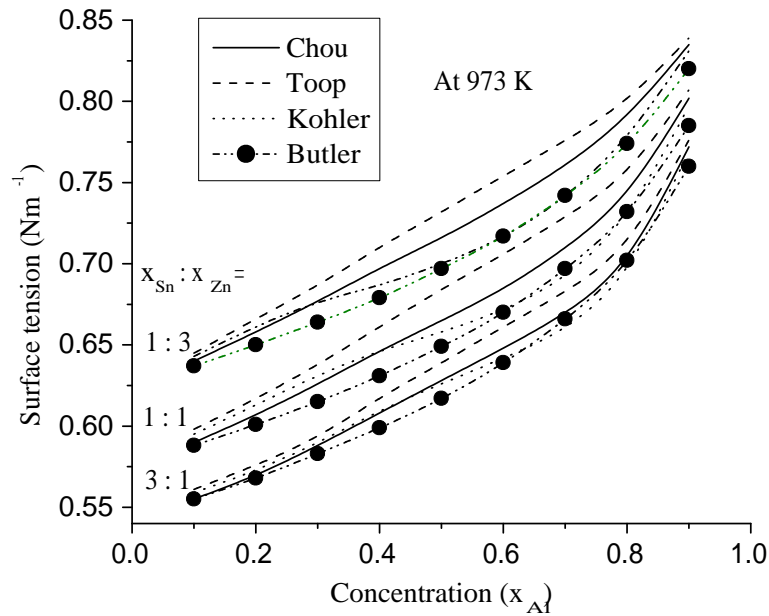


Figure 28: Variation of surface tension of Al–Sn–Zn liquid alloys at 973 K from Al corner at three different cross-sections.

other. However, slight deviation between these results may be due to the variation in the input parameters like surface tension and temperature coefficients of surface tension of the individual components present in this ternary alloy system. For a given bulk concentration of Al, the surface tension was found to be the highest at $x_{\text{Sn}} : x_{\text{Zn}} = 1 : 3$ and the least at $x_{\text{Sn}} : x_{\text{Zn}} = 1 : 3$. These observations suggest that the surface tension of each component contributes significantly to the surface tension of ternary alloys due to the effect of interaction between them.

When the variation of surface tension was observed from the Sn corner (Figure 29), the obtained curves at the cross-sections $x_{\text{Zn}} : x_{\text{Al}} = 3 : 1, 1 : 1$ and $1 : 3$ were not distinctly separated from each other as it from the Al corner (Figure 28). This graphical study showed that the surface tension does not change significantly on changing the bulk concentration of Al and Zn at a fixed concentration of Sn in the alloy. This could be due to the comparable values of surface tensions of Al and Zn at 973 K and the lowest value of surface tension of Sn in its pure state among the constituent atoms. These results show the similar result of variation of surface tension as analysed from ternary plot in Figure 27. Furthermore, the computed values of the surface tensions using the geometrical models and the Butler equation agreed well with each other and varied in a similar fashion. The maximum deviation found between the computed values of surface tensions from all chosen models was 5.4%, which was within a considerable range.

The maximum deviation between data computed using the Toop and the Butler models

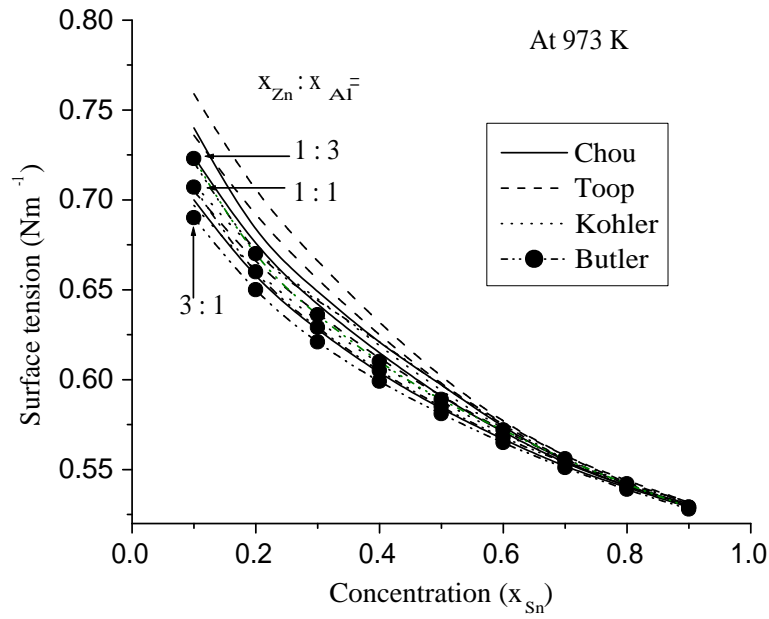


Figure 29: Variation of surface tension of Al-Sn-Zn liquid alloys at 973 K from Sn corner at three different cross-sections.

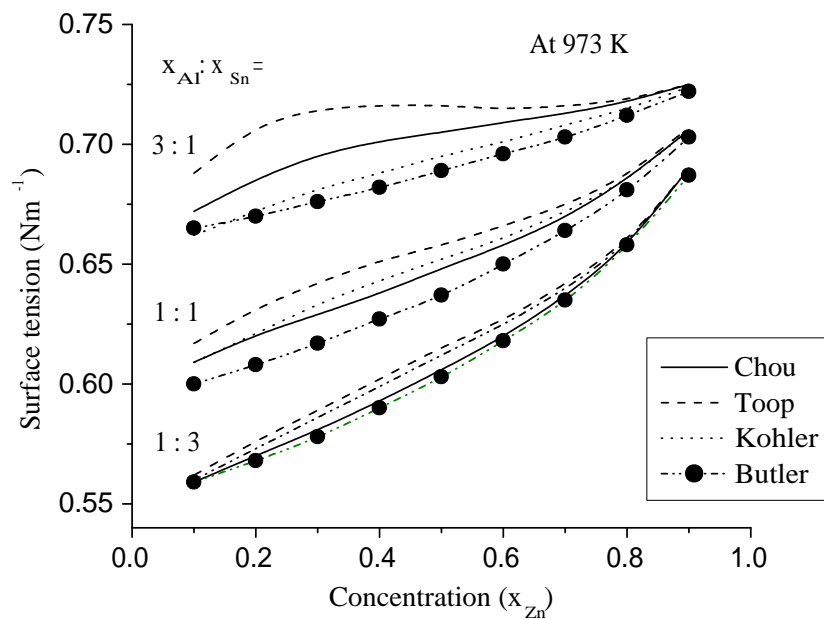


Figure 30: Variation of surface tension of Al-Sn-Zn liquid alloys at 973 K from Zn corner at three different cross-sections.

was found when observed from Sn corner. At all cross-sections, the Kohler and the Butler model yields in the smallest variation in the surface tension values computed.

The compositional dependence curves of surface tensions of this ternary alloys from Zn

corner at cross-sections $x_{Al} : x_{Sn} = 3 : 1$, $1 : 1$ and $1 : 3$ were well separated from each other which is displayed in Figure 30. This large gap in surface tension values were seen at the three cross-sections due to the greatest differential in surface tension between Al and Sn among the constituents of this alloy at 973 K. The computed values of the surface tensions using the four models agreed well with each other at cross-section $x_{Al} : x_{Sn} = 1 : 3$. The range of variation among these values was found to be relatively higher (varying from 0.559 N m^{-1} to 0.687 N m^{-1}) than those of the other two cross-sections. A maximum deviation of 2.7 % was found among the computed values of surface tension using the four geometrical models at the mentioned cross-sections.

The surface tension of the ternary alloy system was also computed at 973, 1073, 1173, and 1273 K using the Butler equation. The computed values of surface tensions at five different bulk concentrations are presented in Table 25 and plotted as a function of temperature in Figure 31. The surface tension of the alloys were found to decrease with the increase in temperature at all compositions showing the negative value of

Table 25: Surface Tension of Al–Sn–Zn liquid ternary alloys at different temperatures

Temperature (K)	Surface Tension (N m^{-1}) at Bulk concentrations $x_{Al} : x_{Sn} : x_{Zn}$				
	10 : 80 : 10	10 : 10 : 80	80 : 10 : 10	90 : 9 : 1	90 : 1 : 9
973	0.540	0.681	0.732	0.847	0.857
1073	0.532	0.662	0.724	0.824	0.829
1173	0.523	0.651	0.712	0.797	0.800
1273	0.514	0.548	0.696	0.769	0.770

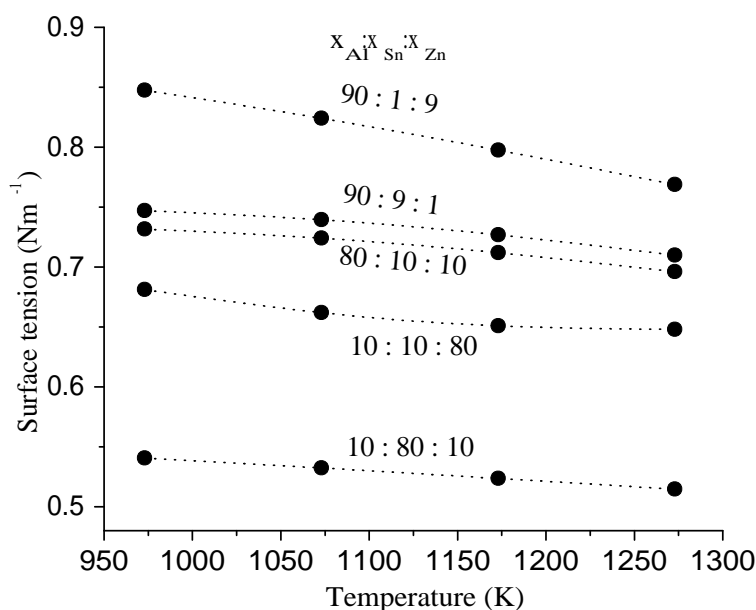


Figure 31: Variation of surface tension (N m^{-1}) of Al–Sn–Zn liquid ternary alloys with temperature (K) at five different bulk compositions.

temperature coefficients of surface tension ($\partial\sigma/\partial T$). The value of $\partial\sigma/\partial T$ was found to be $-0.000086 \text{ N m}^{-1}\text{K}^{-1}$ at $x_{\text{Al}} : x_{\text{Sn}} : x_{\text{Zn}} = 10 : 80 : 10$ in the temperature range from 973 K to 1273 K. This value of $\partial\sigma/\partial T$ in the Sn rich concentration was found to be closer to that of pure Sn ($0.000090 \text{ N m}^{-1}\text{K}^{-1}$) (Gale & Totemeier, 2004). The value of $\partial\sigma/\partial T$ was found to be $-0.00029 \text{ N m}^{-1}\text{K}^{-1}$ at composition $x_{\text{Al}} : x_{\text{Sn}} : x_{\text{Zn}} = 90 : 1 : 9$. This value of $\partial\sigma/\partial T$ in the Al rich concentration was found to be slightly less than that of pure aluminium ($-0.00035 \text{ N m}^{-1}\text{K}^{-1}$). The surface tension as well as the value of $\partial\sigma/\partial T$ of the ternary alloys have been changed significantly on interchanging the bulk concentration of Sn and Zn at constant bulk concentration of Al (at bulk compositions $x_{\text{Al}} : x_{\text{Sn}} : x_{\text{Zn}} = 90 : 9 : 1$ and $90 : 1 : 9$ in Figure 31). The value of $\partial\sigma/\partial T$ was decreased rapidly to the value of $0.00012 \text{ N m}^{-1}\text{K}^{-1}$ at the composition $x_{\text{Al}} : x_{\text{Sn}} : x_{\text{Zn}} = 10 : 80 : 10$. This large reduction in the value of $\partial\sigma/\partial T$ with the considerable decrement in bulk concentration of Al may be due to the large variation in surface concentration of Al at the two compositions. The surface concentrations of Al at the compositions $x_{\text{Al}} : x_{\text{Sn}} : x_{\text{Zn}} = 90 : 1 : 9$ and $10 : 80 : 10$ were found to be 0.68 and 0.33 respectively. The value of $\partial\sigma/\partial T$ at the Zn rich composition $x_{\text{Al}} : x_{\text{Sn}} : x_{\text{Zn}} = 10 : 10 : 80$ was found to be $0.00011 \text{ N m}^{-1}\text{K}^{-1}$ which very close to that of pure Zn ($0.00012 \text{ N m}^{-1}\text{K}^{-1}$). These values were estimated using the data presented in Table 25. These computed data reveal that the value of $\partial\sigma/\partial T$ of ternary alloys have been mainly adjusted by the surface concentrations and $\partial\sigma/\partial T$ of the components of the alloys.

4.4 Al–Cu–Fe ternary system

The first known naturally occurring quasicrystal phase is icosahedrite having the chemical composition $\text{Al}_{63}\text{Cu}_{24}\text{Fe}_{13}$ (Bindi et al., 2011) with a five-fold symmetry (Huttunen-Saarivirta, 2004) which is a forbidden symmetry for crystalline solids. Many metallic quasicrystalline materials are unsuitable for most applications due to their thermal instability. Due to the presence of dislocations in quasi-crystals, they have a variety of unique properties like exceptional brittleness and hardness, strong corrosion and oxidation resistance, high tensile strength, low frictional coefficients, and low electrical and thermal conductivity (Lityńska-Dobrzyńska et al., 2016; Babilas et al., 2020). In comparison to other systems, stable Al–Cu–Fe quasi-crystals are more popular due to their inexpensive, accessible, recyclable, and non-toxic components (Lityńska-Dobrzyńska et al., 2014). They have an icosahedral structure and are available in the range of atomic compositions of 20–28 % Cu and 10–14 % Fe and up to the temperature of 1133 K (Huttunen-Saarivirta, 2004). Tsai et al. (1987) studied the quasicrystalline phase of the Al–Cu–Fe alloys by rapid solidification and observed the formation of icosahedral

quasicrystals in the vicinity of the composition $\text{Al}_{65}\text{Cu}_{20}\text{Fe}_{15}$. Furthermore, they observed the formation of an icosahedral quasicrystalline phase in the Al–Cu–Fe alloys for a narrow composition range of 16–24 at.% Cu and 11–17 at.% Fe. S. M. Lee et al. (2001) examined the icosahedral quasicrystalline phase in the alloys $\text{Al}_{62}\text{Cu}_{25.5}\text{Fe}_{12.5}$ and $\text{Al}_{55}\text{Cu}_{25.5}\text{Fe}_{12.5}\text{Be}_7$ experimentally and observed that the icosahedral quasicrystalline phase forming ability was significantly increased when aluminium in $\text{Al}_{62}\text{Cu}_{22.5}\text{Fe}_{12.5}$ was partially replaced by 7 at.% of beryllium.

Mehta, Yadav, Koirala, & Adhikari (2020) investigated the surface properties of the ternary alloy system at various concentrations and temperatures using several theoretical approaches and found that the results obtained from the Chou model and the Butler equations were in good agreement at all compositions.

4.4.1 Excess Gibbs free energy of mixing of Al–Cu, Al–Fe and Cu–Fe binary systems

Two sets of interaction energy parameters for G_M^{xs} of Al–Cu binary alloys are available in the literature (Ansara et al., 1998; Witusiewicz et al., 2004). However, the computed values of G_M^{xs} of the Al–Cu binary liquid alloys were in good agreement with the experimental data (Hultgren et al., 1973). The computed values of G_M^{xs} of the Al–Cu binary system using the interaction energy parameters given in Witusiewicz et al. (2004) was found more closer to the experimental data and therefore these sets of T-dependent interaction energy parameters were employed in this work. The interaction energy parameters for G_M^{xs} of the Al–Fe binary liquid alloys were optimised using the experimental data (Desai, 1987) of H_M and S_M^{xs} . Similarly, the experimental data (Hultgren et al., 1973) of H_M and S_M^{xs} were used to optimise the interaction energy parameters for G_M^{xs} of the Cu–Fe binary liquid alloys. These interaction energy parameters of these three

Table 26: Optimised coefficients of R-K polynomial for G_M^{xs} of binary subsystems of Al–Cu–Fe liquid ternary alloys

Systems	Optimised parameters (A^K) (J/mol)		Ref.
Al–Cu	A^0	$-67094 + 8.555T$	(Witusiewicz et al., 2004)
	A^1	$32148 - 7.118T$	
	A^2	$5915 - 5.889T$	
	A^3	$-8175 + 6.049T$	
Al–Fe	A^0	$-78925 + 16.068T$	
	A^1	$-16314 + 5.681T$	
	A^2	$-1767 - 0.380T$	
Cu–Fe	A^0	$35621 - 2.654T$	
	A^1	$-3914 + 2.442T$	
	A^2	$7997 - 1.943T$	

binary subsystems of the Al–Cu–Fe ternary alloys are presented in Table 26. The G_M^{xs} of Al–Cu, Cu–Fe and Fe–Al were computed using these interaction energy parameter of the respective systems using Equation (3.22) and obtained data are presented in Table 27.

Both the computed and experimental values of G_M^{xs} of the binary alloys are presented in Table 27 and are plotted as a function of concentration in Figure 32. The observed and computed values of G_M^{xs} were respectively found to be (-13.724 ± 0.6320) kJ/mol (Hultgren et al., 1973) and -13.837 kJ/mol for Al–Cu system at 1373 K, $(+7.679 \pm 0.419)$ kJ/mol (Hultgren et al., 1973) and $+7.696$ kJ/mol for Cu–Fe system at 1823 K, and

Table 27: G_M^{xs} (kJ/mol) of binary subsystems of Al–Cu–Fe liquid ternary alloys.

x_1	Al–Cu at 1373 K		Cu–Fe at 1823 K		Al–Fe at 1873 K	
	Calculated	Expt.*	Calculated	Expt.*	Calculated	Expt.**
0.1	-6.723	-6.172	2.988	2.976	-4.129	-4.121
0.2	-11.133	-10.725	5.130	5.150	-7.411	-7.418
0.3	-13.577	-13.561	6.569	6.609	-9.861	-9.877
0.4	-14.379	-14.453	7.405	7.424	-11.471	-11.484
0.5	-13.837	-13.724	7.696	7.679	-12.207	-12.196
0.6	-12.230	-11.987	7.456	7.420	-12.015	-12.002
0.7	-9.815	-9.582	6.659	6.642	-10.814	-10.806
0.8	-6.828	-6.713	5.233	5.238	-8.500	-8.500
0.9	-3.489	-3.497	3.066	3.072	-4.946	-4.949

*Hultgren et al. (1973), **Desai (1987)

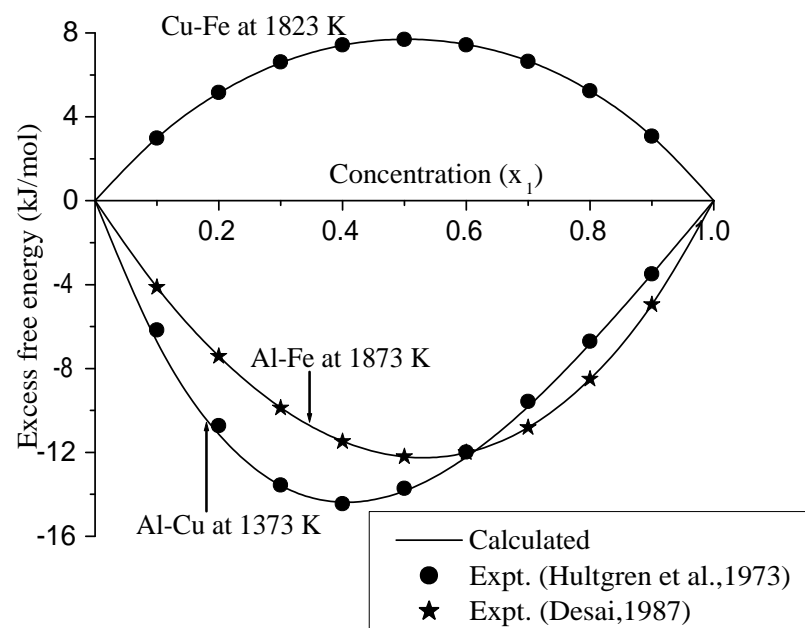


Figure 32: Variation of G_M^{xs} of binary subsystems of Al–Cu–Fe liquid alloys with concentration.

(-12.196 ± 2.5) kJ/mol (Desai, 1987) and -12.207 kJ/mol for Al–Fe system at 1873 K. These computed values agreed well with the experimental data of all the three binary systems. The extremum value of G_M^{xs} of the Al–Cu binary alloys were found to be -14.380 kJ/mol at the mole fraction concentration $x_{Al} : x_{Cu} = 0.41 : 0.59$. It can be concluded that the system preferred to form the complex Al_2Cu_3 in its solid phase at that composition. However, phase diagrams in the literature (Hultgren et al., 1973; Raghavan, 2005) show that the complexes AlCu, Al_2Cu and Al_2Cu_3 exist in the solid solution depending on the composition of components in the alloys. The maximum negative values of G_M^{xs} for the Fe–Al system was found to be -12.207 kJ/mol at the equi-atomic bulk concentration, indicating that it is ordering in nature.

Hultgren et al. (1973) reported the formation of AlFe, Al_6Fe , Al_5Fe_2 , Al_3Fe and $AlFe_3$ stable phases in solid solution of this binary alloys. The Cu–Fe binary liquid alloys were found to be segregating as the values of G_M^{xs} were found to be positive at all compositions (Figure 32) and no intermediate phase exist in the system (Ansara et al., 1998).

4.4.2 Surface tensions of binary subsystems of Al–Cu–Fe alloys

We computed the surface tensions of Al–Cu, Cu–Fe, and Fe–Al binary alloys using the Butler equation (Equation 3.70) with the help of data taken from Gale & Totemeier (2004) and presented in Table 3 . The computed values of the surface tensions of the three sub-binaries at 1823 K are presented in Table 28. These data of the surface tension are plotted as the function of bulk concentration in Figure 33. The surface tensions of Al, Cu and Fe liquid metals in their pure state at 1823 K were found to be 0.603, 1.196, and 1.865 $N m^{-1}$ respectively. As the surface tension of Al was the lowest among the constituent elements, the surface tensions of Al–Cu and Fe–Al liquid alloys decreased with the increase in bulk concentration of Al. The surface tension of the Al–Cu liquid alloys was found to change from 0.760 $N m^{-1}$ to 1.299 $N m^{-1}$ at 1373

Table 28: Surface tension ($N m^{-1}$) of binary subsystems of Al–Cu–Fe liquid alloys at 1823 K

Bulk concentration (x_1)	Surface tension ($N m^{-1}$)		
	Al–Cu	Cu–Fe	Fe–Al
0.1	1.119	1.675	0.639
0.2	1.030	1.563	0.684
0.3	0.944	1.484	0.737
0.4	0.868	1.421	0.798
0.5	0.804	1.370	0.870
0.6	0.750	1.326	0.955
0.7	0.704	1.289	1.058
0.8	0.665	1.255	1.192
0.9	0.631	1.225	1.390

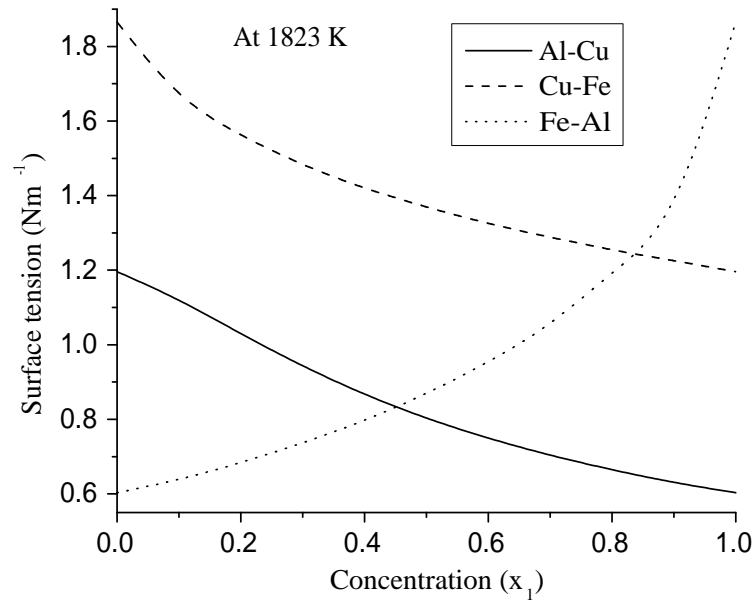


Figure 33: Variation of surface tension of binary subsystems of Al–Cu–Fe liquid ternary alloys with concentration at 1823 K.

K when the mole fraction concentration of Cu was increased from 0 to 1. Schmitz et al. (2009) investigated the surface tension of the Al–Cu liquid alloys computationally and experimentally over a wide concentration and temperature range. They reported the variation of surface tension from 0.80 to 1.31 (± 0.03) N m^{-1} at 1373 K when the bulk concentration of Cu was increased from 0 to 1. The computed values of surface tension of $\text{Al}_{90}\text{Fe}_{10}$ at 1673 K was found to be 0.690 N m^{-1} while the experimental value of 0.76 N m^{-1} was reported at this bulk composition in the work of Egry et al. (2008).

For the same composition ($\text{Al}_{90}\text{Fe}_{10}$) at 1873 K, the computed value of surface tension was found to be 0.622 N m^{-1} in this work and Yadav (2018) reported the value of 0.620 N m^{-1} . Different experimental techniques used for the measurement of the surface tensions of pure components of liquid mixtures most often show deviations. Keene (1988) averaged the twenty seven different results for surface tension of pure Fe at 1823 K and expected it to be 1.865 N m^{-1} with a standard deviation of 0.050 N m^{-1} . This value of surface tension of pure Fe agrees well with the data (Gale & Totemeier, 2004) used in this work. According to Molina et al. (2007), there was still a 25% doubt concerning the fundamental value of surface tension of aluminium and reported that the value of surface tension measured using different techniques by several experimentalists lies between 0.85 to 1.10 N m^{-1} at its melting temperature. The value of the surface tension of aluminium used in this work as input parameter is 0.914 N m^{-1} (Gale & Totemeier, 2004) at melting temperature of 933 K.

The surface tension of the Cu–Fe liquid alloys was found to decrease rapidly with the increase in bulk concentration of Cu at its lower bulk concentration. At higher bulk concentration of Cu in the alloy, the surface tension was found to decrease at lower rate with the increase in its bulk concentration. A similar variation of surface tension of the Cu–Fe binary alloys were studied by Keene (1988) in which surface tension was found to vary from 1.23 N m⁻¹ of pure Cu to 1.83 N m⁻¹ of pure Fe at 1873 K. In this work, surface tension of this alloy was found to vary from 1.184 N m⁻¹ for pure copper to 1.841 N m⁻¹ for pure Fe. The studies showed that the rate of increase of surface concentration of Cu was substantially faster than the rate at which bulk concentration was raised in the region of its lower bulk concentration in the alloy.

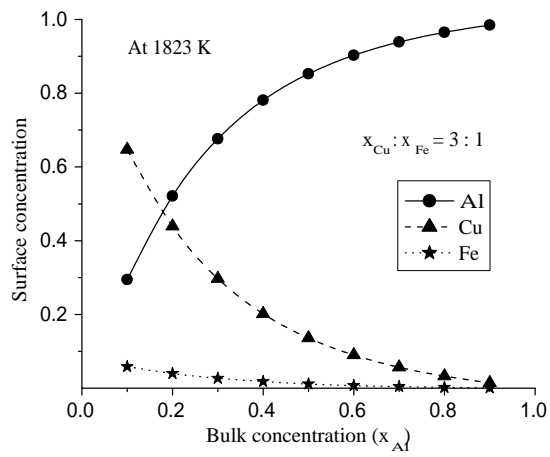
4.4.3 Surface properties of Al–Cu–Fe liquid ternary alloys

4.4.3.1 Surface concentrations of components in Al–Cu–Fe liquid ternary alloys

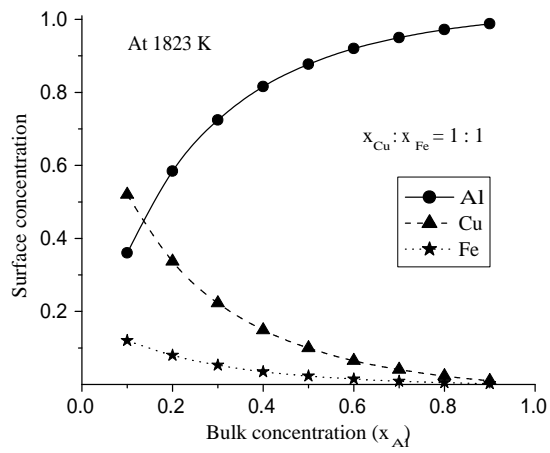
We used Equation (3.47) to compute the G_i^{xs} of components Al, Cu, and Fe of the ternary alloys from Al, Cu and Fe corners at the three cross-sections of 3 : 1, 1 : 1 and 1 : 3. These computed values are presented in Tables 44-46 of Appendix A. We computed the surface concentrations of these components from all three corners and the above mentioned cross-sections using Butler equation. These values are presented in Tables 29, 30 and 31. The variation of surface concentration of the components from Al corner at the three cross-sections are depicted in Figures 34 (a-c). When the variation of surface concentration was studied from Al corner, it was found that the surface concentrations of components increased or decreased with the increase or decrease of their respective bulk concentrations at all three cross-sections. These usual trends of variations from Al corner may be due to the identical interaction level of Al atoms with

Table 29: Surface concentration of components in Al–Cu–Fe liquid ternary alloys from Al corner at 1823 K

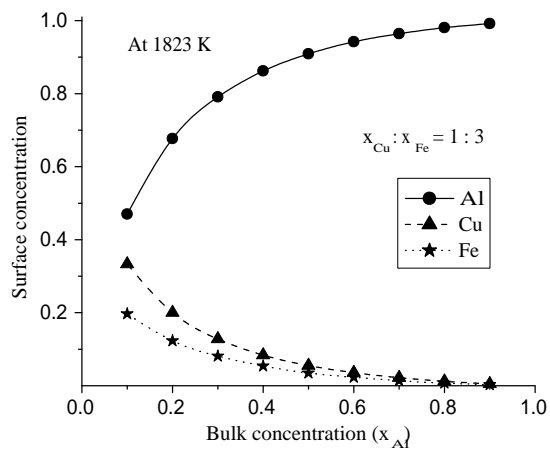
x_{Al}	Surface Concentration								
	$x_{Cu} : x_{Fe} = 3 : 1$			$x_{Cu} : x_{Fe} = 1 : 1$			$x_{Cu} : x_{Fe} = 1 : 3$		
	Al	Cu	Fe	Al	Cu	Fe	Al	Cu	Fe
0.1	0.294	0.647	0.059	0.360	0.520	0.120	0.470	0.333	0.197
0.2	0.521	0.439	0.040	0.584	0.337	0.080	0.677	0.200	0.123
0.3	0.676	0.297	0.027	0.724	0.223	0.053	0.791	0.128	0.081
0.4	0.781	0.201	0.018	0.816	0.149	0.035	0.862	0.084	0.054
0.5	0.853	0.136	0.012	0.877	0.100	0.023	0.909	0.055	0.035
0.6	0.903	0.090	0.007	0.920	0.065	0.015	0.942	0.036	0.023
0.7	0.939	0.057	0.004	0.950	0.041	0.009	0.964	0.022	0.014
0.8	0.965	0.033	0.002	0.972	0.023	0.005	0.981	0.012	0.007
0.9	0.985	0.014	0.001	0.988	0.010	0.002	0.992	0.005	0.003



(a)

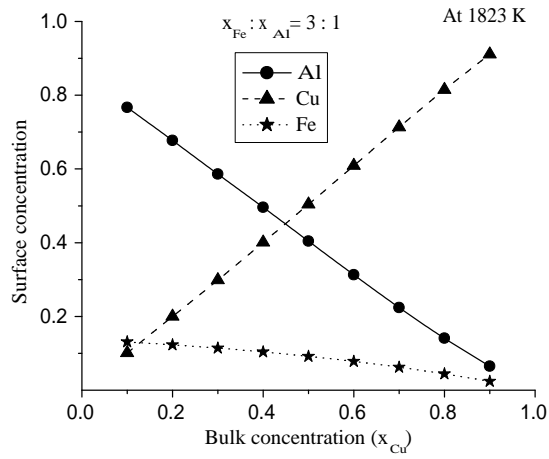


(b)

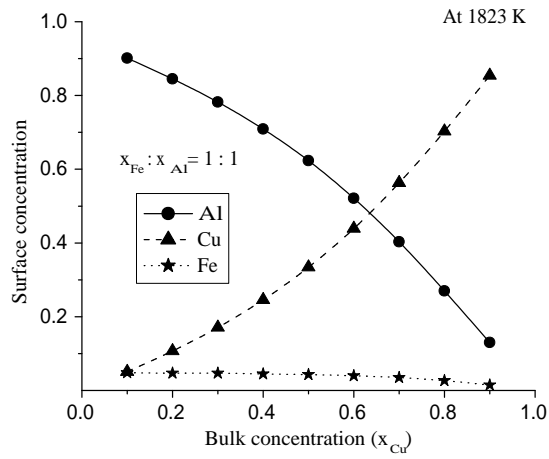


(c)

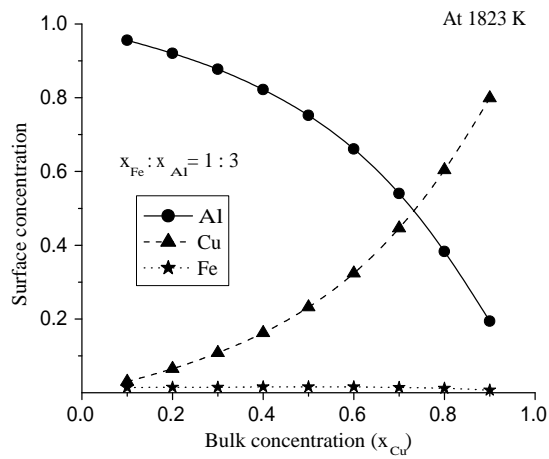
Figure 34: Variation of surface concentration of components in Al–Cu–Fe ternary alloys with bulk concentration from Al corner at three bulk concentrations.



(a)



(b)



(c)

Figure 35: Variation of surface concentration of components in Al–Cu–Fe ternary alloys with bulk concentration from Cu corner at three bulk concentrations.

Table 30: Surface concentration of components in Al–Cu–Fe liquid ternary alloys from Cu corner at 1823 K

x_{Cu}	Surface Concentration								
	$x_{Fe} : x_{Al} = 3 : 1$			$x_{Fe} : x_{Al} = 1 : 1$			$x_{Fe} : x_{Al} = 1 : 3$		
	Al	Cu	Fe	Al	Cu	Fe	Al	Cu	Fe
0.1	0.767	0.101	0.131	0.901	0.051	0.048	0.956	0.030	0.014
0.2	0.677	0.200	0.123	0.845	0.107	0.047	0.920	0.065	0.015
0.3	0.586	0.299	0.114	0.782	0.171	0.047	0.877	0.108	0.015
0.4	0.496	0.401	0.104	0.709	0.246	0.045	0.822	0.162	0.016
0.5	0.404	0.504	0.092	0.623	0.334	0.043	0.752	0.232	0.016
0.6	0.313	0.609	0.078	0.521	0.439	0.040	0.661	0.324	0.016
0.7	0.224	0.713	0.062	0.403	0.563	0.035	0.540	0.446	0.014
0.8	0.141	0.815	0.044	0.270	0.703	0.027	0.383	0.604	0.012
0.9	0.065	0.911	0.024	0.130	0.854	0.015	0.194	0.799	0.007

Table 31: Surface concentration of components in Al–Cu–Fe liquid ternary alloys from Fe corner at 1823 K

x_{Fe}	Surface Concentration								
	$x_{Al} : x_{Cu} = 3 : 1$			$x_{Al} : x_{Cu} = 1 : 1$			$x_{Al} : x_{Cu} = 1 : 3$		
	Al	Cu	Fe	Al	Cu	Fe	Al	Cu	Fe
0.1	0.933	0.060	0.006	0.814	0.176	0.010	0.545	0.436	0.019
0.2	0.920	0.065	0.015	0.791	0.185	0.024	0.521	0.439	0.040
0.3	0.904	0.070	0.026	0.767	0.193	0.040	0.498	0.438	0.064
0.4	0.884	0.074	0.042	0.741	0.198	0.061	0.476	0.433	0.092
0.5	0.860	0.077	0.064	0.712	0.201	0.088	0.453	0.422	0.125
0.6	0.828	0.078	0.093	0.677	0.200	0.123	0.427	0.405	0.169
0.7	0.785	0.078	0.137	0.632	0.194	0.174	0.395	0.378	0.228
0.8	0.717	0.074	0.208	0.569	0.178	0.253	0.350	0.333	0.317
0.9	0.586	0.061	0.353	0.453	0.140	0.407	0.271	0.248	0.481

Cu and Fe atoms in the initial melt. The surface concentration of Al was found to be more than its bulk concentration, whereas that of iron was found to be much less than its bulk concentration at all compositions of the alloy. When the bulk concentration of Al was maintained low and that of Fe was high in the liquid ternary alloys, the surface concentration of Cu was found to be higher than its ideal value (bulk concentration). However, surface concentration of Cu was found less than its ideal value at high Al and low Fe content in the ternary alloys. Calculations show that the surface concentrations of Cu were found to be 0.404 and 0.090 at compositions $x_{Al} : x_{Cu} : x_{Fe} = 10 : 30 : 60$ and $60 : 30 : 10$ respectively at 1823 K. The bulk concentration and surface concentration of Cu were found almost same when observed from the Cu corner at the cross-section $x_{Fe} : x_{Al} = 3 : 1$. Surface mole fraction concentration of Al, Cu and Fe was found to be 0.759, 0.195, and 0.046 respectively at equi-atomic bulk composition at 1823 K. The surface tension of Al was the least ($\sigma_{Al} = 0.602 \text{ N m}^{-1}$) and that of Fe was the highest ($\sigma_{Fe} = 1.865 \text{ N m}^{-1}$) among the constituent elements while the surface tension of pure

Cu ($\sigma_{\text{Cu}} = 1.196 \text{ N m}^{-1}$) has the intermediate value. These observations suggest that the component having a lower value of surface tension segregates more on the surface phase of the alloy.

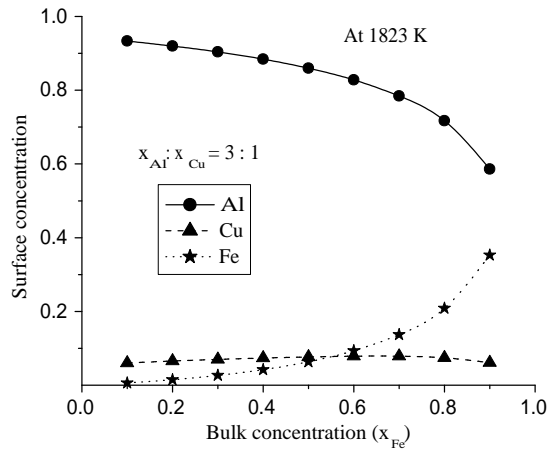
When the variation of surface concentration was studied from Cu corner at cross-sections $x_{\text{Fe}} : x_{\text{Al}} = 3 : 1$ and $1 : 1$ (Figures 35 (a, b)), the surface concentration of Al and Fe was found to decrease and that of Cu was increase. This is due to the increase in the bulk concentration of Cu and the decrease in the bulk concentrations of Fe and Al. These kinds of variations in surface concentrations with bulk concentration of components are termed as usual trends. When the variation was observed at cross-section $x_{\text{Fe}} : x_{\text{Al}} = 1 : 3$ (Figure 35 (c)), the surface concentration of Fe was found to be increasing at a very slow rate from 0.014 to 0.016 in the region where the bulk concentration of Fe had been decreased significantly from 0.225 to 0.125.

The computed values of the surface concentrations of components of the ternary alloy system at 1823 K from the Fe corner at the three cross-sections are presented in Table 31. When the variation of surface concentration was viewed from the Fe corner, the surface concentration of Al was found to decrease with decrease of its bulk concentration and the surface concentration of Fe was found to increase with increase in its bulk concentration (Figure 36).

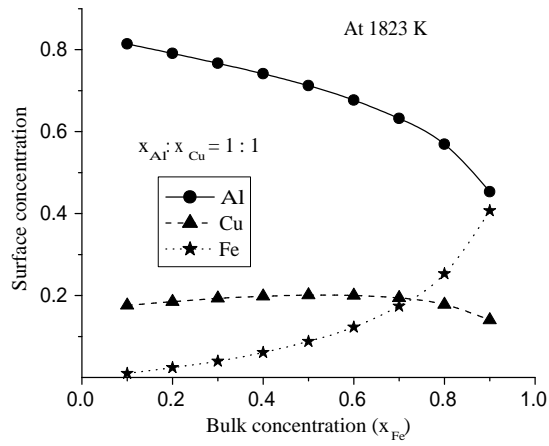
The surface concentration of Cu was found to increase in the beginning and then start to decrease, even though the bulk concentration of Cu decreased continuously in the entire range of compositions. Its value increased from 0.060 to 0.081 when its bulk concentration was decreased from 0.225 to 0.088 at cross-section $x_{\text{Al}} : x_{\text{Cu}} = 3 : 1$. When the bulk concentration of Cu was decreased from 0.450 to 0.250 at a cross-section $x_{\text{Al}} : x_{\text{Cu}} = 1 : 1$, its surface concentration increased from 0.176 to 0.201 and then decreased gradually. This unusual trend may be due to the hetero-coordinating tendency between Fe and Al atoms and the homo-coordinating tendencies between Fe and Cu.

The surface concentration of Fe was found to be much lower than its bulk concentration at all the compositions. When the bulk concentration of Fe was increased continuously, Fe atoms formed a complex with more Al atoms in the bulk phase. The surface concentration of Al decreased more rapidly, leading to a greater concentration of Cu atoms on the surface phase.

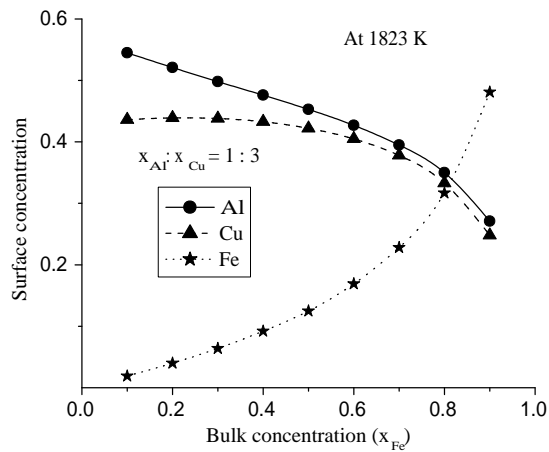
We also computed the surface concentrations of these components using the Butler equation at temperatures of 1823, 1923, 2023, and 2123 K. Table 32 contains surface concentrations of components at the above mentioned temperatures for a fixed bulk concentration of $x_{\text{Al}} : x_{\text{Cu}} : x_{\text{Fe}} = 10 : 45 : 45$. At this bulk composition, the surface concentrations of Al, Cu and Fe were found to be 0.360, 0.520 and 0.120 at 1823



(a)



(b)



(c)

Figure 36: Variation of surface concentration of components in Al–Cu–Fe ternary alloys with bulk concentration from Fe corner at three cross-sections.

Table 32: Surface concentration of components in Al–Cu–Fe liquid alloys at different temperature for a fixed bulk composition $x_{Al} : x_{Cu} : x_{Fe} = 0.1 : 0.45 : 0.45$.

Temperature (K)	Surface Concentration		
	Al	Cu	Fe
1823	0.360	0.520	0.120
1923	0.355	0.512	0.133
2023	0.350	0.504	0.146
2123	0.345	0.497	0.159

K. Figure 37 depicts the variation of surface concentrations of these components with increase in temperature at the fixed bulk composition. At this bulk composition, the surface concentration of Al was much higher than its ideal value (bulk concentration) while that of Cu was slightly higher than its ideal value. This causes to decrease the surface concentration of Al at higher rate than the rate of decrease of Cu with the increase in temperature. The surface concentration of Fe was found to be much less than its ideal value at 1873 K so that its surface concentration tends to increase at the elevated temperature. This observation revealed that the bulk concentrations of the components tend to shift toward the ideal at higher temperatures.

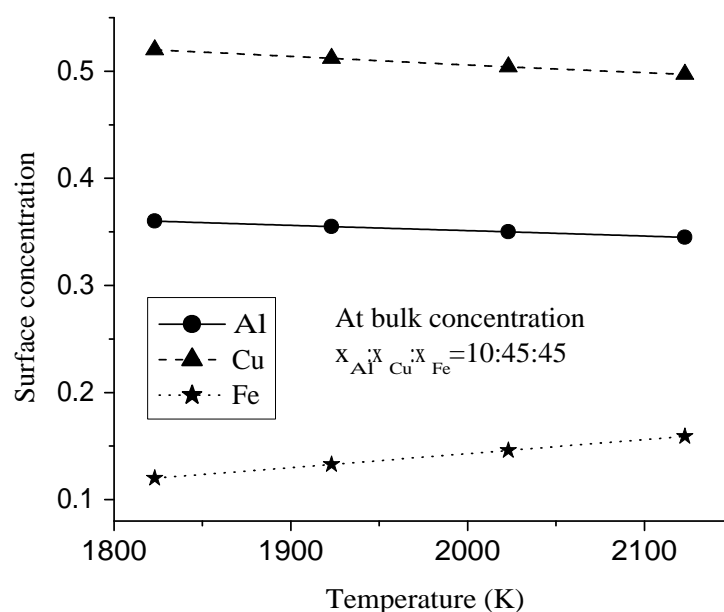


Figure 37: Variation of surface concentration of components in the Al–Cu–Fe ternary alloys with temperature at a fixed bulk concentration.

4.4.3.2 Surface tension of Al–Cu–Fe liquid ternary alloys

We computed the ideal values of the surface tensions of the binary subsystems using Equation (3.72) which was then used to find the excess surface tensions of these binary systems using Equation (3.73) at 973, 1073, 1173, and 1273 K. The computed values of excess surface tensions of the binary systems were used to optimise the T-dependent coefficients of R-K polynomials using the least deviation method and are presented in Table 33. We used these optimised parameters in Equations (3.33), (3.34) and (3.44) to compute the surface tension of the liquid ternary alloys using Kohler, Toop and Chou models respectively. In order to apply the Toop model, Cu was selected as the symmetrical element and we have chosen a bulk concentration of Cu as x_1 , Fe as x_2 and Al as x_3 for the purpose. The reasons behind these selections were the similar variations of excess surface tension of Al–Cu and Cu–Fe and different kinds of variation of excess surface tension of Fe–Al liquid alloys. We also used the Butler equation (Equation (3.70)) to calculate the surface tension of the liquid ternary alloys. The computed values of surface tensions of the ternary alloy system from Al, Cu and Fe corners and

Table 33: Optimised coefficients of R-K polynomial for excess surface tension of binary subsystems of Al–Cu–Fe liquid ternary alloys

Systems	Optimised parameters (L^K) (N m^{-1})	
Al–Cu	L^0	$-0.263 - 6.590 \times 10^{-4}T$
	L^1	$-0.248 + 1.410 \times 10^{-4}T$
	L^2	$0.430 - 1.357 \times 10^{-4}T$
	L^3	$-0.183 + 1.341 \times 10^{-4}T$
Al–Fe	L^0	$-2.116 - 3.881 \times 10^{-4}T$
	L^1	$1.565 - 3.578 \times 10^{-4}T$
	L^2	$-3.472 + 1.104 \times 10^{-3}T$
	L^3	$3.257 - 1.100 \times 10^{-3}T$
Cu–Fe	L^0	$-1.474 + 4.620 \times 10^{-4}T$
	L^1	$1.140 - 4.138 \times 10^{-4}T$
	L^2	$-1.442 + 5.812 \times 10^{-4}T$
	L^3	$1.208 - 4.997 \times 10^{-4}T$

Table 34: Surface tension of Al–Cu–Fe ternary alloys from Al corner at 1823 K

x_{Al}	Surface Tension (N m^{-1}) of Al–Cu–Fe liquid alloys											
	$x_{\text{Cu}} : x_{\text{Fe}} = 3 : 1$				$x_{\text{Cu}} : x_{\text{Fe}} = 1 : 1$				$x_{\text{Cu}} : x_{\text{Fe}} = 1 : 3$			
	Chou	Toop	Kohler	Butler	Chou	Toop	Kohler	Butler	Chou	Toop	Kohler	Butler
0.1	1.154	1.136	1.150	1.172	1.201	1.153	1.166	1.229	1.255	1.197	1.204	1.298
0.2	1.050	1.041	1.056	1.068	1.076	1.044	1.061	1.106	1.099	1.050	1.061	1.147
0.3	0.960	0.953	0.965	0.974	0.978	0.960	0.978	1.002	0.996	0.965	0.979	1.030
0.4	0.882	0.874	0.885	0.892	0.896	0.881	0.900	0.914	0.915	0.894	0.909	0.935
0.5	0.816	0.808	0.819	0.823	0.826	0.810	0.829	0.840	0.842	0.825	0.839	0.855
0.6	0.759	0.753	0.763	0.763	0.765	0.750	0.767	0.776	0.775	0.760	0.772	0.788
0.7	0.712	0.708	0.716	0.713	0.714	0.704	0.716	0.721	0.717	0.707	0.715	0.729
0.8	0.671	0.669	0.675	0.670	0.672	0.668	0.675	0.675	0.673	0.668	0.673	0.679
0.9	0.635	0.635	0.637	0.633	0.638	0.637	0.639	0.635	0.640	0.639	0.640	0.637

Table 35: Surface tension of Al–Cu–Fe ternary alloys from Cu corner at 1823 K

x_{Cu}	Surface Tension ($N m^{-1}$) of Al–Cu–Fe liquid alloys											
	$x_{Fe} : x_{Al} = 3 : 1$				$x_{Fe} : x_{Al} = 1 : 1$				$x_{Fe} : x_{Al} = 1 : 3$			
	Chou	Toop	Kohler	Butler	Chou	Toop	Kohler	Butler	Chou	Toop	Kohler	Butler
0.1	1.089	1.053	1.058	1.134	0.885	0.869	0.879	0.898	0.726	0.716	0.727	0.741
0.2	1.099	1.050	1.061	1.147	0.906	0.887	0.906	0.928	0.760	0.750	0.767	0.776
0.3	1.119	1.068	1.083	1.159	0.937	0.921	0.940	0.960	0.801	0.792	0.807	0.815
0.4	1.140	1.093	1.108	1.171	0.974	0.959	0.976	0.994	0.848	0.839	0.851	0.858
0.5	1.158	1.118	1.133	1.181	1.014	1.000	1.015	1.030	0.900	0.891	0.901	0.907
0.6	1.173	1.141	1.155	1.190	1.057	1.041	1.056	1.068	0.958	0.948	0.958	0.961
0.7	1.185	1.161	1.174	1.196	1.099	1.084	1.098	1.106	1.021	1.011	1.021	1.022
0.8	1.194	1.180	1.189	1.200	1.139	1.128	1.139	1.143	1.085	1.078	1.086	1.085
0.9	1.199	1.194	1.197	1.200	1.173	1.168	1.173	1.174	1.146	1.143	1.147	1.147

Table 36: Surface tension of Al–Cu–Fe ternary alloys from Fe corner at 1823 K

x_{Fe}	Surface Tension ($N m^{-1}$) of Al–Cu–Fe liquid alloys											
	$x_{Al} : x_{Cu} = 3 : 1$				$x_{Al} : x_{Cu} = 1 : 1$				$x_{Al} : x_{Cu} = 1 : 3$			
	Chou	Toop	Kohler	Butler	Chou	Toop	Kohler	Butler	Chou	Toop	Kohler	Butler
0.1	0.724	0.717	0.728	0.727	0.844	0.839	0.848	0.851	1.017	1.012	1.024	1.026
0.2	0.765	0.750	0.767	0.776	0.886	0.876	0.890	0.900	1.050	1.041	1.056	1.068
0.3	0.816	0.798	0.817	0.831	0.933	0.919	0.937	0.953	1.088	1.068	1.083	1.112
0.4	0.875	0.857	0.873	0.892	0.983	0.960	0.979	1.010	1.130	1.092	1.108	1.159
0.5	0.940	0.918	0.930	0.961	1.037	1.000	1.016	1.074	1.178	1.124	1.138	1.212
0.6	1.010	0.982	0.990	1.042	1.099	1.050	1.061	1.147	1.235	1.175	1.185	1.273
0.7	1.096	1.067	1.070	1.139	1.183	1.132	1.138	1.233	1.311	1.257	1.264	1.347
0.8	1.228	1.204	1.206	1.263	1.312	1.273	1.275	1.345	1.422	1.387	1.389	1.442
0.9	1.458	1.447	1.448	1.445	1.521	1.506	1.506	1.508	1.594	1.582	1.582	1.582

at cross-sections of 3 : 1, 1 : 1 and 1 : 3 using the Chou, the Toop, the Kohler and the Butler equations are presented in the Tables 34, 35, and 36. The computed values using the above mentioned modelling equations were in good agreement with each other. The maximum deviation of 8.4 % was found between the computed values using the Butler and Toop models at bulk concentration $x_{Al} : x_{Cu} : x_{Fe} = 20 : 20 : 60$.

Figure 38 depicts the concentration-dependent surface tension of this liquid ternary alloys using the iso-surface tension lines in ternary plot at 1823 K. The data used to plot the iso-surface tension lines are presented in Appendix A (Table 49). The surface tension of this liquid ternary alloys was found to be decreasing with the increase in bulk concentration of Al and increasing with the Fe content. Furthermore, the rate of change of surface tension of Al–Cu–Fe alloys were found to be decreasing gradually with the increase in bulk concentration of Al. This can be explained by comparing variations in surface concentrations of components in the alloys with changes in their bulk concentrations. When $x_{Al} < 0.3$, the surface concentration of aluminium increases at a faster rate than the bulk concentration. For example, the surface concentration of Al was found to be increased from 0 to 0.360 when its bulk concentration had been increased from 0 to 0.1 at equal contents of Cu and Fe in the alloys. Similarly, when the bulk concentration of Al was above 0.4, the surface concentration of Al was found to increase at a slower rate than the rate at which the bulk concentration was increased at all

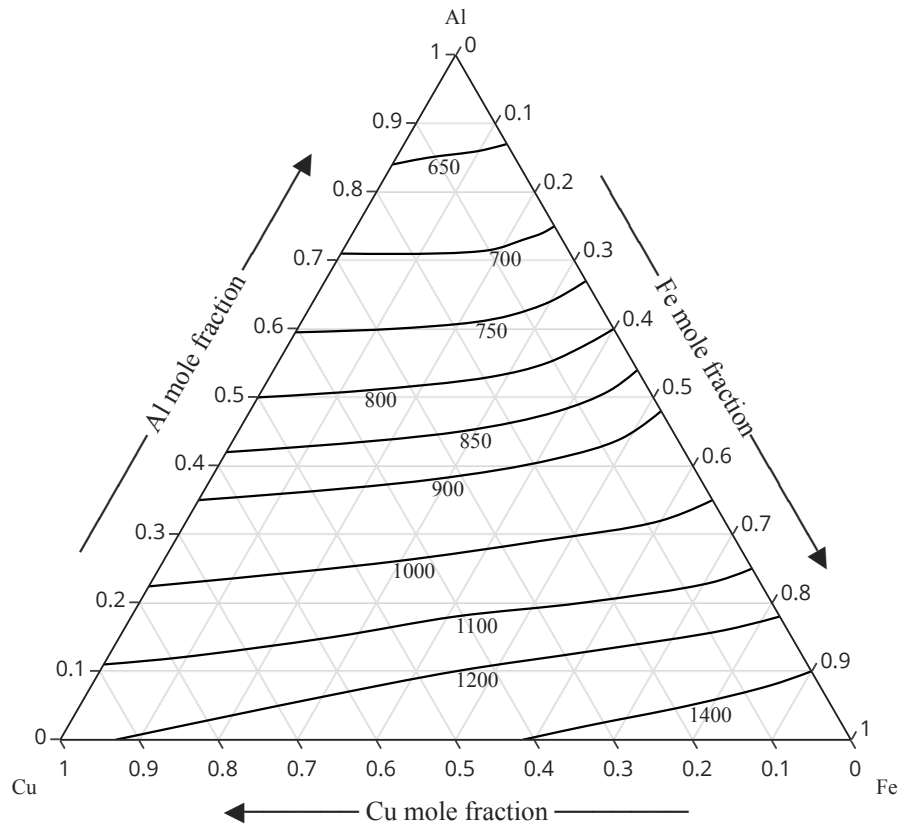


Figure 38: Iso-surface tension lines (mN m^{-1}) of Al–Cu–Fe liquid alloys at 1823 K.

three cross-sections (Table 29). This could explain why the surface tension of this alloy reduces faster at lower bulk concentrations of Al than at its higher bulk concentrations. On the specific iso-surface tension line of the ternary plot (Figure 38), bulk concentration of Al was not changing significantly while the significant change in bulk concentration of Cu and Fe were observed. For reference, the bulk concentration of Al was adjusted from 0.22 to 0.35 on the iso-surface tension line of 1000 mN m^{-1} . However, the bulk concentration of Cu was reduced from 0.776 to 0, while the bulk concentration of Fe was raised from 0 to 0.650 (Table 49 in Appendix A). This indicated that changing the bulk concentrations of Cu and Fe in the alloy for a given bulk concentration of Al had no major effect on the value of the surface tension of the alloy.

The variation of surface tension of this ternary alloys with the bulk concentration from Al corner at the above mentioned cross-sections are shown in Figure 39. The surface tension values obtained using geometrical models were found to be in good agreement with each other as well as with the computed values using the Butler equation. The results estimated using the Chou modelling equation exhibited the lowest deviation when compared to those retrieved using the Butler equation at all the cross-sections. There is no substantial change in surface tension of the ternary alloys when the bulk

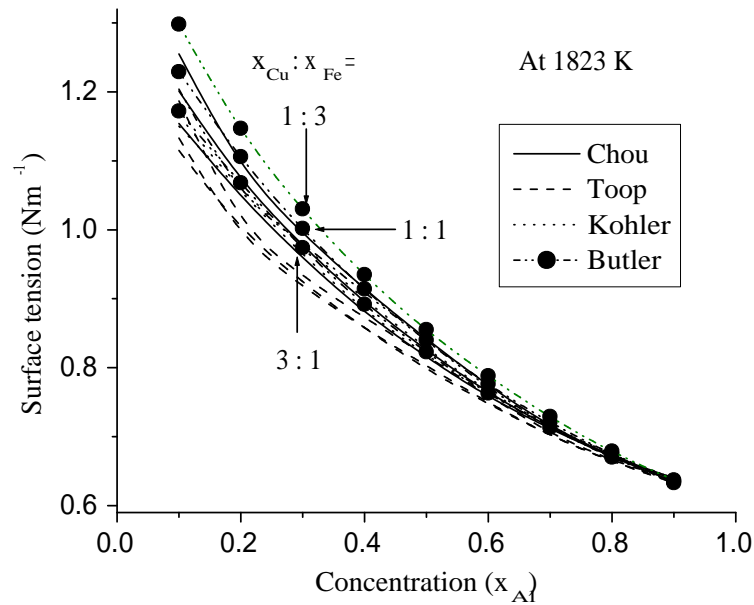


Figure 39: Variation of surface tension of Al–Cu–Fe liquid alloys at 1823 K from Al corner at three different cross-sections.

concentrations of Cu and Fe are interchanged for a given bulk concentration of Al. This is the reason why the graphs at the three cross-sections tend to coincide with each other. For a fixed concentration $x_{Al} = 0.1$, the surface tension of the Al–Cu–Fe ternary alloys were found to vary from 1.154 N m^{-1} at cross-section $x_{Cu} : x_{Fe} = 3 : 1$ to 1.255 N m^{-1} at cross-section $x_{Cu} : x_{Fe} = 1 : 3$. The difference between the computed values of surface tension at these cross-section becomes narrower and narrower with the increase of Al contents in the alloys. The rate of increase of surface concentration of Fe was much slower than the rate at which bulk concentration was raised. Due to this, at a higher bulk concentration of Al, the variation in the surface tensions between the above mentioned cross-sections gradually decreases. At very high concentration of Al, the values of surface tension coincide exactly at a point (Figure 39).

When the variation of surface tension was studied from Cu corner, the obtained graphs at three cross-sections are well separated from each other at the lower bulk concentration of Cu illustrated in Figure 40. This wide separation among these graphs may be due to the large variation in surface tension due to partial replacement of Al by Fe content in the alloys for a fixed bulk concentration of Cu. At the significantly greater bulk concentration of Cu, the surface tension was contributed by Cu only as the amount of Al and Fe were very in the alloy. As a result, these plots tend to overlap at a single point at very high bulk concentrations of Cu. Surface tensions predicted using the four modelling equations were in fair agreement at larger bulk concentrations of Al (at $x_{Fe} : x_{Al} = 1 : 3$), however, there were minor variations at higher Fe contents in the

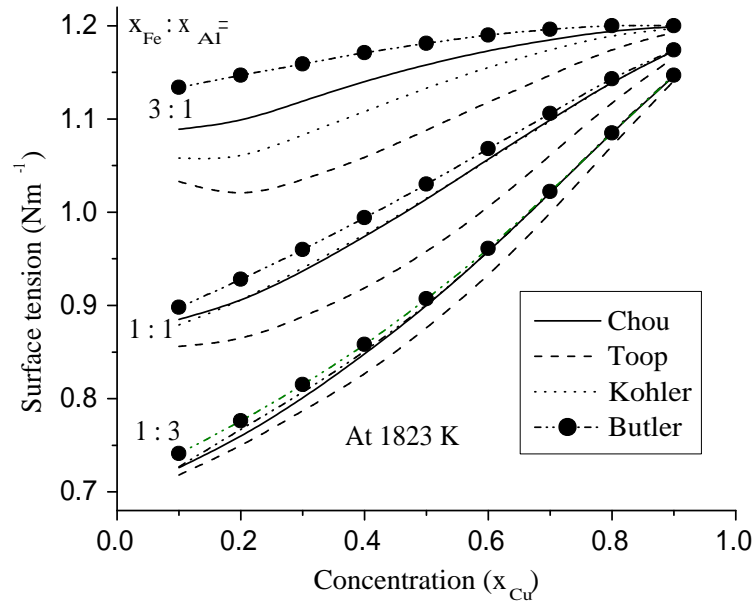


Figure 40: Variation of surface tension of Al–Cu–Fe liquid alloys at 1823 K from Cu corner at three different cross-sections.

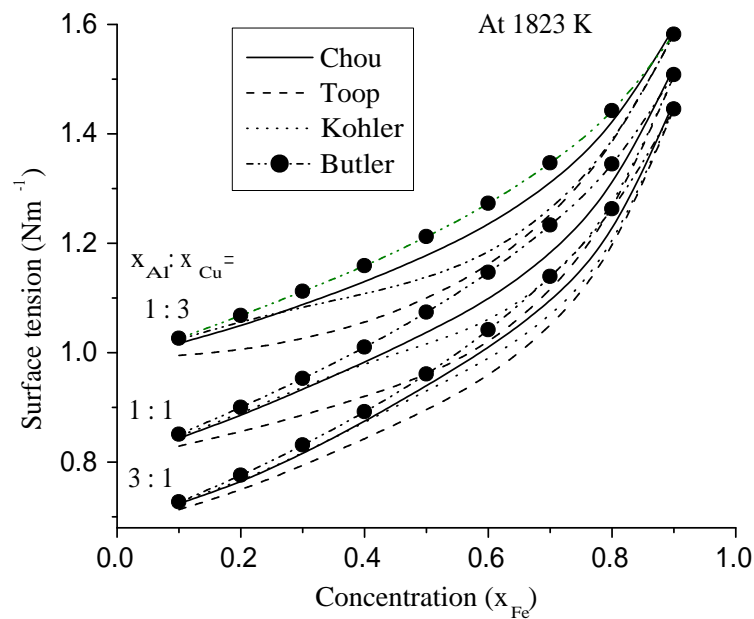


Figure 41: Variation of surface tension of Al–Cu–Fe liquid alloys at 1823 K from Fe corner at three different cross-sections.

alloy ($x_{\text{Fe}} : x_{\text{Al}} = 3 : 1$).

It can be observed that the surface tension of the alloy was found to increase at all the three cross-sections from Fe corner with the increase in its bulk concentration (Figure

41). There was some deviations in the values of surface tension computed using the preferred models. The deviation of computed values of the surface tension using the Chou model was the least in comparison to other geometrical model when compared with the data retrieved using the Butler model. However, the nature of the variance in compositional-dependence of surface tensions was uniform across all models.

The surface tension of the Al–Cu–Fe liquid ternary alloys were also calculated at 1823, 1923, 2023 and 2123 K at five fixed bulk compositions using the Chou model. The computed values of surface tension are presented in Table 37 and plotted as function of temperature in Figure 42. The surface tension of the ternary alloy system was found to decrease gradually with the increase in temperature at all compositions of the alloys. The values of $\partial\sigma/\partial T$ at compositions $x_{\text{Al}} : x_{\text{Cu}} : x_{\text{Fe}} = 80 : 10 : 10$ was found to be $-0.00034 \text{ N m}^{-1}\text{K}^{-1}$ which is slightly less than that of pure Al ($-0.00035 \text{ N m}^{-1}\text{K}^{-1}$ (Gale & Totemeier, 2004)). At this composition, computed value of the surface concentration of Al was found to be 0.970 which shows that the whole liquid

Table 37: Surface Tension of Al–Cu–Fe liquid ternary alloys at different temperatures.

Temperature (K)	Surface Tension (N m^{-1}) at Bulk concentrations $x_{\text{Al}} : x_{\text{Cu}} : x_{\text{Fe}} =$				
	10 : 10 : 80	10 : 80 : 10	40 : 20 : 40	40 : 40 : 20	80 : 10 : 10
1823	1.316	1.143	0.915	0.880	0.675
1923	1.296	1.116	0.887	0.852	0.641
2023	1.272	1.089	0.858	0.824	0.608
2123	1.247	1.062	0.828	0.796	0.574

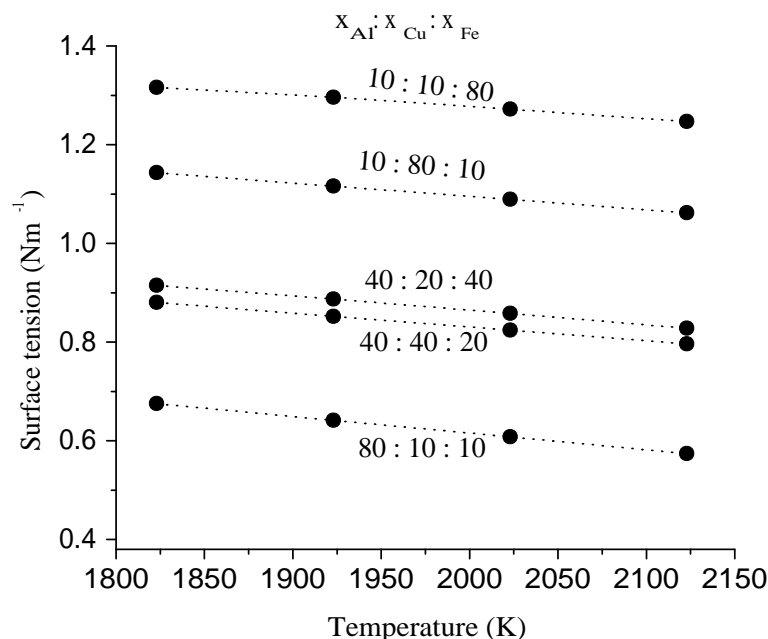


Figure 42: Variation of surface tension (N m^{-1}) of Al–Cu–Fe liquid ternary alloys with temperature at five different compositions.

surface was occupied by Al atoms only. The value of $\partial\sigma/\partial T$ at composition $x_{\text{Al}} : x_{\text{Cu}} : x_{\text{Fe}} = 10 : 10 : 80$ was estimated to be $-0.00024 \text{ N m}^{-1}\text{K}^{-1}$ and surface concentration of Fe at this composition was found to be 0.250 at 1823 K. The negative value of $\partial\sigma/\partial T$ gradually increased with increase in bulk concentration of Al. This may be due to the movement of Al atoms from the surface to the bulk phase and that of Fe atoms from the bulk to the surface phase because of the non-equilibrium conditions imposed by the increase in temperature.

CHAPTER 5

5. CONCLUSIONS AND RECOMMENDATIONS

5.1 Conclusions

The presented work is focused on the study of the effect of interaction between the atoms on the surface properties of ternary liquid alloys. For this purpose, three ternary liquid alloys Fe–Si–Ti, Al–Sn–Zn and Al–Cu–Fe ternary liquid alloys were taken under investigation. Each of these ternary alloys consist of three binary pairs and hence, there are three kinds of interaction energy involved in ternary alloys. All the binary subsystems of Fe–Si–Ti ternary liquid alloys are ordering in nature. Among them, Si–Ti binary system is strongly interacting, Fe–Si is moderately interacting and Al–Fe system is weakly interacting in nature. All the binary subsystems in the Al–Sn–Zn ternary alloys are of segregating nature. Similarly, Al–Cu and Al–Fe are of ordering nature while Cu–Fe is of segregating nature in the Al–Cu–Fe ternary liquid alloys. The Butler equation is employed for the study of surface concentration and surface tension of the sub-binaries and ternary liquid alloys close to their respective melting temperatures. To include the effect of interaction between the atoms in the surface properties of alloy, G_M^{xs} of a ternary alloy system were used for computation of partial excess free energy of mixing of the components. These data of partial excess free energies of components were then used in the Butler equation for the study of surface properties of the ternary liquid alloys.

Furthermore, geometrical models were also employed to comprehend the surface tension of the above mentioned ternary liquid alloys at different temperatures and compositions. For this purpose, temperature-dependent coefficients of R-K polynomials for excess surface tension of the binary subsystems were optimised using the data of surface tension of the respective binary alloys. These optimised parameters for excess surface tension of binary subsystems of a ternary alloys were then used in Kohler, Toop and Chou equation for computation of surface tension of that ternary alloys. Our study has led us to the following conclusions.

- i. The extent of interaction among the constituent atoms in the ternary alloy system is greatly affected by the nature of interaction between the constituent atoms in its binary subsystems. These effects are clearly observed in the surface properties of the preferred ternary alloy systems. Because of the presence of weak and strong ordering sub-binary pairs in a ternary liquid alloys, the surface concentration

of a specific component may increase in the vicinity of a decrease in its bulk concentration.

- ii. In the Fe–Si–Ti ternary alloy system, when the bulk concentration of Ti decreased from 0.225 to 0.075 at cross-section $x_{\text{Si}} : x_{\text{Ti}} = 3 : 1$, its surface concentration increased from 0.009 to 0.022. The surface tensions of the components of the ternary alloy system and its sub-binary pairs seemed to be greatly affected by the strength of interaction among the atoms resulting in above discussed remarkable fluctuation in surface concentration of Ti. As a result of having the highest value of surface tension among the constituent pairs, Fe was observed to have a surface concentration significantly lower than its bulk concentrations whereas that of Si was significantly higher than its bulk concentrations.
- iii. In ternary liquid alloys consisting of all segregating binary subsystems, the surface concentrations of the constituents atoms increased or decreased with the respective increase or decrease in their corresponding bulk concentration. From all corners and at all preferred cross-sections, it is evident that the surface concentrations of the constituents of the Al–Sn–Zn ternary liquid alloy increased or decreased with the increase or decrease in their respective bulk concentrations.
- iv. In the region of lower bulk concentrations of Al and higher bulk concentrations of Sn in Al–Sn–Zn ternary liquid alloys, the surface concentration of Zn was found to be lower than its bulk concentration. However, in the region of very high Al bulk concentrations and very low Sn bulk concentrations, it was determined to be greater than its bulk concentration.
- v. The unusual trends were observed in the compositional dependence curves of the surface concentration of the constituents of Al–Cu–Fe ternary liquid alloys. When the variation was observed at the cross-section $x_{\text{Fe}} : x_{\text{Al}} = 1 : 3$, the surface concentration of Fe was found to be increasing at a very slow rate from 0.014 to 0.016 in the region where the bulk concentration of Fe had decreased significantly from 0.225 to 0.125.
- vi. The degree of atomic interaction among the atoms of the preferred liquid ternary alloy systems decreased at the elevated temperatures and the behaviour of the solution tends to shift towards ideality. As a result, surface concentrations of the components shifted toward the ideal value and the surface tensions decreased when the temperature of the ternary alloy systems were increased.
- vii. The temperature coefficient of surface tension ($\partial\sigma/\partial T$) of liquid alloys was observed to be negative and concentration dependent at all compositions. The surface tension of the alloys were found to decrease rapidly with the increase in bulk concen-

tration of the component having the lowest value of surface tension in the vicinity of its lower bulk concentration. In this region of variation of composition of the alloys, the surface concentration of this component increases more rapidly than the rate at which bulk concentration was raised.

5.2 Recommendations of the work

This theoretical study used to assess the surface properties of the ternary alloys Fe–Si–Ti, Al–Sn–Zn and Al–Cu–Fe could not address some of the issues identified during the work in the specified time frame due to some limitations. These limitations, however, can be resolved through collaborative work. In this section, we provide some recommendations for future studies that the researchers could consider.

- i. Due to the unavailability of an experimental database, it was not possible to compare the computed values related to the surface properties of this work. Therefore, experimental techniques should be devised for the measurement of surface tension of ternary liquid alloys for comparison with the computed values. Solid ternary alloys can be prepared and their surface concentration can be estimated using the x-ray diffraction techniques.
- ii. The theoretical modeling concept used to study ternary liquid alloys can be extended to evaluate thermodynamic and surface properties of higher order liquid alloys useful to industrial and other applications.

CHAPTER 6

6. SUMMARY

As stated previously, the surface properties of three different ternary liquid alloys, including Fe–Si–Ti, Al–Sn–Zn and Al–Cu–Fe, were studied at different temperatures and concentrations. In this work, we have used the thermodynamic database of the binary subsystems to optimise the temperature-dependent interaction energy parameters for G_M^{XS} in the frame of R-K polynomial for the respective binary systems. These partial excess free energies of mixing were obtained using Chou equation, which were then used in the Butler equation for the calculation of the surface properties of the ternary alloy systems. The surface tensions of the binary liquid alloys at different temperatures (computed using the Butler equation) were used to find the excess surface tensions of the binary subsystems. These values were then used to optimise the coefficients of the R-K polynomial for excess surface tension of the respective binary systems. These optimised parameters were then used for calculation of surface tensions of the ternary liquid alloy at different temperatures and concentrations using Chou, Toop and Kohler modelling equations.

The present work can be summarised as follows:

I. Fe–Si–Ti ternary system

- a. The computed values of G_M^{XS} for Fe–Si, Si–Ti and Fe–Ti binary subsystems of Fe–Si–Ti ternary liquid alloy using the optimised parameters of this work were in excellent agreement with the experimental and literature data which were used for the optimisation.
- b. The Fe–Si and Fe–Ti binary liquid systems were found to be moderately interacting whereas the Si–Ti system was found to be strongly interacting in nature. All these binary subsystems were found to be ordering in nature at their respective melting temperatures.
- c. The surface tension of Fe–Si was found to increase with the increase in bulk concentrations of Fe whereas that of Si–Ti was found to decrease with the increase in bulk concentration of Si. The surface tension of Fe–Ti did not change significantly with the change in composition of Ti.
- d. The surface concentration of Si was found to be much higher than its bulk concentration while that of Fe and Ti were found to be lower than their respective bulk concentrations at all compositions.

- e. The surface concentration of Fe and Ti gradually increased and that of Si gradually decreased with the increase in temperature of the alloy at all compositions.
- f. The surface tension of the Fe–Si–Ti ternary liquid alloy was immune to change on interchanging the bulk concentration of Fe and Ti for a given bulk concentration Si. However, surface tension decreases rapidly with the increase in bulk concentration of Si in the vicinity of its lower bulk concentration.
- g. The surface tension of the ternary alloy system decreased linearly with the increase in temperature at all compositions. The negative value of temperature coefficients of surface tension increased with the increase in Fe contents in the ternary alloy system.

II. Al–Sn–Zn ternary system

- a. The computed values of G_M^{xs} of the binary subsystems of Al–Sn–Zn ternary liquid alloy were found to be positive at all compositions indicating them to be segregating in nature. The computed values of G_M^{xs} of these binary subsystems were in excellent agreement with their corresponding experimental data used for optimisation of the interaction energy parameters.
- b. Surface tension of Al–Sn and Al–Zn systems increased with the increase in bulk concentration of Al and that of the Sn–Zn binary system decreased with the increase in bulk concentration of Sn.
- c. The surface concentration of Al was found to be much lower than its bulk concentration and that of Sn was found to be much higher in compared to its bulk concentration at all compositions. The surface concentration of Zn was found to be lower than its bulk concentration in the region of lower bulk concentration of Al and higher bulk concentration of Sn. But, it was found to be higher than its bulk concentration in the region of very high bulk concentration of Al and very low bulk concentration Sn.
- d. The surface concentration of Al was found to be increasing while that of Sn was found to be decreasing with the increase in temperature of the alloy at all compositions.
- e. There is no significant change in surface tension of this ternary alloy on interchanging the bulk composition of Al and Zn for a given bulk concentration of Sn. At the lower value of bulk concentration of Sn, surface tension of the ternary alloy was found to increase rapidly with an increase in its bulk concentration.
- f. The surface tension of the Al–Sn–Zn alloy gradually decreased with the increase in its temperature at all compositions. The negative value of temperature

coefficients of surface tension gradually increased with the gradual increase in bulk concentration of Al of the ternary alloy system.

III. Al–Cu–Fe ternary system

- a. The computed values of G_M^{xs} for binary subsystems Al–Cu and Al–Fe were found to be negative and that of Cu–Fe binary system was found to be positive at all compositions. Among them, Al–Cu and Al–Fe were found to be moderately interacting and ordering in nature whereas Cu–Fe was found to be segregating in nature. The computed value of G_M^{xs} of these binary subsystems were in excellent agreement with their respective experimental values.
- b. The surface tensions of the Al–Cu and Fe–Al binary subsystems decreased with the increase in Al concentration. But the surface tension of Cu–Fe binary system increased with the increase in the bulk concentration of Fe.
- c. The surface concentrations of Al was found to be higher than its bulk concentration whereas the surface concentration of Fe was found to be lower than its bulk concentration at all compositions of the Al–Sn–Zn ternary liquid alloy.
- d. The surface concentration of Cu was found to be greater than its bulk concentration at lower Al and higher Fe contents. At higher bulk concentrations of Al and lower bulk concentrations of Fe, the surface concentration of Cu was found to be less than its bulk concentration.
- e. The surface concentration of Al was found to be decreasing while that of Fe was found to be increasing with the increase in temperature of the ternary alloy. There was no significant change in surface concentration of Cu at higher temperatures.
- f. The surface tension of Al–Cu–Fe ternary liquid alloy was found to increase rapidly with the increase in Fe contents and rather slowly with the increase in Cu contents in ternary alloy system. The surface tension of the alloy was found to be decreasing rapidly with the increase of Al contents in the alloy near its low concentration.
- g. The surface tension of the Al–Cu–Fe ternary alloy gradually decreased with the increase in its temperature at all preferred compositions. The negative value of the temperature coefficient of surface tension of this alloy was found to increase with a increase in bulk concentration of Al and decrease in bulk concentration of Fe.

REFERENCES

- Adhikari, D. (2011). Inhomogeneity in structure of MgPb liquid alloy. *Physica B*, 406(3), 445–448. doi: 10.1016/j.physb.2010.11.009
- Adhikari, D. (2013). *Regular associated solution model for the properties of binary liquid alloys* (PhD dissertation, T. M. Bhagalpur University, Bhagalpur, India). Retrieved from <http://103.69.125.248:8080/xmlui/handle/123456789/309>
- Adhikari, D., Jha, I. S., & Singh, B. P. (2010). Structural asymmetry in liquid Fe–Si alloys. *Philosophical Magazine*, 90(20), 2687–2694. doi: 10.1080/14786431003745302
- Adhikari, D., Singh, B. P., & Jha, I. S. (2010). Structural and energetic asymmetry in liquid Ag–Al alloys. *Physics and Chemistry of Liquids*, 48(6), 787–796. doi: 10.1080/00319101003699008
- Adhikari, D., Singh, B. P., & Jha, I. S. (2011). Concentration fluctuation in long wavelength limit in liquid magnesium alloy. *Himalayan Physics*, 2, 47–49. doi: 10.3126/hj.v2i2.5211
- Akinlade, O., & Boyo, A. (2022). Thermodynamics and surface properties of Fe–V and Fe–Ti liquid alloys. *International Journal of Materials Research*, 95(5), 387–395. doi: 10.1515/ijmr-2004-0081
- Allen, M. P., & Tildesley, D. J. (1987). *Computer simulation of liquids*. Oxford University Press.
- Ansara, I., Dinsdale, A. T., & Rand, M. H. (1998). *Thermochemical database for light metal alloys (COST 507)*. European Commission.
- Arroyave, R., Eagar, T. W., & Kaufman, L. (2003). Thermodynamic assessment of the Cu–Ti–Zr system. *Journal of Alloys and Compounds*, 351(1-2), 158–170. doi: 10.1016/S0925-8388(02)01035-6
- Arslan, H., & Dogan, A. (2019a). Determination of surface tension of liquid ternary Ni–Cu–Fe and sub-binary alloys. *Philosophical Magazine*, 99(10), 1206–1224. doi: 10.1080/14786435.2019.1576937
- Arslan, H., & Dogan, A. (2019b). Surface tension and surface tension assessment of Ag–Au–Cu ternary and sub-Binary alloy systems. In *Hysteresis of composites* (p. 77). IntechOpen. doi: 10.5772/intechopen.84701

- Babilas, R., Bajorek, A., Spilka, M., Radoń, A., & Łoński, W. (2020). Structure and corrosion resistance of Al–Cu–Fe alloys. *Progress in Natural Science: Materials International*, 30(3), 393–401. doi: 10.1016/j.pnsc.2020.06.002
- Balanetskyy, S., Pavlyuchkov, D., Velikanova, T., & Grushko, B. (2015). The Al-rich region of the Al–Fe–Mn alloy system. *Journal of Alloys and Compounds*, 619, 211–220. doi: 10.1016/j.jallcom.2014.08.232
- Belova, I. V., Ahmed, T., Sarder, U., Wang, W. Y., Kozubski, R., Liu, Z.-K., . . . Murch, G. E. (2019). Computer simulation of thermodynamic factors in Ni–Al and Cu–Ag liquid alloys. *Computational Materials Science*, 166, 124–135. doi: 10.1016/j.commatsci.2019.04.048
- Bhatia, A. B., & Hargrove, W. H. (1974). Concentration fluctuations and thermodynamic properties of some compound forming binary molten systems. *Physical Review B*, 10(8), 3186–3196. doi: 10.1103/PhysRevB.10.3186
- Bhatia, A. B., & Thornton, D. E. (1970). Structural aspects of the electrical resistivity of binary alloys. *Physical Review B*, 2(8), 3004–3012. doi: 10.1103/PhysRevB.2.3004
- Bindi, L., Steinhardt, P. J., Yao, N., & Lu, P. J. (2011). Icosahedrite, Al₆₃Cu₂₄Fe₁₃, the first natural quasicrystal. *American Mineralogist*, 96(5-6), 928–931. doi: 10.2138/am.2011.3758
- Bo, H., Duarte, L. I., Zhu, W. J., Liu, L. B., Liu, H. S., Jin, Z. P., & Leinenbach, C. (2013). Experimental study and thermodynamic assessment of the Cu–Fe–Ti system. *Calphad*, 40, 24–33. doi: 10.1016/j.calphad.2012.12.001
- Bouchard, D., & Bale, C. W. (1995). Ti–Si interactions in liquid iron. *Canadian metallurgical quarterly*, 34(4), 343–346. doi: 10.1016/0008-4433(95)00026-T
- Brillo, J., & Egry, I. (2005). Surface tension of nickel, copper, iron and their binary alloys. *Journal of Materials Science*, 40(9-10), 2213–2216. doi: 10.1007/s10853-005-1935-6
- Brillo, J., Egry, I., & Matsushita, T. (2006). Density and surface tension of liquid ternary Ni–Cu–Fe alloys. *Zeitschrift für Metallkunde*, 97(1), 28–34. doi: 10.1007/s10765-006-0121-7
- Butler, J. A. V. (1932). The thermodynamics of the surfaces of solutions. *Proceedings of the Royal Society of London*, 135(827), 348–375. doi: 10.1098/rspa.1932.0040

- Chen, H. L., Du, Y., Xu, H., & Xiong, W. (2009). Experimental investigation and thermodynamic modeling of the ternary Al–Cu–Fe system. *Journal of Materials Research*, 24(10), 3154–3164. doi: 10.1557/JMR.2009.0376
- Chou, K. C. (1987). A new solution model for predicting ternary thermodynamic properties. *Calphad*, 11(3), 293–300. doi: 10.1016/0364-5916(87)90048-4
- Chou, K. C. (1995). A general solution model for predicting ternary thermodynamic properties. *Calphad*, 19(3), 315–325. doi: 10.1016/0364-5916(95)00029-E
- Chou, K. C., & Chang, Y. A. (1989). A study of ternary geometrical models. *Berichte der Bunsengesellschaft für Physikalische Chemie*, 93(6), 735–741. doi: 10.1002/bbpc.19890930615
- Chou, K. C., Li, W. C., Li, F., & He, M. (1996). Formalism of new ternary model expressed in terms of binary regular-solution type parameters. *Calphad*, 20(4), 395–406. doi: 10.1016/S0364-5916(97)00002-3
- Chou, K. C., & Wei, S. K. (1997). A new generation solution model for predicting thermodynamic properties of a multicomponent system from binaries. *Metallurgical and Materials Transactions B*, 28(3), 439–445. doi: 10.1007/s11663-997-0110-7
- Chushak, Y. A., & Baumketner, A. (1999). Theoretical and computer simulation study of density fluctuations in liquid binary alloys. *The European Physical Journal B-Condensed Matter and Complex Systems*, 7(1), 129–136. doi: 10.1007/s100510050595
- Colinet, C. (1967). *Estimation des grandeurs thermodynamiques des alliages ternaires*. des (PhD dissertation). Université Grenoble, France.
- Costa, C., Delsante, S., Borzone, G., Zivkovic, D., & Novakovic, R. (2014). Thermodynamic and surface properties of liquid Co–Cr–Ni alloys. *Journal of Chemical Thermodynamics*, 69, 73–84. doi: 10.1016/j.jct.2013.09.034
- Desai, P. D. (1987). Thermodynamic properties of selected binary aluminum alloy systems. *Journal of Physical and Chemical Reference Data*, 16(1), 109–124. doi: 10.1063/1.555788
- Dogan, A., & Arslan, H. (2016). Geometric modelling of viscosity of copper-containing liquid alloys. *Philosophical Magazine*, 96(5), 459–472. doi: 10.1080/14786435.2015.1133938

- Dogan, A., & Arslan, H. (2018). Thermophysical properties of Cu–In–Sn liquid Pb-free alloys: viscosity and surface tension. *Philosophical Magazine*, 98(1), 37–53. doi: 10.1080/14786435.2017.1392053
- Dreval, L. A., Agraval, P. G., & Turchanin, M. A. (2018). Calorimetric investigation of the mixing enthalpy of liquid Co–Cu–Ti alloys at 1873 K. *Physics and Chemistry of Liquids*, 56(5), 674–684. doi: 10.1080/00319104.2017.1376058
- Duan, S., Shi, X., Yang, W., Guo, H., & Guo, J. (2018). Determination of thermodynamic properties in full composition range of Ti–Al binary melts based on atom and molecule coexistence theory. *Trans Nonferrous Metals Soc. China*, 28(6), 1256–1264. doi: 10.1016/S1003-6326(18)64764-8
- Egry, I., Brillo, J., Holland-Moritz, D., & Plevachuk, Y. (2008). The surface tension of liquid aluminium-based alloys. *Materials Science and Engineering: A*, 495(1-2), 14–18. doi: 10.1016/j.msea.2007.07.104
- Egry, I., Brillo, J., & Matsushita, T. (2005). Thermophysical properties of liquid Cu–Fe–Ni alloys. *Materials Science and Engineering: A*, 413, 460–464. doi: 10.1016/j.msea.2005.09.007
- Egry, I., Holland-Moritz, D., Novakovic, R., Ricci, E., Wunderlich, R., & Sobczak, N. (2010). Thermophysical properties of liquid AlTi-based alloys. *International Journal of Thermophysics*, 31(4), 949–965. doi: 10.1007/s10765-010-0704-1
- Egry, I., Ricci, E., Novakovic, R., & Ozawa, S. (2010). Surface tension of liquid metals and alloys—recent developments. *Advances in Colloid and Interface Science*, 159(2), 198–212. doi: 10.1016/j.cis.2010.06.009
- Fima, P. (2012). Surface tension and density of liquid Sn–Ag–Cu alloys. *International Journal of Materials Research*, 103(12), 1455–1461. doi: 10.3139/146.110819
- Fima, P., & Kucharski, M. (2008). The surface tension and density of Ag–Bi–Sn alloys. *International Journal of Materials Research*, 99(2), 159–161. doi: 10.3139/146.101619
- Fima, P., & Novakovic, R. (2018). Surface tension modelling of liquid Cd–Sn–Zn alloys. *Philosophical Magazine*, 98(17), 1608–1624. doi: 10.1080/14786435.2018.1448124
- Gale, W. F., & Totemeier, T. C. (2004). *Smithells metals reference book*. Elsevier Butterworth-Heinemann. Retrieved from <https://www.worldcat.org/title/smithells-metals-reference-book/oclc/50783126>

- Gibbs, J. W. (1879). On the equilibrium of heterogeneous substances. *Transactions of the Connecticut Academy of Arts and Science*, *111*, 108–248, 343–524. Retrieved from <http://www.archive.org/details/transactions03conn>
- Giorgi, M. L., Diawara, J., Rivollier, M., Duval, H., & Koltsov, A. (2018). Improvement of wettability between steel and liquid Zn–Al alloy by forced wetting. *ISIJ International*, *58*(9), 1592–1599. doi: 10.2355/isijinternational.ISIJINT-2018-147
- Gohivar, R. K., Mehta, U., Yadav, S. K., Koirala, R. P., Jha, I. S., & Adhikari, D. (2021). Thermodynamic, surface and transport properties of ternary Al–Sn–Zn liquid alloy and its sub binaries. *Philosophical Magazine*, *101*(11), 1380–1399. doi: 10.1080/14786435.2021.1912845
- Goumiri, L., Joud, J. C., Desre, P., & Hicter, J. M. (1979). Tensions superficielles d’alliages liquides binaires présentant un caractère dimmiscibilité: Al–Pb, Al–Bi, Al–Sn et Zn–Bi. *Surface Science*, *83*(2), 471–486. doi: 10.1016/0039-6028(79)90086-4
- Guggenheim, E. A. (1945). Statistical thermodynamics of the surface of a regular solution. *Transactions of the Faraday Society*, *41*, 150–156. doi: 10.1039/TF9454100150
- Guggenheim, E. A. (1952). *Mixtures*. Oxford University Press, Amen House, London.
- Han, J., Wang, W. Y., Wang, C., Wang, Y., Liu, X., & Liu, Z. (2013). Accurate determination of thermodynamic properties for liquid alloys based on ab initio molecular dynamics simulation. *Fluid Phase Equilibria*, *360*, 44–53. doi: 10.1016/j.fluid.2013.09.006
- Hillert, M. (1980). Empirical methods of predicting and representing thermodynamic properties of ternary solution phases. *Calphad*, *4*(1), 1–12. doi: 10.1016/0364-5916(80)90016-4
- Hillert, M. (1983). Application of thermodynamic models in phase diagram assessment. *Berichte der Bunsengesellschaft für Physikalische Chemie*, *87*(9), 762–769. doi: 10.1002/bbpc.19830870909
- Hoar, T. P., & Melford, D. A. (1957). The surface tension of binary liquid mixtures: lead + tin and lead + indium alloys. *Transactions of the Faraday Society*, *53*, 315–326. doi: 10.1039/TF9575300315
- Hong, B., Jiang, W., Duarte, L., Leinenbach, C., Liu, L., Liu, H., & JIN, Z. (2012). Thermodynamic re-assessment of Fe–Ti binary system. *Transac-*

- tions of Nonferrous Metals Society of China*, 22(9), 2204–2211. doi: 10.1016/S1003-6326(11)61450-7
- Hultgren, R., Desai, P. D., Hawkins, D. T., Gleiser, M., & Kelley, K. K. (1973). *Selected values of the thermodynamic properties of binary alloys*. Metal Park, Ohio: ASM.
- Huttunen-Saarivirta, E. (2004). Microstructure, fabrication and properties of quasicrystalline Al–Cu–Fe alloys: a review. *Journal of Alloys and Compounds*, 363(1-2), 154–178. doi: 10.1016/S0925-8388(03)00445-6
- Jha, I. S., Adhikari, D., & Singh, B. P. (2012). Mixing behaviour of sodium-based liquid alloys. *Physics and Chemistry of Liquids*, 50(2), 199–209. doi: 10.1080/00319104.2011.569887
- Jordan, A. S. (1970). A theory of regular associated solutions applied to the liquidus curves of the Zn–Te and Cd–Te systems. *Metallurgical Transactions*, 1(1), 239–249. doi: 10.1007/BF02819267
- Jordan, M. I., & Mitchell, T. M. (2015). Machine learning: Trends, perspectives, and prospects. *Science*, 349(6245), 255–260. doi: 10.1126/science.aaa8415
- Kamal, M., Meikhail, M. S., El-bediwi, A. B., & Gouda, E. (2005). Study of structural changes and properties for Sn–Zn₉ lead-free solder alloy with addition of different alloying elements. *Radiation Effects & Defects in Solids*, 160(1-2), 45–52. doi: 10.1080/10420150500085810
- Kaptay, G. (2004). A new equation for the temperature dependence of the excess Gibbs energy of solution phases. *Calphad*, 28(2), 115–124. doi: 10.1016/j.calphad.2004.08.005
- Kaptay, G. (2005a). A method to calculate equilibrium surface phase transition lines in monotectic systems. *Calphad*, 29(1), 56–67. doi: 10.1016/j.calphad.2005.04.004
- Kaptay, G. (2005b). Modelling interfacial energies in metallic systems. In *Materials Science Forum* (Vol. 473, pp. 1–10). doi: 10.4028/www.scientific.net/MSF.473-474.1
- Kaptay, G. (2015). Partial surface tension of components of a solution. *Langmuir*, 31(21), 5796–5804. doi: 10.1021/acs.langmuir.5b00217
- Kaptay, G. (2016). Modelling equilibrium grain boundary segregation, grain boundary energy and grain boundary segregation transition by the extended Butler

- equation. *Journal of Materials Science*, 51(4), 1738–1755. doi: 10.1007/s10853-015-9533-8
- Kaptay, G. (2017). The exponential excess Gibbs energy model revisited. *Calphad*, 56, 169–184. doi: 10.1016/j.calphad.2017.01.002
- Keene, B. J. (1988). Review of data for the surface tension of iron and its binary alloys. *International Materials Reviews*, 33(1), 1–37. doi: 10.1179/imr.1988.33.1.1
- Knott, S., Flandorfer, H., & Mikula, A. (2005). Calorimetric investigations of the two ternary systems Al–Sn–Zn and Ag–Sn–Zn. *International Journal of Materials Research*, 96(1), 38–44. doi: 10.3139/ijmr-2005-0006
- Knott, S., & Mikula, A. (2002). Thermodynamic properties of liquid Al–Sn–Zn alloys: A possible new lead-free solder material. *Materials Transactions*, 43(8), 1868–1872. doi: 10.2320/matertrans.43.1868
- Kohler, F. (1960). Estimation of the thermodynamic data for a ternary system from the corresponding binary systems. *Monatsh. Chem*, 91(4), 738–740.
- Koirala, I., Jha, I. S., Singh, B. P., & Adhikari, D. (2013). Thermodynamic , transport and surface properties in In–Pb liquid alloys. *Physica B*, 423, 49–53. doi: 10.1016/j.physb.2013.04.051
- Koirala, R. P., Kumar, J., Singh, B. P., & Adhikari, D. (2014). Bulk and surface properties of Co–Fe and Fe–Pd liquid alloys. *Journal of Non-Crystalline Solids*, 394, 9–15. doi: 10.1016/j.jnoncrysol.2014.04.001
- Koirala, R. P., Singh, B. P., Jha, I. S., & Adhikari, D. (2013). Thermodynamic, structural and surface properties of liquid Cd–Zn alloys. *Journal of Molecular Liquids*, 179, 60–66. doi: 10.1016/j.molliq.2012.12.008
- Kostov, A., Friedrich, B., & Živković, D. (2008). Thermodynamic calculations in alloys Ti–Al, Ti–Fe, Al–Fe and Ti–Al–Fe. *Journal of Mining and Metallurgy, Section B: Metallurgy*, 44(1), 49–61. doi: 10.2298/JMMB0801049K
- Kostov, A., Živković, D., & Friedrich, B. (2007). Thermodynamic predicting of Si–Me (Me= Ti, Al) binary systems. *Journal of Mining and Metallurgy B: Metallurgy*, 43(1), 29–38. doi: 10.2298/JMMB0701029K
- Lee, J., Kiyose, A., Nakatsuka, S., Nakamoto, M., & Tanaka, T. (2004). Improvements in surface tension measurements of liquid metals having low capillary constants by the constrained drop method. *ISIJ international*, 44(11), 1793–1799. doi: 10.2355/isijinternational.44.1793

- Lee, J., Kiyose, A., Tanaka, M., & Tanaka, T. (2006). Surface tension of liquid Fe–Ti alloys at 1823 K. *ISIJ international*, *46*(4), 467–471. doi: 10.2355/isijinternational.46.467
- Lee, S. M., Kim, B. H., Kim, D. H., & Kim, W. T. (2001). Quasicrystalline phase formation in $\text{Al}_{62}\text{Cu}_{25.5}\text{Fe}_{12.5}$ and $\text{Al}_{55}\text{Cu}_{25.5}\text{Fe}_{12.5}\text{Be}_7$ alloys. *Journal of Materials Research*, *16*(6), 1535–1540. doi: 10.1557/JMR.2001.0213
- Lele, S., & Ramachandrarao, P. (1981). Estimation of complex concentration in a regular associated solution. *Metallurgical Transactions B*, *12*(4), 659–666. doi: 10.1007/BF02654134
- Lityńska-Dobrzyńska, L., Dutkiewicz, J., Stan-Głowińska, K., Dembinski, L., Coddet, C., & Ochinnik, P. (2014). Characterization of rapidly solidified $\text{Al}_{65}\text{Cu}_{20}\text{Fe}_{15}$ alloy in form of powder or ribbon. *Acta Physica Polonica, A*, *126*(2), 512–515. doi: 10.12693/APhysPolA.126.512
- Lityńska-Dobrzyńska, L., Mitka, M., Góral, A., Stan-Głowińska, K., & Dutkiewicz, J. (2016). Microstructure and mechanical properties of aluminium matrix composites reinforced by $\text{Al}_{62}\text{Cu}_{25.5}\text{Fe}_{12.5}$ melt spun ribbon. *Materials Characterization*, *117*, 127–133. doi: 10.1016/j.matchar.2016.04.025
- Manasijević, D., Živković, D., & Živković, V. (2003). Prediction of the thermodynamic properties for the Ga–Sb–Pb ternary system. *Calphad*, *27*(4), 361–366. doi: 10.1016/j.calphad.2003.12.004
- Mehta, U., Koirala, I., Yadav, S. K., Koirala, R. P., & Adhikari, D. (2020). Prediction of thermodynamic and surface properties of ternary Ti–Si–Fe liquid alloy. *Modelling and Simulation in Materials Science and Engineering*, *28*(6), 1–16. doi: 10.1088/1361-651X/aba053
- Mehta, U., Yadav, S. K., Koirala, I., & Adhikari, D. (2020). Thermo-physical properties of ternary Al–Cu–Fe alloy in liquid state. *Philosophical Magazine*, *100*(19), 2417–2435. doi: 10.1080/14786435.2020.1775907
- Mehta, U., Yadav, S. K., Koirala, I., & Adhikari, D. (2022). Thermodynamic, surface and viscous properties of ternary Al–Fe–Mn alloy using theoretical modellings. *Physics and Chemistry of Liquids*, *60*(1), 111–128. doi: 10.1080/00319104.2021.1916933
- Mehta, U., Yadav, S. K., Koirala, I., Koirala, R. P., & Adhikari, D. (2021). Thermodynamic and surface properties of liquid Ti–Al–Fe alloy at different temperatures. *Physics and Chemistry of Liquids*, *59*(4), 585–596. doi: 10.1080/00319104.2020.1793333

- Mekler, C., & Kaptay, G. (2008). Calculation of surface tension and surface phase transition line in binary Ga–Tl system. *Materials Science and Engineering: A*, 495(1-2), 65–69. doi: 10.1016/j.msea.2007.10.111
- Mills, K. C., & Su, Y. C. (2006). Review of surface tension data for metallic elements and alloys: Part 1–pure metals. *International Materials Reviews*, 51(6), 329–351. doi: 10.1179/174328006X102510
- Molina, J. M., Voytovych, R., Louis, E., & Eustathopoulos, N. (2007). The surface tension of liquid aluminium in high vacuum: the role of surface condition. *International Journal of Adhesion and Adhesives*, 27(5), 394–401. doi: 10.1016/j.ijadhadh.2006.09.006
- Moser, Z., Dutkiewicz, J., Gasiór, W., & Salawa, J. (1985). The Sn–Zn (Tin-Zinc) system. *Bulletin of Alloy Phase Diagrams*, 6(4), 330–334. doi: 10.1007/BF02880511
- Moser, Z., Sebo, P., Gasiór, W., Svec, P., & Pstruś, J. (2009). Effect of indium on wettability of Sn–Ag–Cu solders. Experiment vs. modeling, Part I. *Calphad*, 33(1), 63–68. doi: 10.1016/j.calphad.2008.10.001
- Muggianu, Y. M., Gambino, M., & Bros, J. P. (1975). Enthalpies of formation of liquid alloys bismuth-gallium-tin at 723 K—choice of an analytical representation of integral and partial thermodynamic functions of mixing for this ternary system. *Journal de Chimie Physique et de Physico-Chimie Biologique*, 72(1), 83–88.
- Nogi, K., Chung, W. B., McLean, A., & Miller, W. A. (1991). Surface tension of liquid Fe–(Cu, Sn, Cr) and Ni–(Cu, Sn) binary alloys. *Materials Transactions, JIM*, 32(2), 164–168. doi: 10.2320/matertrans1989.32.164
- Novakovic, R. (2010). Thermodynamics, surface properties and microscopic functions of liquid Al–Nb and Nb–Ti alloys. *Journal of Non-Crystalline Solids*, 356(31-32), 1593–1598. doi: 10.1016/j.jnoncrysol.2010.05.055
- Novakovic, R., Giuranno, D., Delsante, S., & Borzone, G. (2014). Bulk and surface properties of liquid Cr–Nb–Re alloys. *Journal of Phase Equilibria and Diffusion*, 35(4), 445–457. doi: 10.1007/s11669-014-0316-8
- Novakovic, R., Giuranno, D., Lee, J., Mohr, M., Delsante, S., Borzone, G., . . . Fecht, H. (2022). Thermophysical properties of Fe–Si and Cu–Pb melts and their effects on solidification related processes. *Metals*, 12(2), 336. doi: 10.3390/met12020336
- Novakovic, R., Giuranno, D., Ricci, E., Tuissi, A., Wunderlich, R., Fecht, H., & Egry, I. (2012). Surface, thermodynamic and structural properties of liquid Al–Ti

- alloys. *Applied Surface Science*, 258(7), 3269–3275. doi: 10.1016/j.apsusc.2011.11.080
- Novakovic, R., Ricci, E., Amore, S., & Lanata, T. (2006). Surface and transport properties of Cu–Sn–Ti liquid alloys. *Rare Metals*, 25(5), 457–468. doi: 10.1016/S1001-0521(06)60085-5
- Oduote, Y. A., Popoola, A. I., Adedayo, K. D., & Ogunjo, S. T. (2017). Thermodynamic properties of Al in ternary lead-free solder Al–Sn–Zn alloys. *Materials Science-Poland*, 35(3), 583–593. doi: 10.1515/msp-2017-0080
- Oduote, Y. A., Popoola, A. I., & Oluyamo, S. S. (2016). Bulk and surface properties of demixing liquid Al–Sn and Sn–Ti alloys. *Applied Physics A*, 122, 1–9. doi: 10.1007/s00339-015-9591-4
- Park, J. M., Kim, D. H., Kim, K. B., & Eckert, J. (2010). Improving the plasticity of a high strength Fe–Si–Ti ultrafine composite by introduction of an immiscible element. *Applied Physics Letters*, 97(25), 251915. doi: 10.1063/1.3532100
- Picha, R., Vřešťál, J., & Kroupa, A. (2004). Prediction of alloy surface tension using a thermodynamic database. *Calphad*, 28(2), 141–146. doi: 10.1016/j.calphad.2004.06.002
- Plevachuk, Y. U., Sklyarchuk, V., Gerbeth, G., Eckert, S., & Novakovic, R. (2011). Surface tension and density of liquid Bi–Pb, Bi–Sn and Bi–Pb–Sn eutectic alloys. *Surface Science*, 605(11-12), 1034–1042. doi: 10.1016/j.susc.2011.02.026
- Prasad, L. C., & Mikula, A. (2006a). Surface segregation and surface tension in Al–Sn–Zn liquid alloys. *Physica B: Condensed Matter*, 373(1), 142–149. doi: 10.1016/j.physb.2005.11.113
- Prasad, L. C., & Mikula, A. (2006b). Thermodynamics of liquid Al–Sn–Zn alloys and concerned binaries in the light of soldering characteristics. *Physica B: Condensed Matter*, 373(1), 64–71. doi: 10.1016/j.physb.2005.11.073
- Prasad, L. C., Singh, R. N., Singh, V. N., & Chatterjee, S. K. (1995). Compound formation in Sn-based liquid alloys. *Physica B: Condensed Matter*, 215(2-3), 225–232. doi: 10.1016/0921-4526(95)00393-N
- Prigogine, I., & Defay, R. (1954). Chemical thermodynamics. volume 1 of treatise on thermodynamics. *London, Great Britain: Longmans Green and Co.*
- Pstrus, J. (2013). Surface tension and density of liquid In–Sn–Zn alloys. *Applied Surface Science*, 265, 50–59. doi: 10.1016/j.apsusc.2012.10.098

- Pstrus, J., Moser, Z., Gasior, W., & Debski, A. (2006). Surface tension and density measurements of liquid Sn-Zn alloys. experiment vs. SURDAT database of Pb-free solders. *Archives of Metallurgy and Materials*, 51(3), 335–343. Retrieved from <https://www.researchgate.net/publication>
- Raghavan, V. (2005). Al–Cu–Fe (aluminum-copper-iron). *Journal of Phase Equilibria and Diffusion*, 26(1), 59–64. doi: 10.1007/s11669-005-0061-0
- Raghavan, V. (2009). Fe–Si–Ti (iron-silicon-titanium). *Journal of Phase Equilibria and Diffusion*, 30(4), 393–396. doi: 10.1007/s11669-009-9555-5
- Redlich, O., & Kister, A. T. (1948). Algebraic representation of thermodynamic properties and the classification of solutions. *Industrial & Engineering Chemistry*, 40(2), 345–348. doi: 10.1021/ie50458a036
- Sabooni, S., Karimzadeh, F., & Abbasi, M. H. (2012). Thermodynamic aspects of nanostructured Ti_5Si_3 formation during mechanical alloying and its characterization. *Bulletin of Materials Science*, 35(3), 439–447. doi: 10.1007/s12034-012-0298-2
- Schmitz, J., Brillo, J., Egry, I., & Schmid-Fetzer, R. (2009). Surface tension of liquid Al–Cu binary alloys. *International Journal of Materials Research*, 100(11), 1529–1535. doi: 10.3139/146.110221
- Seyhan, I., & Egry, I. (1999). The surface tension of undercooled binary iron and nickel alloys and the effect of oxygen on the surface tension of Fe and Ni. *International Journal of Thermophysics*, 20(4), 1017–1028. doi: 10.1023/A:1022638400507
- Singh, B. P., Koirala, I., Jha, I. S., & Adhikari, D. (2014). The segregating nature of Cd–Pb liquid binary alloys. *Physics and Chemistry of liquids*, 52(4), 457–470. doi: 10.1080/00319104.2013.871668
- Singh, R. N. (1987). Short-range order and concentration fluctuations in binary molten alloys. *Canadian Journal of Physics*, 65(3), 309–325. doi: 10.1139/p87-038
- Singh, R. N., & Sommer, F. (1997). Segregation and immiscibility in liquid binary alloys. *Reports on Progress in Physics*, 60(1), 57–150. doi: 10.1088/0034-4885/60/1/003
- Skapski, A. S. (1948). The temperature coefficient of the surface tension of liquid metals. *The Journal of Chemical Physics*, 16(4), 386–389. doi: 10.1063/1.1746896
- Sklyarchuk, V., Plevachuk, Y. u., Kaban, I., & Novaković, R. (2012). Surface properties and wetting behaviour of liquid Ag–Sb–Sn alloys. *Journal of Mining and Metallurgy, Section B: Metallurgy*, 48(3), 443–448. doi: 0.2298/JMMB120719055S

- Srikanth, S., Goel, R. P., & Ramachandrarao, P. (1999). Limitations of a regular associated solution approximation in describing the thermodynamic behaviour of complex liquid alloys. *Calphad*, 23(1), 85–100. doi: 10.1016/S0364-5916(99)00015-2
- Srikanth, S., & Jacob, K. T. (1988). Volume effects and associations in liquid alloys. *Metallurgical Transactions B*, 19(3), 465–470.
- Tadmor, R. (2009). Marangoni flow revisited. *Journal of Colloid and Interface Science*, 332(2), 451–454. doi: 10.1016/j.jcis.2008.12.047
- Tanaka, T., Hack, K., Iida, T., & Hara, S. (1996). Application of thermodynamic databases to the evaluation of surface tensions of molten alloys, salt mixtures and oxide mixtures. *Zeitschrift für Metallkunde*, 87(5), 380–389. doi: 10.1515/ijmr-1996-870509
- Tanaka, T., Hara, S., Ogawa, M., & Ueda, T. (1998). Evaluation of surface tension of molten salt mixtures. In *Retrospective Collection* (Vol. 25, pp. 213–216). doi: 10.3139/ijmr-1998-0065
- Tanaka, T., & Iida, T. (1994). Application of a thermodynamic database to the calculation of surface tension for iron-base liquid alloys. *Steel Research*, 65(1), 21–28. doi: 10.1002/srin.199400921
- Thiedemann, U., Qin, J., Schaefer, K., Rösner-Kuhn, M., & Froberg, M. G. (1995). Mixing enthalpy measurements of liquid Fe–Ti alloys by levitation alloying calorimetry and calculation of the thermodynamic properties of mixing. *ISIJ International*, 35(12), 1518–1522. doi: 10.2355/isijinternational.35.1518
- Toop, G. W. (1965). Predicting ternary activities using binary data. *Transactions of the Metallurgical Society of AIME*, 223, 850–855.
- Trybula, M. E., Gancarz, T., & Gąsior, W. (2016). Density, surface tension and viscosity of liquid binary Al–Zn and ternary Al–Li–Zn alloys. *Fluid Phase Equilibria*, 421, 39–48. doi: 10.1016/j.fluid.2016.03.013
- Trybula, M. E., Szafranski, P. W., & Korzhavyi, P. A. (2018). Structure and chemistry of liquid Al–Cu alloys: molecular dynamics study versus thermodynamics-based modelling. *Journal of Materials Science*, 53(11), 8285–8301. doi: 10.1007/s10853-018-2116-8
- Tsai, A. P., Inoue, A., & Masumoto, T. (1987). Preparation of a new Al–Cu–Fe quasicrystal with large grain sizes by rapid solidification. *Journal of Materials Science Letters*, 6(12), 1403–1405. doi: 10.1007/BF01689302

- Turchanin, M. A., Velikanova, T. Y., Agraval, P. G., Abdulov, A. R., & Dreval, L. A. (2008). Thermodynamic assessment of the Cu-Ti-Zr system. III. Cu-Ti-Zr system. *Powder Metallurgy and Metal Ceramics*, 47(9), 586–606. doi: 10.1007/s11106-008-9062-y
- Ushioda, K., Takahashi, J., Takebayashi, S., Maeda, D., Hayashi, K., & Abe, Y. R. (2011). Challenges toward the further strengthening of sheet steel. In *Advanced steels* (pp. 229–240). Springer. doi: 10.1007/978-3-642-17665-4_23
- Wang, H. P., Luo, B. C., Qin, T., Chang, J., & Wei, B. (2008). Surface tension of liquid ternary Fe-Cu-Mo alloys measured by electromagnetic levitation oscillating drop method. *The Journal of Chemical Physics*, 129(12), 124706. doi: 10.1063/1.2981833
- Wang, J., Liu, C., Leinenbach, C., Klotz, U. E., Uggowitzer, P. J., & Löffler, J. (2011). Experimental investigation and thermodynamic assessment of the Cu-Sn-Ti ternary system. *Calphad*, 35(1), 82–94. doi: 10.1016/j.calphad.2010.12.006
- Wang, L., Chou, K. C., & Seetharaman, S. (2007). A comparison of traditional geometrical models and mass triangle model in calculating the surface tensions of ternary sulphide melts. *Calphad*, 32(1), 49–55. doi: 10.1016/j.calphad.2007.11.006
- Wang, W., Chen, H., Larsson, H., & Mao, H. (2019). Thermodynamic constitution of the Al-Cu-Ni system modeled by Calphad and ab initio methodology for designing high entropy alloys. *Calphad*, 65, 346–369. doi: 10.1016/j.calphad.2019.03.011
- Watson, J. D., & Brown, G. G. (1974). The strength and ductility of precipitation-hardened Fe-Si-Ti Alloys. *Metal Science*, 8(1), 9–20. doi: 10.1179/msc.1974.8.1.9
- Weitzer, F., Schuster, J. C., Naka, M., Stein, F., & Palm, M. (2008). On the reaction scheme and liquidus surface in the ternary system Fe-Si-Ti. *Intermetallics*, 16(2), 273–282. doi: 10.1016/j.intermet.2007.10.006
- Witusiewicz, V. T., Hecht, U., Fries, S. G., & Rex, S. (2004). The Ag-Al-Cu system: Part I: Reassessment of the constituent binaries on the basis of new experimental data. *Journal of Alloys and Compounds*, 385(1-2), 133–143. doi: 10.1016/j.jallcom.2004.04.126
- Xuyang, L., Xuwei, L. v., Chunxin, L., Jie, C., & Chenguang, B. (2017). Surface tension of liquid Ti-Al alloys. *Rare Metal Materials and Engineering*, 46(1), 39–44. doi: 10.1016/S1875-5372(17)30074-7

- Yadav, S. K. (2018). *Ordering and segregating in liquid alloys* (PhD dissertation, Tribhuvan University, Kirtipur, Nepal). Retrieved from <https://elibrary.tucl.edu.np/handle/123456789/15515>
- Yadav, S. K., Jha, L. N., & Adhikari, D. (2015). Thermodynamic and structural properties of Bi-based liquid alloys. *Physica B: Condensed Matter*, 475, 40–47. doi: 10.1016/j.physb.2015.06.015
- Yadav, S. K., Jha, L. N., & Adhikari, D. (2018). Modeling equations to predict the mixing behaviours of Al–Fe liquid alloy at different temperatures. *Bibechana*, 15, 60–69. doi: 10.3126/bibechana.v15i0.18624
- Yadav, S. K., Jha, L. N., Jha, I. S., Singh, B. P., Koirala, R. P., & Adhikari, D. (2016). Prediction of thermodynamic and surface properties of Pb–Hg liquid alloys at different temperatures. *Philosophical Magazine*, 96(18), 1909–1925. doi: 10.1080/14786435.2016.1181281
- Yadav, S. K., Mehta, U., & Adhikari, D. (2021). Optimization of thermodynamic and surface properties of ternary Ti–Al–Si alloy and its sub-binary alloys in molten state. *Heliyon*, 7(3), 1–10. doi: 10.1016/j.heliyon.2021.e06511
- Yadav, S. K., Mehta, U., Gohivar, R. K., Dhungana, A., Koirala, R. P., & Adhikari, D. (2020). Reassessments of thermo-physical properties of Si–Ti melt at different temperatures. *Bibechana*, 17, 146–153. doi: 10.3126/bibechana.v17i0.26877
- Yan, L., Zheng, S., Ding, G., Xu, G., & Qiao, Z. (2007). Surface tension calculation of the Sn–Ga–In ternary alloy. *Calphad*, 31(1), 112–119. doi: 10.1016/j.calphad.2006.09.005
- Yi, W., Liu, G., Gao, J., & Zhang, L. (2021). Boosting for concept design of casting aluminum alloys driven by combining computational thermodynamics and machine learning techniques. *Journal of Materials Informatics*, 1(2), 11–40. doi: 10.20517/jmi.2021.10
- Young, H. D., Freedman, R. A., & Ford, A. L. (2013). *University Physics with Modern Physics*. Pearson Education.
- Young, W. H. (1992). Structural and thermodynamic properties of NFE liquid metals and binary alloys. *Reports on Progress in Physics*, 55(10), 1769. doi: 10.1088/0034-4885/55/10/003
- Yu, S. P., Wang, M. C., & Hon, M. H. (2001). Formation of intermetallic compounds at eutectic Sn–Zn–Al solder/Cu interface. *Journal of Materials Research*, 16(1), 76–82. doi: 10.1557/JMR.2001.0015

- Zhang, F., Chen, S. L., Chang, Y. A., & Kattner, U. R. (1997). A thermodynamic description of the Ti–Al system. *Intermetallics*, 5(6), 471–482. doi: 10.1016/S0966-9795(97)00030-7
- Zheng, W., Mao, H., Lu, X. G., He, Y., Li, L., Selleby, M., & Agren, J. (2018). Thermodynamic investigation of the Al–Fe–Mn system over the whole composition and wide temperature ranges. *Journal of Alloys and Compounds*, 742, 1046–1057. doi: 10.1016/j.jallcom.2018.01.291
- Zhou, K., Wang, H. P., Chang, J., & Wei, B. (2011). Surface tension measurement of metastable liquid Ti–Al–Nb alloys. *Applied Physics A*, 105(1), 211–214. doi: 10.1007/s00339-011-6491-0
- Zhu, T. J., Zhao, X. B., & Hu, S. H. (2001). Phase transition of FeSi₂ and Fe₂Si₅ based alloys prepared by melt spinning. *Journal of Materials Science Letters*, 20(19), 1831–1833. doi: 10.1023/A:1012563906690
- Živković, D., Grgurić, T. H., Gojić, M., Čubela, D., Šimišić, Z. S., Kostov, A., & Kožuh, S. (2014). Calculation of thermodynamic properties of Cu–Al–(Ag, Au) shape memory alloy systems. *Transactions of the Indian Institute of Metals*, 67(2), 285–289. doi: 10.1007/s12666-013-0328-9
- Zou, C., Li, J., Wang, W. Y., Zhang, Y., Lin, D., Yuan, R., . . . others (2021). Integrating data mining and machine learning to discover high-strength ductile titanium alloys. *Acta Materialia*, 202, 211–221. doi: 10.1016/j.actamat.2020.10.056

APPENDIX

A: Data for Partial excess free energy of mixing of components in ternary liquid alloys.

Table 38: Partial excess free energy of components in Fe–Si–Ti ternary liquid alloy at 1873 K from Fe corner at three cross-section

Bulk concentration			Partial excess free energy (kJ/mol)		
Fe	Si	Ti	Fe	Si	Ti
0.100	0.675	0.225	-37.01	-6.58	-114.22
0.200	0.600	0.200	-35.73	-10.37	-103.91
0.300	0.525	0.175	-33.02	-15.11	-93.69
0.400	0.450	0.150	-27.91	-22.17	-84.06
0.500	0.375	0.125	-20.86	-32.76	-75.96
0.600	0.300	0.100	-13.20	-47.34	-70.30
0.700	0.225	0.075	-6.49	-65.05	-67.44
0.800	0.150	0.050	-1.99	-83.23	-66.75
0.900	0.075	0.025	-0.19	-95.95	-67.03
0.100	0.450	0.450	-17.10	-45.50	-58.10
0.200	0.400	0.400	-19.10	-46.934	-56.11
0.300	0.350	0.350	-18.68	-49.61	-53.97
0.400	0.300	0.300	-15.90	-54.50	-52.37
0.500	0.250	0.250	-11.64	-62.19	-52.00
0.600	0.200	0.200	-7.04	-72.50	-53.24
0.700	0.150	0.150	-3.20	-84.257	-55.96
0.800	0.100	0.100	-0.82	-95.10	-59.40
0.900	0.050	0.050	0.02	-101.38	-62.13
0.100	0.225	0.675	-28.36	-114.95	-13.96
0.200	0.200	0.600	-25.25	-106.51	-17.60
0.300	0.175	0.525	-20.81	-100.74	-21.62
0.400	0.150	0.450	-15.60	-98.14	-26.38
0.500	0.125	0.375	-10.40	-98.61	-32.05
0.600	0.100	0.300	-5.93	-101.36	-38.54
0.700	0.075	0.225	-2.68	-104.90	-45.48
0.800	0.050	0.150	-0.81	-107.20	-52.20
0.900	0.025	0.075	-0.09	-105.82	-57.94

Table 39: Partial excess free energy of components in Fe–Si–Ti ternary liquid alloy at 1873 K from Si corner at at three cross-section

Bulk concentration			Partial excess free energy (kJ/mol)		
Fe	Si	Ti	Fe	Si	Ti
0.225	0.100	0.675	-33.66	-132.58	-8.57
0.200	0.200	0.600	-25.25	-106.51	-17.60
0.175	0.300	0.525	-19.50	-78.71	-31.92
0.150	0.400	0.450	-17.84	-52.74	-51.11
0.125	0.500	0.375	-20.78	-31.073	-73.69
0.100	0.600	0.300	-27.94	-15.10	-97.16
0.075	0.700	0.225	-38.24	-5.16	-118.06
0.050	0.800	0.150	-49.98	-0.55	-132.06
0.025	0.900	0.075	-61.06	-0.36	-134.16
0.450	0.100	0.450	-14.39	-109.36	-24.47
0.400	0.200	0.400	-14.32	-82.97	-33.85
0.350	0.300	0.350	-16.66	-58.39	-47.81
0.300	0.400	0.300	-21.37	-37.53	-65.41
0.250	0.500	0.250	-27.97	-21.45	-84.90
0.200	0.600	0.200	-35.73	-10.37	-103.91
0.150	0.700	0.150	-43.90	-3.84	-119.63
0.100	0.800	0.100	-51.98	-0.82	-129.10
0.050	0.900	0.050	-60.05	-0.00	-129.56
0.675	0.100	0.225	-3.23	-98.71	-46.19
0.600	0.200	0.200	-7.04	-72.50	-53.24
0.525	0.300	0.175	-14.14	-48.52	-63.69
0.450	0.400	0.150	-23.28	-29.27	-77.28
0.375	0.500	0.125	-32.89	-15.64	-92.47
0.300	0.600	0.100	-41.49	-7.24	-107.00
0.225	0.700	0.075	-48.22	-2.89	-118.39
0.150	0.800	0.050	-53.36	-1.03	-124.57
0.075	0.900	0.025	-58.90	-0.29	-124.49

Table 40: Partial excess free energy of components in Fe–Si–Ti ternary liquid alloy at 1873 K from Ti corner at three cross-sections

Bulk concentration			Partial excess free energy (kJ/mol)		
Fe	Si	Ti	Fe	Si	Ti
0.675	0.225	0.100	-6.81	-65.01	-64.93
0.600	0.200	0.200	-7.04	-72.50	-53.24
0.525	0.175	0.300	-8.86	-82.32	-41.67
0.450	0.150	0.400	-12.62	-94.23	-30.81
0.375	0.125	0.500	-18.52	-107.96	-21.12
0.300	0.100	0.600	-26.59	-123.13	-13.01
0.225	0.075	0.700	-36.56	-139.13	-6.79
0.150	0.050	0.800	-47.69	-155.03	-2.64
0.075	0.025	0.900	-58.61	-169.36	-0.52
0.450	0.450	0.100	-28.63	-20.76	-86.86
0.400	0.400	0.200	-22.88	-31.23	-73.61
0.350	0.350	0.300	-18.78	-45.42	-58.48
0.300	0.300	0.400	-17.43	-63.14	-43.24
0.250	0.250	0.500	-19.52	-83.83	-29.28
0.200	0.200	0.600	-25.25	-106.51	-17.60
0.150	0.150	0.700	-34.28	-129.74	-8.86
0.100	0.100	0.800	-45.61	-151.55	-3.28
0.050	0.050	0.900	-57.44	-169.36	-0.60
0.225	0.675	0.100	-45.79	-3.96	-116.29
0.200	0.600	0.200	-35.73	-10.37	-103.91
0.175	0.525	0.300	-25.98	-22.20	-84.87
0.150	0.450	0.400	-19.29	-39.92	-63.40
0.125	0.375	0.500	-17.39	-63.10	-42.77
0.100	0.300	0.600	-20.98	-90.36	-25.28
0.075	0.225	0.700	-29.71	-119.42	-12.32
0.050	0.150	0.800	-42.16	-147.01	-4.30
0.025	0.075	0.900	-55.82	-168.91	-0.70

Table 41: Partial excess free energy of components in Al–Sn–Zn ternary liquid alloy at 973 K from Al corner at three cross-sections

Bulk concentration			Partial excess free energy (kJ/mol)		
Al	Sn	Zn	Al	Sn	Zn
0.100	0.675	0.225	6.995	0.250	1.947
0.200	0.600	0.200	6.036	0.560	1.696
0.300	0.525	0.175	5.046	1.047	1.560
0.400	0.450	0.150	4.041	1.767	1.574
0.500	0.375	0.125	3.048	2.787	1.777
0.600	0.300	0.100	2.107	4.184	2.203
0.700	0.225	0.075	1.270	6.039	2.873
0.800	0.150	0.050	0.600	8.427	3.788
0.900	0.075	0.025	0.158	11.411	4.912
0.100	0.450	0.450	5.850	0.898	1.247
0.200	0.400	0.400	5.053	1.336	1.090
0.300	0.350	0.350	4.241	1.926	1.042
0.400	0.300	0.300	3.399	2.710	1.168
0.500	0.250	0.250	2.545	3.756	1.523
0.600	0.200	0.200	1.726	5.144	2.143
0.700	0.150	0.150	1.005	6.945	3.024
0.800	0.100	0.100	0.449	9.208	4.103
0.900	0.050	0.050	0.108	11.930	5.235
0.100	0.225	0.675	4.970	2.367	0.553
0.200	0.200	0.600	4.143	2.789	0.602
0.300	0.175	0.525	3.495	3.393	0.688
0.400	0.150	0.450	2.851	4.147	0.900
0.500	0.125	0.375	2.159	5.105	1.340
0.600	0.100	0.300	1.452	6.356	2.080
0.700	0.075	0.225	0.812	7.989	3.124
0.800	0.050	0.150	0.331	10.043	4.363
0.900	0.025	0.075	0.066	12.457	5.532

Table 42: Partial excess free energy of components in Al–Sn–Zn ternary liquid alloy at 973 K from Sn corner at three cross-sections

Bulk concentration			Partial excess free energy (kJ/mol)		
Al	Sn	Zn	Al	Sn	Zn
0.225	0.100	0.675	3.658	3.939	0.495
0.200	0.200	0.600	4.143	2.789	0.602
0.175	0.300	0.525	4.707	1.898	0.808
0.150	0.400	0.450	5.325	1.226	1.083
0.125	0.500	0.375	5.971	0.736	1.399
0.100	0.600	0.300	6.623	0.399	1.727
0.075	0.700	0.225	7.260	0.186	2.040
0.050	0.800	0.150	7.861	0.067	2.311
0.025	0.900	0.075	8.412	0.013	2.523
0.450	0.100	0.450	2.409	5.064	1.063
0.400	0.200	0.400	3.020	3.608	0.963
0.350	0.300	0.350	3.717	2.476	1.017
0.300	0.400	0.300	4.470	1.621	1.183
0.250	0.500	0.250	5.250	0.996	1.421
0.200	0.600	0.200	6.036	0.560	1.696
0.150	0.700	0.150	6.807	0.276	1.978
0.100	0.800	0.100	7.549	0.107	2.243
0.050	0.900	0.050	8.250	0.023	2.474
0.675	0.100	0.225	1.001	7.274	2.825
0.600	0.200	0.200	1.726	5.144	2.143
0.525	0.300	0.175	2.570	3.518	1.768
0.450	0.400	0.150	3.485	2.306	1.621
0.375	0.500	0.125	4.435	1.428	1.637
0.300	0.600	0.100	5.389	0.814	1.762
0.225	0.700	0.075	6.324	0.409	1.955
0.150	0.800	0.0500	7.226	0.162	2.184
0.075	0.900	0.025	8.087	0.036	2.427

Table 43: Partial excess free energy of components in Al–Sn–Zn ternary liquid alloy at 973 K from Zn corner at three cross-section

Bulk concentration			Partial excess free energy (kJ/mol)		
Al	Sn	Zn	Al	Sn	Zn
0.675	0.225	0.100	1.392	5.729	2.714
0.600	0.200	0.200	1.726	5.144	2.143
0.525	0.175	0.300	2.132	4.715	1.553
0.450	0.150	0.400	2.547	4.448	1.098
0.375	0.125	0.500	2.914	4.304	0.804
0.300	0.100	0.600	3.230	4.241	0.622
0.225	0.075	0.700	3.595	4.252	0.476
0.150	0.050	0.800	4.248	4.410	0.305
0.075	0.025	0.900	5.614	4.899	0.111
0.450	0.450	0.100	3.711	2.036	1.727
0.400	0.400	0.200	3.819	2.033	1.438
0.350	0.350	0.300	3.931	2.117	1.146
0.300	0.300	0.400	4.017	2.279	0.916
0.250	0.250	0.500	4.072	2.503	0.746
0.200	0.200	0.600	4.143	2.789	0.602
0.150	0.150	0.700	4.347	3.170	0.447
0.100	0.100	0.800	4.893	3.732	0.267
0.050	0.050	0.900	6.085	4.622	0.090
0.225	0.675	0.100	6.216	0.451	1.902
0.200	0.600	0.200	6.036	0.560	1.696
0.175	0.525	0.300	5.821	0.736	1.466
0.150	0.450	0.400	5.578	0.983	1.236
0.125	0.375	0.500	5.342	1.315	1.006
0.100	0.300	0.600	5.188	1.757	0.768
0.075	0.225	0.700	5.232	2.362	0.521
0.050	0.150	0.800	5.635	3.207	0.280
0.025	0.075	0.900	6.594	4.395	0.084

Table 44: Partial excess free energy of components in Al–Cu–Fe ternary liquid alloy at 1823 K from Al corner at three cross-sections

Bulk concentration			Partial excess free energy (kJ/mol)		
Al	Cu	Fe	Al	Cu	Fe
0.100	0.675	0.225	-53.909	1.049	16.577
0.200	0.600	0.200	-37.896	-1.705	13.737
0.300	0.525	0.175	-26.118	-5.255	8.897
0.400	0.450	0.150	-17.454	-9.280	2.537
0.500	0.375	0.125	-11.111	-13.591	-5.057
0.600	0.300	0.100	-6.540	-18.070	-13.730
0.700	0.225	0.075	-3.375	-22.602	-23.411
0.800	0.150	0.050	-1.362	-27.021	-34.062
0.900	0.075	0.025	-0.303	-31.059	-45.638
0.100	0.450	0.450	-51.405	5.721	7.881
0.200	0.400	0.400	-37.896	2.767	6.160
0.300	0.350	0.350	-27.463	-0.730	2.810
0.400	0.300	0.300	-19.342	-4.616	-1.932
0.500	0.250	0.250	-13.012	-8.829	-7.953
0.600	0.200	0.200	-8.134	-13.354	-15.228
0.700	0.150	0.150	-4.498	-18.187	-23.786
0.800	0.100	0.100	-1.975	-23.314	-33.699
0.900	0.050	0.050	-0.490	-28.702	-45.072
0.100	0.225	0.675	-46.615	13.280	2.562
0.200	0.200	0.600	-35.837	9.548	1.313
0.300	0.175	0.525	-27.098	5.582	-1.197
0.400	0.150	0.450	-19.916	1.380	-4.898
0.500	0.125	0.375	-13.985	-3.111	-9.814
0.600	0.100	0.300	-9.134	-7.985	-16.044
0.700	0.075	0.225	-5.285	-13.360	-23.742
0.800	0.050	0.150	-2.434	-19.391	-33.117
0.900	0.025	0.075	-0.635	-26.278	-44.437

Table 45: Partial excess free energy of components in Al–Cu–Fe ternary liquid alloy at 1823 K from Cu corner at three cross-sections

Bulk concentration			Partial excess free energy (kJ/mol)		
Al	Cu	Fe	Al	Cu	Fe
0.225	0.100	0.675	-31.861	13.215	-0.856
0.200	0.200	0.6	-35.837	9.548	1.313
0.175	0.300	0.525	-39.790	6.913	3.782
0.150	0.400	0.450	-43.935	4.991	6.526
0.125	0.500	0.375	-48.426	3.539	9.591
0.100	0.600	0.300	-53.360	2.391	13.097
0.075	0.700	0.225	-58.793	1.456	17.222
0.050	0.800	0.150	-64.751	0.711	22.196
0.025	0.900	0.075	-71.255	0.197	28.286
0.450	0.100	0.450	-16.827	1.061	-7.698
0.400	0.200	0.400	-19.873	-0.817	-4.034
0.350	0.300	0.350	-23.276	-1.809	-0.027
0.300	0.400	0.300	-27.263	-2.160	4.276
0.250	0.500	0.250	-32.057	-2.072	8.860
0.200	0.600	0.200	-37.896	-1.705	13.737
0.150	0.700	0.150	-45.054	-1.191	18.917
0.100	0.800	0.100	-53.867	-0.646	24.385
0.050	0.900	0.050	-64.772	-0.196	30.063
0.675	0.100	0.225	-5.993	-13.160	-21.673
0.600	0.200	0.200	-8.134	-13.354	-15.228
0.525	0.300	0.175	-10.802	-12.529	-8.467
0.450	0.400	0.150	-14.259	-11.013	-1.522
0.375	0.500	0.125	-18.815	-9.045	5.524
0.300	0.600	0.100	-24.871	-6.814	12.584
0.225	0.700	0.075	-32.974	-4.508	19.509
0.150	0.800	0.050	-43.868	-2.359	26.030
0.075	0.900	0.025	-58.551	-0.695	31.688

Table 46: Partial excess free energy of components in Al–Cu–Fe ternary liquid alloy at 1823 K from Fe corner at three cross-sections

Bulk concentration			Partial excess free energy (kJ/mol)		
Al	Cu	Fe	Al	Cu	Fe
0.675	0.225	0.100	−4.374	−20.465	−21.092
0.600	0.200	0.200	−8.134	−13.354	−15.228
0.525	0.175	0.300	−12.303	−7.095	−10.586
0.450	0.150	0.400	−16.780	−1.421	−7.019
0.375	0.125	0.500	−21.481	3.931	−4.370
0.300	0.100	0.600	−26.338	9.216	−2.486
0.225	0.075	0.700	−31.295	14.679	−1.228
0.150	0.050	0.800	−36.297	20.567	−0.469
0.075	0.025	0.900	−41.278	27.142	−0.098
0.450	0.450	0.100	−13.280	−12.554	0.199
0.400	0.400	0.200	−18.241	−7.835	0.824
0.350	0.350	0.300	−22.992	−3.415	1.274
0.300	0.300	0.400	−27.532	0.839	1.505
0.250	0.250	0.500	−31.834	5.093	1.511
0.200	0.200	0.600	−35.837	9.548	1.313
0.150	0.150	0.700	−39.445	14.440	0.962
0.100	0.100	0.800	−42.511	20.041	0.541
0.050	0.050	0.900	−44.833	26.670	0.168
0.225	0.675	0.100	−33.436	−4.148	17.864
0.200	0.600	0.200	−37.896	−1.705	13.737
0.175	0.525	0.300	−41.515	0.904	10.547
0.15	0.45	0.400	−44.451	3.695	8.004
0.125	0.375	0.500	−46.781	6.759	5.897
0.100	0.300	0.600	−48.499	10.265	4.095
0.075	0.225	0.700	−49.512	14.454	2.542
0.050	0.150	0.800	−49.645	19.645	1.262
0.025	0.075	0.900	−48.636	26.236	0.355

B: Data for iso-surface tension lines of ternary liquid alloys.

Table 47: Ternary concentrations of Fe–Si–Ti liquid alloy for iso-surface tension lines at 1873 K

Surface Tension (mN m ⁻¹)	Ternary bulk concentrations
900	(0.00, 0.83, 0.17), (0.05, 0.84, 0.11), (0.10, 0.85, 0.05), (0.16, 0.84, 0.00),
950	(0.00, 0.74, 0.26), (0.05, 0.74, 0.21), (0.10, 0.74, 0.16), (0.15, 0.73, 0.12), (0.22, 0.73, 0.05), (0.27, 0.73, 0.00)
1000	(0.00, 0.69, 0.31), (0.07, 0.67, 0.26), (0.14, 0.66, 0.20), (0.21, 0.65, 0.14), (0.28, 0.64, 0.08), (0.35, 0.65, 0.00),
1100	(0.00, 0.60, 0.40), (0.08, 0.58, 0.34), (0.16, 0.56, 0.28), (0.22, 0.54, 0.24), (0.28, 0.53, 0.19), (0.36, 0.52, 0.12), (0.42, 0.52, 0.06), (0.48, 0.52, 0.00)
1200	(0.00, 0.53, 0.46), (0.08, 0.50, 0.42), (0.16, 0.48, 0.36), (0.28, 0.45, 0.27), (0.39, 0.44, 0.17), (0.51, 0.43, 0.06), (0.57, 0.43, 0.00)
1300	(0.00, 0.47, 0.53), (0.05, 0.45, 0.50), (0.12, 0.42, 0.46), (0.20, 0.40, 0.40), (0.29, 0.38, 0.33), (0.38, 0.36, 0.26), (0.49, 0.36, 0.15), (0.61, 0.35, 0.04), (0.65, 0.35, 0.00)
1400	(0.00, 0.41, 0.59), (0.10, 0.36, 0.54), (0.20, 0.33, 0.47), (0.30, 0.31, 0.39), (0.40, 0.30, 0.30), (0.60, 0.28, 0.12), (0.69, 0.28, 0.03), (0.715, 0.285, 0.00)
1500	(0.00, 0.33, 0.67), (0.10, 0.29, 0.61), (0.20, 0.26, 0.54), (0.30, 0.24, 0.46), (0.40, 0.23, 0.37), (0.50, 0.22, 0.28), (0.60, 0.22, 0.18), (0.70, 0.22, 0.08), (0.78, 0.22, 0.00)
1600	(0.00, 0.24, 0.76), (0.10, 0.20, 0.70), (0.20, 0.18, 0.62), (0.30, 0.17, 0.53), (0.40, 0.16, 0.44), (0.50, 0.16, 0.34), (0.60, 0.16, 0.24), (0.70, 0.16, 0.04), (0.80, 0.16, 0.04), (0.84, 0.16, 0)
1700	(0.90, 0.10, 0.00), (0.87, 0.09, 0.04), (0.82, 0.09, 0.09), (0.73, 0.10, 0.17), (0.66, 0.10, 0.24), (0.55, 0.10, 0.35), (0.42, 0.09, 0.49), (0.30, 0.07, 0.63), (0.23, 0.06, 0.71), (0.18, 0.04, 0.78), (0.13, 0.00, 0.87)

Table 48: Ternary concentrations of Al–Sn–Zn liquid alloy for iso-surface tension lines at 973 K

Surface Tension (mN m ⁻¹)	Ternary bulk concentrations
540	(0.00, 0.77, 0.23), (0.05, 0.77, 0.18), (0.10, 0.77, 0.13), (0.15, 0.78, 0.07), (0.19, 0.81, 0.00)
555	(0.00, 0.65, 0.35), (0.06, 0.64, 0.30), (0.12, 0.64, 0.24), (0.17, 0.65, 0.18), (0.23, 0.67, 0.10), (0.30, 0.70, 0.00)
575	(0.00, 0.51, 0.49), (0.07, 0.52, 0.41), (0.14, 0.53, 0.33), (0.21, 0.54, 0.25), (0.28, 0.56, 0.16), (0.36, 0.59, 0.05), (0.40, 0.60, 0.00)
600	(0.00, 0.36, 0.64), (0.07, 0.39, 0.54), (0.14, 0.41, 0.45), (0.20, 0.42, 0.38), (0.28, 0.44, 0.28), (0.35, 0.46, 0.19), (0.43, 0.48, 0.09), (0.51, 0.49, 0.00)
625	(0.00, 0.24, 0.76), (0.09, 0.28, 0.63), (0.18, 0.32, 0.50), (0.27, 0.345, 0.385), (0.36, 0.36, 0.28), (0.45, 0.38, 0.17), (0.55, 0.38, 0.07), (0.64, 0.36, 0.00)
650	(0.00, 0.16, 0.84), (0.09, 0.20, 0.71), (0.17, 0.23, 0.60), (0.25, 0.25, 0.50), (0.34, 0.28, 0.38), (0.42, 0.29, 0.29), (0.50, 0.30, 0.20), (0.60, 0.29, 0.11), (0.70, 0.27, 0.03), (0.74, 0.26, 0.00)
700	(0.00, 0.05, 0.95), (0.10, 0.08, 0.82), (0.20, 0.10, 0.70), (0.30, 0.13, 0.57), (0.40, 0.15, 0.45), (0.50, 0.17, 0.33), (0.60, 0.17, 0.23), (0.70, 0.17, 0.13), (0.77, 0.16, 0.07), (0.85, 0.15, 0.00)
750	(0.15, 0.00, 0.85), (0.25, 0.02, 0.73), (0.35, 0.04, 0.61), (0.45, 0.06, 0.49), (0.55, 0.08, 0.37), (0.65, 0.09, 0.26), (0.73, 0.09, 0.18), (0.82, 0.09, 0.09), (0.90, 0.10, 0)

Table 49: Ternary concentrations of Al–Cu–Fe liquid alloy for iso-surface tension lines at 1823 K

Surface Tension (mN m ⁻¹)	Ternary bulk concentrations
650	(0.84, 0.16, 0.00), (0.85, 0.11, 0.04), (0.86, 0.04, 0.10), (0.87, 0.00, 0.13)
700	(0.72, 0.10, 0.18), (0.73, 0.05, 0.22), (0.74, 0.02, 0.24), (0.75, 0.00, 0.25)
750	(0.60, 0.40, 0), (0.60, 0.28, 0.12), (0.61, 0.17, 0.22), (0.62, 0.12, 0.26), (0.64, 0.06, 0.30), (0.67, 0.00, 0.33)
800	(0.50, 0.50, 0.00), (0.51, 0.36, 0.13), (0.53, 0.19, 0.28), (0.55, 0.11, 0.34), (0.58, 0.04, 0.38), (0.60, 0.00, 0.40)
850	(0.42, 0.58, 0.00), (0.45, 0.27, 0.28), (0.48, 0.13, 0.39), (0.51, 0.05, 0.44), (0.54, 0.00, 0.46)
900	(0.35, 0.65, 0.00), (0.38, 0.34, 0.28), (0.41, 0.17, 0.42), (0.44, 0.07, 0.49), (0.48, 0.00, 0.52)
1000	(0.22, 0.78, 0), (0.26, 0.45, 0.29), (0.29, 0.25, 0.46), (0.32, 0.08, 0.60), (0.35, 0.00, 0.65)
1100	(0.11, 0.89, 0.00), (0.12, 0.79, 0.09), (0.15, 0.58, 0.27), (0.18, 0.41, 0.41), (0.20, 0.24, 0.56), (0.23, 0.06, 0.71), (0.25, 0.00, 0.75)
1200	(0.00, 0.93, 0.07), (0.06, 0.65, 0.29), (0.10, 0.45, 0.45), (0.13, 0.26, 0.61), (0.16, 0.08, 0.76), (0.18, 0.00, 0.82)
1400	(0.00, 0.42, 0.58), (0.02, 0.32, 0.66), (0.05, 0.18, 0.77), (0.08, 0.06, 0.86), (0.10, 0.00, 0.90)

C: Paper published in international journals

- Gohivar, R. K., Mehta, U., Yadav, S. K., Koirala, R. P., Jha, I. S., & Adhikari, D. (2021). Thermodynamic, surface and transport properties of ternary Al–Sn–Zn liquid alloy and its sub binaries. *Philosophical Magazine*, *101*(11), 1380–1399. doi: 10.1080/14786435.2021.1912845
- Mehta, U., Koirala, I., Yadav, S. K., Koirala, R. P., & Adhikari, D. (2020). Prediction of thermodynamic and surface properties of ternary Ti–Si–Fe liquid alloy. *Modelling and Simulation in Materials Science and Engineering*, *28*(6), 1-16. doi: 10.1088/1361-651X/aba053
- Mehta, U., Yadav, S. K., Koirala, I., & Adhikari, D. (2020). Thermo-physical properties of ternary Al–Cu–Fe alloy in liquid state. *Philosophical Magazine*, *100*(19), 2417–2435. doi: 10.1080/14786435.2020.1775907
- Mehta, U., Yadav, S. K., Koirala, I., & Adhikari, D. (2022). Thermodynamic, surface and viscous properties of ternary Al–Fe–Mn alloy using theoretical modellings. *Physics and Chemistry of Liquids*, *60*(1), 111–128. doi: 10.1080/00319104.2021.1916933
- Mehta, U., Yadav, S. K., Koirala, I., Koirala, R. P., & Adhikari, D. (2021). Thermodynamic and surface properties of liquid Ti–Al–Fe alloy at different temperatures. *Physics and Chemistry of Liquids*, *59*(4), 585–596. doi: 10.1080/00319104.2020.1793333
- Mehta, U., Yadav, S. K., Koirala, I., Koirala, R. P., Shrestha, G. K., & Adhikari, D. (2020). Study of surface tension and viscosity of Cu–Fe–Si ternary alloy using a thermodynamic approach. *Helvion*, *6*(8), e04674. doi: 10.1016/j.helivon.2020.e04674
- Yadav, S. K., Mehta, U., & Adhikari, D. (2021). Optimization of thermodynamic and surface properties of ternary Ti–Al–Si alloy and its sub-binary alloys in molten state. *Helvion*, *7*(3), 1–10. doi: 10.1016/j.helivon.2021.e06511

D: Paper published in national journals

- Mehta, U., Yadav, S. K., Koirala, I., & Adhikari, D. (2020). Surface Properties of Al–Fe–Si Liquid Alloy Using Thermodynamic Database. *Journal of Nepal Physical Society*, *6*(2), 10–19. doi: 10.3126/jnphysoc.v6i2.34849

Yadav, S. K., Mehta, U., Gohivar, R. K., Dhungana, A., Koirala, R. P., & Adhikari, D. (2020). Reassessments of thermo-physical properties of Si–Ti melt at different temperatures. *Bibechana*, *17*, 146–153. doi: 10.3126/bibechana.v17i0.26877

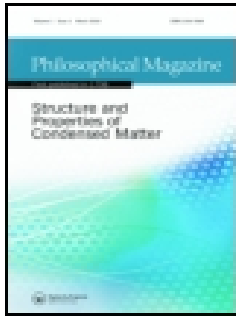
E: Participation in Conferences and Workshops

Conferences

- **3rd International Conference on Condensed Matter & Applied Physics**, 14–15 October, 2019, **Department of Physics, Government Engineering College**, Bikaner, Rajasthan, India.
- **On Scientific Session of 37th Annual Convention**, 6th February 2021, **Nepal Physical Society**, Ghantaghar, Kathmandu, Nepal.
- **International Conference on Material Science and Characterization Technology (ICMSCT)**, 26 -28 September, 2021, **St. Xavier’s College**, Maitighar, Kathmandu, Nepal

Workshop Participation

- Workshop on Research Writing and Publishing, 29–30 March, 2019, Nepal Physical Society, Eastern Chapter.
- Workshop on Research Writing and Publishing, 8–11 May, 2019, M. M. A. M. Campus, T. U., Biratnagar, Nepal.
- NPS School of Computing–2020, 4 July 2020 to 31 January 2021, Nepal Physical Society.



Thermo-physical properties of ternary Al–Cu–Fe alloy in liquid state

U. Mehta , S. K. Yadav , I. Koirala & D. Adhikari

To cite this article: U. Mehta , S. K. Yadav , I. Koirala & D. Adhikari (2020): Thermo-physical properties of ternary Al–Cu–Fe alloy in liquid state, Philosophical Magazine, DOI: [10.1080/14786435.2020.1775907](https://doi.org/10.1080/14786435.2020.1775907)

To link to this article: <https://doi.org/10.1080/14786435.2020.1775907>



Published online: 09 Jun 2020.



Submit your article to this journal [↗](#)







View related articles [↗](#)



View Crossmark data [↗](#)



Thermo-physical properties of ternary Al–Cu–Fe alloy in liquid state

U. Mehta ^{a,b}, S. K. Yadav ^b, I. Koirala ^a and D. Adhikari ^b

^aCentral Department of Physics, T.U., Kathmandu, Nepal; ^bDepartment of Physics, MMAMC, T.U. Biratnagar, Nepal

ABSTRACT

The thermodynamic and surface properties of the ternary Al–Cu–Fe alloy in the liquid state have been computed using different models. The thermodynamic properties, such as activity and excess free energy of mixing and the surface properties, such as surface tension have been calculated. The temperature dependence of activity and surface concentration of the components of the ternary Al–Cu–Fe alloy in fixed proportion of any two components have also been calculated. The surface tension of the alloy with respect to the change in temperature in the range 1823–2073 K has also been studied.

ARTICLE HISTORY

Received 29 March 2020
Accepted 25 May 2020

KEYWORDS

Al–Cu–Fe alloy;
thermodynamic properties;
surface properties

1. Introduction

Several investigations have long been carried out to explain the compositional dependence of surface tension of a liquid solution [1–17]. Some of these investigations were focused to study the surface tension of the binary liquid solutions [1,2,5,7,12,14,17] while others were developed for the ternary liquid systems [3,4,7,13]. A model for the estimation of concentration based surface tension of binary liquid alloys was developed by Speiser et al. [5] and Yeum et al. [6] which was later modified by Tanaka et al. [18] by taking into account the change in binding energy in the surface phase, and β (ratio of coordination numbers in surface phase and bulk phase) = 0.83 in the place of 0.75. In both of these approaches for the estimation of surface tension of binary liquid alloys surface entropy was neglected [19]. However, studies show that surface entropy term cannot be neglected in order to get good results of surface tension for binary liquid solutions as it contributes significantly in the values of surface tension [19].

The present work is focused to study the thermodynamic [1,8] and surface properties [20–23] of Al–Cu–Fe alloys in the liquid state at temperatures 1823, 1873, 1973 and 2073 K at different compositions using different models.

CONTACT D. Adhikari  adksbdev@yahoo.com  Department of Physics, Mahendra Morang A. M. Campus, T.U., Biratnagar, Nepal

© 2020 Informa UK Limited, trading as Taylor & Francis Group

The sub-binary system Al–Cu of the alloy has several intermediate phases like AlCu, Al₂Cu, Al₂Cu₃, etc. [24–26], whereas the phase diagram of sub-binary system Al–Fe depicts number of stable phases including Al₂Fe, Al₃Fe and Al₅Fe₂ [26, 27]. However, there is no intermediate phase for Cu–Fe alloys [25, 26]. The sub-binary alloys Al–Cu and Al–Fe are ordering in nature while the sub-binary alloy Cu–Fe is segregating in nature [26]. The studies on the ternary Al–Cu–Fe alloys by several researchers show that there are number of stable ternary phases like Al₂₃CuFe₄, Al₁₀Cu₁₀Fe, Al₁₈CuFe, Al₆Cu₂Fe, etc. [25,28–30] for this alloy. The melting temperature of this alloy system changes considerably with the variation of Fe content in the alloy which can be estimated from the phase diagram. From the phase diagram of ternary Al–Cu–Fe alloy, it is seen that this alloy exists in the liquid state above 1800 K at all compositions. In this work, firstly the thermodynamic and surface properties of the concerned sub-binary systems have been calculated using appropriate models and secondly these results have been used to compute the thermodynamic and surface properties of the preferred ternary alloys.

The mathematical modeling of the work is presented in Section 2, the results and discussion is presented in Section 3 and the conclusions are listed in Section 4.

2. Mathematical modeling

The partial excess Gibbs free energy (G_i^{xs}) of i th component of a multi-component alloy can be expressed in terms of integral excess Gibbs free energy (G_M^{xs}) as [31–34]

$$G_i^{xs} = G_M^{xs} + \sum_{j=1}^m (\delta_{ij} - x_j) \frac{\partial G_M^{xs}}{\partial x_j} \quad (1a)$$

where $i, j = 1, 2$ for binary and $i, j = 1, 2, 3$ for ternary liquid alloys. δ_{ij} is the Kronecker delta function, and $\delta_{ij} = 1$ if $i = j$ and $\delta_{ij} = 0$ if $i \neq j$. For binary system ($m = 2$), the above equation can be expressed as

$$G_1^{xs} = G_M^{xs} + x_2 \left(\frac{\partial G_M^{xs}}{\partial x_1} - \frac{\partial G_M^{xs}}{\partial x_2} \right) \quad \text{and} \quad G_2^{xs} = G_M^{xs} - x_1 \left(\frac{\partial G_M^{xs}}{\partial x_1} - \frac{\partial G_M^{xs}}{\partial x_2} \right) \quad (1b)$$

and for ternary system ($m = 3$), Equation (1a) can be obtained as

$$\begin{aligned} G_1^{xs} &= G_M^{xs} + \frac{\partial G_M^{xs}}{\partial x_1} - \left(x_1 \frac{\partial G_M^{xs}}{\partial x_1} + x_2 \frac{\partial G_M^{xs}}{\partial x_2} + x_3 \frac{\partial G_M^{xs}}{\partial x_3} \right), G_2^{xs} \\ &= G_M^{xs} + \frac{\partial G_M^{xs}}{\partial x_2} - \left(x_1 \frac{\partial G_M^{xs}}{\partial x_1} + x_2 \frac{\partial G_M^{xs}}{\partial x_2} + x_3 \frac{\partial G_M^{xs}}{\partial x_3} \right) \quad (1c) \\ \text{and} \quad G_3^{xs} &= G_M^{xs} + \frac{\partial G_M^{xs}}{\partial x_3} - \left(x_1 \frac{\partial G_M^{xs}}{\partial x_1} + x_2 \frac{\partial G_M^{xs}}{\partial x_2} + x_3 \frac{\partial G_M^{xs}}{\partial x_3} \right) \end{aligned}$$

The compositional dependence of the integral excess Gibbs free energy of binary liquid alloys can be expressed in terms of Redlich-Kister (R-K) polynomial as [35–37]

$$G_M^{xs} = x_i x_j \sum_{k=0}^n A_{ij}^k (x_i - x_j)^k \quad (2)$$

where A_{ij}^k are coefficients of R-K polynomial of binary system ‘ij’ for excess Gibbs free energy, and x_i and x_j are the mole fractions of the components in the binary alloy. The A_{ij}^k are concentration independent and linear temperature dependent terms. According to Chou model [21], the excess free energy of mixing for ternary system can be given as

$$G_M^{xs} = x_1 x_2 \sum_{k=0}^n A_{12}^k (x_1 - x_2)^k + x_2 x_3 \sum_{k=0}^n A_{23}^k (x_2 - x_3)^k + x_3 x_1 \sum_{k=0}^n A_{31}^k (x_3 - x_1)^k + f x_1 x_2 x_3 \quad (3)$$

where f is the ternary interaction term and can be given as [22]

$$\begin{aligned} f = & (2\xi_{12} - 1)[A_{12}^3(3(x_1 - x_2)^2 x_3 + 3(x_1 - x_2)x_3^2(2\xi_{12} - 1) + x_3^3(2\xi_{12} - 1)^2) \\ & + A_{12}^2((2\xi_{12} - 1)x_3 + 2(x_1 - x_2)) + A_{12}^1] \\ & + (2\xi_{23} - 1)[A_{23}^3(3(x_2 - x_3)^2 x_1 + 3(x_2 - x_3)x_1^2(2\xi_{23} - 1) + x_1^3(2\xi_{23} - 1)^2) \\ & + A_{23}^2((2\xi_{23} - 1)x_1 + 2(x_2 - x_3)) + A_{23}^1] \\ & + (2\xi_{31} - 1)[A_{31}^3(3(x_3 - x_1)^2 x_2 + 3(x_3 - x_1)x_2^2(2\xi_{31} - 1) + x_2^3(2\xi_{31} - 1)^2) \\ & + A_{31}^2((2\xi_{31} - 1)x_2 + 2(x_3 - x_1)) + A_{31}^1] \end{aligned} \quad (4)$$

The terms ξ_{ij} in Equation (4) are the similarity indexes and are expressed as

$$\xi_{12} = \frac{\eta_1}{\eta_1 + \eta_{11}}, \quad \xi_{23} = \frac{\eta_{11}}{\eta_{11} + \eta_{111}}, \quad \xi_{31} = \frac{\eta_{111}}{\eta_{111} + \eta_1} \quad (5)$$

The term η is the deviation sum of squares and can be estimated as

$$\begin{aligned} \eta_1 &= \int_0^1 (G_{12}^{xs} - G_{13}^{xs})^2 dx_1, \quad \eta_{11} = \int_0^1 (G_{21}^{xs} - G_{23}^{xs})^2 dx_2, \\ \eta_{111} &= \int_0^1 (G_{31}^{xs} - G_{32}^{xs})^2 dx_3 \end{aligned} \quad (6)$$

The terms x_1 , x_2 and x_3 are the mole fractions of components in the ternary alloy. The values of partial excess free energy for binary liquids are obtained using Equation (2) in Equation (1b). Similarly, the values of partial excess free energy for ternary alloys are obtained using Equation (3) in Equation (1c).

The partial excess free energy of components in the alloy are related with their respective activities (a_i) as [38]

$$G_i^{xs} = RT \ln \left(\frac{a_i}{x_i} \right) \quad (7)$$

where R is universal gas constant and T is absolute temperature.

According to Kohler model [8], the expression for integral excess Gibbs free energy of ternary liquid alloy in terms of integral excess Gibbs free energy of sub-binary systems are given as

$$\begin{aligned} G_M^{xs} = & (x_1^2 + x_2^2) G_{12}^{xs} \left(\frac{x_1}{x_1 + x_2}, \frac{x_2}{x_1 + x_2} \right) \\ & + (x_2^2 + x_3^2) G_{23}^{xs} \left(\frac{x_2}{x_2 + x_3}, \frac{x_3}{x_2 + x_3} \right) \\ & + (x_3^2 + x_1^2) G_{31}^{xs} \left(\frac{x_3}{x_3 + x_1}, \frac{x_1}{x_3 + x_1} \right) \end{aligned} \quad (8)$$

where G_{ij}^{xs} are integral excess Gibbs free energy of binary alloys defined by Equation (2) at binary concentration $\left(\frac{x_i}{x_i + x_j}, \frac{x_j}{x_i + x_j} \right)$. The Toop model is an asymmetrical model in which a symmetrical element has to be chosen. According to this model, the expression for excess thermodynamic for a symmetrical element x_1 is given as [8]

$$\begin{aligned} G_M^{xs} = & \frac{x_2}{(x_2 + x_3)} G_{12}^{xs}(x_1, 1 - x_1) + (x_2^2 + x_3^2) G_{23}^{xs} \left(\frac{x_2}{x_2 + x_3}, \frac{x_3}{x_2 + x_3} \right) \\ & + \frac{x_3}{(x_2 + x_3)} G_{13}^{xs}(x_1, 1 - x_1) \end{aligned} \quad (9)$$

The surface tension of binary and ternary liquid alloy using Butler equation is given as [1]

$$\sigma = \sigma_i + \frac{RT}{\alpha_i} \ln \left(\frac{x_i^s}{x_i^b} \right) + \frac{G_{s,i}^{xs} - G_{b,i}^{xs}}{\alpha_i} \quad (10)$$

where σ_i are the surface tension of pure components i ($i = 1, 2$ for binary and $i = 1, 2, 3$ for ternary liquid components). x_i^s and x_i^b are surface and bulk concentrations of individual components in the liquid mixture. $G_{s,i}^{xs}$ and $G_{b,i}^{xs}$ are the partial excess free energy for surface and bulk phase respectively which are related as $G_{s,i}^{xs} = \beta G_{b,i}^{xs}$ [15,31–34,39–41]. The value of β depends on crystal

structure and is taken as 0.82 for the liquid phase [15,41]. The molar surface area α_i of the pure component in the alloy is given as [15,31–34,39–41]

$$\alpha_i = f N_A^{1/3} \left(\frac{M_i}{\rho_i} \right)^{2/3} \quad (11)$$

where N_A is the Avogadro's number, and M_i and ρ_i are molar mass and density of the pure components of the liquid alloy. f is geometric factor and its value for an average simple liquid metal is taken to be 1.00 [15,41]. The temperature dependence of surface tension (σ) and density (ρ) of pure element in the liquid alloy are expressed as [42]

$$\sigma = \sigma_0 + \frac{\partial \sigma}{\partial T} (T - T_0), \quad \text{and} \quad \rho = \rho_0 + \frac{\partial \rho}{\partial T} (T - T_0) \quad (12)$$

where σ_0 and ρ_0 are the surface tension and density of pure component at its melting temperature T_0 and T is the temperature of interest. $\frac{\partial \sigma}{\partial T}$ and $\frac{\partial \rho}{\partial T}$ are the temperature derivative terms of surface tension and density respectively.

The excess surface tension of the ternary liquid alloys using Chou, Kohler and Toop model are obtained by using the same Equations (3), (8) and (9) respectively those are used for integral excess Gibbs free energy by replacing G_M^{xs} by σ^{xs} . The values of coefficients of R-K polynomial (A_{ij}^k) in these equations for G_M^{xs} have to be replaced by the coefficients (L_{ij}^k) for σ^{xs} . σ^{xs} of sub-binary and ternary liquid alloys is defined as the deviation of the surface tensions from the value obtained using additive rule and given by the relation

$$\sigma^{xs} = \sigma - \sum_i (\sigma_i x_i) \quad (13)$$

where σ_1 , σ_2 and σ_3 are the surface tensions of the pure components of the liquid mixture.

3. Results and discussion

The partial excess Gibbs free energy of individual component of sub-binary systems was computed using the values of coefficients of R-K polynomial (A_{ij}^k) [43] from Table 1 for sub-binary systems Al–Cu and Cu–Fe in Equations. (1)

Table 1. Coefficients of R-K polynomials (A_{ij}^k) of G_M^{xs} for sub-binary liquid alloys.

Systems	Coefficients (A_{ij}^k) [J mol ⁻¹]		
	A^0	A^1	A^2
Al–Cu [43]	$-66622 + 8.1 T$	$46800 - 90.8 T + 10 T \cdot \ln T$	-2812
Cu–Fe [43]	$36088.0 - 2.32968 T$	$324.53 - 0.03270 T$	$10355.40 - 3.60297 T$
Al–Fe [This work]	$-90335.45 \cdot \exp\left(-\frac{T}{32800}\right)$	$-31734.57 \cdot \exp\left(-\frac{T}{69980}\right)$	$-4458.50 \cdot \exp\left(-\frac{T}{165600}\right)$

and (2). These parameters are described as a linear functions of temperatures in the form $A_{ij}^k = a_{ij}^k - b_{ij}^k \cdot T$ where a_{ij}^k is the enthalpy-like semi-empirical coefficient in J mol^{-1} for the k th order interaction energy of the A-B liquid phase and b_{ij}^k is the entropy-like semi-empirical coefficient (with opposite sign) in $\text{J mol}^{-1} \text{K}^{-1}$ for the k th order interaction energy of the A-B liquid phase. It has been observed that in linear model, if $a_{ij}^0 < 0$ and if $b_{ij}^0 > 2.R$, then there appears high temperature calculated artifact [44,45]. The values of parameters presented in COST 507 [43] for the Al-Fe liquid alloy fall in this domain. In order to avoid artifact, the exponential T-dependence of the interaction energy parameters for excess Gibbs energy called exponential model have been employed for Al-Fe melt. According to this model, the exponential T-dependence of the interaction energy parameters (A_{ij}^k) is expressed as [44,45]

$$A_{ij}^k = h_{ij}^k \cdot \exp\left(-\frac{T}{\tau_{ij}^k}\right) \quad (14)$$

where h_{ij}^k (J mol^{-1}) and τ_{ij}^k (K) are the modeling parameters.

The exponential temperature-dependent interaction energy parameters for Al-Fe sub-binary system have been optimised using Equation (14) and the experimental data [26]. The values so obtained are presented in Table 1. These values were then used to calculate the partial excess free energy of individual components of the Al-Fe alloy with the help of Equations (1) and (2). These partial excess free energies were then used to compute the activities of the respective components of the above-mentioned sub-systems in Equation (7). The compositional dependence of activity and excess Gibbs free energy for sub-binary Al-Cu alloy is computed at 1373 K while these for the Al-Fe and Cu-Fe alloys were computed at 1873 and 1823 K, respectively (Figure 1(a-d)). This was done due to availability of the data for the respective systems at these temperatures. The computed values of activity and excess Gibbs free energy of Al-Cu alloy at 1373 K were found to be in well agreement with the respective observed values [26] and the values obtained by Kanibolotsky et al. [46] (Figure 1(a,d)). The computed values of activities and excess Gibbs free energy of Al-Fe liquid alloy at 1873 K were also found to be in good agreement with the work of Adhikari et al. [47] and observed values [26] (Figure 1(b,d)). The activity and Gibbs free energy of Cu-Fe alloy at 1823 K are all in a very good agreement with the observed value [26] (Figure 1(c,d)). The Gibbs free energy of this alloy is found to be positive (Figure 1(d)) which indicates that it shows demixing tendency or is segregating in nature. As a result, the compositional dependence of activities of Cu and Fe show positive deviations from Raoult's law and hence their plots reflect unusual trends (Figure 1(c)).

The activities of the components of ternary Al-Cu-Fe liquid alloy at five different cross-sections ($x_{\text{Cu}}/x_{\text{Fe}} = 1:9, 3:7, 5:5, 7:3$ and $9:1$) have been calculated from Al corner (x_{Al}) at 1823 K (Figure 2(a-e)) using Equations (1c) and values

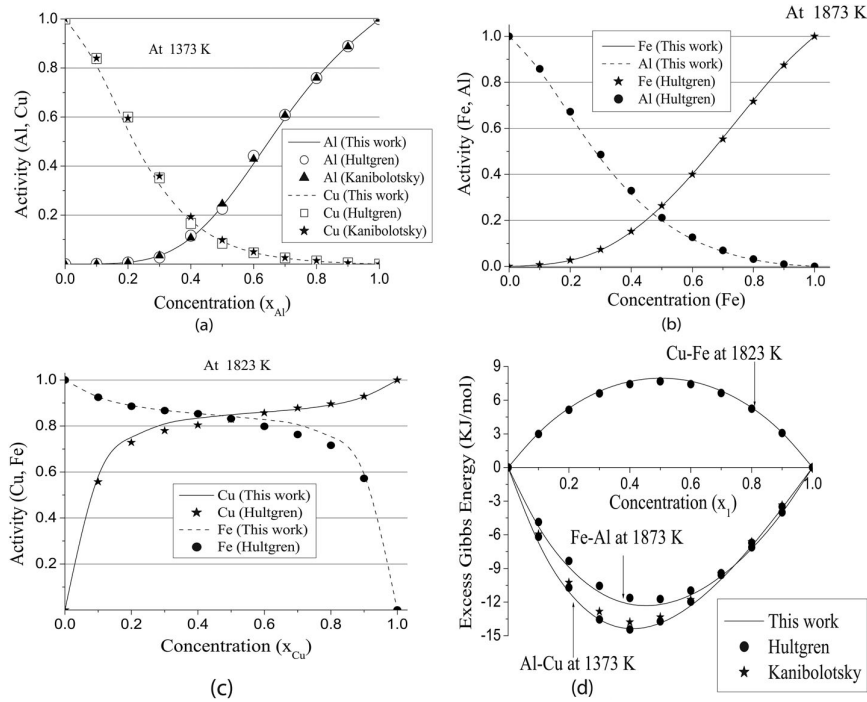


Figure 1. (a) Variation of activity of Al and Cu with concentration of Al in Al–Cu alloy at 1373 K. (b) Variation of activity of Al and Fe with concentration Fe at 1873 K. (c) Variation of activity of Cu and Fe with concentration Cu at 1823 K. (d) Compositional dependence of excess free energy of mixing of binary sub-systems Al–Cu, Al–Fe and Cu–Fe at 1373, 1873 and 1823 K respectively.

from Table 1. It was found that the activity of the component Al increases with an increase in the concentration of Al at all considered cross-sections in the ternary alloy. However, the behavior of Cu and Fe as regards of activity was not the same at different ratios of Cu and Fe ($x_{Cu}/x_{Fe} = 1:9, 5:5$ and $3:7$) with respect to the variation of the concentration of Al (Figure 2(a–e)). When the concentration of Cu was lesser than the concentration of Fe ($x_{Cu}/x_{Fe} = 1:9$ and $3:7$) in ternary Al–Cu–Fe alloy, the activity of Cu was also lesser at all composition of Al (Figure 2(a,b)). When the concentration Cu was equal to the concentration of Fe ($x_{Cu}/x_{Fe} = 5:5$) in the ternary alloy, the activity of Cu was found to be greater in the region $x_{Al} < 0.5$ and lesser in the region $x_{Al} > 0.5$ than that of Fe (Figure 1(c)). As the concentration of Cu increased and became greater than that of Fe ($x_{Cu}/x_{Fe} = 7:3$ and $9:1$), the activity of Cu also exceeded the activity of Fe (Figure 2(d,e)). Such behavior of the ternary alloy as regards of the activity of components may be due to the segregating or phase separating tendency of Cu and Fe in the liquid solution.

The compositional dependence of G_M^{XS} have been computed from Al corners at above mentioned cross-sections in the framework of Chou, Kohler and Toop models at 1873 K using Equations. (3), (8) and (9) and values from Table 1. The

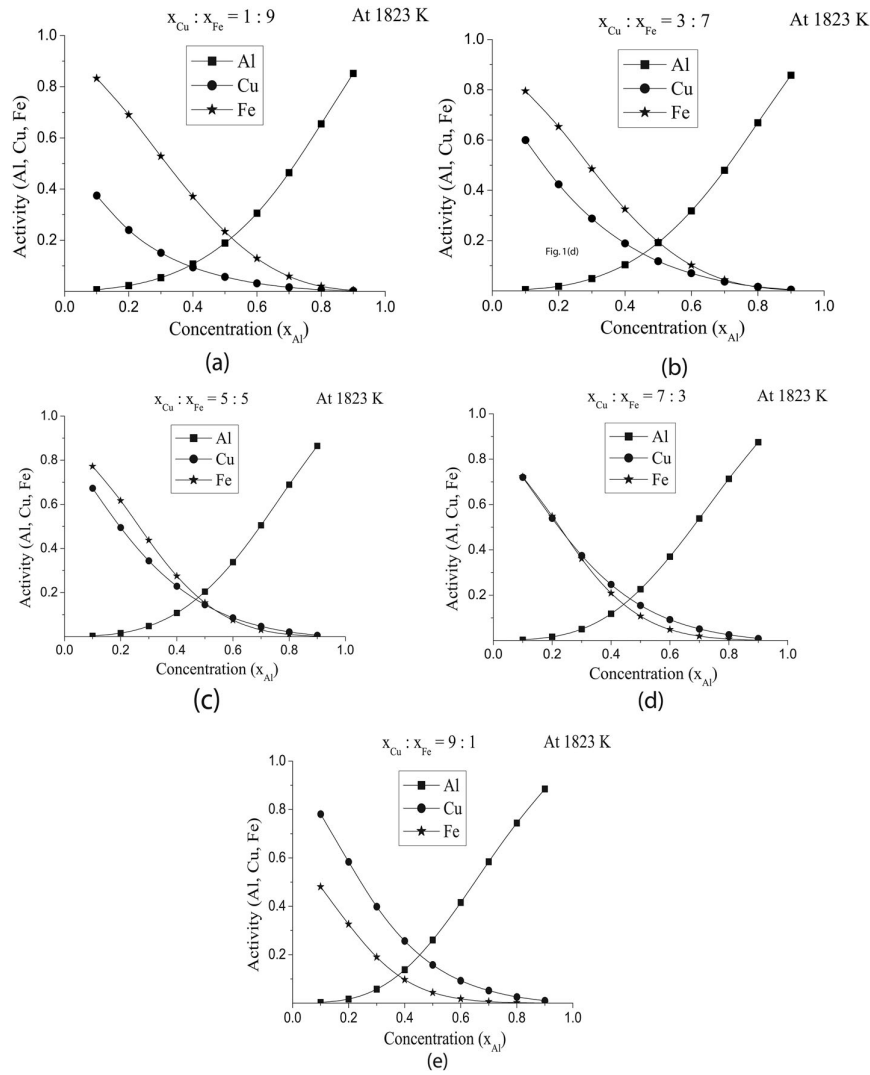


Figure 2. (a) Variation of activity of Al, Cu and Fe from Al corner at Cu:Fe = 1:9 in Al–Cu–Fe alloy at 1823 K. (b) Variation of activity of Al, Cu and Fe from Al corner at Cu:Fe = 3:7 in Al–Cu–Fe alloy at 1823 K. (c) Variation of activity of Al, Cu and Fe from Al corner at Cu:Fe = 5:5 in Al–Cu–Fe alloy at 1823 K. (d) Variation of activity of Al, Cu and Fe from Al corner at Cu:Fe = 7:3 in Al–Cu–Fe alloy at 1823 K. (e) Variation of activity of Al, Cu and Fe from Al corner at Cu:Fe = 9:1 in Al–Cu–Fe alloy at 1823 K.

values so computed were found to be in good agreement with one another (Figure 3(a–e)). The peak value of the excess Gibbs free energy of Al–Cu–Fe alloy in liquid state computed from Al corners at any composition ratio of Cu and Fe and just reversing the composition did not change significantly. The compositional dependence of G_M^{XS} from Fe (x_{Fe}) corners at three different cross-sections ($x_{Al}/x_{Cu} = 1:9, 5:5$ and $9:1$) have also been computed at 1823 K

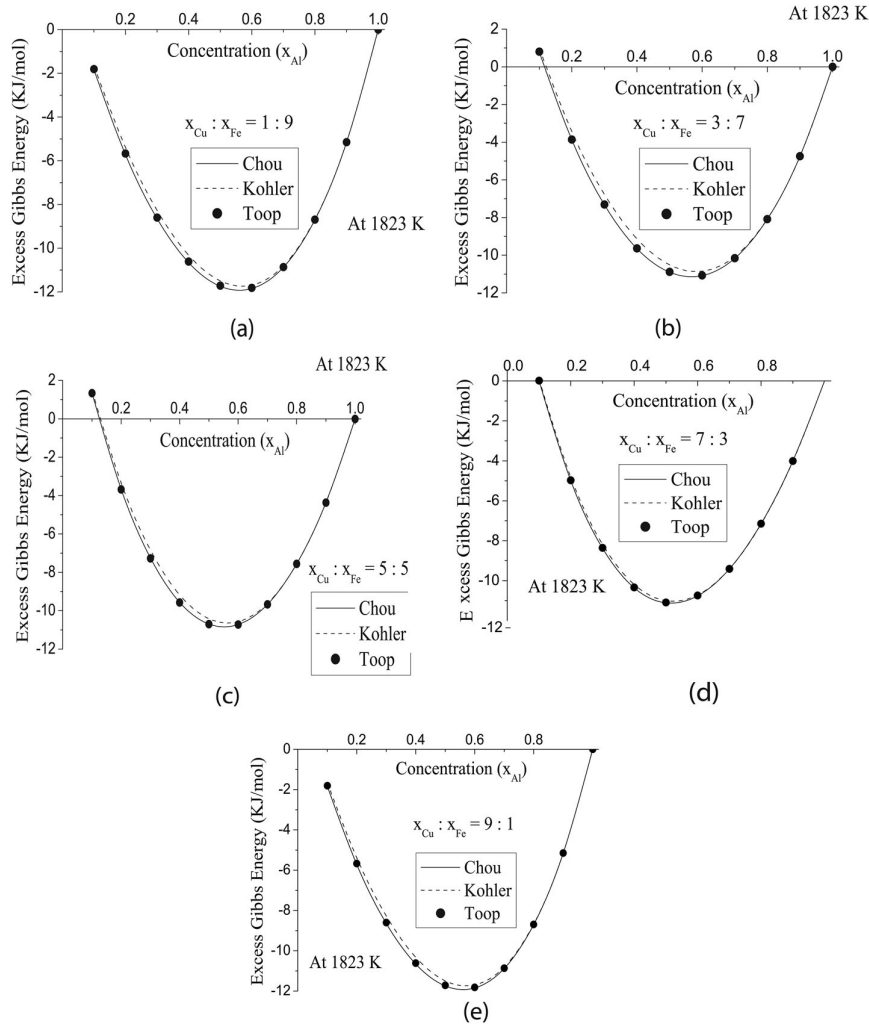


Figure 3. (a) Variation of excess free energy (in KJ/mol) of mixing of Al–Cu–Fe alloy from Al corner at Cu:Fe = 1:9 in Al–Cu–Fe alloy at 1823 K. (b) Variation of excess free energy (in KJ/mol) of mixing of Al–Cu–Fe alloy from Al corner at Cu:Fe = 3:7 in Al–Cu–Fe alloy at 1823 K. (c) Variation of excess free energy (in KJ/mol) of mixing of Al–Cu–Fe alloy from Al corner at Cu:Fe = 5:5 in Al–Cu–Fe alloy at 1823 K. (d) Variation of excess free energy (in KJ/mol) of Al–Cu–Fe alloy from Al corner at Cu:Fe = 7:3 in Al–Cu–Fe alloy at 1823 K. (e) Variation of excess free energy (in KJ/mol) of mixing of Al–Cu–Fe alloy from Al corner at Cu:Fe = 9:1 in Al–Cu–Fe alloy at 1823 K.

(Figure 4(a–c)). When the concentration of Al was very low ($x_{Al}/x_{Cu} = 1:9$), the compositional dependence of G_M^{XS} was found to be positive in the region $x_{Fe} > 0.2$ and all models used here to compute the G_M^{XS} agree with each other (Figure 4(a)). As the content of Al in the ternary alloy was increased, the G_M^{XS} became negative (Figure 4(b, c)).

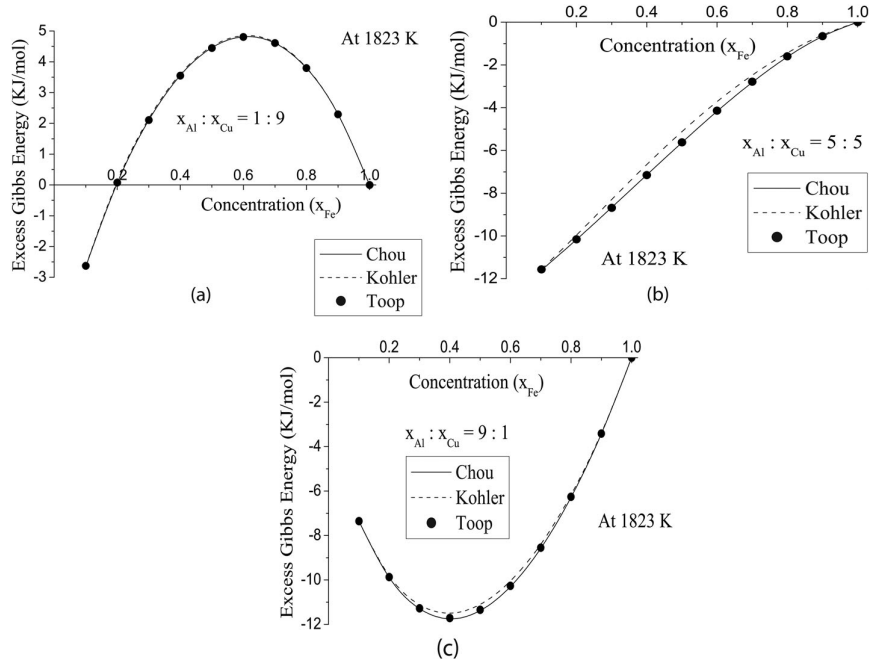


Figure 4. (a) Variation of excess free energy (in KJ/mol) of mixing of Al–Cu–Fe alloy from Fe corner at Cu:Fe = 1:9 in Al–Cu–Fe alloy at 1823 K. (b) Variation of excess free energy (in KJ/mol) of mixing of Al–Cu–Fe alloy from Fe corner at Cu:Fe = 5:5 in Al–Cu–Fe alloy at 1823 K. (c) Variation of excess free energy (in KJ/mol) of mixing of Al–Cu–Fe alloy from Fe corner at Cu:Fe = 9:1 in Al–Cu–Fe alloy at 1823 K.

Table 2. Values of density (ρ_0) and surface tension (σ_0) of Al, Fe and Cu near their melting temperatures (T_0) and variation of density and surface tension with temperature.

Elements	T_0 (K)	ρ_0 (kg m^{-3})	$\frac{\partial \rho}{\partial T}$ ($\text{kg m}^{-3}\text{K}^{-1}$)	σ_0 (Nm^{-1})	$\frac{\partial \sigma}{\partial T}$ ($\text{N m}^{-1}\text{K}^{-1}$)
Al	933	2385	-0.28	0.914	-0.00035
Fe	1809	7030	-0.833	1.872	-0.00049
Cu	1360	8000	-0.801	1.285	-0.00013

In order to compute the surface tension (σ) and surface concentration (x_i^S ; $i = 1, 2$) of sub-binary systems requires the surface tension and density of pure components and their variations with temperature. The required values were taken from the ref. [42] and are listed in Table 2. The values of compositional dependence of x_i^S and σ for Al–Cu, Al–Fe and Cu–Fe at 1823 K are then computed using Equations (10–12) and Table 2 (Figure 5(a–d)). The excess surface tension (σ^{xs}) and surface concentration for sub-binary systems Al–Cu, Al–Fe and Cu–Fe were computed using respective partial excess free

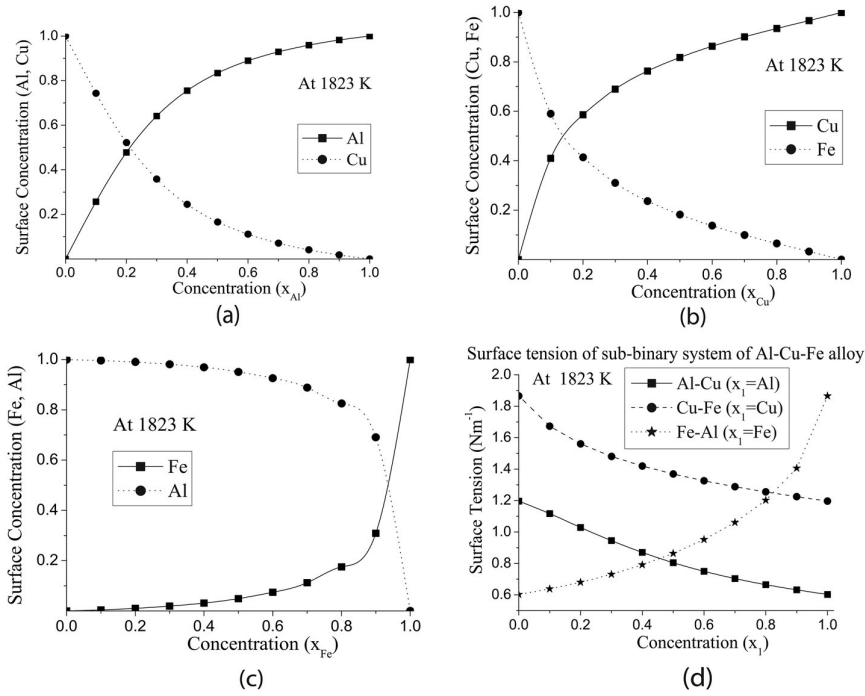


Figure 5. (a) Variation of surface concentrations of Al and Cu with concentration of Al in Al–Cu liquid alloy at 1823 K. (b) Variation of surface concentrations of Cu and Fe with concentration of Cu in Cu–Fe liquid alloy at 1823 K. (c) Variation of surface concentrations of Al and Fe with concentration of Fe in Al–Fe liquid alloy at 1823 K. (d) Compositional dependence of surface tensions of binary sub-systems Al–Cu, Al–Fe and Cu–Fe at 1823 K.

Table 3. Optimized values of coefficients of R-K polynomials for excess surface tension of sub-binary systems used in calculation of surface tension (Chou, Toop and Kohler models). The temperature (K) dependent optimized parameters (L_{ij}^k) are for the temperature range of 1823–2073 K.

Systems	Coefficients (L_{ij}^k) [$N m^{-1}$]
Al–Cu	$L^0 = -6.7140 \times 10^{-5}T - 0.2561$
	$L^1 = 1.0508 \times 10^{-4}T - 0.1937$
	$L^2 = -1.4584 \times 10^{-4}T - 0.4289$
	$L^3 = 8.6536 \times 10^{-5}T - 0.2745$
Cu–Fe	$L^0 = 4.7557 \times 10^{-4}T - 1.5031$
	$L^1 = -4.1258 \times 10^{-4}T - 1.1503$
	$L^2 = 6.0323 \times 10^{-4}T - 1.4916$
	$L^3 = -5.3145 \times 10^{-4}T - 1.2674$
Fe–Al	$L^0 = 3.9122 \times 10^{-4}T - 2.1101$
	$L^1 = 3.6858 \times 10^{-4}T - 1.5993$
	$L^2 = 1.1457 \times 10^{-3}T - 3.5833$
	$L^3 = 1.1138 \times 10^{-3}T - 3.3383$

energy and the coefficients of R-K polynomials for excess surface tension were optimised as a function of temperature in the range 1823–2073 K. The optimised values of R-K polynomials for sub-binary alloys are listed in Table 3.

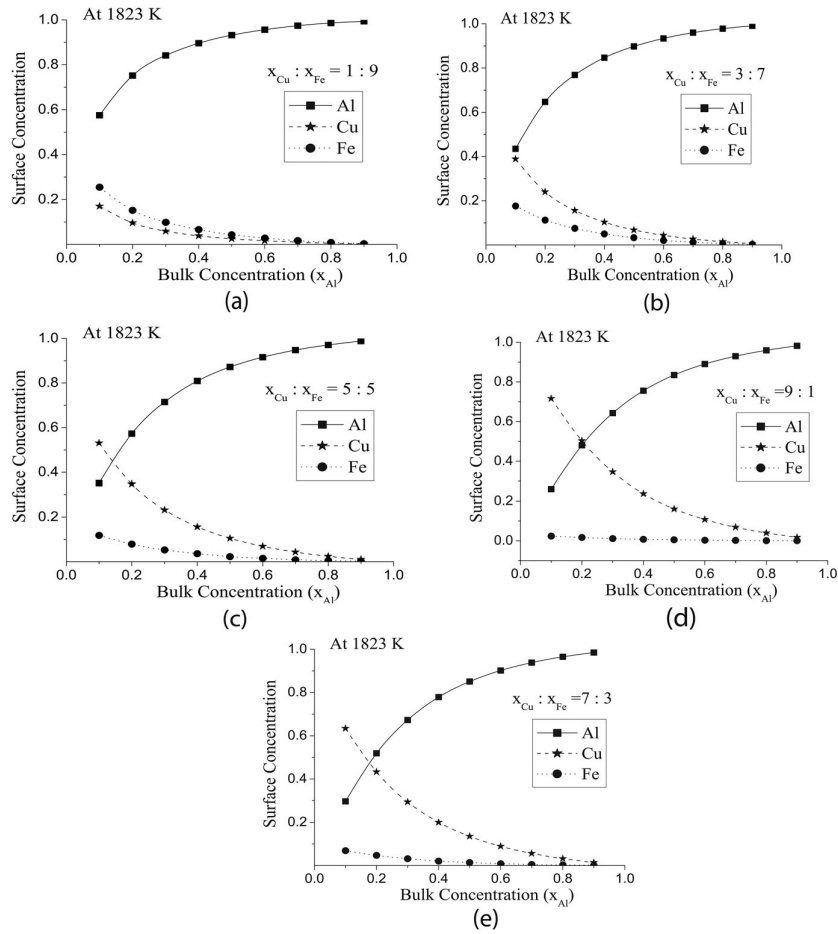


Figure 6. (a) Variation of surface concentration of different components with bulk concentration from Al corners at Cu:Fe = 1:9 in Al-Cu-Fe alloy at 1823 K. (b) Variation of surface concentration of different components with bulk concentration from Al corners at Cu:Fe = 3:7 in Al-Cu-Fe alloy at 1823 K. (c) Variation of surface concentration of different components with bulk concentration from Al corners at Cu:Fe = 5:5 in Al-Cu-Fe alloy at 1823 K. (d) Variation of surface concentration of different components with bulk concentration from Al corners at Cu:Fe = 7:3 in Al-Cu-Fe alloy at 1823 K. (e) Variation of surface concentration of different components with bulk concentration from Al corners at Cu:Fe = 9:1 in Al-Cu-Fe alloy at 1823 K.

The surface concentration of the constituents of the ternary Al-Cu-Fe alloy was computed from the corner of Al at above mentioned five cross-sections (Figure 6(a-e)) at 1823 K using Equation (10). The surface concentration of Al was found to be much higher than that of other components at all regions when concentration of Cu is lower as compared to the concentration of Fe ($x_{Cu}/x_{Fe} = 1:9$ and $3:7$) in Al-Cu-Fe alloy (Figure 6(a,b)). This is due to the lower value of surface tension of Al as compared to that of Cu and Fe. As the concentration of Cu was increased in the ratio of Cu and Fe in Al-Cu-Fe

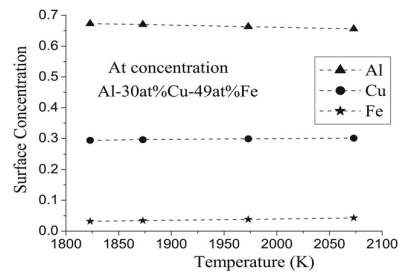


Figure 7. Variation of surface concentration of the components of Al–Cu–Fe alloy with temperature at composition Al–30at%Cu–49at%Fe.

alloy, the surface concentration of Cu exceeded the surface concentration of Al at the lower concentration region of Al (Figure 6(c–e)). However, at higher concentration region of Al again the Al atoms segregate more in the surface. The surface concentration of the constituents of ternary Al–Cu–Fe alloy with fixed composition of the constituents (Al–30at%Cu–49at%Fe) at different temperatures (1873–2100 K) have also been computed and plotted in Figure 7. It is clearly observed that the Al atoms segregate higher than any other components of Al–Cu–Fe alloy in the surface at all temperatures. It was found that most of the Fe atoms remain in the bulk of the solution at any temperatures and concentration which is due to the highest value of surface tension among the constituents of Al–Cu–Fe alloy (Figure 7).

The excess surface tensions obtained for sub-binary system were then used in Equations. (8), (9) and (11) to compute excess surface tension of the ternary Al–Cu–Fe alloy. The computed excess surface tension for the ternary alloy was used in Equation (13) to compute the surface tension of the alloy using Chou, Kohler and Toop models. Equation (10) was used to compute the surface tension of the ternary alloy using the Butler model. The surface tension of the ternary Al–Cu–Fe alloy computed from the Al corner at aforementioned cross-sections at 1823 K is plotted in Figure 7(a–e). The surface tension computed using different models at all cross-sections were found to agree well with each other. It is also evident from the figures that the surface tension of the alloy decreases with an increase in the concentration of Al as expected. The surface tension of the ternary Al–Cu–Fe alloy at 1823 K from the Fe corner at three different fixed composition ratio of Al and Cu ($x_{Cu}/x_{Fe} = 1:9, 5:5$ and $9:1$) using different models (Figure 9(a–c)). It was found that the surface tension of the alloy increases with increase in the concentration of Fe. This is not beyond the expectation as the surface tension of Fe is the greatest among the constituents of Al–Cu–Fe alloy.

The temperature dependence of activity and surface tension in the ternary Al–Cu–Fe alloy have also been studied. The activities of the components Al, Cu and Fe of the alloy with fixed composition Al–35at%Cu–30at%Fe in the

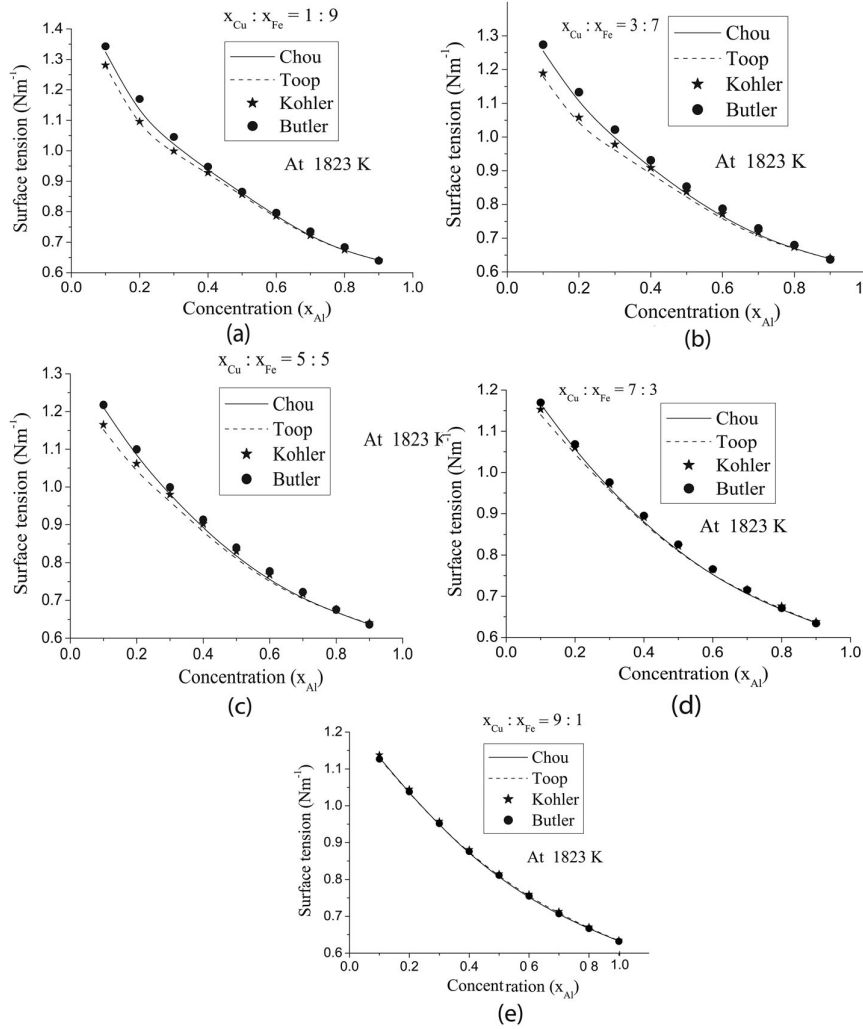


Figure 8. (a) Variation of surface tension of Al-Cu-Fe alloy with bulk concentration from Al corners at Cu:Fe = 1:9 in Al-Cu-Fe alloy at 1823 K. (b) Variation of surface tension of Al-Cu-Fe alloy with bulk concentration from Al corners at Cu:Fe = 3:7 in Al-Cu-Fe alloy at 1823 K. (c) Variation of surface tension of Al-Cu-Fe alloy with bulk concentration from Al corners at Cu:Fe = 5:5 in Al-Cu-Fe alloy at 1823 K. (d) Variation of surface tension of Al-Cu-Fe alloy with bulk concentration from Al corners at Cu:Fe = 7:3 in Al-Cu-Fe alloy at 1823 K. (e) Variation of surface tension of Al-Cu-Fe alloy with bulk concentration from Al corners at Cu:Fe = 9:1 in Al-Cu-Fe alloy at 1823 K.

ternary alloys have been computed in the temperature range 1873–2073 K and plotted in Figure 10. It was found that the activity of Al and Cu increased linearly at a very small rate with the increase in temperature. The activity of the component Fe was observed to be almost non-responsive to the temperature change. As stated earlier, the surface tension of the ternary Al-Cu-Fe alloy at

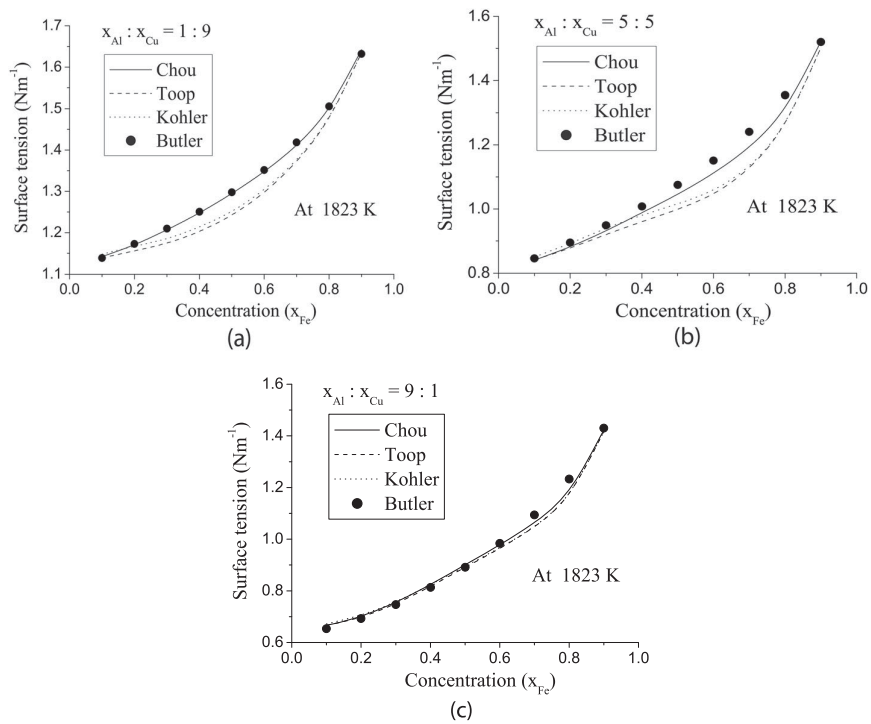


Figure 9. (a) Variation of surface tension of Al–Cu–Fe alloy with bulk concentration from Fe corners at Al:Cu = 1:9 in Al–Cu–Fe alloy at 1823 K. (b) Variation of surface tension of Al–Cu–Fe alloy with bulk concentration from Fe corners at Al:Cu = 5:5 in Al–Cu–Fe alloy at 1823 K. (c) Variation of surface tension of Al–Cu–Fe alloy with bulk concentration from Fe corners at Al:Cu = 9:1 in Al–Cu–Fe alloy at 1823 K.

different compositions, such as Al–10at%Cu–81at%Fe, Al–30at%Cu–49at%Fe, Al–35at%Cu–15at%Fe and Al–35at%Cu–30at%Fe have been calculated using Chou model in the temperature above range and plotted in Figure 11. It is interesting to note that the surface tension of the alloy was found to be decreasing

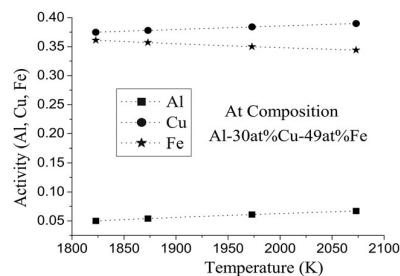


Figure 10. Variation of activity of Al, Cu and Fe with temperature at composition Al–30at%Cu–49at%Fe in the Al–Cu–Fe liquid alloy.

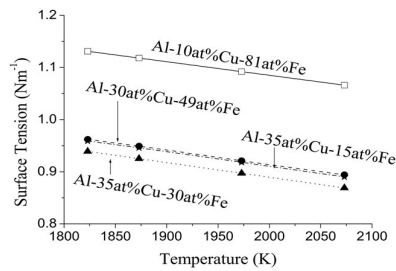


Figure 11. Variation of surface tension (in Nm^{-1}) with temperature at different compositions Al-10at%Cu-81at%Fe, Al-30at%Cu-49at%Fe, Al-35at%Cu-15at%Fe and Al-35at%Cu-30at%Fe in Al-Cu-Fe liquid alloy using Chou model.

linearly with the increase in temperature at all compositions. The results obtained in this work are in accordance with the findings in ref. [48].

4. Conclusions

From the above study the following conclusions can be drawn:

- The sub-binary Al-Cu and Al-Fe alloys are ordering systems whereas the sub-binary Cu-Fe alloy is segregating system.
- The activity of the component Al increases with the increase in the concentration of Al irrespective of the composition ratio of Cu and Fe in the ternary alloy.
- The activity of the component Fe is almost non-responsive to the temperature change.
- The peak value of the excess free energy of the alloy computed from the Al corners is independent of the composition ratio of Cu and Fe in the ternary alloy.
- The Al atoms segregate higher than any other components of Al-Cu-Fe alloy in the surface at all temperatures.
- The surface tension of the alloy decreases with the increase in the concentration of Al in the alloy.
- The surface tension of the alloy decreases linearly with the increase in temperature at all compositions.

Acknowledgement

Authors are grateful to University Grants Commission (UGC) Nepal for providing financial support to pursue this work under the grant FRG-S&T-73/74-14.

Disclosure statement

No potential conflict of interest was reported by the author(s).

Funding

This work was supported by University Grants Commission- Nepal: [Grant Number FRG-S&T-73/74-14].

ORCID

U. Mehta  <http://orcid.org/0000-0003-1024-2436>
 S. K. Yadav  <http://orcid.org/0000-0003-2525-216X>
 I. Koirala  <http://orcid.org/0000-0002-8838-1674>
 D. Adhikari  <http://orcid.org/0000-0002-6022-3615>

References

- [1] J.A.V. Butler, *The thermodynamics of the surfaces of solutions*. Proc. R. Soc. A 135 (1932), pp. 348–375.
- [2] R.I. Defay, I. Prigogine, A. Bellemans and D.H. Everett, *Surface Tension and Adsorption*, Longmans, London, 1966.
- [3] Y. Kawai, K. Mori, M. Kishimoto, K. Ishikura and T. Shimada, *Surface tension of liquid Fe-C-Si alloys*. Tetsu-to-Hagane 60 (1974), pp. 29–37.
- [4] K. Ogino, K. Nogi and C. Hosoi, *Surface tension of molten Fe-O-S alloy*. Tetsu-to-Hagane 69 (1983), pp. 1989–1999.
- [5] R. Speiser, D.R. Poirier and K. Yeum, *Surface tension of binary liquid alloys*. Scripta Metallurgica 21 (1987), pp. 687–692.
- [6] K.S. Yeum, R. Speiser and D.R. Poirier, *Estimation of the surface tensions of binary liquid alloys*. Metall. Mater. Transact. B 20 (1989), pp. 693–703.
- [7] J. Brillo and I. Egly, *Surface tension of nickel, copper, iron and their binary alloys*. J. Mater. Sci. 40 (2005), pp. 2213–2216.
- [8] L. Yan, S. Zheng, G. Ding, G. Xu and Z. Qiao, *Surface tension calculation of the Sn-Ga-In ternary alloy*. Comput. Coupl. Phase Diagrams Thermochem. 31 (2007), pp. 112–119.
- [9] R. Novakovic, E. Ricci, F. Gnecco, D. Giuranno and G. Borzone, *Surface and transport properties of Au-Sn liquid alloys*. Surf. Sci. 599 (2005), pp. 230–247.
- [10] J. Brillo, I. Egly and T. Matsushita, *Density and surface tension of liquid ternary Ni-Cu-Fe alloys*. Int. J. Thermophys. 97 (2006), pp. 28–34.
- [11] I. Egly, E. Ricci, R. Novakovic and S. Ozawa, *Surface tension of liquid metals and alloys - recent developments*. Adv. Colloid Interface Sci. 159 (2010), pp. 198–212.
- [12] D. Giuranno, A. Tuissi, R. Novakovic and E. Ricci, *Surface tension and density of Al-Ni Alloys*. J. Chem. Eng. Data 55 (2010), pp. 3024–3028.
- [13] J. Brillo, Y. Plevachuk and I. Egly, *Surface tension of liquid Al-Cu-Ag ternary alloys*. J. Mater. Sci. 45 (2010), pp. 5150–5157.
- [14] R.P. Koirala, D. Adhikari and B.P. Singh, *Surface tension of two weakly interacting liquid alloys*. BECHANA 9 (2013), pp. 103–112.
- [15] G. Kaptay, *Improved derivation of the Butler equations for surface tension of solutions*. Langmuir 35 (2019), pp. 10987–10992.
- [16] G. Kaptay, *Partial surface tension of components of a solution*. Langmuir 31 (2015), pp. 5796–5804.
- [17] I.S. Jha, R. Khadka, R.P. Koirala, B.P. Singh and D. Adhikari, *Theoretical assessment on mixing properties of liquid Tl-Na alloys*. Phil. Mag. 96 (2016), pp. 1664–1683.

- [18] T. Tanaka, K. Hack, T. Iida and S. Hara, *Application of thermodynamic databases to the evaluation of surface tensions of molten alloys, salt mixtures and oxide mixtures*. *Zeitschrift für Metallkunde* 87 (1996), pp. 380–389.
- [19] K. Mukai, T. Matsushita, K.C. Mills, S. Seetharaman, and T. Furuzono, *Surface tension of liquid alloys—a thermodynamic Approach*. *Metall. Mater. Transact. B* 39 (2008), pp. 561–569.
- [20] K.C. Chou and C.Y. Austin, *A study of ternary Geometrical models*. *BerBunsenges Phys Chem* 93 (1989), pp. 735–741.
- [21] K.C. Chou, *A general solution model for predicting ternary thermodynamic properties*. *Calphad* 19 (1995), pp. 315–325.
- [22] K.C. Chou, W.C. Li, F.S. Li and M.H. He, *Formalism of new ternary model expressed in terms of binary regular-solution type parameters*. *Calphad* 20 (1996), pp. 395–406.
- [23] L. Yan, S. Zheng and G. Ding, *Surface tension calculation of the Sn–Ga–In ternary alloy*. *Calphad* 31 (2007), pp. 112–119.
- [24] T.B. Massalski, *The Al–Cu (Aluminum–Copper) system*. *Bullet. Alloy Phase Diagrams* 1 (1980), pp. 27–33.
- [25] V. Raghavan, *Al–Cu–Fe (aluminum–copper–iron)*. *J. Phase Equilibria Diffus.* 26 (2005), pp. 59–64.
- [26] R. Hultgren, P.D. Desai, D.T. Hawkins, M. Gleiser and K.K. Kelley, *Selected Values of the Thermodynamic Properties of Binary Alloys*, ASM International, Metal Park, OH, 1973.
- [27] U. R. Kattner, B. P. Burton, *Al–Fe (Aluminum–Iron)*, *Phase Diagrams of Binary Iron Alloys*, H. Okamoto, Ed., ASM International, 1993, pp. 12–28.
- [28] V. Raghavan, *The Al–Cu–Fe (Aluminum–Copper–Iron System)*, *Phase Diagrams of Ternary Iron Alloys: Part 6*, Indian Institute of Metals, Calcutta, 1992, pp. 86–95.
- [29] L. Zhang and R. Luck, *Phase diagram of the Al–Cu–Fe Quasi-crystal Forming Alloy system: IV. Formation and Stability of the $Al_{10}Cu_{10}Fe$ phase*. *Z. Metallkunde* 94 (2003), pp. 341–344.
- [30] A.J. Bradley and H.J. Goldschmidt, *An X-ray study of Slowly Cooled Iron–Copper–Aluminum alloys: Part II. alloys Rich in Aluminum*. *J. Inst. Met.* 65 (1939), pp. 403–418.
- [31] I. Egry, D. Holland-Moritz and R. Novakovic, *Thermophysical properties of liquid Al–Ti-based alloys*. *Int. J. Thermophys.* 31 (2010), pp. 949–965.
- [32] C. Costa, S. Delsante and G. Borzone, *Thermodynamic and surface properties of liquid Co–Cr–Ni alloys*. *J. Chem. Thermodyn.* 69 (2014), pp. 73–84.
- [33] R. Nowak, T. Lanata and N. Sobczak N, *Surface tension of Ti–Al based alloys*. *J. Mater. Sci* 45 (2010), pp. 1993–2001.
- [34] V. Sklyarchuk, Y. Plevachuk and I. Kaban, *Surface properties and wetting behaviour of liquid Ag–Sb–Sn alloys*. *J. Min. Metall. B* 48 (2012), pp. 443–448.
- [35] R. Picha, J. Vreštal and A. Kroupa, *Prediction of alloy surface tension using a thermodynamic database*. *Calphad* 28 (2004), pp. 141–146.
- [36] R.N. Singh and F. Sommer, *Segregation and immiscibility in liquid binary alloys*. *Rep. Prog. Phys.* 60 (1997), pp. 57–150.
- [37] O. Redlich and A.T. Kister, *Algebraic representation of thermodynamic properties and the classification of solutions*. *Ind. Eng. Chem.* 40 (1948), pp. 345–348.
- [38] S. Marjanovic, D. Manašijevic and D. Živkovic, *Calculation of thermodynamic properties for ternary Ag–Cu–Sn system*. *RMZ-Mater. Geoenviron.* 56 (2009), pp. 30–37.
- [39] T. Tanaka, S. Hara and M. Ogawa, *Evaluation of surface tension of molten salt mixtures*. *Retrospect. Collect.* 25 (1998), pp. 213–216.
- [40] I. Koirala, I.S. Jha, B.P. Singh and D. Adhikari, *Thermodynamic, transport and surface properties in In–Pb liquid alloys*. *Physica B* 423 (2013), pp. 49–53.

- [41] G. Kaptay, *A unified model for the cohesive enthalpy, critical temperature, surface tension and volume thermal expansion coefficient of liquid metals of bcc, fcc and hcp crystals*. Mater. Sci. Eng. A 495 (2008), pp. 19–26.
- [42] E.A. Brandes and G.B. Brook, *Smithells Metals Reference Book*, Elsevier, Oxford, 2013.
- [43] I. Ansara, A. T. Dinsdale, M. H. Rand, *Thermochemical Database for Light Metal Alloys (Cost 507)*, 1998.
- [44] G. Kaptay, *A new equation for the temperature dependence of the excess Gibbs energy of solution phases*. Calphad 28 (2004), pp. 115–124.
- [45] G. Kaptay, *The exponential excess Gibbs energy model revisited*. Calphad 56 (2017), pp. 169–184.
- [46] D.S. Kanibolotsky, O.A. Bieloborodova, N.V. Kotova and V.V. Lisnyak, *Thermodynamic properties of liquid Al–Si and Al–Cu Alloys*. J. Therm. Anal. Calorimetry 70 (2002), pp. 975–983.
- [47] D. Adhikari, S.K. Yadav and L.N. Jha, *Thermo-physical properties of Al–Fe melt*. J. Chin. Adv. Mater. Soc. 2 (2014), pp. 149–158.
- [48] I. L. Ferreira and A. Garcia, *The application of numerical and analytical approaches for the determination of thermophysical properties of Al–Si–Cu–Mg alloys*. Continuum Mech. Thermodyn. 31(6) (2019.[doi:10.1007/s00161-019-00836-5](https://doi.org/10.1007/s00161-019-00836-5)).

Prediction of thermodynamic and surface properties of ternary Ti–Si–Fe liquid alloy

U Mehta^{1,2}, I Koirala¹, S K Yadav², R P Koirala²
and D Adhikari^{2,3} 

¹ Central Department of Physics, Tribhuvan University, Kathmandu, Nepal

² Department of Physics, Mahendra Morang A.M.Campus, Tribhuvan University, Biratnagar, Nepal

E-mail: devendra.physics@yahoo.com

Received 17 April 2020, revised 15 June 2020

Accepted for publication 26 June 2020

Published 24 July 2020



CrossMark

Abstract

Thermodynamic and surface properties of the ternary Ti–Si–Fe liquid alloy have been assessed at temperatures 1873 K, 1973 K, 2073 K and 2173 K. For this purpose, the optimized linear temperature dependent coefficients of Redlich–Kister (R–K) polynomials for excess free energy of mixing for sub-binary systems Ti–Si, Fe–Si and Ti–Fe have been computed considering available experimental and literature data. The thermodynamic properties of ternary liquid alloy, such as activity have been studied using general solution model (GSM) and excess free energy of mixing has been studied using GSM, Kohler and Toop models. In surface properties, surface concentration has been computed using Butler’s equation and surface tension of the liquid alloy has been studied using all the four above mentioned models feeding the database of liquid Fe–Si, Si–Ti and Ti–Fe sub-binary systems. The values of surface tension computed using GSM and Toop model are in well agreement with each other at all concentrations. Moreover, the computed values of excess free energy of mixing and surface tension decrease at elevated temperatures from all corners and at all considered cross-sections indicating the decrease in ordering tendency of the alloy.

Keywords: Ti–Si–Fe liquid alloy, sub-binary system, surface tension, surface concentration

1. Introduction

The mixing behaviour of alloys in liquid state plays a vital role for the development of desired materials in solid state. Without having a good understanding of thermodynamic, surface,

³ Author to whom any correspondence should be addressed.

transport, electrical and magnetic properties of an alloy and its constituents in liquid state it is not possible to develop a new materials with desired mechanical, electrical or magnetic properties in solid state. Moreover, the properties of alloys changes significantly with the variation of compositions of the components. Therefore, several metal scientists have long been working to understand the mixing behaviours of alloys in liquid state [1–10].

Unlike crystalline solids, liquid is a disorder system and does not have long range order. This complex behaviour of liquid generates manifold interest to the researchers. Various theoretical models [11–17] have been developed by researchers to understand the complexity in the mixing properties of liquid alloys. In this work, we have computed thermodynamic and surface properties of Ti–Si–Fe alloy in liquid state at different compositions and temperatures using different models. The ductility and strength of Ti–Si–Fe alloy has been studied by Watson and Brown [18]. The deformation mechanism of this alloy has been investigated by Jack and Guiu [19] at lower temperature. The crystal structure and phases of the Ti–Si–Fe alloy has also been studied by the researchers [20–23]. The intermediate phases FeSi_2Ti , FeSiTi , $\text{Fe}_4\text{Si}_3\text{Ti}$, $\text{Fe}_{10}\text{Si}_{44}\text{Ti}_{46}$, $\text{Fe}_{15}\text{Si}_{40}\text{Ti}_{45}$, $\text{Fe}_7\text{Si}_2\text{Ti}$ have been detected in the Ti–Si–Fe alloy over the entire range of concentration. The ternary Ti–Si–Fe alloys has three sub-binary systems: Fe–Si, Ti–Si and Fe–Ti. The binary Fe–Si system which has Fe_2Si , Fe_5Si_3 , FeSi , αFeSi_2 (orthorhombic) and βFeSi_2 (tetragonal) intermediate phases [24, 25], has been studied by several researchers [26–29]. The binary Fe–Ti system has two intermediate phases Fe_2Ti and FeTi [30]. The ductility and strength of this binary system has been studied by Louzguine *et al* [31]. Similarly, the sub-binary Si–Ti alloy has Ti_3Si , Ti_5Si_3 and Ti_5Si_4 intermediate phases [32].

As per the knowledge of authors on the basis of literature survey, the complete thermo-physical dataset of Ti–Si–Fe is not available till date. Therefore, an attempt has been made in this work to study and predict the thermo-physical properties of the system. With this regard, the activity of components of the Ti–Si–Fe alloy in liquid state has been computed using Chou equation [33, 34]. The excess free energy of mixing has been computed using Chou [33, 34], Kohler [35] and Toop models [36]. The surface concentration and surface tension of sub-binary and ternary alloy has been computed using Butler model [37]. Further, surface tension of sub-binary alloys is used to determine the excess surface tension of sub-binary systems which are then used to optimize the coefficients of R–K polynomial [38] for excess surface tension. These values of coefficient are then used to determine the surface tension of the ternary alloy using Chou [33, 34], Kohler [35] and Toop model [36].

2. Theory

2.1. Thermodynamic properties

Excess Gibbs free energy of mixing (G_{ij}^{xs}) of binary system ‘*ij*’ are frequently expressed in terms of R–K polynomial given as [38–42]

$$G_{ij}^{xs} = x_i x_j \sum_{\nu=0}^n A_{ij}^{\nu} (x_i - x_j)^{\nu} \quad (1)$$

where A_{ij}^{ν} are called coefficients of R–K polynomial for binary system ‘*ij*’ and x_i and x_j are the mole fraction of components in the alloy. For the computation of excess free energy of mixing of ternary alloy using Chou model [33, 34], the equation used is given as

$$G^{xs} = x_1 x_2 \sum_{\nu=0}^n A_{12}^{\nu} (x_1 - x_2)^{\nu} + x_2 x_3 \sum_{\nu=0}^n A_{23}^{\nu} (x_2 - x_3)^{\nu} + x_3 x_1 \sum_{\nu=0}^n A_{31}^{\nu} (x_3 - x_1)^{\nu} + f x_1 x_2 x_3 \quad (2)$$

where x_1 , x_2 and x_3 are mole fraction of components in the ternary alloy and A_{ij}^{ν} are called coefficients of R–K polynomial of sub-binary system of the ternary alloy. The term f is called the ternary interaction term explained by Chou [33, 34] and given as

$$\begin{aligned} f = & (2\xi_{12} - 1) [A_{12}^3 (3(x_1 - x_2)^2 x_3 + 3(x_1 - x_2) x_3^2 (2\xi_{12} - 1) + x_3^3 (2\xi_{12} - 1)^2) \\ & + A_{12}^2 ((2\xi_{12} - 1) x_3 + 2(x_1 - x_2)) + A_{12}^1] \\ & + (2\xi_{23} - 1) [A_{23}^3 (3(x_2 - x_3)^2 x_1 + 3(x_2 - x_3) x_1^2 (2\xi_{23} - 1) + x_1^3 (2\xi_{23} - 1)^2) \\ & + A_{23}^2 ((2\xi_{23} - 1) x_1 + 2(x_2 - x_3)) + A_{23}^1] \\ & + (2\xi_{31} - 1) [A_{31}^3 (3(x_3 - x_1)^2 x_2 + 3(x_3 - x_1) x_2^2 (2\xi_{31} - 1) + x_2^3 (2\xi_{31} - 1)^2) \\ & + A_{31}^2 ((2\xi_{31} - 1) x_2 + 2(x_3 - x_1)) + A_{31}^1] \end{aligned} \quad (3)$$

where ξ in the above equation are called similarity indexes and expressed as

$$\xi_{12} = \frac{\eta_1}{\eta_1 + \eta_{11}}, \quad \xi_{23} = \frac{\eta_{11}}{\eta_{11} + \eta_{111}}, \quad \xi_{31} = \frac{\eta_{111}}{\eta_{111} + \eta_1}. \quad (4)$$

The deviation sum of squares (η) can be estimated as

$$\eta_1 = \int_0^1 (G_{12}^{xs} - G_{13}^{xs})^2 dx_1, \quad \eta_{11} = \int_0^1 (G_{21}^{xs} - G_{23}^{xs})^2 dx_2, \quad \eta_{111} = \int_0^1 (G_{31}^{xs} - G_{32}^{xs})^2 dx_3. \quad (5)$$

The activity (a_i) of the components ' i ' in binary and ternary alloy are related with their respective partial excess free energy (G_i^{xs}) expressed as [44]

$$G_i^{xs} = RT \ln \left(\frac{a_i}{x_i} \right) \quad (6)$$

where R is the molar gas constant and T is the absolute temperature. The values of G_i^{xs} are obtained in terms of G^{xs} and connected by the relation [39–44]

$$G_i^{xs} = G^{xs} + \sum_{j=1}^m (\delta_{ij} - x_j) \frac{\partial G^{xs}}{\partial x_j} \quad (7)$$

where δ_{ij} is the Kronecker delta function defined as $\delta_{ij} = 1$ when $i = j$ and $\delta_{ij} = 0$ when $i \neq j$. The value of G^{xs} is replaced by G_{ij}^{xs} using equation (1) for binary alloy and putting $m = 2$. Similarly, value of G^{xs} is used from equation (2) for ternary alloy and putting $m = 3$.

Table 1. Optimized coefficients of R–K polynomials (A_{ij}^v) for excess Gibbs free energy (G_M^{xs}) of sub-binary systems of Ti–Si–Fe liquid alloy for this work.

System	A_{ij}^v (Jmol ⁻¹)
Fe–Si	$A^0 = -151\,620 + 29.39 T, A^1 = -38\,960 - 2.58 T, A^2 = 36\,970 - 12.76 T$
Si–Ti	$A^0 = -231\,200 + 12.50 T, A^1 = 42\,500, A^2 = 58\,400$
Ti–Fe	$A^0 = -86\,950 + 7.85 T, A^1 = -18\,720 + 6.31 T, A^2 = 20\,300 - 6.66 T$

Kohler model is a symmetrical model and excess free energy of ternary alloy using Kohler model is given by the equation [45–47]

$$G^{xs} = (x_1 + x_2)^2 G_{12}^{xs} \left(\frac{x_1}{x_1 + x_2}, \frac{x_2}{x_1 + x_2} \right) + (x_2 + x_3)^2 G_{23}^{xs} \left(\frac{x_2}{x_2 + x_3}, \frac{x_3}{x_2 + x_3} \right) + (x_3 + x_1)^2 G_{31}^{xs} \left(\frac{x_3}{x_3 + x_1}, \frac{x_3}{x_3 + x_1} \right). \quad (8)$$

In this equation, the excess free energy of mixing (G_{ij}^{xs}) for binary system ‘ ij ’ are evaluated at binary concentrations ($x_i/(x_i + x_j)$) and ($x_j/(x_i + x_j)$).

The Toop model is an asymmetrical model and a symmetrical element is to be determined. For a symmetrical model x_1 in the ternary alloy, the excess free energy using Toop model is evaluated by the relations [45–47]

$$G^{xs} = \left(\frac{x_2}{x_2 + x_3} \right) G_{12}^{xs}(x_1, 1 - x_1) + \left(\frac{x_3}{x_2 + x_3} \right) G_{13}^{xs}(x_1, 1 - x_1) + (x_2 + x_3)^2 G_{23}^{xs} \left(\frac{x_2}{x_2 + x_3}, \frac{x_3}{x_2 + x_3} \right). \quad (9)$$

2.2. Surface properties

The surface concentration and surface tension of binary and multi-component liquid alloy are given by the Butler equation [1] and used by many researchers [28, 39, 48, 49]

$$\begin{aligned} \sigma &= \sigma_1 + \frac{RT}{\alpha_1} \ln \left(\frac{x_1^s}{x_1^b} \right) + \frac{G_{s,1}^{xs} - G_{b,1}^{xs}}{\alpha_1} \\ \sigma &= \sigma_2 + \frac{RT}{\alpha_2} \ln \left(\frac{x_2^s}{x_2^b} \right) + \frac{G_{s,2}^{xs} - G_{b,2}^{xs}}{\alpha_2} \\ \sigma &= \sigma_3 + \frac{RT}{\alpha_3} \ln \left(\frac{x_3^s}{x_3^b} \right) + \frac{G_{s,3}^{xs} - G_{b,3}^{xs}}{\alpha_3} \end{aligned} \quad (10)$$

where σ is the surface tension of binary or ternary liquid alloy. The surface tensions of the binary liquid alloy is obtained by simultaneously solving the first two expressions of equation (10) whereas that of ternary system is obtained by simultaneously solving all three expressions. The terms σ_i ($i = 1, 2, 3$) are the surface tensions of pure components and x_i^b and x_i^s are bulk and surface concentrations of individual components in the liquid mixture. x_i^s are obtained by employing the successive approximation methodology. $G_{b,i}^{xs}$ and $G_{s,i}^{xs}$ are the partial excess free energy for bulk and surface phase of individual components respectively. The ratio

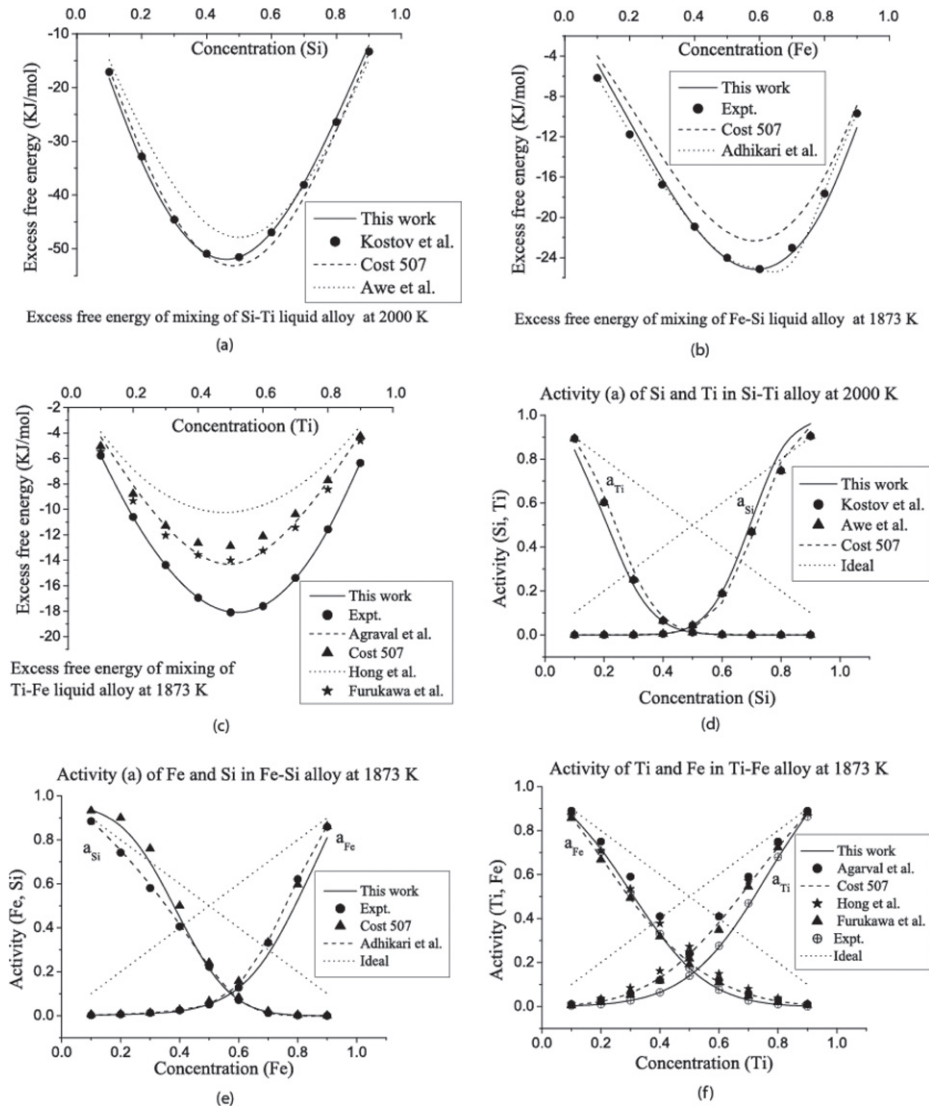


Figure 1. Variation of compositional dependence of excess free energy of mixing and activity of binary sub-systems of Ti-Si-Fe liquid alloy. (a) Excess free energy of mixing for Si-Ti at 2000 K. (b) Excess free energy of mixing for Fe-Si at 1873 K. (c) Excess free energy of mixing for Ti-Fe at 1873 K. (d) Activity of Si-Ti at 2000 K. (e) Activity of Fe-Si at 1873 K. (f) Activity of Ti-Fe at 1873 K.

of these two quantities is a constant and its value depends on crystal structure [42, 45]. For liquid phase, the value of this ratio is taken to be 0.83 in this work. And the value of β depends on crystal structure and is taken as 0.83 [42, 50] for liquid phase. The term α_i are the mono-layer surface areas of 1 mol of pure component 'i' and its value is evaluated using the relations [42, 45]

$$\alpha_i = 1.091N_A^{1/3}V_i^{2/3} \quad (11)$$

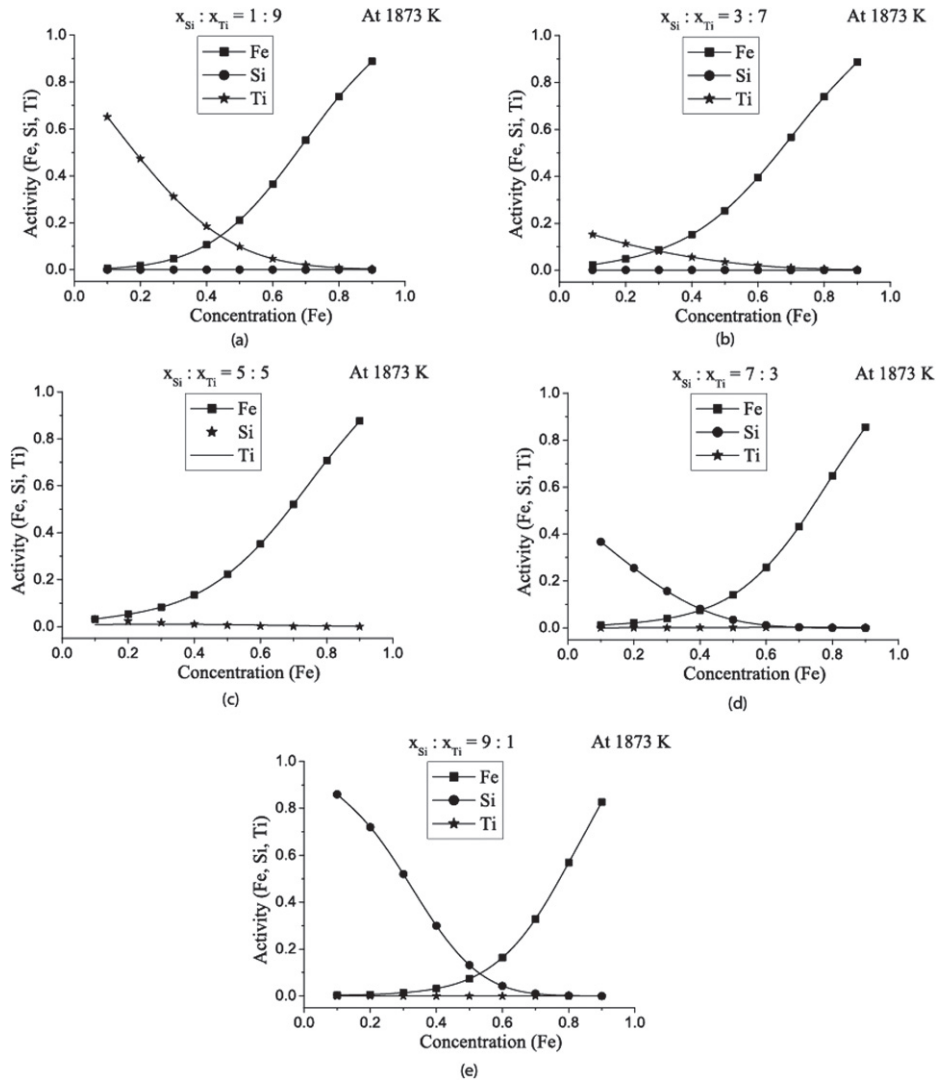


Figure 2. Variation of activity of Fe, Si and Ti in Ti–Si–Fe alloy at 1873 K from Fe corner at cross-sections (a) $x_{\text{Si}} : x_{\text{Ti}} = 1 : 9$ (b) $x_{\text{Si}} : x_{\text{Ti}} = 3 : 7$ (c) $x_{\text{Si}} : x_{\text{Ti}} = 5 : 5$ (d) $x_{\text{Si}} : x_{\text{Ti}} = 7 : 3$ (e) $x_{\text{Si}} : x_{\text{Ti}} = 9 : 1$.

where $N_A = 6.023 \times 10^{23}$ is called Avogadro's number and V_i is the volume of 1 mol of pure elements at concerned temperature of the liquid alloy and evaluated by the relation $V_i = (M_i/\rho_i)$. The density (ρ_i) and surface tension (σ_i) are linear temperature dependent quantities and their values at elevated temperature T is given by the relation [51]

$$\rho_i = \rho_{0,i} + \frac{\partial \rho}{\partial T}(T - T_0), \quad \text{and} \quad \sigma_i = \sigma_{0,i} + \frac{\partial \sigma}{\partial T}(T - T_0). \quad (12)$$

The terms $\rho_{0,i}$ and $\sigma_{0,i}$ are density and surface tension of pure components respectively near their melting temperature T_0 . The excess surface tension (σ^{xs}) of binary and ternary liquid alloy

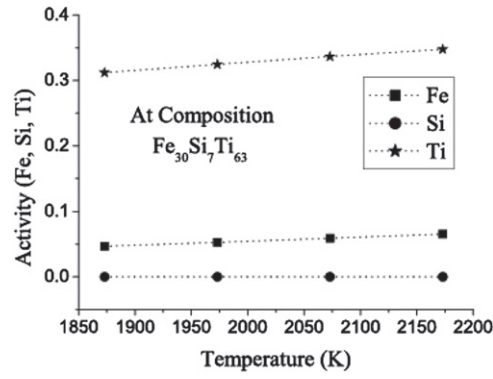


Figure 3. Variation of activity of Fe, Si and Ti in ternary liquid alloy with temperature for a given composition $x_{\text{Fe}} : x_{\text{Si}} : x_{\text{Ti}} = 30 : 7 : 63$.

are computed using the relation [52]

$$\sigma^{xs} = \sigma - \sigma^{\text{ideal}} \quad \text{and} \quad \sigma^{\text{ideal}} = \sum_i x_i \sigma_i = x_1 \sigma_1 + x_2 \sigma_2. \quad (13)$$

The excess surface tension using Chou, Kohler and Toop model are evaluated in the similar fashion as used for excess Gibbs free energy. The coefficients of R–K polynomial A_{ij}^y for excess Gibbs free energy of sub-binary are replaced by L_{ij}^y called coefficient of R–K polynomial for excess surface tension. The excess free energy of mixing (G_{ij}^{xs}) in equations (5) are replaced by excess surface tension of binary system (σ_{ij}^{xs}).

3. Results and discussion

3.1. Thermodynamic properties

The optimized coefficients of R–K polynomials for excess free energy of mixing (G_M^{XS}) for sub-binary systems Ti–Si, Fe–Si and Ti–Fe have been computed using available literature [53] and literature data [24, 54], and equation (1) by the method of least square fitting. The values so obtained are presented in table 1. The validity of the optimized parameters has been tested by plotting the compositional dependence of G_M^{XS} for sub-binary systems (figures 1(a)–(c)). The computed values of G_M^{XS} were found to be in well agreement with the reference data at their respective melting temperatures (figures 1(a)–(c)). Activity (a) is one of the important thermodynamic properties which are directly computed from the experimental techniques. The validity of the optimized parameters would only be established if it could explain the activity. Therefore, the activities of the components of sub-binary systems have been computed with the aid of parameters from table 1 and equations (1), (6) and (7). The computed values of activities of the monomers of sub-binary systems were also found to be in well agreement with respect to their sources mentioned above (figures 1(d)–(f)). The theoretical investigations thus showed that optimized coefficients not only explained G_M^{XS} but also have successfully reproduced activity of the concerned systems thereby establishing the fruitfulness of optimized parameters. The computed values of G_M^{XS} and a were also compared with other available literature data [27, 30, 55–58].

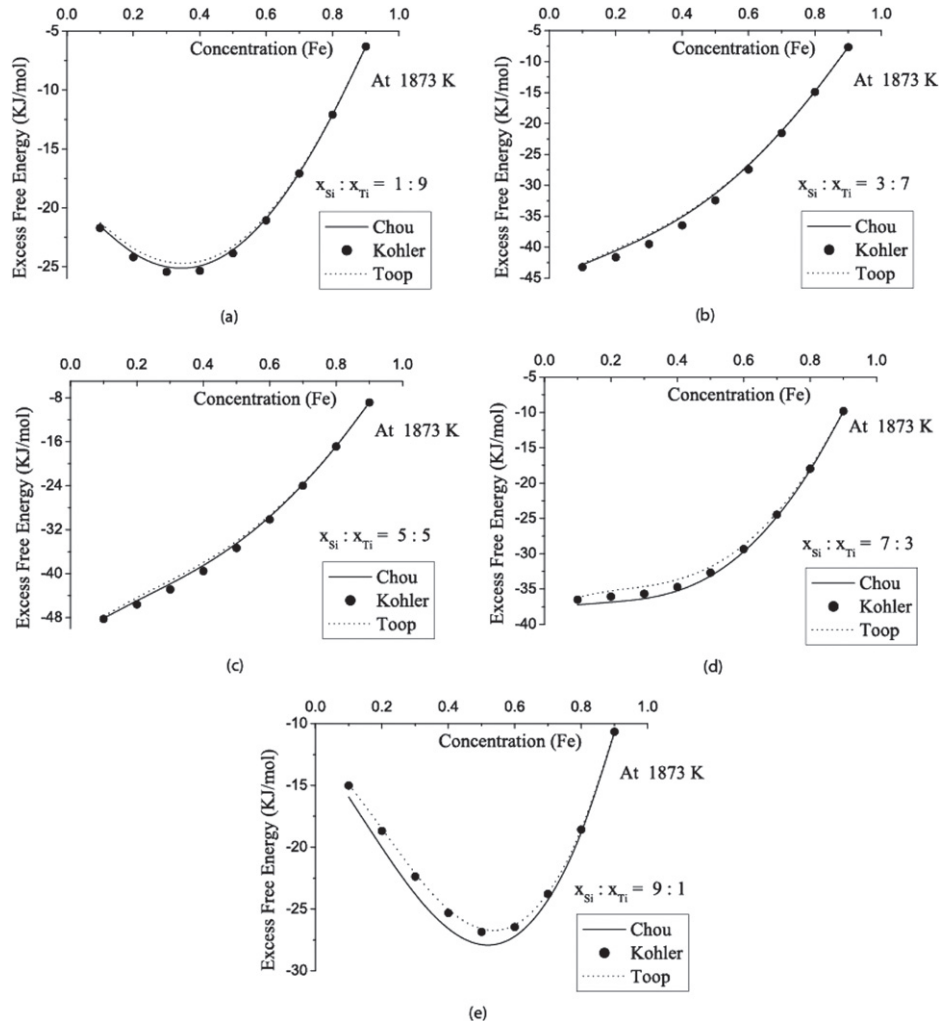


Figure 4. Variation of Gibbs free energy of mixing of Ti–Si–Fe alloy at 1873 K from Fe corner computed using three different models at cross-sections (a) $x_{\text{Si}} : x_{\text{Ti}} = 1 : 9$ (b) $x_{\text{Si}} : x_{\text{Ti}} = 3 : 7$ (c) $x_{\text{Si}} : x_{\text{Ti}} = 5 : 5$ (d) $x_{\text{Si}} : x_{\text{Ti}} = 7 : 3$ (e) $x_{\text{Si}} : x_{\text{Ti}} = 9 : 1$.

The partial excess Gibbs free energy of individual components of sub-binary systems were computed using the coefficients of R–K polynomial (A_{ij}^{ν}) from table 1 for the concerned sub-binary systems in equations (1)–(3). The computed value of partial excess free energy of individual components were then used to compute the activities of the components Ti, Si and Fe in the above mentioned sub-binary systems at temperature 1873 K. We then computed the activities of Ti, Si and Fe in the ternary Ti–Si–Fe alloy at five different cross-sections ($x_{\text{Si}}/x_{\text{Ti}} = 1 : 9, 3 : 7, 5 : 5, 7 : 3, 9 : 1$) from Fe corner (figures 2(a)–(e)). The activity of Fe was found to be increased with increase in the concentration of Fe at all compositions of Si and Ti. But the activities of Si and Ti were found to be decreased with increase in the concentration of Fe. It was also found that the activity of each component in the alloy increased with the rise of its concentration. This clearly indicates that the component with greater bulk concentration in the

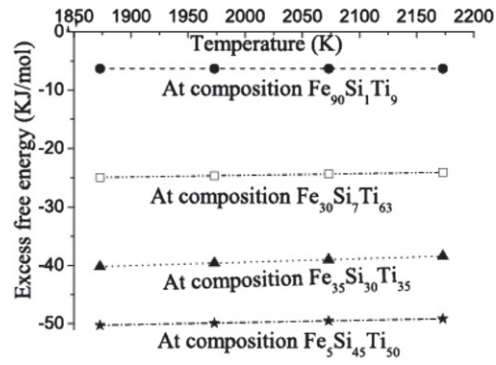


Figure 5. Variation of excess Gibbs free energy of mixing of ternary liquid alloy with temperature for four different compositions.

Table 2. Values of density (ρ_0) and surface tension (σ_0) of Si, Fe and Ti near their melting temperature (T_0) and variation of density and surface tension with temperature [51].

Elements	T_0 (K)	ρ_0 (Kg m ⁻³)	$\partial\rho/\partial T$ (Kg m ⁻³ K ⁻¹)	σ_0 (N m ⁻¹)	$\partial\sigma/\partial T$ (N m ⁻¹ K ⁻¹)
Si	1683	2530	-0.35	0.865	-0.00013
Fe	1809	7015	-0.883	1.872	-0.00049
Ti	1958	4110	-0.23	1.650	-0.00026

Table 3. Optimized values of coefficients of R-K polynomial (L_{ij}^v) for excess surface tension (σ^{XS}) of sub-binary systems of Ti-Si-Fe liquid alloy.

	L_{ij}^v (Nm ⁻¹)
L_{Fe-Si}^0	$7.34 \times 10^{-4} T - 2.34$
L_{Fe-Si}^1	$-2.41 \times 10^{-7} T^2 + 1.35 \times 10^{-3} T - 1.77$
L_{Fe-Si}^2	$-4.77 \times 10^{-7} T^2 + 2.16 \times 10^{-3} T - 2.11$
L_{Fe-Si}^3	$-4.12 \times 10^{-7} T^2 + 1.85 \times 10^{-3} T - 1.94$
L_{Si-Ti}^0	$3.30 \times 10^{-4} T - 0.809$
L_{Si-Ti}^1	$1.51 \times 10^{-7} T^2 - 4.10 \times 10^{-4} T - 0.985$
L_{Si-Ti}^2	$-3.97 \times 10^{-4} T + 1.16$
L_{Si-Ti}^3	$-3.01 \times 10^{-7} T^2 + 1.30 \times 10^{-3} T - 0.695$
L_{Ti-Fe}^0	$-9.70 \times 10^{-8} T^2 + 4.88 \times 10^{-4} T - 0.361$
L_{Ti-Fe}^1	$1.57 \times 10^{-4} T - 0.416$
L_{Ti-Fe}^2	$3.20 \times 10^{-8} T^2 - 1.16 \times 10^{-4} T + 0.018$
L_{Ti-Fe}^3	$4.78 \times 10^{-8} T^2 - 2.50 \times 10^{-4} T + 0.333$

alloy has tendency to exist in pure state. The activities of the components of the alloy at different temperatures were also computed for Fe₃₀Si₇Ti₆₃ in the ternary Ti-Si-Fe alloy (figure 3). The activity of Ti was found to be maximum followed by Fe and Si at all temperatures. The variation of activities with temperature was almost linear for all components.

The compositional dependence of the excess free energy of mixing (G_M^{XS}) for the ternary Ti-Si-Fe alloy in liquid state was also computed from Fe corners at five different

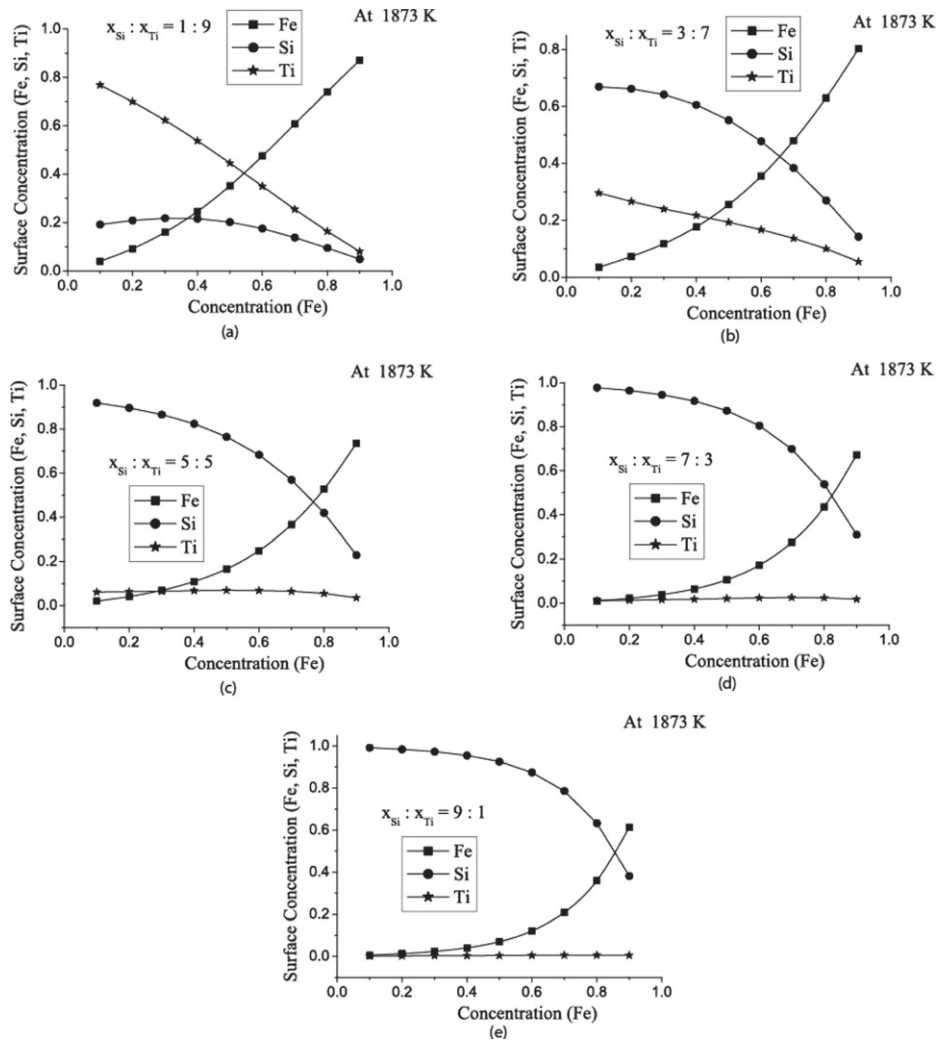


Figure 6. Variation of surface concentration of individual components Fe, Si and Ti in Ti–Si–Fe alloy at 1873 K from Fe corner at cross-sections (a) $x_{\text{Si}} : x_{\text{Ti}} = 1 : 9$ (b) $x_{\text{Si}} : x_{\text{Ti}} = 3 : 7$ (c) $x_{\text{Si}} : x_{\text{Ti}} = 5 : 5$ (d) $x_{\text{Si}} : x_{\text{Ti}} = 7 : 3$ (e) $x_{\text{Si}} : x_{\text{Ti}} = 9 : 1$.

cross-sections ($x_{\text{Si}}/x_{\text{Ti}} = 1 : 9, 3 : 7, 5 : 5, 7 : 3, 9 : 1$) using general solution model (GSM), Kohler and Toop models (figures 4(a)–(e)). Considering three significant figures, the deviation between the computed values of G_M^{XS} using Toop and Kohler models with respect to GSM were maximum with 6.70% ($x_{\text{Si}}/x_{\text{Ti}} = 9 : 1$) at $x_{\text{Fe}} = 0.2$ and 7.72% ($x_{\text{Si}}/x_{\text{Ti}} = 9 : 1$) at $x_{\text{Fe}} = 0.2$ respectively. As these deviations were within the considerable range, therefore, it can be concluded that the values of the G_M^{XS} computed from different models agreed well with one another. The peak value of the G_M^{XS} was found to depend on the concentration ratio of the components. The excess Gibbs free energy of Ti–Si–Fe alloy in liquid state has large negative values for all corners and at all cross-sections at 1873 K. This implies that the alloy is highly interacting in nature near its melting temperature. However the G_M^{XS} was found to be large negative value at the equal composition of Si and Ti (figure 4(c)). This indicates that the

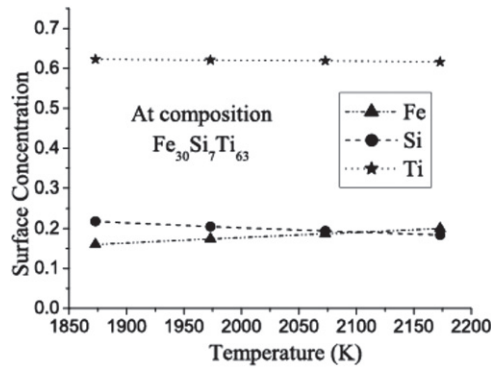


Figure 7. Variation of surface concentration of Fe, Si and Ti in liquid ternary alloy with temperature for a given composition $x_{\text{Fe}} : x_{\text{Si}} : x_{\text{Ti}} = 30 : 7 : 63$.

alloy is in most stable state when Si and Ti are mixed at equal compositions in liquid state. The variation of computed values of the G_M^{XS} of the alloy with temperature at four different cross-sections ($\text{Fe}_{90}\text{Si}_{10}\text{Ti}_0$, $\text{Fe}_{30}\text{Si}_7\text{Ti}_{63}$, $\text{Fe}_{35}\text{Si}_{30}\text{Ti}_{35}$ and $\text{Fe}_5\text{Si}_{45}\text{Ti}_{50}$) is shown in figure 5. It can be observed that the negative values of the G_M^{XS} decreases with the rise in temperature of the alloy (figure 5). This indicates that the ordering tendency of the system gradually decreases as the temperature increases. This is usual behaviour as liquid alloys shows ideal mixing tendency at elevated temperature. It was also found that the G_M^{XS} became less negative when there was higher concentration of Fe component in the ternary Ti–Si–Fe alloy. This means the Fe component makes the ternary Ti–Si–Fe alloy less stable. The values of the G_M^{XS} was also affected by the compositions of other components in the alloy.

3.2. Surface properties

The experimental values of surface tensions ($\sigma_{o,i}$) and densities ($\rho_{o,i}$) of pure components and their variations with temperatures required to compute the surface tension and surface concentration of the alloy were taken from Smithells Metals Reference Book [51] which are listed in table 2. The surface tensions of sub-binary systems Fe–Si, Si–Ti, Fe–Ti were computed by using partial excess free energy of mixing of respective systems in Butler's equation (equations (10)–(12)). These surface tensions were then used to determine the excess surface tension of aforementioned sub-binary systems with the help of equation (13). The ideal value of surface tension was computed using additive rule in equation (13). The excess surface tensions of the sub-binary systems were used to optimize the coefficients of R–K polynomial (L_{ij}^v) as a function of temperature ranging from the temperature 1873–2173 K using least square methods and are listed in table 3. These optimized coefficients were then used to find excess surface tension of the ternary Ti–Si–Fe alloy using Chou, Kohler and Toop model.

The values of partial excess free energy were used in Butler equation to compute surface concentration and surface tension of binary and ternary alloy. The surface concentration of the constituents of the ternary Ti–Si–Fe alloy was computed from the corner of Fe at five different cross-sections ($x_{\text{Si}}/x_{\text{Ti}} = 1 : 9, 3 : 7, 5 : 5, 7 : 3, 9 : 1$) at 1873 K using equation (10) (figures 6(a)–(e)). The surface concentration of Si was found to be much higher than that of other components at the lower end of Fe whereas the surface concentration of Ti is the lowest in all regions in Ti–Si–Fe alloy. The Si atoms segregate most in the surface due to the lowest

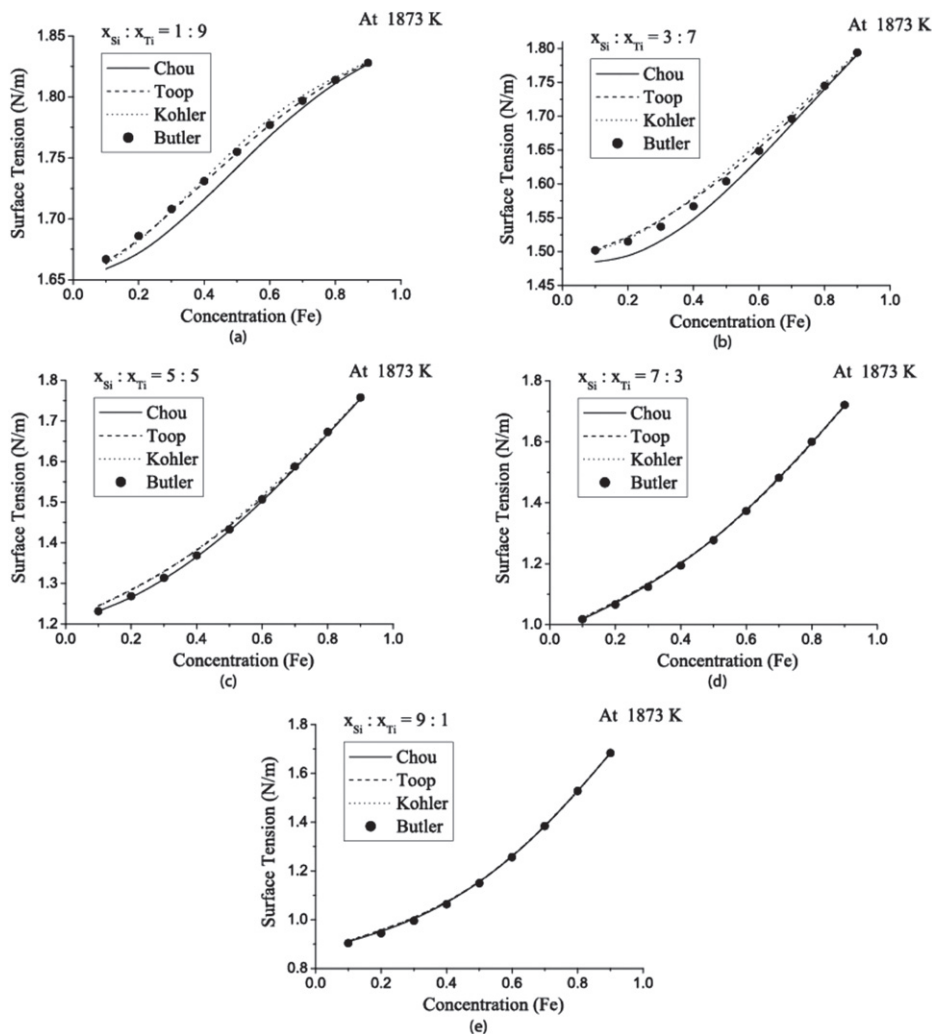


Figure 8. Variation of surface tension of Ti–Si–Fe ternary alloy at 1873 K from Fe corner computed using four different models at cross-sections (a) $x_{\text{Si}} : x_{\text{Ti}} = 1 : 9$ (b) $x_{\text{Si}} : x_{\text{Ti}} = 3 : 7$ (c) $x_{\text{Si}} : x_{\text{Ti}} = 5 : 5$ (d) $x_{\text{Si}} : x_{\text{Ti}} = 7 : 3$ (e) $x_{\text{Si}} : x_{\text{Ti}} = 9 : 1$.

value of its surface tension among the three components. Of the two components Fe and Ti, the surface tension of Ti is lesser. But Fe atoms segregate more in the surface than that of Ti. This may be due to the fact that surface tension of Fe and Ti are comparable but molar surface area of monolayer surface of Ti is larger than that of Fe. Calculation showed that when equal amount of these elements were mixed at liquid state, then surface concentration of Fe, Si, Ti were about 9%, 84% and 7% respectively (figure 6(c)). It was evident from the computation that when the concentration of Fe was increased in the ratio of Si and Ti in Ti–Si–Fe alloy the surface concentration of Fe exceeded the surface concentration of Si at the higher concentration region of Fe.

We studied the variation of surface concentration of different components in the ternary alloy with temperature at fixed ratio of Si : Ti : Fe = 7 : 63 : 30 (figure 7). The surface

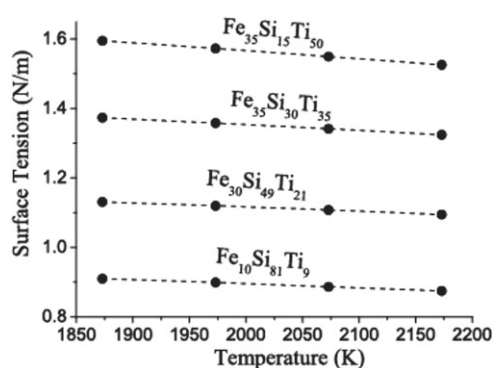


Figure 9. Variation of surface tension of the ternary alloy computed using Chou model with temperature for four different compositions.

concentration of components in the alloy tended to change towards ideal value with the rise of temperature. The surface concentration of Si decreased with the rise of temperature as shown in figure 7. Similarly, surface concentration of Ti was found to be decreased while that of Fe was found to be increased at the elevated temperature.

The surface tension (σ) of the ternary Ti–Si–Fe alloy at 1873 K was computed using Chou, Kohler, Toop and Butler models from Fe corners at above mentioned five different cross-sections. The surface tension of the ternary Ti–Si–Fe alloy computed at 1873 K using Chou, Kohler and Toop models in the framework of optimized parameters of R–K polynomials were then compared with that computed from Butler’s model (figures 8(a)–(e)). Considering three significant figures, the deviation between the computed values of σ using Chou, Toop and Kohler models with respect to Butler’s model were maximum with 1.35% ($x_{\text{Si}}/x_{\text{Ti}} = 3 : 7$), 1.28% ($x_{\text{Si}}/x_{\text{Ti}} = 9 : 1$) and 1.34% ($x_{\text{Si}}/x_{\text{Ti}} = 9 : 1$) at $x_{\text{Fe}} = 0.3, 0.2$ and 0.2 respectively. As these deviations were within the considerable range, it can be concluded that the values of surface tension so computed were in very good agreement with one another for all cross-sections. The surface tension of the alloy increases as the concentrations of Fe and Ti in the mixture were increased which is obvious. We also studied the variation of surface tension of the ternary Ti–Si–Fe alloy with temperature at different compositions of the components ($\text{Fe}_{35}\text{Si}_{30}\text{Ti}_{50}$, $\text{Fe}_{35}\text{Si}_{30}\text{Ti}_{35}$, $\text{Fe}_{30}\text{Si}_{49}\text{Ti}_{21}$ and $\text{Fe}_{10}\text{Si}_{81}\text{Ti}_9$) using Chou model (figure 9). The surface tension of Ti–Si–Fe liquid alloy decreased linearly with the rise in its temperature at all compositions of the components as expected. The variation of surface tension with temperature using other models has also been found to be similar as that in Chou model but the graph is not mentioned in this paper.

4. Conclusions

Theoretical investigations predict that the component with greater bulk concentration in the alloy has tendency to exist in the pure state. The variation of activities with temperature is almost linear for all components in the ternary Ti–Si–Fe alloy. The excess free energy of mixing of the ternary Ti–Si–Fe alloy is negative at all compositions showing the compound forming tendency at all compositions. Moreover, the Si atoms segregate higher than any other components of the ternary Ti–Si–Fe alloy in the surface at all temperatures. The surface tension of the alloy decreases linearly with the increase in temperature as well as with the increase in the concentration of Si.

Acknowledgments

Authors are grateful to University Grants Commission, Nepal, for providing partial financial support to conduct this research work.

ORCID iDs

D Adhikari  <https://orcid.org/0000-0002-6022-3615>

References

- [1] Bhatia A B and Singh R N 1984 A quasi-lattice theory compound forming molten alloys *Phys. Chem. Liq.* **13** 177–90
- [2] Sommer F 1990 Thermodynamic properties of compound-forming liquid alloys *J. Non-Cryst. Solids* **117** 505–12
- [3] Singh R and Sommer F 1992 Temperature dependence of the thermodynamic functions of strongly interacting liquid alloys *J. Phys.: Condens. Matter.* **4** 5345
- [4] Novakovic R 2010 Thermodynamic, surface properties and microscopic functions of liquid Al–Nb and Nb–Ti alloys *J. Non-Cryst. Solids* **356** 1593–8
- [5] Kaptay G and Sytchev J 1999 Thermodynamic properties of phases and the electrochemical synthesis diagram for the Mo–B system *Ukr. Khim. Zh.* **65** 34–41
- [6] Hoshino K 1983 On the temperature dependence of the structure factor of the liquid Li–Pb alloy *J. Phys. F: Met. Phys.* **13** L189
- [7] Young W H 1992 Structural and thermodynamic properties of NFE liquid metals and binary alloys *Rep. Prog. Phys.* **55** 1769
- [8] Ruppertsberg H and Reiter H 1982 Chemical short-range order in liquid LiPb alloys *J. Phys. F: Met. Phys.* **12** 1311
- [9] Adhikari D, Jha I S and Singh B P 2010 Structural asymmetry in liquid Fe–Si alloys *Phil. Mag.* **90** 2687–94
- [10] Singh R N and Sommer F 1997 Segregation and immiscibility in liquid binary alloys *Rep. Prog. Phys.* **60** 57–150
- [11] Adhikari D 2011 Disorder in liquid Cu–Pd alloy *Phase Transit.* **84** 308–14
- [12] Kaptay G 2004 A new equation for the temperature dependence of the excess Gibbs energy of solution phases *CALPHAD, Comput. Coupling Phase Diagr. Thermochem.* **28** 115–24
- [13] Jha I S, Adhikari D, Kumar J and Singh B P 2011 Anomaly in mixing properties of lithium–magnesium liquid alloy *Phase Transit.* **84** 1075–83
- [14] Flory P J 1942 Thermodynamics of high polymer solutions *J. Chem. Phys.* **10** 51–61
- [15] Jordan A S 1970 A theory of regular associated solution applied to the liquid us curves of the Zn–Te and Cd–Te system *Metall. Trans.* **1** 239–49
- [16] March N H and Alonso J A 2008 Non–monotonic behaviour with concentration of the surface tension of certain binary liquid alloys *Phys. Chem. Liq.* **46** 522–6
- [17] Bhatia A B and Hargrove W H 1974 Concentration fluctuation and thermodynamic properties of some compound forming binary molten alloys *Phys. Rev. B* **10** 3186–96
- [18] Watson J D and Brown G G 1974 The strength and ductility of precipitation-hardened Fe–Si–Ti alloys *Met. Sci.* **8** 9–20
- [19] Jack D H and Guiu F 1975 Low-temperature deformation mechanisms in an Fe–Si–Ti alloy *J. Mater. Sci.* **10** 1161–8
- [20] Raghavan V 1987 *The Fe–Si–Ti (Iron–Silicon–Titanium) System, Phase Diagrams of Ternary Iron Alloys* (Materials Park, OH: ASM) pp 65–72
- [21] Weitzer F, Schuster J C, Naka M, Stein F and Palm M 2008 On the reaction scheme and liquidus surface in the ternary system Fe–Si–Ti *Intermetallics* **16** 273–82
- [22] Raghavan V 2009 Fe–Si–Ti (iron–silicon–titanium) *J. Phase Equilib. Diffus.* **30** 393–6
- [23] Park J M, Kim D H, Kim K B and Eckert J 2010 Improving the plasticity of a high strength Fe–Si–Ti ultrafine composite by introduction of an immiscible element *Appl. Phys. Lett.* **97** 251915

- [24] Hultgren R, Desai P D, Hawkins D T, Gleiser M and Kelly K K 1973 *Selected Values of the Thermodynamic Properties of Binary Alloys* (Metal Park: ASM)
- [25] Ohnuma I, Abe S, Shimenouchi S, Omori T, Kainuma R and Ishida K 2012 Experimental and thermodynamic studies of the Fe–Si binary system *ISIJ Int.* **52** 540–8
- [26] Ustinovshchikov Y I and Sapegina I V 2005 Ordering of Fe–Si phases *Inorg. Mater.* **41** 24–31
- [27] Adhikari D, Jha I S and Singh B P 2010 Structural asymmetry in liquid Fe–Si alloys *Phil. Mag.* **96** 2687–94
- [28] Wicks J K, Smith R F, Fratanduono D E, Coppari F, Kraus R G, Newman M G, Rygg J R, Eggert Jon H and Duffy T S 2018 Crystal structure and equation of state of Fe–Si alloys at super-Earth core conditions *Sci. Adv.* **4** eaao586
- [29] Choi Y W, Koo Y M, Kwon S K and Vitos L 2018 Ordered phases in Fe–Si alloys: a first-principles study *J. Korean Phys. Soc.* **72** 737–40
- [30] Hong B O, Jiang W, Duarte L, Leinenbach C, Liu L B, Liu H S and Jin Z P 2012 Thermodynamic re-assessment of Fe–Ti binary system *Trans. Nonferrous Metals Soc. China* **22** 2204–11
- [31] Louzguine D V, Kato H and Inoue A 2004 High strength and ductile binary Ti–Fe composite alloy *J. Alloys Compd.* **384** L1–3
- [32] Sabooni S, Karimzadeh F and Abbasim H 2012 Thermodynamic aspects of nanostructured Ti_5Si_3 formation during mechanical alloying and its characterization *Bull. Mater. Sci.* **35** 439–47
- [33] Chou K C et al 1996 Formalism of new ternary model expressed in terms of binary regular-solution type parameters *Calphad* **20** 395–406
- [34] Chou K C and Austin Chang Y 1989 A study of ternary geometrical models *BerBunsenges Phys. Chem.* **93** 735–41
- [35] Lijun Y, Shaobo Z, Guoji D, Gaotian X and Zhiyu Q 2007 Surface tension calculation of the Sn–Ga–In ternary alloy *CALPHAD, Comput. Coupling Phase Diagr. Thermochem.* **31** 112–9
- [36] Jiran E and Jacob K T 1986 Computation of thermodynamic properties of multi-component solutions: extension of Toop model *Metall. Trans. A.* **17** 1102–4
- [37] Butler J A V 1932 The thermodynamics of the surfaces of solutions *Proc. R. Soc. A* **135** 348–75
- [38] Redlich O and Kister A 1948 *Ind. Eng. Chem.* **40** 345
- [39] Egry I, Holland-Moritz D, Rada N, Enrica R, Wunderlich R and Sobczak N 2010 Thermophysical properties of liquid Al–based alloys *Int. J. Thermophys.* **31** 949–65
- [40] Fima P and Novakovic R 2018 Surface tension modelling of liquid Cd–Sn–Zn alloys *Phil. Mag.* **98** 1608–24
- [41] Yan X-Y, Zhang F and Chang Y A 2000 A thermodynamic analysis of the Mg–Si system *J. Phase Equilibria* **21** 379–84
- [42] Radim P, Jan V and Aleš K 2004 Prediction of alloy surface tension using a thermodynamic database *Calphad* **28** 141–6
- [43] Saša M, Dragan M S, Dragana Ž, Dragoslav G U S and Minić D 2009 Calculation of thermodynamic properties for ternary Ag–Cu–Sn system *RMZ Mater. Geoenviron* **56** 30–7
- [44] Sklyarchuk V, Yu P, Kaban I and Novaković R 2012 Surface properties and wetting behaviour of liquid Ag–Sb–Sn alloys *J. Min. Metall. B* **48** 443–8
- [45] Nowak R, Lanata T, Sobczak N, Ricci E, Giuranno D, Novakovic R, Holland-Moritz D and Egry I 2010 Surface tension of γ -TiAl-based alloys *J. Mater. Sci.* **45** 1993–2001
- [46] Manasijević D, Zivkovic D and Zivkovic Z 2003 Prediction of the thermodynamic properties for the Ga–Sb–Pb ternary system *CALPHAD, Comput. Coupling Phase Diagr. Thermochem.* **27** 361–66
- [47] Manasijević D, Živković D and Živković Ž 2003 Prediction of the thermodynamic properties for the ga–sb–pb ternary system *Calphad* **27** 361–6
- [48] Fima P 2012 Surface tension and density of liquid Sn–Ag–Cu alloys *Int. J. Mat. Res.* **103** 1455–61
- [49] Costa C, Delsante S, Borzone G, Zivkovic D and Novakovic R 2014 Thermodynamic and surface properties of liquid Co–Cr–Ni alloys *J. Chem. Thermodyn.* **69** 73–84
- [50] Tanaka T, Hara S, Ogawa M and Ueda T 1998 Evaluation of surface tension of molten salt mixtures *Retrospective Collection* vol 25 (Trans Tech Publication) pp 213–6
- [51] Smithells C J, Brandes E A and Brook G B 2004 *Smithells Metals Reference Book* (Amsterdam: Elsevier)
- [52] Arslan H and Dogan A 2019 Determination of surface tension of liquid ternary Ni–Cu–Fe and sub-binary alloys *Phil. Mag.* **99** 1206–24

- [53] Kostov A, Živković D and Friedrich G 2007 Thermodynamic prediction of Si–Me (Me = Ti, Al) binary systems *J. Min. Metall. B* **43** 29–38
- [54] Thiedemann U, Qin J, Scaefers K, Rosner-Kuhn M and Frohberg M G 1995 Mixing enthalpy measurements of liquid Fe–Ti alloys by levitation alloying calorimetry and calculation of thermodynamic properties of mixing *ISIJ Int.* **35** 1518–22
- [55] Ansara I, Dinsdale A T and Rand M H 1998 Cost 507 *Thermochemical Database for Light Metal Alloys*
- [56] Agraval P G, Dreval L A and Turchanin M A 2017 Thermodynamic properties of iron melts with titanium, zirconium and hafnium *Powder Metall. Met. Ceram.* **55** 707–16
- [57] Awe O E, Odusote Y A, Hussain L A and Akinlade O 2011 Temperature dependence of thermodynamic properties of Si–Ti binary liquid alloys *Thermochim. Acta* **519** 1–5
- [58] Furukawa T and Kato E 1975 Thermodynamic properties of liquid Fe–Ti alloys by mass-spectrometry *Tetsu-to-Hagane* **61** 3060–8



Thermodynamic, surface and transport properties of ternary Al–Sn–Zn liquid alloy and its sub binaries

R. K. Gohivar, U. Mehta, S. K. Yadav, R. P. Koirala, I. S. Jha & D. Adhikari

To cite this article: R. K. Gohivar, U. Mehta, S. K. Yadav, R. P. Koirala, I. S. Jha & D. Adhikari (2021): Thermodynamic, surface and transport properties of ternary Al–Sn–Zn liquid alloy and its sub binaries, Philosophical Magazine, DOI: [10.1080/14786435.2021.1912845](https://doi.org/10.1080/14786435.2021.1912845)

To link to this article: <https://doi.org/10.1080/14786435.2021.1912845>



Published online: 17 Apr 2021.



Submit your article to this journal [↗](#)



Article views: 11








View related articles [↗](#)



View Crossmark data [↗](#)



Thermodynamic, surface and transport properties of ternary Al–Sn–Zn liquid alloy and its sub binaries

R. K. Gohivar ^{a,b}, U. Mehta ^{a,b}, S. K. Yadav ^b, R. P. Koirala ^b, I. S. Jha^b and D. Adhikari ^b

^aCentral Department of Physics, Tribhuvan University, Kirtipur, Nepal; ^bDepartment of Physics, Mahendra Morang Adarsha Multiple Campus, Tribhuvan University, Biratnagar, Nepal

ABSTRACT

The excess free energies of sub-binary Al–Sn, Sn–Zn and Zn–Al alloys and ternary Al–Sn–Zn alloy were computed using the optimised exponential parameters of R–K polynomial at 973, 1073, 1173 and 1273 K. The computed values of free energy of mixing, enthalpy of mixing and activity of the ternary alloy were compared with the available experimental data. The surface concentrations of the monomers of the ternary Al–Sn–Zn alloy were computed using Butler model. The surface tension of the ternary liquid alloy was calculated in the framework of Chou, Kohler, Toop and Bulter models using optimised parameters for the excess surface tension. The viscosity of the sub-binary systems have been computed using Kaptay equation with the help of calculated results of enthalpy of mixing, and the viscosity of the ternary alloy were computed in the framework of Chou, Kohler and Toop model using optimised parameter for the excess viscosity.

ARTICLE HISTORY

Received 8 December 2020
Accepted 30 March 2021

KEYWORDS

R–K polynomial; glass-forming nature; exponential parameters; surface tension; viscosity

1. Introduction

Lead containing soldering materials is not preferable for the appliances because of their adverse effect on human health. However, the substitute of lead-free solders must have superior properties regarding mechanical strength, electrical conductivity, wettability, corrosion resistance and appropriate melting temperature, etc. Therefore, the research work for the development of lead-free materials having desirable properties is of great interest to many workers.

Sn-based alloys are mostly used in designing lead-free solders [1–6]. Among many Sn-based binary and ternary alloys, ternary Al–Sn–Zn alloy is considered as one of the important candidate for lead-free systems under investigation. Knott and Mikula [1] determined the partial excess free energy of Al in Al–Zn–Sn alloy using galvanic cell EMF method and the integral Gibbs energy and integral enthalpy of the ternary Al–Zn–Sn alloys at 973 K using Gibbs–

CONTACT D. Adhikari  adksbdev@yahoo.com  Department of Physics, Mahendra Morang Adarsha Multiple Campus, Tribhuvan University, Biratnagar, Nepal

© 2021 Informa UK Limited, trading as Taylor & Francis Group

Duhem integration. Knott et al. [2] also carried out the calorimetric investigation of the Al–Sn–Zn alloy to examine the enthalpy of mixing at 973 K. Prasad and Mikula [3,4] studied the thermodynamic and surface properties of the Al–Sn–Zn alloy and its sub-binaries using regular solution model, self-association model and quasi-chemical approximation in the framework of Kohler model [7] and GSM model [8,9]. Their theoretical investigation on the sub-binaries Al–Sn, Sn–Zn and Al–Zn systems showed that these systems are segregating in nature. Odusote et al. [5] used molecular interaction volume model to predict the activity of Al content in ternary Al–Sn–Zn liquid alloy by analysing activities of the components of the binaries Al–Sn, Sn–Zn and Al–Zn. Zhang et al. [10] investigated the effect of alloying Zn with the binary Al–Sn alloy on the hydrogen generation performance and found that Zn can enhance the hydrogen generation rate and yield by promoting pitting corrosion. Cheng and Zhang [6] also reassessed the thermodynamics of Al–Sn–Zn alloy by using the calculation of phase diagram (CALPHAD) method by adopting thermodynamics of binary sub-systems from previous literature and enthalpy of mixing and activity of Al content in ternary system from experiment. Sidorov et al. [11] studied density (by gamma-absorption method), electrical resistivity (by contactless method in rotating magnetic field) and magnetic susceptibility (by Faraday's method) of some Al–Sn–Zn alloys containing up to 10% of aluminum and up to 65% of zinc and found that the increase of the Zn content mostly decreased density and susceptibility values but did not affect the resistivity of the sample of ternary alloy.

In the present work, the thermodynamic, surface and transport properties of the ternary Al–Sn–Zn liquid alloy and its liquid sub-binaries Al–Sn, Sn–Zn and Al–Zn systems have been investigated in the framework of R–K polynomial [12,13] using exponential temperature-dependent parameters [14]. In most of the theoretical investigations, the linear temperature-dependent interaction parameters have been used to compute the thermodynamic and other properties of alloys in liquid state. But the authors of the present work have found that some asymmetric artifacts appear at higher temperatures in the properties of most of the alloys when linear temperature-dependent parameters are used. This indicates that the interaction parameters do not vary linearly on temperature when investigation is done at higher temperature. However, the artifacts do not appear when the interaction parameters are assumed to be exponentially dependent on temperature [14,15]. So the reassessment of the thermodynamic, surface and transport properties of the ternary Al–Sn–Zn and its sub-binaries have been done theoretically using the optimised exponential parameters.

2. Theoretical basis

Thermodynamic properties like excess Gibbs free energy of mixing (ΔG^{xs}), enthalpy of mixing (ΔH) and excess entropy of mixing (ΔS^{xs}) of liquid A–B

alloy can be calculated in framework of Redlich–Kistler (R–K) polynomial [12,13] in terms of temperature-dependent parameters. The excess Gibbs free energy of mixing is related with enthalpy of mixing and excess entropy of mixing by well-known relation

$$\Delta G^{xs} = \Delta H - T\Delta S^{xs} \quad (1)$$

The excess entropy of mixing is calculated by taking partial derivative of excess Gibbs free energy of mixing as

$$\Delta S^{xs} = \frac{-\partial(\Delta G^{xs})}{\partial T} \quad (2)$$

Thermodynamic property (ΔZ) of liquid A–B alloy is calculated using R–K polynomials [12,13]

$$\Delta Z = x_1 x_2 \sum_{i=0}^n K_i (x_1 - x_2)^i \quad (3)$$

where x_1 and x_2 are concentration of components A and B of liquid A–B alloy and K_i is coefficient of R–K polynomials and its value is different for $\Delta Z = \Delta G^{xs}$, ΔH and ΔS^{xs} .

For excess Gibbs free energy of mixing (ΔG^{xs}), K_i is also known as interaction parameters between components A and B is similar to the linear temperature dependence (A_i) such that

$$A_i = a_i - b_i T \quad (4)$$

where a_i and b_i are coefficients of R–K polynomials for enthalpy of mixing and excess entropy of mixing, respectively.

Using Equation (4) in Equation (3), we get

$$\Delta G^{xs} = x_1 x_2 \sum_{i=0}^n (a_i - b_i T)(x_1 - x_2)^i \quad (5)$$

Using Equation (5) in Equation (3) then excess entropy of mixing is obtained as

$$\Delta S^{xs} = x_1 x_2 \sum_{i=0}^n b_i (x_1 - x_2)^i; K_i = b_i \quad (6)$$

Using Equations (5) and (6) in Equation (1) we obtain enthalpy of mixing as

$$\Delta H = x_1 x_2 \sum_{i=0}^n a_i (x_1 - x_2)^i \text{ here } K_i = a_i \quad (7)$$

Kaptay [14,15] suggested interaction parameter A_i for excess Gibbs free energy

of mixing to be exponential temperature-dependent as

$$A_i = h_i \exp\left(\frac{-T}{\tau_i}\right) \quad (8)$$

where h_i and τ_i are exponential parameters.

Similarly, using Equation (8), Equations (6) and (7) can be written as

$$\Delta S^{xs} = x_1 x_2 \sum_{i=0}^n \left(\frac{1}{\tau_i}\right) h_i \exp\left(\frac{-T}{\tau_i}\right) (x_1 - x_2)^i \quad (9)$$

and

$$\Delta H_M = x_1 x_2 \sum_{i=0}^n \left(1 + \frac{T}{\tau_i}\right) h_i \exp\left(\frac{-T}{\tau_i}\right) (x_1 - x_2)^i \quad (10)$$

For ternary liquid alloy, three different models namely Chou, Kohler and Toop models [7–9] can be used to compute excess Gibbs free energy of mixing. The partial excess Gibbs free energy of mixing of liquid alloy can be determined from the expanded form of the following equation [16]

$$G_i^{xs} = G_M^{xs} + \sum_{j=1}^m (\delta_{ij} - x_j) \frac{\partial G_M^{xs}}{\partial x_j} \quad (11)$$

where δ_{ij} is Kronecker delta function.

The activities of the components of a liquid alloy are computed with the help of the equation

$$a_1 = x_1 \exp\left(\frac{G_1^{xs}}{RT}\right) \quad \text{and} \quad a_2 = x_2 \exp\left(\frac{G_2^{xs}}{RT}\right) \quad (12)$$

The well-known Butler equation [17,18] for the calculation of the surface tension of a ternary liquid alloy using the values of partial excess free energy of each component is

$$\sigma = \sigma_i + \frac{RT}{\alpha_i} \ln\left(\frac{x_i^s}{x_i^b}\right) + \frac{G_{s,i}^{xs} - G_{b,i}^{xs}}{\alpha_i} \quad \text{for } i = 1, 2, 3 \quad (13)$$

where σ_i are the surface tension of pure components, α_i are the molar surface areas of pure components and x_i^s and x_i^b are surface and bulk concentrations of individual components in the liquid mixture, respectively. $G_{s,i}^{xs}$ and $G_{b,i}^{xs}$ are the partial excess free energy for surface and bulk phase, respectively, which are related as $G_{s,i}^{xs} = \beta G_{b,i}^{xs}$

The value of β depends on crystal structure and is taken as 0.82 for liquid phase. The molar surface area of the pure component in the alloy [19] is

given as

$$\alpha_i = 1.0 N_A^{1/3} \left(\frac{M_i}{\rho_i} \right)^{2/3}$$

where N_A is Avogadro's number and M_i and ρ_i are molar mass and density of the pure components of the liquid alloy, respectively.

The surface tension (σ) and density (ρ) of pure elements in the liquid alloy vary with temperature accordingly [20]

$$\sigma = \sigma_0 + \frac{\partial \sigma}{\partial T}(T - T_0) \text{ and } \rho = \rho_0 + \frac{\partial \rho}{\partial T}(T - T_0) \quad (14)$$

where σ_0 and ρ_0 are the surface tension and density of pure component at their melting temperature T_0 and T is the temperature of interest. $\frac{\partial \sigma}{\partial T}$ and $\frac{\partial \rho}{\partial T}$ are the temperature derivative terms of surface tension and density, respectively.

For the constituent components of a ternary liquid alloys the variation of viscosity with temperature can be determined by the relation [21]

$$\eta = \eta_0 \exp\left(\frac{E}{RT}\right) \quad (15)$$

where η_0 and E are constants, and are given in the Table for liquid metals and R is the gas constant whose value is $8.31 \text{ J K}^{-1} \text{ mol}^{-1}$.

Kaptay equation [22] for the viscosity of binary alloy in terms of cohesion energy of the alloy and the activation energy of viscous flow for which viscosity increases with the increase in the cohesion energy is

$$\eta = \left(\frac{hN_A}{x_1 v_1 + x_2 v_2 + v^E} \right) \exp\left(\frac{x_1 G_1^i + x_2 G_2^i - (0.155 \pm 0.015)H_M}{RT} \right) \quad (16)$$

where G_i^i is the Gibb's energy of activation of the viscous flow in pure components i and is computed by the expression

$$G_i^i = RT \ln\left(\frac{\eta_i v_i}{hN_A}\right) \quad (17)$$

where N_A is Avogadro's number, v_i are n the molar volumes of components i ($i = 1, 2$), h is Planck's constant and v^E is the excess volume upon alloy formation which can be neglected [23].

$$\eta = \left(\frac{hN_A}{x_1 v_1 + x_2 v_2 + v^E} \right) \exp\left(\frac{x_1 G_1^i + x_2 G_2^i - (0.155 \pm 0.015)H_M}{RT} \right) \quad (18)$$

Using the above relations, the optimised values for the coefficients of the R-K polynomial for binary sub-systems can be determined and using those values in

the standard Chou, Toop and Kohler's relations, one can find the excess value of viscosity for ternary liquid alloys.

3. Results and discussion

The coefficients of R–K polynomials of Equation (3) can be expressed in the forms of linear temperature-dependent (T-dependent) and exponential T-dependent interaction parameters. The linear T-dependent interaction parameters of R–K polynomial for the liquid sub-binaries Al–Sn, Sn–Zn and Zn–Al of the ternary Al–Sn–Zn liquid alloy were optimised using observed data of Hultgren et al. [24] for enthalpy of mixing and entropy of mixing of the respective systems using Equations (6) and (7). These linear parameters of the coefficients were then used to optimise the exponential T-dependent interaction parameters of R–K polynomials which are listed in Table 1. The optimised exponential parameters were used in Equation (3) to compute the excess free energy of mixing of the sub-binary Al–Sn, Sn–Zn and Zn–Al liquid alloys at different compositions and temperatures. The computed excess free energy of mixing for sub-binary systems were found to be in good agreement with the observed values [24] at all compositions (Figure 1). The excess free energy of mixing for all sub-binaries was found to be positive which agrees with the observed results. These positive values of the excess free energy of mixing predict that the sub-binary systems are segregating in nature. The maximum value of the computed excess free energy of mixing for Al–Sn at 973 K was found to be 2888 J/mol at $x_{Al} = 0.6$ which is equal to the observed value (2884 J/mol) at the same composition and temperature [24]. Similarly, the maximum value of the computed value of the excess free energy of mixing of Sn–Zn alloy (=1563 J/mol at $x_{Sn}=0.4$) at 750 K and Zn–Al alloy (=1660 J/mol at $x_{Zn}=0.5$) at 1000 K was found to be exactly matching with the observed values at the corresponding concentrations and temperatures.

The partial excess free energies of the components of sub-binary alloys were computed using Equation (11) and optimised exponential parameters in Table 1. These partial excess free energies were then used in Equation (12) to

Table 1. Optimised exponential parameters for excess free energy of mixing of liquid Al–Sn, Sn–Zn and Zn–Al alloys.

Optimised exponential parameter for excess free energy of mixing (J/mol)		
Al–Sn	A_0	17274.46 $\exp(-4.25 \times 10^{-4} T)$
	A_1	3368.43 $\exp(-1.49 \times 10^{-4} T)$
	A_2	49682.76 $\exp(-4.6 \times 10^{-3} T)$
	A_3	6666.35 $\exp(-2.91 \times 10^{-3} T)$
Sn–Zn	A_0	17091.62 $\exp(-1.4 \times 10^{-3} T)$
	A_1	-5459.05 $\exp(-1.08 \times 10^{-3} T)$
	A_2	7494.39 $\exp(-2.93 \times 10^{-3} T)$
	A_3	302944.08 $\exp(-9.47 \times 10^{-3} T)$
Zn–Al	A_0	11564.54 $\exp(-5.55 \times 10^{-4} T)$

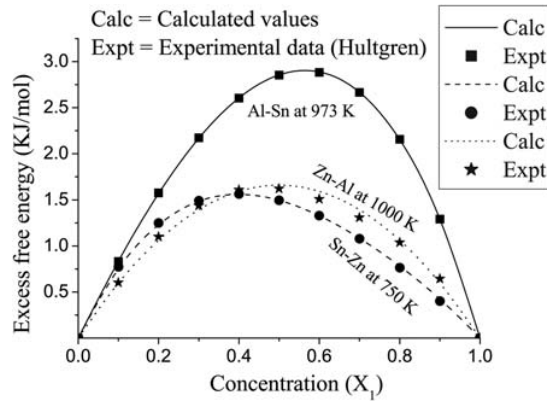


Figure 1. Calculated excess free energy of mixing of liquid binary Al–Sn, Sn–Zn and Zn–Al alloys at temperatures 973, 750 and 1000 K, respectively, and compared with experimental data of Hultgren et al. [24].

compute the activities of the corresponding components. The activities of the components of the sub-binaries Al–Sn, Sn–Zn and Zn–Al were computed at respective temperatures 973, 750 and 1000 K and plotted in Figure 2(a–c).

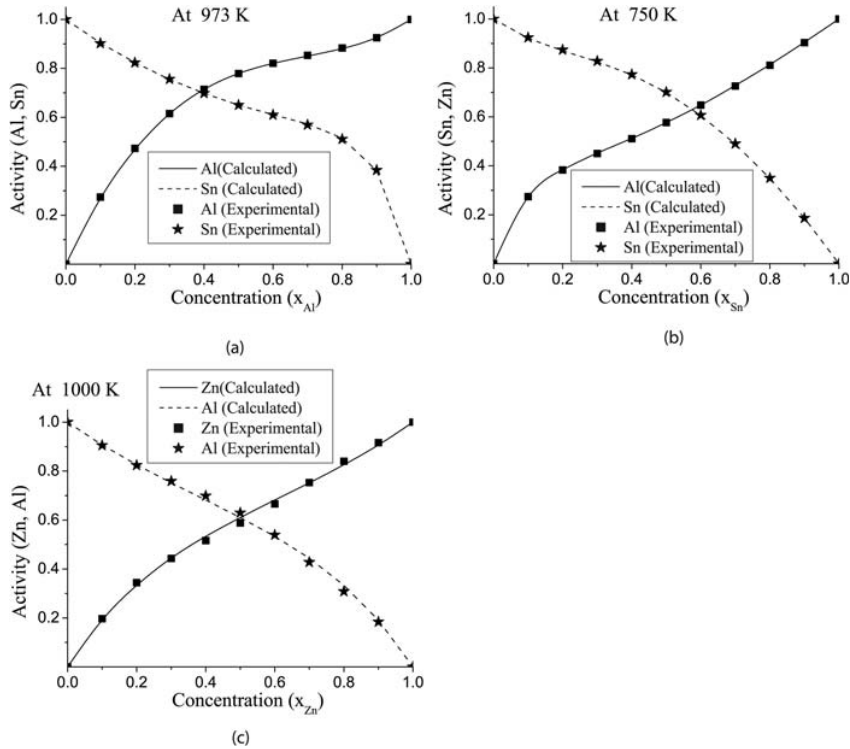


Figure 2. Activity of components of liquid binary (a) Al–Sn alloy at 973 K (b) Sn–Zn alloy at 750 K and (c) Zn–Al alloy at 1000 K.

The computed activities of the components of the corresponding sub-binaries were found to be in good agreement with the corresponding observed values [24]. The computed values of activities of the components of the sub-binary systems were found to be slightly higher than their corresponding ideal values (Raoult's law). These findings are similar to the results predicted by the excess free energy of mixing in the earlier section. Activity is a very important thermodynamic function which is obtained directly from experiment and can be used to obtain concentration fluctuation in long wavelength limit ($S_{cc}(0)$) by using a relation $S_{CC}(0) = xa \left(\frac{\partial a}{\partial x} \right)_{T,P}^{-1}$ [25,26]. The $S_{cc}(0)$ can be used to understand the nature of atomic order in the binary liquid alloys. At a given composition, if $S_{cc}(0) < S_{CC}^{id}(0)$, ordering in liquid alloy is expected and if $S_{cc}(0) > S_{CC}^{id}(0)$, there is tendency of segregation.

The excess free energy of mixing of the ternary Al–Sn–Zn liquid alloy was computed using Chou, Kohler and Toop models [7–9] and the exponential parameters from Al corners at different cross-sections ($x_{Sn}:x_{Zn} = 1:9, 3:7, 5:5, 7:3$ and $9:1$) at temperature 973 K. The excess free energy of mixing of the ternary Al–Sn–Zn alloys was found to be positive at all aforementioned compositions and temperature. This indicates that the ternary Al–Sn–Zn alloy is of glass-forming in nature at 973 K. The values of excess free energy of mixing of the ternary alloys computed from different models were found to be in excellent agreement with one another at all cross-sections. The excess free energy of mixing of the ternary alloy was found to be increasing with the increase in the concentration of Sn from Al corner and became maximum at near 50 at% of Al content (Figure 3(a–e)). The computed and observed values [1] of excess free energy of mixing of the ternary alloy were compared in Figure 3 (c) and found in well agreement with one another at all compositions. The excess free energy of mixing of the ternary alloy was also investigated in the temperature range from 973 to 1273 K. The excess free energy of mixing of the ternary Al–Sn–Zn alloy was found to be decreasing with the rise of temperature at all compositions (Figure 4).

The activities of the monomers of the ternary Al–Sn–Zn were computed using Equation (12) from Al corners at the cross-sections $x_{Sn}: x_{Zn} = 1:9, 3:7, 5:5, 7:3$ and $9:1$ at temperature 973 K. The activities of the monomers of the ternary alloy were found to be increasing with the increase in the concentration of the corresponding components (Figure 5(a–e)). The activities of all components were found to have positive deviation from Raoult's law. This result, thus, showed that the ternary Al–Sn–Zn alloy in liquid state is glass forming in nature. The variation of the activities of the components of the ternary Al–Sn–Zn alloy with temperature in the range 973 to 1273 K was studied. The activity of the components of the system was found to be decreasing and shifting towards the ideal value with the rise in temperature (Figure 6).

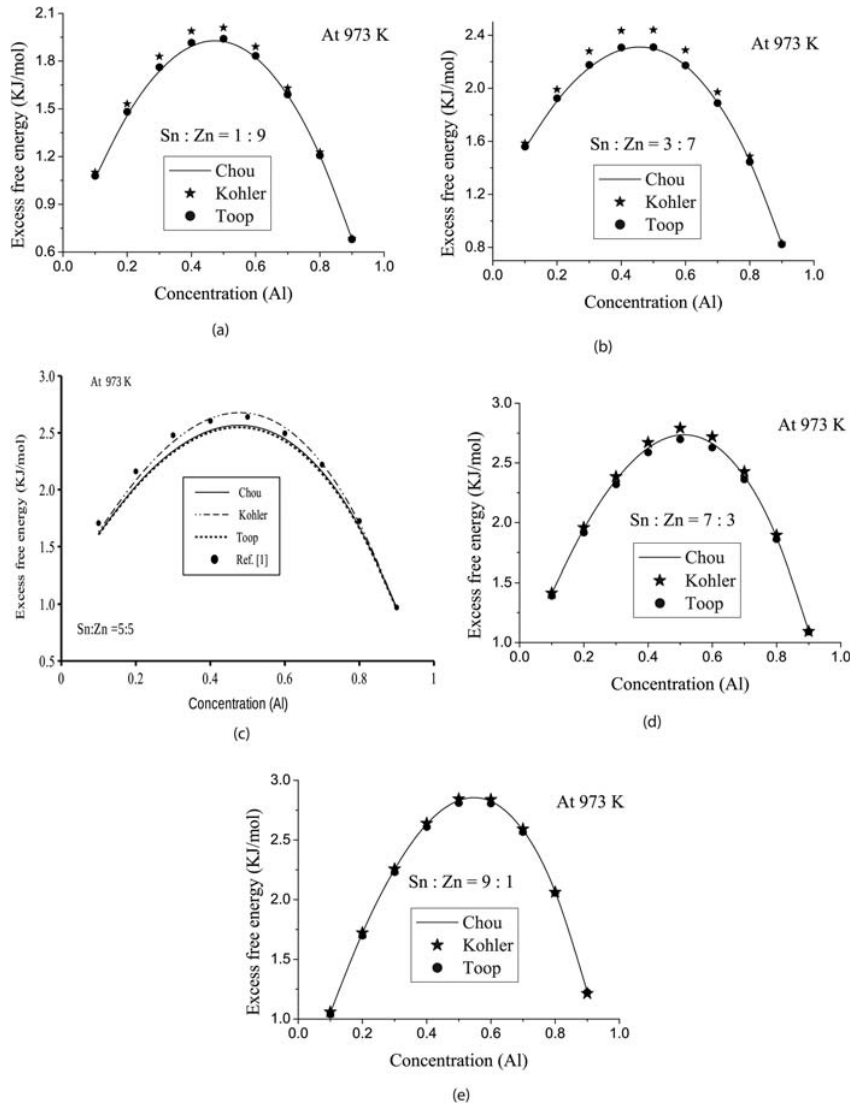


Figure 3. Computed excess free energy of mixing of liquid Al-Sn-Zn alloy using Chou, Kohler and Toop model at cross-sections Sn:Zn (a) 1:9 (b) 3:7 (c) 5:5 (d) 7:3 and (e) 9:1 at temperature 973 K.

Further, the enthalpy of mixing of the ternary Al-Sn-Zn liquid alloy was computed from the Al corner at the cross-sections $x_{\text{Sn}}: x_{\text{Zn}} = 1:2, 1:1$ and $2:1$ with the help of exponential parameters for free energy of mixing listed in Table 1 in the framework of Chou model [8] at temperature 973 K. The computed enthalpy of mixing was compared with observed values [1,2] (Figure 7(a-c)). The computed enthalpy of mixing of the ternary alloy was found to be in reasonably agreement at lower concentration and in well

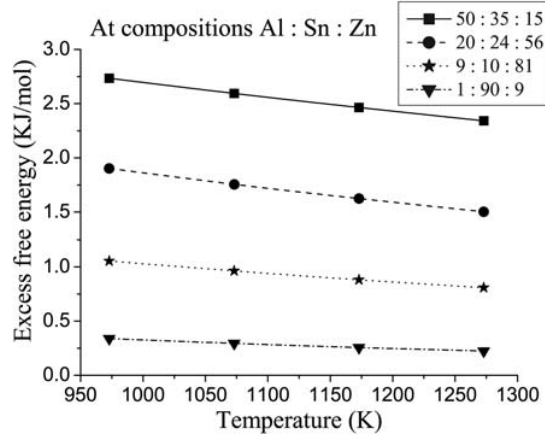


Figure 4. Variation of excess free energy of mixing with temperature at composition Al:Sn:Zn in ratio 50:35:15, 20:24:56, 9:10:81 and 1:90:9.

agreement at higher concentration of Al with the observed value [1,2] (Fig. 7(a-c)). The computed enthalpy of mixing for the ternary Al–Sn–Zn alloy was found to be positive at all compositions and the cross-sections $x_{\text{Sn}}: x_{\text{Zn}} = 1:2$, 1:1 and 2:1.

The partial excess free energies of the components of the alloy were then used in Butler equation to obtain the surface concentrations and surface tensions of sub-binary Al–Sn, Sn–Zn and Zn–Al systems. The computed values of the surface tensions of Al–Sn, Sn–Zn and Zn–Al systems of present work were found to be in satisfactorily agreement with the available experimental and literature data [28–30] (Figure 8). The coefficients of R–K polynomial for excess surface tensions of the sub-binary systems Al–Sn, Sn–Zn and Zn–Al were optimised and are listed in Table 2. The values of surface tension of the ternary Al–Sn–Zn alloy were computed using parameters of Tables 2 and 3 in the framework of Chou, Kohler and Toop equations [7–9] from Al corner at the cross-sections $x_{\text{Sn}}:x_{\text{Zn}} = 1:9$, 3:7, 5:5, 7:3 and 9:1. The surface tension of the ternary Al–Sn–Zn

Table 2. Optimised parameter for excess surface tension of liquid Al–Sn, Sn–Zn and Zn–Al alloy.

Optimised parameter for excess surface tension (N/m)		
Al–Sn	A_0	$5.320 \times 10^{-4} T - 0.9746$
	A_1	$5.143 \times 10^{-4} T - 0.8526$
	A_2	$-1.5804 \times 10^{-6} T^2 + 4.7305 \times 10^{-3} T - 3.6910$
	A_3	$-1.7503 \times 10^{-6} T^2 + 5.071 \times 10^{-3} T - 3.7951$
Sn–Zn	A_0	$1.762 \times 10^{-4} T - 0.3749$
	A_1	$1.2897 \times 10^{-7} T^2 - 4.4992 \times 10^{-4} T + 0.4449$
	A_2	$-3.6610 \times 10^{-7} T^2 + 1.0769 \times 10^{-3} T - 0.8438$
	A_3	$3.6154 \times 10^{-7} T^2 - 1.0281 \times 10^{-3} T + 0.7650$
Zn–Al	A_0	$-1.9883 \times 10^{-7} T^2 + 6.0902 \times 10^{-4} T - 0.4948$
	A_1	$1.5672 \times 10^{-7} T^2 - 4.3797 \times 10^{-4} T + 0.3154$
	A_2	$-1.1305 \times 10^{-7} T^2 + 2.9553 \times 10^{-4} T - 0.1961$
	A_3	$5.9748 \times 10^{-8} T^2 - 1.5190 \times 10^{-4} T + 0.09731$

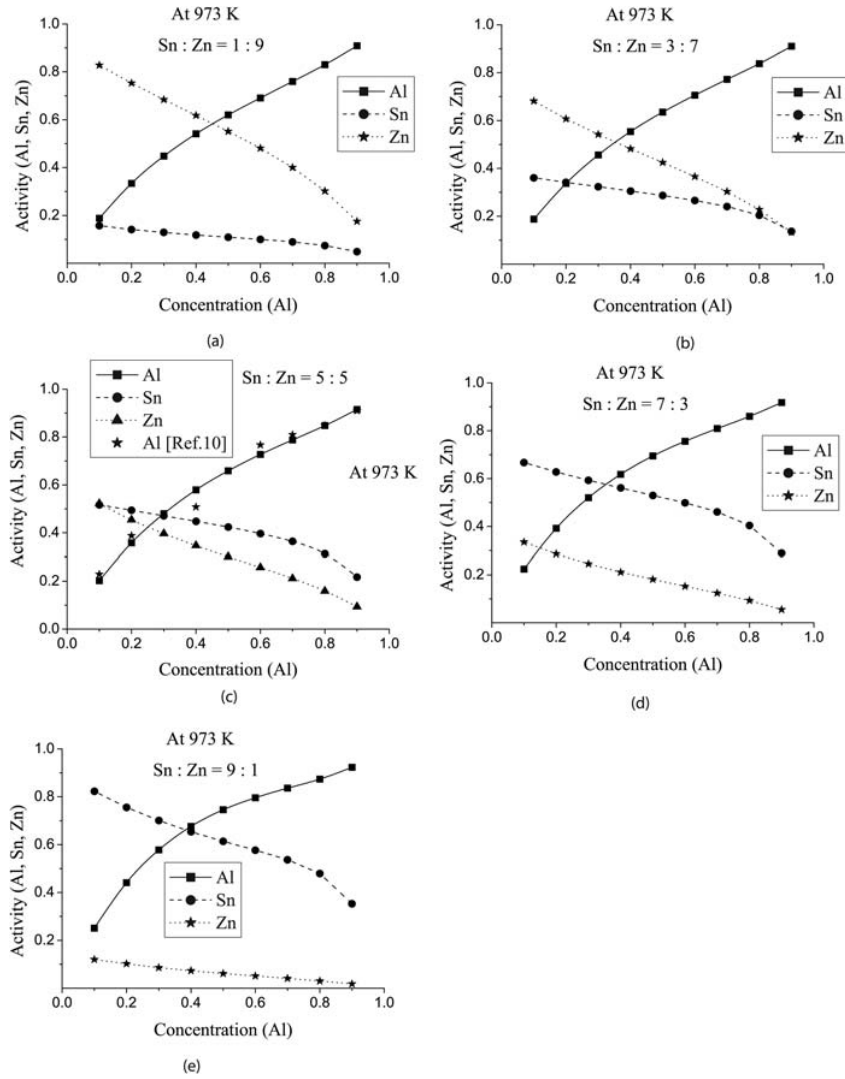


Figure 5. Activity of components of liquid Al–Sn–Zn alloy at cross-section Sn:Zn (a) 1 : 9 (b) 3 : 7 (c) 5 : 5 (d) 7 : 3 and (e) 9 : 1 at temperature 973 K.

alloys computed using these three modeling equations were found to be in good agreement with that obtained from Butler model, Equation (13) (Figure 9(a–e)). The agreement between the values of the surface tension using different

Table 3 . Density (ρ_0) and surface tension (σ_0) of elements Al, Sn and Zn at temperature (T_0) and their variations with temperature and their constant η_0 and E .

Element	T_0 (K)	ρ_0 (Kg/m ³)	$\partial\rho/\partial T$ (Kg m ⁻³ K ⁻¹)	σ_0 (Nm ⁻¹)	$\partial\sigma/\partial T$ (Nm ⁻¹ K ⁻¹)	η_0 (mPa s)	E (J/mol)
Al	933	2385	-0.35	0.914	-0.00035	0.1493	16,500
Sn	505	6980	-0.61	0.560	-9E-05	0.315	8488.6
Zn	692	6575	-0.98	0.782	-0.00017	0.4131	12,700

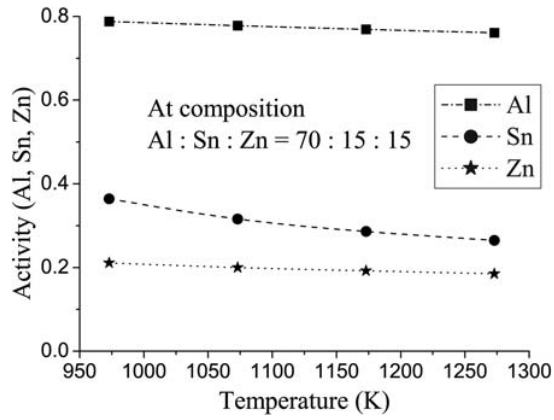


Figure 6. Variation of activity of liquid Al–Sn–Zn alloy with temperature at composition Al:Sn: Zn in ratio 70:15:15.

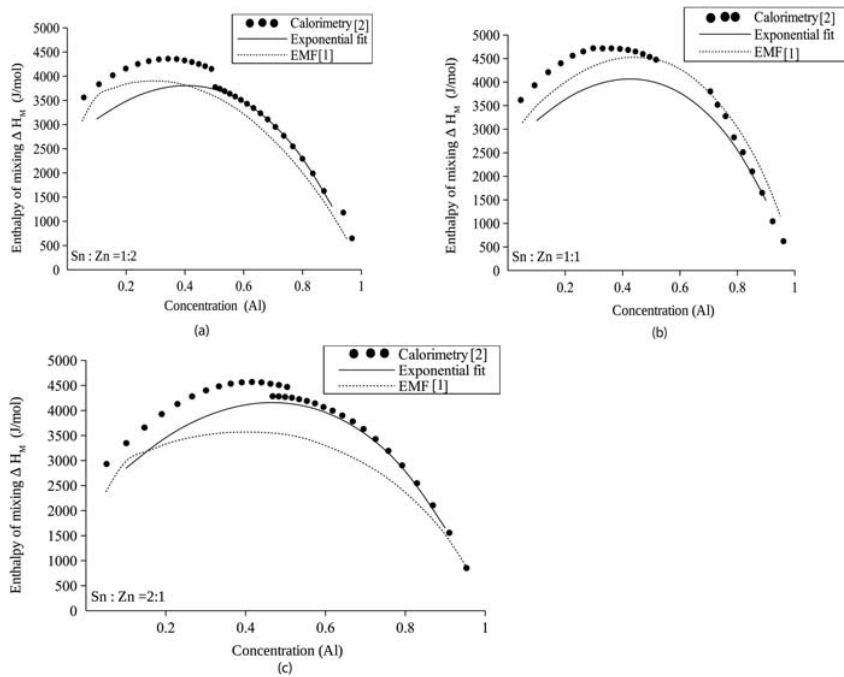


Figure 7. The enthalpy of mixing of liquid Al–Sn–Zn alloy at three different cross-section (a) $x_{Sn}:x_{Zn}=1:2$ (b) $x_{Sn}:x_{Zn}=1:1$ and (c) $x_{Sn}:x_{Zn}=2:1$ at temperature 973 K.

modeling equations proves the validity of optimised parameters of coefficients of R–K polynomial. The surface tension of the ternary alloy was observed to be increasing with the increase in the concentration of Al at all cross-sections. For a given concentration of Al in the ternary alloy, the surface tension was

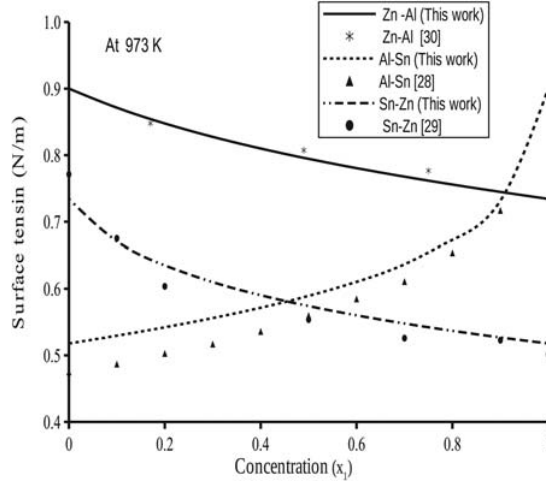


Figure 8. The compositional dependence of surface tension of the sub-binary systems of Al-Sn-Zn ternary liquid alloy at 973 K.

found to be increasing with the increase in the concentration of Zn and decreasing with the increase in the concentration of Sn. This is due to the fact that the surface tension of pure Sn is the lowest and that of Al is the greatest among the constituents of the alloy. While studying the surface tension of the ternary Al-Sn-Zn alloy, it was found that the surface tension of the alloy decreased linearly with the rise in the temperature at all compositions (Figure 10).

The surface concentrations of the components Al, Sn and Zn of the alloy were computed using Butler's model from Al corner at the cross-sections x_{Sn} : $x_{\text{Zn}} = 1:9, 3:7, 5:5, 7:3$ and $9:1$ at 973 K. The surface concentration of each monomer was found to be increasing with the increase in the bulk concentration of the respective components (Figure 11(a-e)). The surface concentration of Sn was found to be much greater than its bulk concentration while the surface concentration of Al and Zn were found to be less than their respective bulk concentrations. At equiatomic composition, surface concentrations of Sn, Al and Zn change to 70 at%, 10 at% and 20 at%, respectively (Figure 11(c)). Further the variation of the surface concentration of each component of the system with the temperature was found to be shifting towards ideal value (Figure 12).

In order to study the transport properties of the ternary Al-Sn-Zn alloy, Equation (17) was used to calculate the viscosity of individual component. The values of η_0 and E for Sn were taken from Ref. [27] and rests were taken from Smithells metal reference book [20] and are listed in Table 3. The enthalpy of mixing of sub-binary systems were used in Equation [16] to compute the viscosity of sub-binary systems at different temperatures. The computed viscosity of the sub-binary systems of the ternary Al-Sn-Zn liquid alloy is plotted in Figure 13. The viscosity of sub-binary Zn-Al alloy was found to be in good

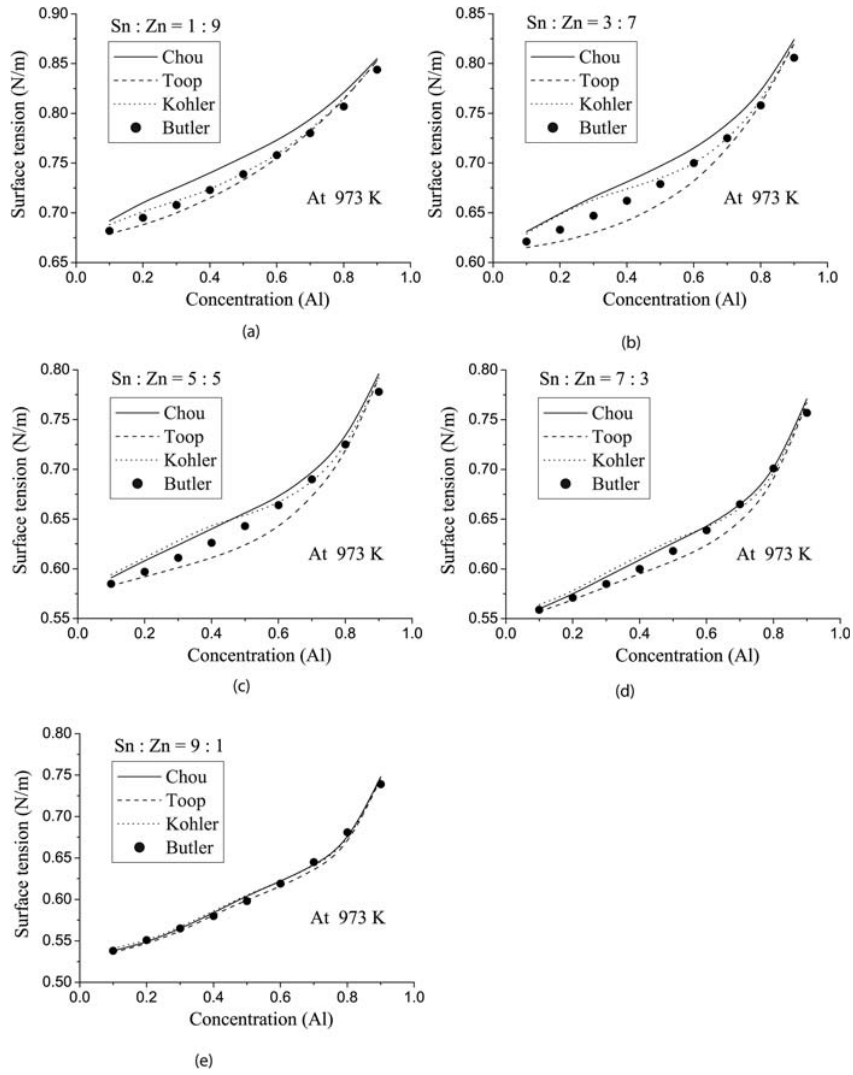


Figure 9. Comparison of surface tension of liquid Al-Sn-Zn alloy using Chou, Kohler and Toop Models with that values computed using Butler model at cross-sections Sn:Zn (a) 1:9 (b) 3:7 (c) 5:5 (d) 7:3 and (e) 9:1 at temperature 973 K.

agreement with the experimental value [30]. The viscosities of the sub-binary systems were then used to optimise the coefficients of R-K polynomial for excess viscosity which are presented in Table 4. These coefficients were used in Chou, Kohler and Toop equations to compute the viscosity of the ternary alloy at different concentrations and temperatures. The variation of viscosity of the ternary alloy at 973 K from Al corner at five different cross-sections are shown in Figure 14(a-e). The viscosity of the alloy was found to decrease gradually with the increase in the concentration of Al in the Zn-rich cross-

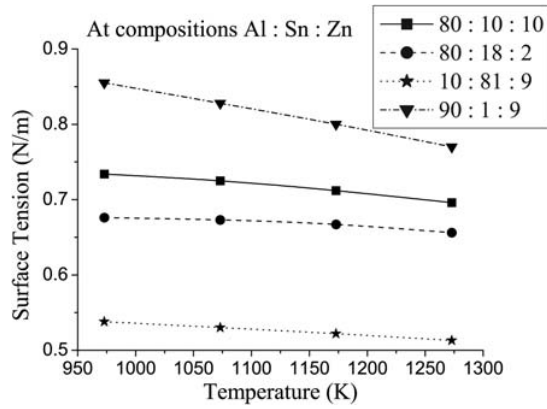


Figure 10. Variation of surface tension of liquid Al–Sn–Zn alloy with temperature at compositions Al:Sn:Zn in ratio 80:10:10, 80:18:2, 10:81:9, and 90:1:9.

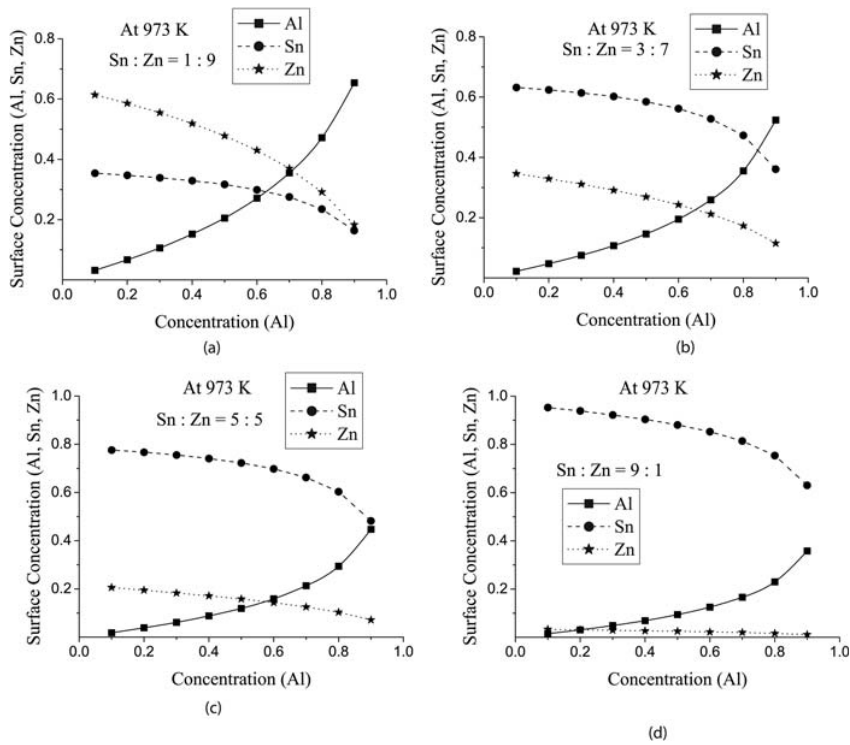


Figure 11. Surface concentrations of the components of liquid Al–Sn–Zn alloy at different cross-sections, Sn:Zn (a) 1:9 (b) 3:7 (c) 5:5 (d) 7:3 (e) 9:1 at 973 K.

section (Figure 14(a, b)). The viscosity of the system was found to decrease slightly and then increases rapidly with the increase in the concentration of Al in the Sn-rich region (Figure 14 (d,e)). The viscosity of the alloy was

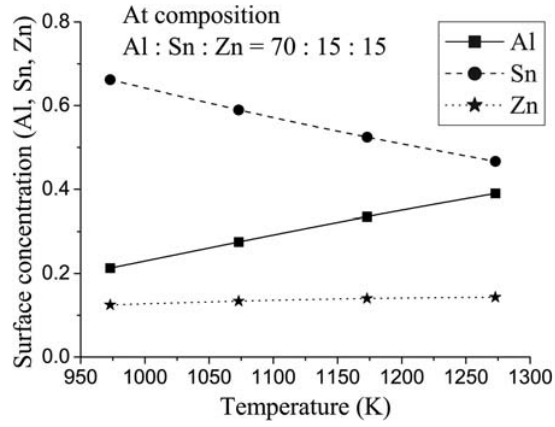


Figure 12. Variation of surface concentration of component of liquid Al-Sn-Zn alloy with temperature at composition Al:Sn:Zn in ratio 70:15:15.

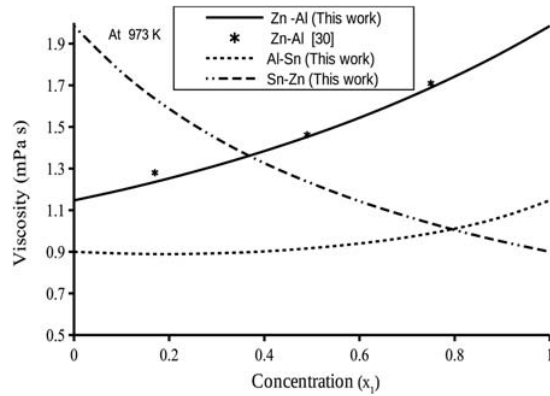


Figure 13. Viscosity of liquid Al-Sn, Sn-Zn and Zn-Al alloys at 973 K.

Table 4 . Optimised parameter for excess viscosity of liquid Al-Sn, Sn-Zn and Zn-Al alloy.

Optimised parameter for excess viscosity (mPa s)		
Al-Sn	A ₀	$-1.4296 \times 10^{-6} T^2 + 3.8975 \times 10^{-3} T - 2.8607$
	A ₁	$-5.8912 \times 10^{-7} T^2 + 1.5860 \times 10^{-3} T - 1.1056$
	A ₂	$-7.1126 \times 10^{-7} T^2 + 1.8433 \times 10^{-3} T - 1.2141$
	A ₃	$-3.2698 \times 10^{-7} T^2 + 8.4940 \times 10^{-4} T - 0.5929$
Sn-Zn	A ₀	$-2.2936 \times 10^{-6} T^2 + 6.4814 \times 10^{-3} T - 4.9930$
	A ₁	$1.10365 \times 10^{-6} T^2 - 3.0817 \times 10^{-3} T + 2.3035$
	A ₂	$-6.6072 \times 10^{-7} T^2 + 1.8047 \times 10^{-3} T - 1.2893$
	A ₃	$1.5215 \times 10^{-7} T^2 - 4.334 \times 10^{-4} T - 0.3230$
Zn-Al	A ₀	$-6.9256 \times 10^{-7} T^2 + 1.9691 \times 10^{-3} T - 1.6864$
	A ₁	$-1.1240 \times 10^{-7} T^2 + 3.3006 \times 10^{-4} T - 0.2900$
	A ₂	$-2.6656 \times 10^{-8} T^2 + 7.5504 \times 10^{-5} T - 0.0605$
	A ₃	$-4.1058 \times 10^{-9} T^2 + 1.1635 \times 10^{-5} T - 0.0091$

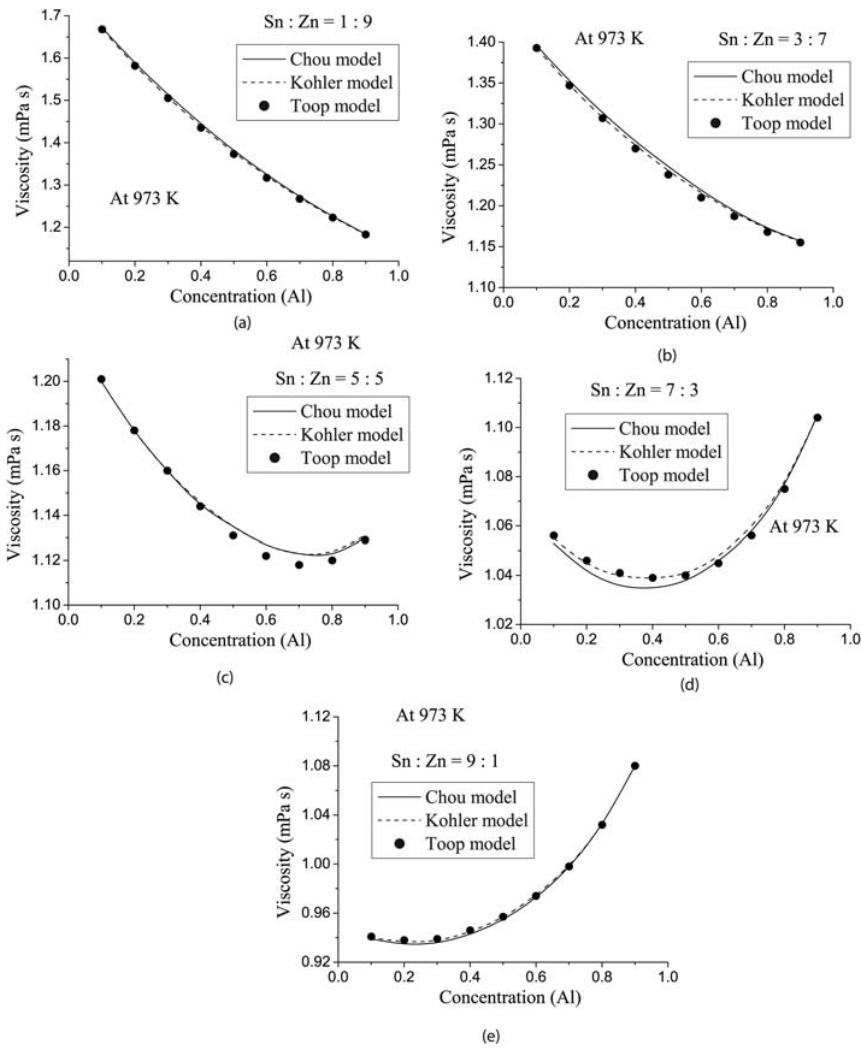


Figure 14. Viscosity of liquid Al–Sn–Zn alloy using Chou, Kohler and Toop model at cross-sections Sn:Zn (a) 1: 9 (b) 3:7 (c) 5:5 (d) 7:3 (e) 9:1 at temperature 973 K.

observed to decrease rapidly at elevated temperatures at all concentrations as shown in Figure 15, which is as expected.

4. Conclusions

The conclusions of the work are as follows:

- i The excess free energies of all the sub-binary and ternary systems are positive with moderate value. This shows that the sub-binary and ternary systems are segregating (glass forming) in nature.

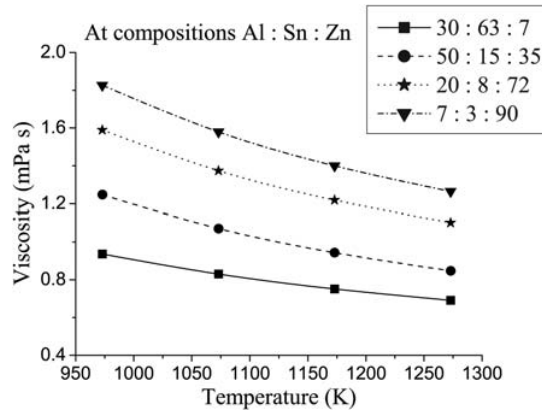


Figure 15. Variation of viscosity of liquid Al–Sn–Zn alloy with temperature at composition Al:Sn:Zn in ratio 30:63:7, 50:15:35, 20:8:72 and 7:3:90.

- ii The activities of the components of the binary and ternary alloys are found to be greater than their respective ideal values (Raoult's law) which also indicate that the alloys are segregating in nature. The activity of Al is found to be relatively greater than that of other components of the alloy showing that the leaving tendency of Al from the mixture is greater and its solubility is relatively low.
- iii The surface concentration of Sn is found to be greater than its bulk concentration while the surface concentration of Al and Zn are found to be less than their respective bulk concentrations. This indicates that the component having lower value of surface tension in pure state segregates more on the surface phase. The surface concentration of Sn decreases while that of Al and Zn increases with the rise of temperature. This shows that the surface concentration changes towards ideal value at elevated temperatures.
- iv Surface tension of the ternary Al–Sn–Zn alloy increases with the increase in the concentration of Al and decreases with the increase in the concentration of Sn contents in the alloy. The surface tension of alloy decreases linearly with temperature at all compositions.
- v The viscosity of the ternary Al–Sn–Zn alloy decreases gradually with increase in the temperature of the system at all compositions.

Acknowledgement

D. Adhikari is grateful to University Grants Commissions (UGC), Nepal for providing financial support to pursue this research (Grant no, FRG-S&T-73/74-14).

Disclosure statement

No potential conflict of interest was reported by the author(s).

Funding

This work was supported by University Grants Commission- Nepal: [Grant Number FRG-S&T-73/74-14].

ORCID

R. K. Gohivar  <http://orcid.org/0000-0002-6154-7443>

U. Mehta  <http://orcid.org/0000-0003-1024-2436>

S. K. Yadav  <http://orcid.org/0000-0003-2525-216X>

R. P. Koirala  <http://orcid.org/0000-0002-7325-6352>

D. Adhikari  <http://orcid.org/0000-0002-6022-3615>

References

- [1] S. Knott and A. Mikula, *Thermodynamic properties of liquid Al – Sn – Zn alloys: A possible new lead-free solder material*. Mater. Trans 43 (2002), pp. 1872.
- [2] S. Knott, H. Flandorfer and A. Mikula, *Calorimetric investigations of the two ternary systems Al – Sn – Zn and Ag – Sn – Zn*. Z. Met 96 (2005), pp. 38–44.
- [3] L.C. Prasad and A. Mikula, *Thermodynamics of liquid Al – Sn – Zn alloys and concerned binaries in the light of soldering characteristics*. Phys. B Condens. Matter 373 (2006), pp. 64–71.
- [4] L.C. Prasad and A. Mikula, *Surface segregation and surface tension in Al-Sn-Zn liquid alloys*. Phys. B Condens. Matter 373 (2006), pp. 142–149.
- [5] Y.A. Odusote, A.I. Popoola and K.D. Adedayo, *Thermodynamic properties of Al in ternary lead-free solder Al-Sn-Zn alloys*. Mater. Sci 35 (2017), pp. 583–593.
- [6] T. Cheng and L. Zhang, *Thermodynamic re-assessment of the Al-Sn-Zn ternary system*. J. Min. Met. Sect. B-Metall 55 (2019), pp. 439–449.
- [7] L. Yan, S. Zheng, G. Ding, G. Xu, and Z. Qiao, *Surface tension calculation of the Sn–Ga–In ternary alloy*. CALPHAD 31 (2007), pp. 112–119.
- [8] K.C. Chou, *A general solution model for predicting ternary thermodynamic properties*. CALPHAD 19 (1995), pp. 315–325.
- [9] K.C. Chou and C.Y. Austin, *A study of ternary geometrical models*. Ber. Bunsenges. Phys. Chem. 93 (1989), pp. 735–741.
- [10] F. Zhang, K. Edalati, M. Arita and Z. Horita, *Hydrolytic hydrogen production on Al–Sn–Zn alloys processed by high-pressure torsion*. Materials (Basel 11 (2018), pp. 1209.
- [11] V. Sidorov, J. Drápala, S. Uporov, A. Sabirzyanov, P. Popel, A. Kurochkin, and K. Grushevskij, *Some physical properties of Al–Sn–Zn melts*. EPJ Web of Conferences 15 (2011), pp. 01022.
- [12] O. Redlich and A.T. Kister, *Algebraic representation of thermodynamic properties and the classification*. Ind. Eng. Chem 40 (1948), pp. 345–348.
- [13] R.N. Singh and F. Sommer, *Segregation and immiscibility in liquid binary alloys*. Rep. Prog. Phys 60 (1997), pp. 57–150.
- [14] G. Kaptay, *A new equation for the temperature dependence of the excess Gibbs energy of solution phases*. CALPHAD 28 (2004), pp. 115–124.
- [15] G. Kaptay, *The exponential excess Gibbs energy model revisited*. CALPHAD 56 (2017), pp. 169–184.
- [16] X. Ding, P. Fan and W. Wang, *Thermodynamic calculation for alloy systems*. Metall. Mater. Trans. B 30 (1999), pp. 7–8.

- [17] J.A.V. Butler, *The thermodynamics of the surfaces of solutions*. Proceedings of The Royal Society A 135 (1932), pp. 348–375.
- [18] P. Fima and R. Novakovic, *Surface tension modelling of liquid Cd-Sn-Zn alloys*. Philos. Mag. 6435 (2018), pp. 1–17.
- [19] C. Costa, S. Delsante, G. Borzone, D. Zivkovic and R. Novakovic, *Thermodynamic and surface properties of liquid Co-Cr-Ni alloys*. J. Chem. Thermodyn 69 (2014), pp. 73–84.
- [20] E.A. Brandes and G.B. Brook, *Smithells Metals Reference Book*, 7th edition, Butterworth-Heinemann, (1999).
- [21] M. Hirai, *Estimation of viscosities of liquid alloys*. ISIJ Int. 33 (1986), pp. 251–258.
- [22] G. Kaptay, *Section metallurgy*, IMAG0675, in Proceeding of micro CAD 2003 conference, University of Miskolc, 2003. pp. 23–28.
- [23] I. Budai and M.Z. Benko, *Gyorgy kaptay*. Mater. Sci. Forum 473–474 (2005), pp. 309–314.
- [24] K.K. Hultgren, R. Desai, P.D. Hawkins, D.T. Gleiser, and M. Kelley, *Selected values of thermodynamic properties of binary alloy*. Met. Park. Ohio ASM. (1973).
- [25] R.N. Singh, *Short-range order and concentration fluctuations in binary molten alloys*. Can. J. Phys 65 (1987), pp. 309–325.
- [26] D. Adhikari, B.P. Singh, I.S. Jha and B.K. Singh, *Chemical ordering and thermodynamic properties of Hg-Na liquid alloys*. J. Non-Cryst. Solids 357 (2011), pp. 2892–2896.
- [27] T. Gancarz, W. Gąsior and H. Henein, *Physicochemical properties of Sb, Sn, Zn, and Sb-Sn system*. Int. J. Thermophys 34 (2013), pp. 250–266.
- [28] Y.A. Odusote, A.I. Popoola and S.S. Oluyamo, *Bulk and surface properties of demixing liquid Al-Sn and Sn-Tl alloys*. Appl. Phys. A 122 (2016), pp. 80.
- [29] J. Pstrus, Z. Moser, W. Gąsior and A. Dębski, *Surface tension and density measurements of liquid Sn-Zn alloys. experiment vs. SURDATdatabase of Pb-free solders*. Arch. Metall. Mater. 51 (2006), pp. 335–343.
- [30] M.E. Trybula, T. Gancarz and W. Gąsior, *Density, surface tension and viscosity of liquid binary Al-Zn and ternary Al-Li-Zn alloys*. Fluid Phase Equilib. 421 (2016), pp. 39–48.

Surface Properties of Al–Fe–Si Liquid Alloy Using Thermodynamic Database

U. Mehta, S. K. Yadav, I. Koirala, D. Adhikari

Journal of Nepal Physical Society

Volume 6, Issue 2, December 2020

ISSN: 2392-473X (Print), 2738-9537 (Online)

Editors:

Dr. Binod Adhikari

Dr. Bhawani Joshi

Dr. Manoj Kumar Yadav

Dr. Krishna Rai

Dr. Rajendra Prasad Adhikari

Mr. Kiran Pudasainee

JNPS, 6 (2), 10-19 (2020)

DOI: <http://doi.org/10.3126/jnphysoc.v6i2.34849>

Published by:

Nepal Physical Society

P.O. Box: 2934

Tri-Chandra Campus

Kathmandu, Nepal

Email: npseditor@gmail.com





Surface Properties of Al–Fe–Si Liquid Alloy Using Thermodynamic Database

U. Mehta^{1,2}, S. K. Yadav², I. Koirala¹, D. Adhikari^{2,*}

¹Central Department of Physics, Tribhuvan University, Kirtipur, Nepal.

²Department of Physics, Mahendra Morang Adarsha Multiple Campus, T. U., Biratnagar, Nepal.

*Corresponding Email : adksbdev@yahoo.com

Received: 25 October, 2020; Revised: 24 November, 2020; Accepted: 26 December, 2020

Abstract

Temperature-dependent interaction parameters for excess free energies of mixing of sub-binary systems of Al-Fe-Si ternary liquid alloys were optimised using the experiment data in the frame of Redlich-Kister (R-K) polynomials. These optimised parameters were then used to compute the partial excess free energy of sub-binary and ternary liquid alloys. The surface tension and surface concentration of sub-binary and the ternary liquid alloys were computed using Butler equation. The temperature dependent coefficients of R-K polynomials for excess surface tensions of the sub-binary systems were optimised which were then used to estimate the surface tension of ternary alloy using Chou, Kohler and Toop modelling equations at temperatures 1773, 1873, 1973 and 2073 K. The surface tension of the ternary alloy obtained using aforementioned models were found to be in good agreement from Fe and Al corners but some deviations were observed from Si corner.

Keywords: R-K polynomials, Al–Fe–Si liquid alloy, sub-binary systems, surface tension, surface concentration.

1. INTRODUCTION

Iron and silicon are mostly used as common alloying ingredient in aluminium alloys to enhance the mechanical strength [1, 2]. Al–Fe–Si system possesses high oxidation resistance and hence are mainly used for food packaging, magnetic materials for transformers, lithographic printing sheets, capacitors [2-4] and building materials [5]. The addition of iron and vanadium to the Al–Si alloy enhances the wear resistance significantly with respect to the conventional Al–Si alloy [6]. The Fe and Si atoms precipitate on solidifying the Al-Fe-Si liquid alloy and forms the hard and brittle ternary phases which enhances the mechanical properties and surface quality of the final products significantly [7]. Due to these multidisciplinary applications, many researchers [1-5, 7-12] have long been working to access the energetic of Al-Fe-Si system.

The effect of cooling rate on solidification of the

system was studied experimentally by Dutta and Rettenmayr [5] and they predicted that different stable and metastable compounds formed on cooling the specimen at different rates. Du et.al. [7] reported the eleven different stable complex of Al-Fe-Si in liquid and solid alloys. Lui and Chang [1] studied the thermodynamic properties and the phase equilibria of the system and reported the formation of different intermetallic compounds like $Al_{66}Fe_{19}Si_5(Al, Si)_{10}$, $Al_{59.8}Fe_{15.2}Si_{10}(Al, Si)_{15}$, $Al_{63.5}Fe_{20.5}Si_{16}$, $Al_{49}Fe_{16}Si_{35}$, $Al_{35}Fe_{37}Si_{28}$, $Al_{54}Fe_{26}Si_{20}$ and $Al_{40}Fe_{25}Si_{35}$. Moreover, Boulouma et al. [4] investigated the phases of Al-Fe-Si system and identified the formation of compounds like $\alpha - Fe_2SiAl_8$, $\beta - FeSiAl_8$, $\gamma - FeSiAl_3$ and $\delta - FeSi_3Al_9$. Pontevichi et al. [8] studied the phase equilibria of the system at 1000 K and found that the compound $\gamma - Al_3FeSi$ to be in equilibrium with the liquid containing 10.5 at.% of Si and 3.2-3.5 at. % of Fe. Novak et al. [3]

prepared the $FeAl_{20}Si_{20}$ alloy by ultrahigh-energy mechanical alloying and spark plasma sintering processes and reported the anomalous compressive strength of about 1100 MPa at room temperature which increased to 1500 MPa at 773 K. Moreover, they observed that the alloy of this composition showed better oxidation resistance at 1273 K than that of 1073 K due to the formation of a highly protective $\alpha - Al_2O_3$ layer on the surface. They further suggested that this alloy can be used as appropriate material for automobile industries and also as a material for aggressive environmental conditions. Further, several researchers had studied the surface tensions of Al-Fe [13, 14], Fe-Si [13, 15, 16] and Si-Al [14, 17] sub-binary liquid alloys of Al-Fe-Si system.

Therefore, the surface properties, such as surface tension and surface concentration of Al-Fe-Si ternary liquid alloy have been studied at 1773 K, 1873 K, 1973 K and 2073 K and different cross-sections in the present work. For this purpose, the activity and excess Gibbs free energy of mixing of sub-binary systems were calculated using the optimised coefficients of R-K polynomials for excess free energy of mixing. The surface concentration and surface tension of the binary and ternary liquid alloys were computed using Butler's equation. For the comparative study, the surface tension of the ternary alloy were also computed using Chou, Kohler and Toop models with the help of temperature-dependent optimised coefficients of R-K polynomial for excess surface tension.

The expressions used for the computations of different physical quantities are presented in the Section 2, the results and discussion are mentioned in the Section 3 and the conclusions are highlighted in the Section 4 of the work.

2. MATHEMATICAL MODELING

According to the Butler model, the surface tension (γ) and the surface concentrations (x^s) of components of binary and multi-component liquid alloys can be expressed as [13, 18-21]

$$\gamma = \gamma_1 + \frac{RT}{\alpha_1} \ln \left(\frac{x_1^s}{x_1^b} \right) + \frac{G_{s,1}^{xs} - G_{b,1}^{xs}}{\alpha_1} \dots\dots\dots (1a)$$

$$= \gamma_2 + \frac{RT}{\alpha_2} \ln \left(\frac{x_2^s}{x_2^b} \right) + \frac{G_{s,2}^{xs} - G_{b,2}^{xs}}{\alpha_2} \dots\dots\dots (1b)$$

$$= \gamma_3 + \frac{RT}{\alpha_3} \ln \left(\frac{x_3^s}{x_3^b} \right) + \frac{G_{s,3}^{xs} - G_{b,3}^{xs}}{\alpha_3} \dots\dots\dots (1c)$$

where γ_i ($i=1, 2, 3$) are the surface tension, x_i^b and x_i^s are the bulk and surface concentrations of the individual component i of the alloy in their pure state and R is the universal gas constant. $G_{s,i}^{xs}$ and $G_{b,i}^{xs}$ are the partial excess free energies for the surface and bulk phases of the individual component i which are related as $G_{s,i}^{xs} = \beta G_{b,i}^{xs}$. The value of β depends on the coordination number of atoms in the surface and bulk phases and its value is taken to be 0.82 [22] for the liquid metal. α_i are the monolayer surface area of one mole of the pure components and its value is computed using the relation [13, 23]

$$\alpha_i = f N_A^{1/3} \left(\frac{M_i}{\rho_i} \right)^{2/3} \dots\dots\dots (2)$$

where f is called geometrical factor and its value is taken to be 1.00 [23]. The terms N_A , M_i and ρ_i are the Avogadro's number, molar mass and density of the element i . The partial excess Gibbs free energy (G_i^{xs}) of component i in binary and multi-component alloys are expressed in terms of integral excess Gibbs free energy of mixing (G_M^{xs}) as [20, 24]

$$G_i^{xs} = G_M^{xs} + \sum_{j=1}^m (\delta_{ij} - x_j) \frac{\partial G_M^{xs}}{\partial x_j} \dots\dots\dots (3)$$

where δ_{ij} is the Kronecker delta function defined as $\delta_{ij} = 0$ for $i \neq j$ and $\delta_{ij} = 1$ for $i = j$. The value of m is 2 for binary and 3 for ternary liquid alloy. The excess free energy of mixing of binary liquid alloy 'ij' having bulk concentrations x_i and x_j are frequently expressed in terms of R-K polynomial of order 'n' as [20, 21]

$$G_M^{xs} = x_i x_j \sum_{k=0}^n \varphi_{ij}^k (x_i - x_j)^k \dots\dots\dots (4)$$

where φ_{ij}^k ($k = 0, 1, 2, 3, \dots$) are called coefficients of R-K polynomial for excess Gibbs free energy of mixing of the binary system such that $\varphi_{ji}^k = (-1)^k \varphi_{ij}^k$. In the present calculations, value of k was taken upto 2 and the higher order terms were dropped out as their contribution to the excess free energy was found to be negligible.

Following Chou [25], the expression for free energy of mixing (G_{123}^{xs}) for ternary alloy can be given as

$$G_{123}^{xs} = x_1 x_2 \sum_{k=0}^n \varphi_{12}^k (x_1 - x_2)^k + x_2 x_3 \sum_{k=0}^n \varphi_{23}^k (x_2 - x_3)^k + x_3 x_1 \sum_{k=0}^n \varphi_{31}^k (x_3 - x_1)^k + F x_1 x_2 x_3 \quad (5)$$

where F is the ternary interaction term and can be given as [25]

$$\begin{aligned} F = & (2\xi_{12} - 1)[\varphi_{12}^3(3(x_1 - x_2)^2 x_3 + 3(x_1 - x_2)x_3^2(2\xi_{12} - 1) + x_3^3(2\xi_{12} - 1)^2) \\ & + \varphi_{12}^2((2\xi_{12} - 1)x_3 + 2(x_1 - x_2)) + \varphi_{12}^1] \\ & + (2\xi_{23} - 1)[\varphi_{23}^3(3(x_2 - x_3)^2 x_1 + 3(x_2 - x_3)x_1^2(2\xi_{23} - 1) + x_1^3(2\xi_{23} - 1)^2) \\ & + \varphi_{23}^2((2\xi_{23} - 1)x_1 + 2(x_2 - x_3)) + \varphi_{23}^1] \\ & + (2\xi_{31} - 1)[\varphi_{31}^3(3(x_3 - x_1)^2 x_2 + 3(x_3 - x_1)x_2^2(2\xi_{31} - 1) + x_2^3(2\xi_{31} - 1)^2) \\ & + \varphi_{31}^2((2\xi_{31} - 1)x_2 + 2(x_3 - x_1)) + \varphi_{31}^1] \end{aligned} \quad (6)$$

The terms x_1 , x_2 and x_3 are the mole fractions of components in the ternary alloy. The term ξ_{ij} are called similarity indexes and are expressed as

$$\xi_{12} = \frac{\eta_1}{\eta_1 + \eta_{11}}, \quad \xi_{23} = \frac{\eta_{11}}{\eta_{11} + \eta_{111}} \quad \text{and} \quad \xi_{31} = \frac{\eta_{111}}{\eta_{111} + \eta_1} \quad (7)$$

The term η are called deviation sum of squares and are computed using the relations [25]

$$\begin{aligned} \eta_1 = & \int_0^1 (G_{12}^E - G_{13}^E)^2 dx_1 \\ = & \frac{1}{30}(\varphi_{12}^0 - \varphi_{13}^0)^2 + \frac{1}{210}(\varphi_{12}^1 - \varphi_{13}^1)^2 + \frac{1}{630}(\varphi_{12}^2 - \varphi_{13}^2)^2 + \frac{1}{1386}(\varphi_{12}^3 - \varphi_{13}^3)^2 \\ & + \frac{1}{105}(\varphi_{12}^0 - \varphi_{13}^0)(\varphi_{12}^2 - \varphi_{13}^2) + \frac{1}{315}(\varphi_{12}^1 - \varphi_{13}^1)(\varphi_{12}^3 - \varphi_{13}^3) \end{aligned} \quad (8a)$$

$$\begin{aligned} \eta_{11} = & \int_0^1 (G_{23}^E - G_{21}^E)^2 dx_2 \\ = & \frac{1}{30}(\varphi_{23}^0 - \varphi_{21}^0)^2 + \frac{1}{210}(\varphi_{23}^1 - \varphi_{21}^1)^2 + \frac{1}{630}(\varphi_{23}^2 - \varphi_{21}^2)^2 + \frac{1}{1386}(\varphi_{23}^3 - \varphi_{21}^3)^2 \\ & + \frac{1}{105}(\varphi_{23}^0 - \varphi_{21}^0)(\varphi_{23}^2 - \varphi_{21}^2) + \frac{1}{315}(\varphi_{23}^1 - \varphi_{21}^1)(\varphi_{23}^3 - \varphi_{21}^3) \end{aligned} \quad (8b)$$

$$\begin{aligned} \eta_{111} = & \int_0^1 (G_{31}^E - G_{32}^E)^2 dx_3 \\ = & \frac{1}{30}(\varphi_{31}^0 - \varphi_{32}^0)^2 + \frac{1}{210}(\varphi_{31}^1 - \varphi_{32}^1)^2 + \frac{1}{630}(\varphi_{31}^2 - \varphi_{32}^2)^2 + \frac{1}{1386}(\varphi_{31}^3 - \varphi_{32}^3)^2 + \\ & \frac{1}{105}(\varphi_{31}^0 - \varphi_{32}^0)(\varphi_{31}^2 - \varphi_{32}^2) + \frac{1}{315}(\varphi_{31}^1 - \varphi_{32}^1)(\varphi_{31}^3 - \varphi_{32}^3) \end{aligned} \quad (8c)$$

The values of partial excess free energy of the components for the binary liquid alloys are obtained using Equation (4) in Equation (3) and putting

$m = 2$. Similarly, the values of partial excess free energies of the individual components in the ternary liquid alloys are obtained using Equation (5) in

Equation (3) and putting $m = 3$. The activity (a_i) of a component i can be expressed in terms of the partial excess free energy (G_i^{xs}) at temperature T using the thermodynamic relation [26]

$$a_i = x_i \exp\left(\frac{G_i^{xs}}{RT}\right) \quad (9)$$

The excess surface tension (σ_{123}^{xs}) of the ternary alloy using the Chou model is obtained by using Equations (5), (6), (7) and (8) and replacing the coefficients φ_{ij}^k for excess free energy by the corresponding coefficients (λ_{ij}^k) for excess surface tension. Kohler model is a symmetric geometrical model and all the elements can be placed at equal footing. The expression for excess surface tension of ternary alloy on the basis of Kohler model is expressed as [20, 27].

$$\begin{aligned} \gamma_{123}^{xs} = & (x_1^2 + x_2^2) \gamma_{12}^{xs} \left(\frac{x_1}{x_1+x_2}, \frac{x_2}{x_1+x_2} \right) + (x_2^2 + \\ & x_3^2) \gamma_{23}^{xs} \left(\frac{x_2}{x_2+x_3}, \frac{x_3}{x_2+x_3} \right) + (x_3^2 + \\ & x_1^2) \gamma_{31}^{xs} \left(\frac{x_3}{x_3+x_1}, \frac{x_1}{x_3+x_1} \right) \end{aligned} \quad (10)$$

where γ_{ij}^{xs} are the excess surface tension of the binary system at concentrations $\left(\frac{x_i}{x_i+x_j}, \frac{x_j}{x_i+x_j} \right)$.

Toop model is an asymmetric geometrical model and a symmetric element is to be selected to apply this model. According to this model, the expression for excess surface tension of ternary alloy for a symmetrical element having bulk concentration x_1 is given by the relation [20, 28].

$$\begin{aligned} \gamma_{123}^{xs} = & \frac{x_2}{(x_2 + x_3)} \gamma_{12}^{xs}(x_1, 1 - x_1) + (x_2 \\ & + x_3)^2 \gamma_{23}^{xs} \left(\frac{x_2}{x_2 + x_3}, \frac{x_3}{x_2 + x_3} \right) \\ & + \frac{x_3}{(x_2 + x_3)} \gamma_{13}^{xs}(x_1, 1 - x_1) \end{aligned} \quad (11)$$

The surface tension (γ) and density (ρ) of a pure element at temperature T are expressed in terms of

its surface tension (σ_0) and density (ρ_0) near melting temperature T_0 using the linear relations [29]

$$\begin{aligned} \gamma = \gamma_0 + \frac{\partial \gamma}{\partial T} (T - T_0), \\ \text{and } \rho = \rho_0 + \frac{\partial \rho}{\partial T} (T - T_0) \end{aligned} \quad (12)$$

where $\partial \gamma / \partial T$ and $\partial \rho / \partial T$ are the temperature derivatives terms of surface tension and density respectively.

The excess surface tension (γ^{xs}) of the liquid alloy is the deviation between surface tension and its ideal value and is given as

$$\gamma^{xs} = \gamma - \gamma^{ideal} = \gamma - \sum_i (x_i \gamma_i) \quad (13)$$

where γ_i are the surface tension of the pure elements at working temperature.

3. RESULTS AND DISCUSSION

The coefficients of R-K polynomials for the integral excess Gibbs free energy of mixing (G_M^{xs}) for the sub-binary systems (Al-Fe, Fe-Si and Si-Al) were optimised using the experimental values [30, 31] of the enthalpy of mixing and excess entropy of mixing and are listed in Table 1. These optimised parameters were then used in Equation (4) to compute G_M^{xs} of the sub-binary systems. The computed values of the present work were found to be in excellent agreement with the experimental values (Figures 1(a-c)). Moreover, the computed values of G_M^{xs} for Al-Fe system was found to be excellent agreement with the work of Adhikari et. al. [32] and Yadav et. al. [33], and that of Al-Si with the work of Adhikari et al. [34]. But the values obtained using the parameters given in Cost 507 [35] and the results of Kostov et al. [36] (for Al-Fe system) were found to deviate from the experimental results. Therefore, the optimised parameters of the present work were considered for further computations. Moreover, the perusal of Figures 1(a-c) correspond that Fe-Si is strongly interacting, Al-Fe is moderately interacting and Si-Al is weakly interacting in nature.

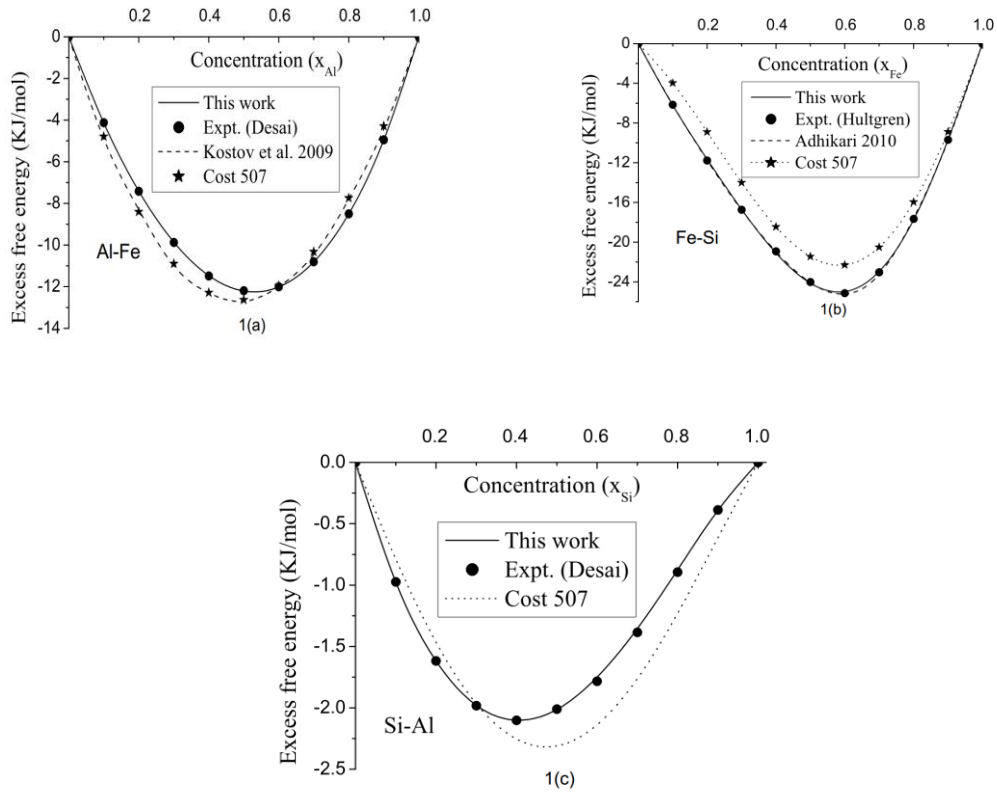


Fig. 1: Variation of excess free energy of mixing for sub-binary systems of Al–Fe–Si ternary liquid alloy with bulk concentration. (a) Al-Fe at 1873 K, (b) Fe-Si at 1873 K and (c) Si-Al at 1700 K.

Table 1: Optimised coefficients of R-K polynomial for excess free energy of mixing for the sub-binary systems of liquid Al–Fe–Si alloy (this work).

Sub-binary system	Optimised parameters (φ^k) [Jmol^{-1}]
Al-Fe	$\varphi^0 = -78925 + 16.068 T$, $\varphi^1 = -16314 + 5.681 T$ $\varphi^2 = -1766 - 0.380 T$
Fe-Si	$\varphi^0 = -151490 + 29.357 T$, $\varphi^1 = -37170 - 2.290 T$ $\varphi^2 = 36570 - 12.6060 T$, $\varphi^3 = 29560 - 1.374 T$
Si-Al	$\varphi^0 = -11263 + 1.890 T$, $\varphi^1 = 4423 - 0.479 T$ $\varphi^2 = 1790 - 0.627 T$, $\varphi^3 = -1565 + 1.330 T$

The activity is an important thermodynamic function of the liquid alloys. The optimised parameters for the excess Gibbs free energy of mixing are considered to be acceptable only when they well reproduces activity. The activities of the constituent atoms of the sub-binary systems were calculated using Equations (3), (4) and (9) with help of parameters of Table 1. The compositional dependence of the activities of the monomers of the sub-binary systems are presented in Figure 2 (a-c). The computed values of activities of Al (a_{Al}) and Fe

(a_{Fe}) of Al-Fe liquid alloy at 1873 K were found to be in good agreement with the respective experimental [30] and literature [32, 33, 36] values (Figure 2(a)). Likewise, the computed values of activities of the components of Fe–Si alloy at 1873 K agree with the experimental data [31] and with the work of Adhikari et al. [34] but some considerable deviations were depicted for the activity of Si in concentration range $0.15 < x_{Fe} < 0.4$ (Figure 2(b)). The computed values of activities of Si (a_{Si}) and Al (a_{Al}) of Si–Al alloys at 1700 K were in good

agreement with the experimental [30] data and the values computed using the parameters from Cost 507 [35] (Figure 2(c)). As the optimised parameters for the excess Gibbs free energy of mixing have well

reproduced the activity of the preferred systems, these parameters were considered for further computations of the surface properties.

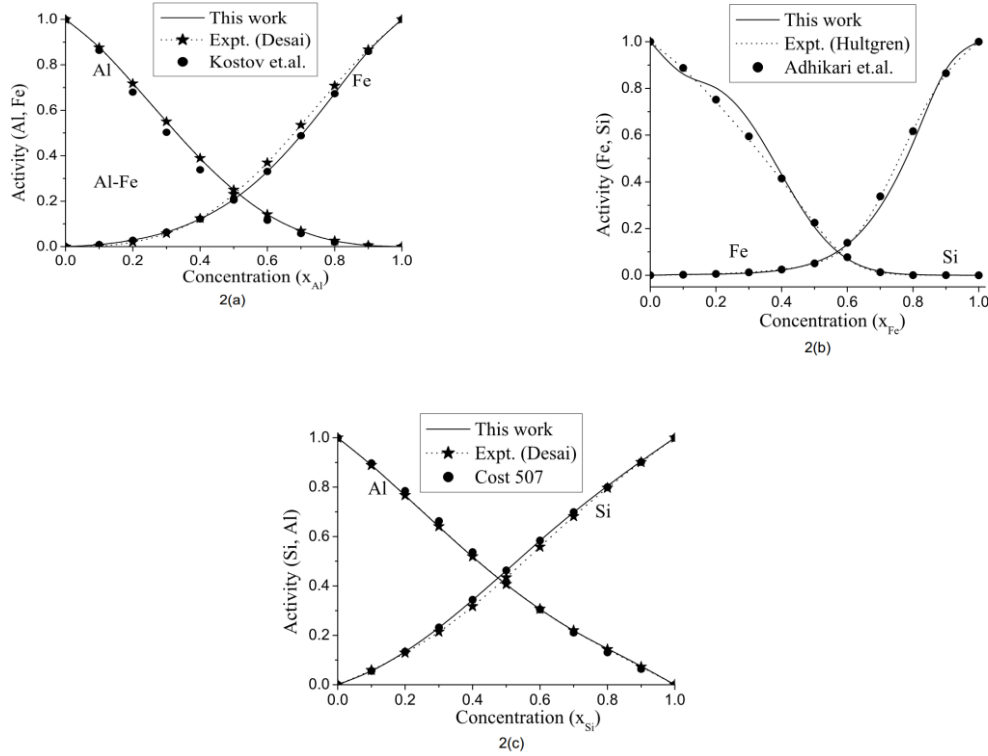


Fig. 2: Variation of activities of the components of the sub-binary systems of liquid Al-Fe-Si ternary alloy with bulk concentration. (a) Al-Fe at 1873 K, (b) Fe-Si at 1873 K and (c) Si-Al at 1700 K.

The surface tensions and densities of the pure elements of the sub-binary systems were calculated at working temperatures using Equation (12) and the data presented in Table 2. The surface tensions of the sub-binary liquid alloys were then computed using Equations (1) and (2) and are plotted in Figure 3. The computed values of the surface tensions for Al-Fe and Fe-Si systems at 1823 K were compared with the work of Tanaka and Lida [13]. There appeared some deviations between

these results and these deviations might be due to the difference in the values of input parameters, such as f and β . In present computations, $f = 1.00$ and $\beta = 0.82$ [33, 37, 38] were taken but Tanaka and Lida carried out the work taking $f = 1.091$ and $\beta = 0.75$. Additionally, the result of this work for the surface tension of Si-Al system at 1773 K was found to be in agreement with the results of Kobatake et al. [17] at higher bulk concentration of Si.

Table 2: Density (ρ_0) and surface tension (σ_0) of elements near their melting temperature (T_0) and their derivatives w.r.t. temperature [28].

Elements	T_0 (K)	ρ_0 (kg m ⁻³)	$\partial\rho/\partial T$ (kg m ⁻³ K ⁻¹)	σ_0 (Nm ⁻¹)	$\partial\sigma/\partial T$ (Nm ⁻¹ K ⁻¹)
Al	933	2385	-0.35	0.914	-0.00035
Fe	1809	7030	-0.88	1.872	-0.00049
Si	1683	2530	-0.35	0.865	-0.00013

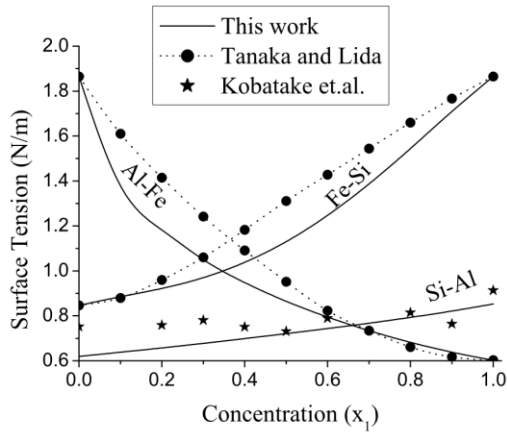


Fig. 3: Variation of surface tensions of sub-binary alloys of Al-Fe-Si ternary system with the bulk concentration.

The Butler equation was used to estimate the surface concentrations of components of the ternary liquid alloy at cross-sections $x_{Fe}/x_{Si} = 5:5$ from Al corner, $x_{Si}/x_{Al} = 5:5$ from Fe corner and $x_{Al}/x_{Fe} = 5:5$ from Si corner. For this purpose, the input parameters from Tables 1 and 2 were used in Equations (1), (2) and (12). The variation of the

surface concentration with the bulk concentration of the system at 1773 K are presented in Figures 4 (a-c). The surface concentration of each component in the alloy was found to increase with the rise of the respective bulk concentration. But some unusual trend had been depicted at $x_{Si}/x_{Al} = 5:5$ from Fe corner in which the surface concentration of Al increases with the decrease in its bulk concentration upto $x_{Fe} \leq 0.6$ (Figure 4(b)). This might be because when the bulk concentration of Fe is gradually increased, Si atoms tend to make complexes with the Fe atoms as Fe-Si system is found to be strongly interacting in nature than that of Al-Fe system due to which Al atoms tend to segregate on the surface phase. At equiatomic bulk concentration of components in ternary alloy, the extent of surface segregation of Al atoms is much higher than that of Si atoms while Fe atoms is less than that of Si (Figures 4 (a-c)). These observations reveal that the component having lower value of surface tension has the greater surface segregation. The surface concentration of Si and Al were found to decrease and that of Fe was found to increase gradually with the rise in temperature of the system at bulk concentration $Si_{33}Al_{33}Fe_{34}$ (Figure 4(d)).

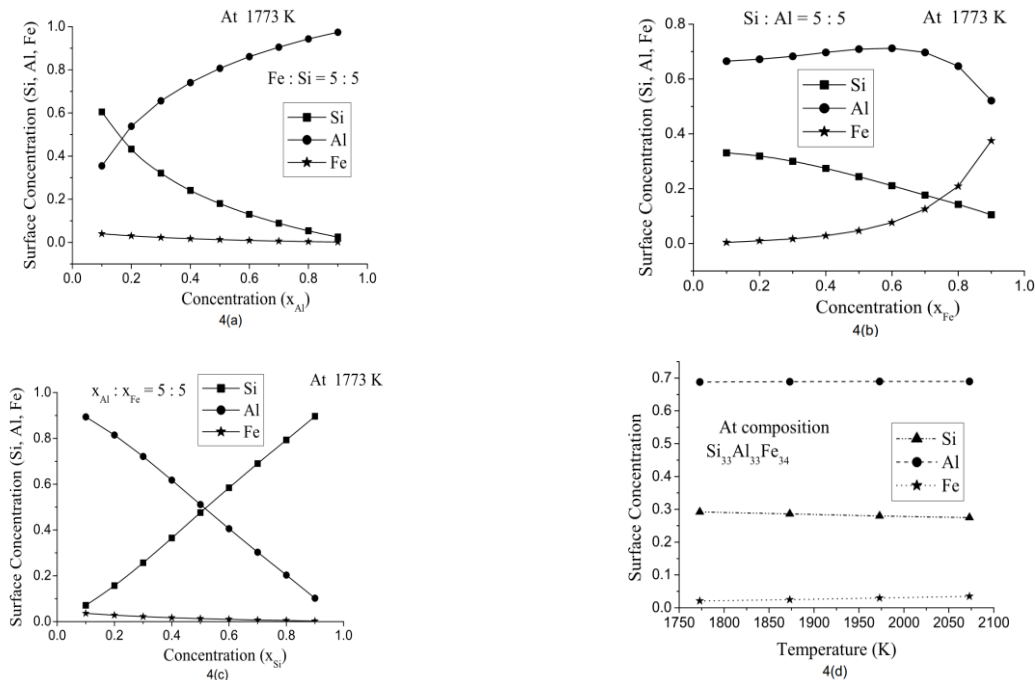


Fig. 4: Variation of surface concentration of the components of the Al-Fe-Si ternary liquid alloy with concentration. (a) at $x_{Fe}/x_{Si} = 5:5$ from Al corner, (b) at $x_{Si}/x_{Al} = 5:5$ from Fe corner, (c) at $x_{Al}/x_{Fe} = 5:5$ from Si corner and (d) Variation of surface concentration of the Al-Fe-Si ternary liquid alloy with temperatures at a fixed concentration $Si_{33}Al_{33}Fe_{34}$.

Table 3: Optimised coefficients of R-K polynomial for excess surface tension of sub-binary systems of Al-Fe-Si alloy (this work).

Sub-binary system	Optimised parameters (λ^k) [Nm^{-1}]
Al-Fe	$\lambda^0 = -2.099 + 3.693 \times 10^{-4}T$, $\lambda^1 = 1.549 - 3.355 \times 10^{-4}T$ $\lambda^2 = -3.540 + 1.098 \times 10^{-3}T$, $\lambda^3 = 3.350 - 1.106 \times 10^{-3}T$
Fe-Si	$\lambda^0 = -2.263 + 7.437 \times 10^{-4}T$, $\lambda^1 = -0.522 + 3.150 \times 10^{-4}T$ $\lambda^2 = -1.195 + 1.582 \times 10^{-3}T - 3.905 \times 10^{-7}T^2$ $\lambda^3 = -1.207 + 1.202 \times 10^{-3}T - 2.909 \times 10^{-7}T^2$
Si-Al	$\lambda^0 = 0.205 - 1.515 \times 10^{-4}T$, $\lambda^1 = 0.074 - 5.191 \times 10^{-5}T$ $\lambda^2 = 0.0172 - 2.095 \times 10^{-5}T$, $\lambda^3 = 0.0145 - 1.487 \times 10^{-5}T$

The excess surface tensions of the sub-binary liquid alloys were computed using Equation (13). These values were then used to optimise the coefficients of R-K polynomial for excess surface tension and are presented in Table 3. The surface tension of the liquid Al-Fe-Si ternary alloy at different temperatures and concentrations were then calculated using Butler (Equation (1)), Chou (Equations (5-8)), Kohler (Equation (10)) and Toop (Equation (11)) models at above mentioned cross-sections and corners. The compositional and the temperature dependence of the surface tension of the ternary system are shown in Figures 5(a-d).

The surface tension of the ternary alloy was found to increase with the rise in concentration of Fe (Figure 5(b)) and decrease with the rise in the concentration of Al (Figure 5(a)). This might be due to the greatest value of the surface tension of Fe and the least for Al among the constituents of the system at 1773 K. As the surface tension of Si lies in between Al and Fe, the variation of the surface tension of the system from Si corner is the least (Figure 5(c)). The surface tension of the system was found to decrease linearly with the increase in its temperature at all ternary concentrations (Figure 5(d)).

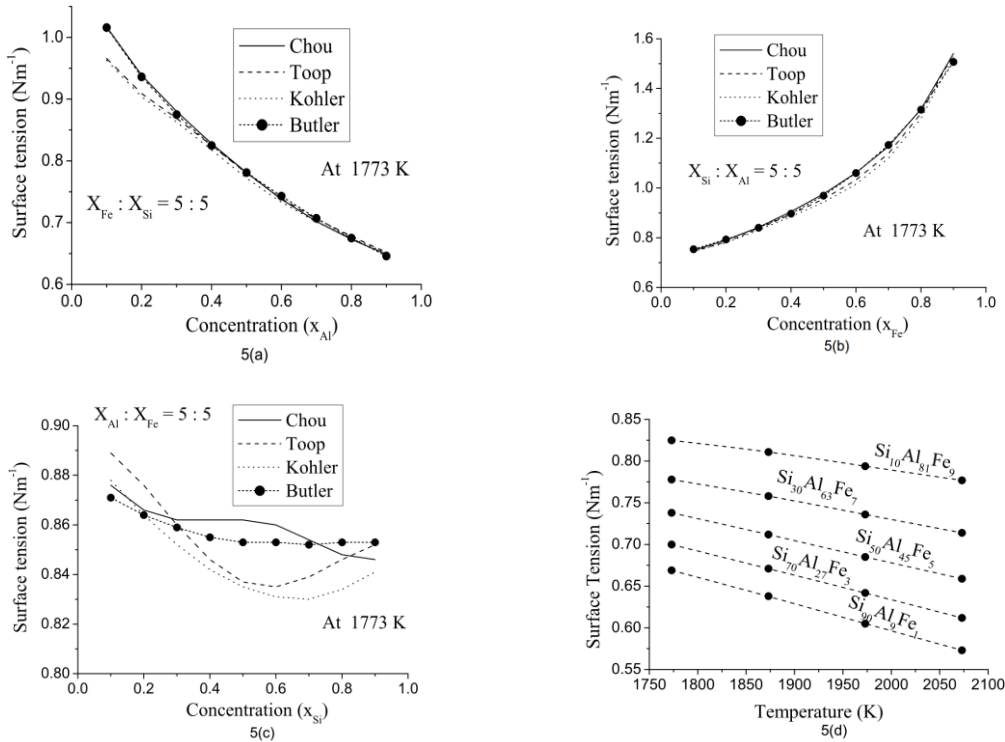


Fig. 5: Variation of surface tension of the liquid Al-Fe-Si ternary alloy with concentration. (a) at $x_{Fe}/x_{Si} = 5:5$ from Al corner, (b) at $x_{Si}/x_{Al} = 5:5$ from Fe corner, (c) at $x_{Al}/x_{Fe} = 5:5$ from Si corner and (d) Variation of surface tension of the liquid Al-Fe-Si ternary alloy with temperatures at five different fixed concentrations.

4. CONCLUSIONS

The computed and the experimental values of the excess Gibbs free energy of mixing and the activity of the sub-binary systems of the liquid Al-Fe-Si alloy were found to be in good agreement which provided the validity of the optimised parameters of this work. Among the three sub-binary systems, Fe–Si was found to be strongly interacting, Al–Fe was found to be moderately interacting and Si–Al was found to be weakly interacting. Surface concentrations of the components of the ternary system were found to increase with the rise in the respective bulk concentrations. The component having lower values of the surface tension segregates more on the surface phase of the initial melt. The surface tension of the ternary system was found to increase with the increase in Fe content and decrease with the increase in Al content. Moreover, the surface tension of the ternary alloy was found to decrease linearly with the rise in temperature.

REFERENCES

- [1] Liu, Z. K. and Chang Y. A. Thermodynamic assessment of the Al-Fe-Si system. *Metallurgical and Materials Transactions A*, **30**(4): 1081–1095 (1999).
- [2] Ghosh, G. Aluminium–Iron–Silicon. In *Iron Systems, Part 1*, 184–266 (2008).
- [3] Novak, P.; Vanka, T.; Nova, K.; Stouilil, J.; Prusa, F.; Kopecek, J.; Hausild, P. and Laufek, F. Structure and properties of Fe–Al–Si alloy prepared by mechanical alloying. *Materials*, **12**(15): 2463 (2019).
- [4] Boulouma, A.; Drici, A.; Benaldjia, A.; Guerioune, M. and Vrel, D. The formation of (Al₈Fe₂Si, Al₁₃Fe₄) phases from Al–Fe–Si system by TE mode. In *AIP Conference Proceedings*. **1653**(1): 020023. AIP Publishing LLC (2015).
- [5] Dutta, B. and Rettenmayr, M. Effect of cooling rate on the solidification behaviour of Al–Fe–Si alloys. *Materials Science and Engineering: A*, **283**: 218–224 (2000).
- [6] Koraman, E.; Baydogan, M.; Sayilgan, S. and Kalkanli, A. Dry sliding wear behavior of Al–Fe–Si–V alloys at elevated temperatures. *Wear*, **322**: 101–107 (2015).
- [7] Du, Y.; Schuster, J. C.; Liu, Z. K.; Hu, R.; Nash, P.; Sun, W.; Zhang, W.; Wang, J.; Zhang, L.; Tang, C. and Zhu, Z. A thermodynamic description of the Al–Fe–Si system over the whole composition and temperature ranges via a hybrid approach of Calphad and key experiments. *Intermetallics*, **16**(4): 554–570 (2008).
- [8] Pontevichi, S.; Bosselet, F.; Barbeau, F.; Peronnet, M. and Viala, J.C. Solid-liquid phase equilibria in the Al-Fe-Si system at 727 °C. *Journal of Phase Equilibria and Diffusion*, **25**(6): 528–537 (2004).
- [9] Raghavan, V. Al–Fe–Si (aluminum-iron-silicon). *Journal of Phase Equilibria and Diffusion*, **30**(2): 184–188 (2009).
- [10] Zakharov, A. M.; Guldin, I. T.; Arnold, A. A. and Matsenko, Y. A. Phase equilibria in multi-component aluminum systems with copper, iron, silicon, manganese and titanium. *Metalloved. Obrab. Tsv. Splavov, RAN. Inst. Metallurgii. M*, 6–17, (1992).
- [11] Anglezio, J. C.; Servant, C. and Ansara, I. Contribution to the experimental and thermodynamic assessment of the Al–Ca–Fe–Si system-I. Al–Ca–Fe, Al–Ca–Si, Al–Fe–Si and Ca–Fe–Si systems. *Calphad*, **18**(3): 273–309 (1994).
- [12] Griger, A. and Stefaniay, V. Equilibrium and non-equilibrium intermetallic phases in Al–Fe and Al-Fe-Si alloys. *Journal of Materials Science*, **31**(24): 6645–6652 (1996).
- [13] Tanaka, T. and Iida T. Application of a thermodynamic database to the calculation of surface tension for iron-base liquid alloys. *Journal of Iron Steel Research International*, **65**(1): 21–28 (1994).
- [14] Bainbridge, I. F. and Taylor, J. A. The surface tension of pure aluminum and aluminum alloys. *Metallurgical and Materials Transactions A*, **44**(8): 3901–3909 (2013).
- [15] Dzhemilev, N. K.; Popel, S. I. and Tsarevskii, B. V. Isotherm of the density and surface tension of iron–silicon melts. *Fiz. Met. Metallved*, **18**(1): 83–87 (1964).
- [16] Kawai, Y.; Mori, K.; Kishimoto, M.; Ishikura, K. and Shimada, T. Surface tension of liquid Fe–C–Si alloys. *Tetsu-to-Hagané*, **60**(1): 29–37 (1974).
- [17] Kobatake, H.; Brillo, J.; Schmitz, J. and Pichon, P. Y. Surface tension of binary Al–Si liquid alloys. *Journal of Materials Science*, **50**(9): 3351–3360 (2015).
- [18] Butler, J. A. V. The thermodynamics of the surfaces of solutions. *Proceedings of the Royal Society of London-A.*, **135**(827): 348–375 (1932).
- [19] Yeum, K. S.; Speiser, R. and Poirier, D. R. Estimation of the surface tensions of binary liquid alloys. *Metallurgical Transactions B*, **20**(5): 693–703 (1989).
- [20] Yan, L.; Zheng, S.; Ding, G.; Xu, G. and Qiao Z. Surface tension calculation of the Sn–Ga–In ternary alloy. *Calphad*, **31**(1): 112–119 (2007).
- [21] Fima, P. and Novakovic, R. Surface tension

- modelling of liquid Cd-Sn-Zn alloys. *Philosophical Magazine*, **6435**: 1–17 (2018).
- [22] Kaptay, G. A method to calculate equilibrium surface phase transition lines in monotectic systems. *Calphad*, **29**(1): 56–67 (2005).
- [23] Mekler, C. and Kaptay, G. Calculation of surface tension and surface phase transition line in binary Ga-Tl system. *Material Science and Engineering A*, **495**(1-2): 65–69 (2008).
- [24] Egry, I.; Holland-Moritz, D.; Novakovic, R.; Ricci, E.; Wunderlich, R. and Sobczak, N. Thermo-physical properties of liquid AlTi-based alloys. *International Journal of Thermophysics*, **1**: 949–965 (2010).
- [25] Chou, K. C.; Li, W. C.; Li, F. and He, M. Formalism of new ternary model expressed in terms of binary regular-solution type parameters. *Calphad*, **20**(4): 395–406, (1996).
- [26] Marjanović, S.; Manašijević, D.; Živković, D.; Gusković, D. and Minić, D. Calculation of thermodynamic properties for ternary Ag–Cu–Sn system. *RMZ-Materials and Geoenvironment*, **56**(1): 30–37 (2009).
- [27] Kohler, F. Zur berechnung der thermodynamischen daten eines ternären systems aus den zugehörigen binären systemen. *Monatshefte für Chemie und verwandte Teile anderer Wissenschaften*, **91**(4): 738–740 (1960).
- [28] Toop G. W. Predicting ternary activities using binary data. *Trans. TMS-AIME*, **223**: 850–855(1965).
- [29] Gale, W. F. and Terry, C. *Smithells Metals Reference Book*. Elsevier (2003).
- [30] Desai, P. D. Thermodynamic properties of selected binary aluminum alloy systems. *Journal of Physical and Chemical Reference Data*, **16**(1): 109–124 (1987).
- [31] Hultgren, R.; Desai, P. D.; Hawkins, D. T. Molly Gleiser, and Kelley, K. K. Selected values of the thermodynamic properties of binary alloys. Technical Report, *National Standard Reference Data System* (1973).
- [32] Adhikari, D.; Yadav, S. K.; Jha, L. N. Thermo-physical properties of Al-Fe melt. *Journal of the Chinese Advanced Materials Society*, **2**(3): 149-158 (2014).
- [33] Yadav, S. K.; Jha, L. N. and Adhikari, D. Modeling equations to predict the mixing behaviour of Al–Fe liquid alloy at different temperatures. *Bibechana*, **15**: 60-69 (2018).
- [34] Adhikari, D.; Jha, I. S. and Singh, B. P. Structural asymmetry in liquid Fe–Si alloys. *Philosophical Magazine*, **90**(20): 2687–2694 (2010).
- [35] Ansara, I., Dinsdale, A. T. and Rand, M. H. *Thermochemical Database for Light Metal Alloys (Cost507)*, (1998).
- [36] Kostov, A.; Friedrich, B. and Živković, D. Thermodynamic calculations in alloys Ti–Al, Ti–Fe, Al–Fe and Ti–Al–Fe. *Journal of Mining and Metallurgy*, **44B**: 49–61 (2008).
- [37] Mehta, U., Koirala, I., Yadav, S. K., Koirala, R. P. and Adhikari, D. Prediction of thermodynamic and surface properties of ternary Ti–Si–Fe liquid alloy. *Modelling and Simulation in Materials Science and Engineering*, **28**(6): 065010 (2020).
- [38] Mehta, U.; Yadav, S. K.; Koirala, I.; Koirala, R. P.; Shrestha, G. K. and Adhikari, D. Study of surface tension and viscosity of Cu–Fe–Si ternary alloy using a thermodynamic approach. *Heliyon*, **6**(8): e04674 (2020).

Certificate of Participations



ICC 2019

3rd International Conference on
Condensed Matter & Applied Physics

Organized By: Department of Physics, Govt. Engineering College, Bikaner



Paper ID : H-0012



Certificate

This is to certify that
Mr. Upendra Mehta
of
Tribhuvan University

has participated in 3rd International Conference on
Condensed Matter & Applied Physics (ICC 2019)
organized by Govt. Engineering College, Bikaner
during Oct. 14-15, 2019
and presented a paper entitled

Surface Properties of Liquid Ti-Al-Fe Alloy at Different Temperatures

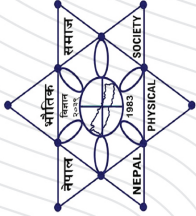


15 October 2019
Bikaner

(Dr. M. S. Shekhawat)
Convener

iccindia.in

Oct. 14-15, 2019, Bikaner, India



Nepal Physical Society

Ghantaghar, Kathmandu

Certificate of Participation

This certificate is awarded to


Mr. Upendra Mehta from

**Central Department of Physics, TU, Nepal, for his presentation entitled
Concentration and Temperature Dependence of Surface Properties
of Cu-Fe-Ti Ternary Liquid Alloy**

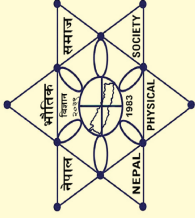
On Scientific Session of 37th Annual Convention, February 6, 2021.


Prof. Dr. Narayan Prasad Chapagain
President
Nepal Physical Society


Dr. Sunil Babu Shrestha
Chief Guest
Vice – Chancellor, NAST


Prof. Dr. Leela Pradhan Joshi
Chair, Scientific Committee
37th Annual Convention, NPS

February 6, 2021



Nepal Physical Society

Ghantaghar, Kathmandu

Certificate of Participation

This certificate is awarded to

Mr. Upendra Mehta from

MMAMC, TU, Biratnagar for his successful participation in

NPS School of Computing - 2020

Conducted from July 4, 2020 to January 31, 2021.

Alchhapagain
.....
Prof. Dr. Narayan Prasad Chapagain
President
Nepal Physical Society

Shrestha
.....
Dr. Sunil Babu Shrestha
Chief Guest
Vice – Chancellor, NAST

Sigdel
.....
Dr. Dibakar Sigdel
Instructor
Data Scientist, UCLA, USA

February 6, 2021



St. Xavier's College

Maitighar, Kathmandu, Nepal

Department of Physics

This e-certificate of appreciation is awarded to **Mr Upendra Mehta** of Mahendra Morang Adarsh Multiple Campus, Biratnagar for oral presentation on the title

Thermodynamics surface and viscous properties of Cu-Fe-Ti liquid ternary alloys in the

“International Conference on Material Science and Characterization Technology (ICMSCT)”

held on **September 26-28, 2021**

Mr. Drabindra Pandit
Head,
Department of Physics

Fr. Dr. Augustine Thomas, S.J.
Principal
St. Xavier's College

Prof. Dr. Bhim Prasad Subedi
Chairperson, University
Grants Commission Nepal